Technische Universität München

Fakultät für Physik

Mechanistic dissection of Kinesin-2 and its conveyance in Intraflagellar transport

Augustine Cleetus

Technische Universität München

Fakultät für Physik

Mechanistic dissection of Kinesin-2 and its conveyance in Intraflagellar transport

Augustine Cleetus

Vollständiger Abdruck der von der Fakultät für Physik der Technischen Universität München zur Erlangung des akademischen Grades eines Doktors der Naturwissenschaften (Dr. rer. nat.) genehmigten Dissertation.

Vorsitzender: Prof. Dr. Ulrich Gerland

Prüfer der Dissertation:

1. TUM Junior Fellow Dr. Zeynep Ökten
2. Prof. Dr. Manfred Schliwa

Die Dissertation wurde am 12.10.2020 bei der Technischen Universität München eingereicht und durch die Fakultät für Physik am 02.12.2020 angenommen.

List of publications

Kinesin-2 from *C. reinhardtii* is an atypically fast and auto-inhibited motor that is activated by heterotrimerization for intraflagellar transport.

Sonar P, Youyen W, **Cleetus A**, Wisanpitayakorn P, Mousavi IS, Stepp WL, Hancock WO, Tuezel E, Okten Z.

Current Biology 2020; 30(6):1160-1166.e5. doi:10.1016/j.cub.2020.01.046

Myosin Va's adaptor protein melanophilin enforces track selection on the microtubule and actin networks *in vitro*.

Oberhofer A, Spieler P, Rosenfeld Y, Stepp WL, **Cleetus A**, Hume AN, Okten Z.

Proc Natl Acad Sci 2017. doi:10.1073/pnas.1619473114.

Summary

Kinesin motors are responsible for the transportation of numerous intracellular components on the microtubule tracks. Cells have evidently established robust means to regulate the kinesin-mediated transport processes, starting with the kinesin motor. When not bound to their cargo, virtually all kinesins are 'switched off', meaning they have the ability to self-inhibit their ATPase activity. Binding to cargo is thus thought to activate the kinesin motor for directional transport on the microtubule network. How cells decide where and when to activate and deactivate a motor, is therefore a central question of intracellular transport. Yet very little is known about the mechanisms that establish motor-cargo specificity and how the motor is activated and deactivated at the right time and place.

To provide answers to the above-mentioned questions, this thesis concentrates on the kinesin-2 motors that are found in the cilium as well as in the cytoplasm. Kinesin-2 subfamily is unique in that it comprises heterotrimeric motors in addition to the prototypical homodimeric kinesins. In the cilium, kinesin-2 is involved in the Intraflagellar Transport and its absence completely disrupts the ciliogenesis from unicellular to mammalian organisms. Much attention has therefore been paid to the working mechanisms of kinesin-2 motors. As it is the case for other kinesins, hetero- and homodimeric kinesin-2 motors are autoinhibited and their binding to cargo is thought to activate the respective motors. Building on this near universal regulatory mechanism, I describe in so far unprecedented detail how a homodimeric kinesin-2 motor is activated by its cargo/adaptor. I further suggest that cargo/adaptor binding does not necessarily represents the activation step of an autoinhibited kinesin motor. From the data presented in this thesis, I propose that a cell simply deploys dedicated switches to activate a motor or to keep it autoinhibited. Notably, these on- and off-switches are kept conserved, suggesting that cells might repurpose motors for different transport processes simply by tailoring them for specific switches.

Using heterotrimeric kinesin-2, I show that the characteristics of kinesin-2 motors are tuned in correspondence with their primary duty inside the cilium. The analogous heterotrimeric motors from different species have adapted their autoregulation and structural domain properties distinctly in response to the different needs inside the respective cilium. Altogether this thesis

provides direct insights into the mechanism of kinesin-2 deployment to separate domains inside the cell body and presents a systematic dissection on unmasking the unique features of the kinesin-2 motors.

Zusammenfassung

Kinesin-Motoren sind für den Transport zahlreicher intrazellulärer Komponenten auf den Fahrbahnen der Mikrotubuli verantwortlich. Zellen haben offensichtlich robuste Mittel etabliert, um die Kinesin-vermittelten Transportprozesse zu regulieren, angefangen beim Kinesin-Motor. Wenn sie nicht an ihre Ladung gebunden sind, werden praktisch alle Kinesine "abgeschaltet", d.h. sie haben die Fähigkeit, ihre ATPase-Aktivität selbst zu hemmen. Durch die Bindung an Ladung soll der Kinesin-Motor für den gerichteten Transport auf dem Mikrotubuli-Netzwerk aktiviert werden. Wie Zellen entscheiden, wo und wann sie einen Motor aktivieren und deaktivieren, ist daher eine zentrale Frage des intrazellulären Transports. Dennoch ist sehr wenig über die Mechanismen bekannt, die die Spezifität der Fracht bestimmen und wie der Motor zur richtigen Zeit und am richtigen Ort aktiviert und deaktiviert wird.

Um Antworten auf die oben genannten Fragen zu geben, konzentriert sich diese Arbeit auf die Kinesin-2-Motoren, die sowohl im Zilium als auch im Zytoplasma zu finden sind. Die Kinesin-2-Unterfamilie ist insofern einzigartig, als sie neben den prototypischen homodimeren Kinesinen auch heterotrimere Motoren umfasst. Im Zilium ist Kinesin-2 am intraflagellären Transport beteiligt, und sein Fehlen stört die Ciliogenese von Einzellern zu Säugetieren vollständig. Daher wurde den Wirkungsmechanismen der Kinesin-2-Motoren viel Aufmerksamkeit geschenkt. Wie bei anderen Kinesinen auch, sind die hetero- und homodimeren Kinesin-2-Motoren autoinhibiert, und es wird angenommen, dass ihre Bindung an Fracht die entsprechenden Motoren aktiviert. Aufbauend auf diesem nahezu universellen Regulationsmechanismus beschreibe ich in bisher nie dagewesener Ausführlichkeit, wie ein homodimerer Kinesin-2-Motor durch seine Ladung/seinen Adapter aktiviert wird. Darüber hinaus stelle ich die These auf, dass die Bindung an Ladung/Adapter nicht notwendigerweise den Aktivierungsschritt eines auto-inhibierten Kinesin-Motors darstellt. Aus den in dieser Arbeit vorgestellten Daten schlage ich vor, dass eine Zelle einfach dedizierte Schalter einsetzt, um einen Motor zu aktivieren oder auto-inhibiert zu halten. Insbesondere wurden diese Ein- und Ausschalter konserviert, was darauf hindeutet, dass die Zellen die Motoren für verschiedene Transportprozesse wiederverwenden könnten, indem sie einfach auf bestimmte Schalter zugeschnitten werden.

Anhand des heterotrimeren Kinesin-2 zeige ich, dass die Eigenschaften von Kinesin-2-Motoren entsprechend ihrer primären Aufgabe im Cilium abgestimmt sind. Die analogen heterotrimeren Motoren verschiedener Spezies haben ihre Autoregulations- und Strukturdomänen-Eigenschaften deutlich an die unterschiedlichen Bedürfnisse innerhalb des jeweiligen Ziliums angepasst. Insgesamt bietet diese Arbeit direkte Einblicke in den Mechanismus der Kinesin-2-Entwicklung zur Trennung der Domänen innerhalb des Zellkörpers und präsentiert eine systematische Dissektion zur Entlarvung der einzigartigen Eigenschaften der Kinesin-2-Motoren.

Table of Contents

1. Introduction

1.1. Cytoskeletal motors are essential for primary cellular functions

Life exists in diverse forms, from unicellular to complex multicellular organisms ranging up to mammals. Cell, often being dubbed as the basic unit of life, exhibits a higher order of sophistication in structure and biological functions within itself [1]. This independent unit is differentiated into distinct systems based on the role they play on the ensemble level and also have to maneuver their tasks depending on the environment they exist. Despite the nonlinear interplay between wide varieties of constituents within cells, they have been able to preserve a higher degree of spatial assembly in a stationary state far from equilibrium.

In such an intricate organization, most cellular assignments are handled by molecular machines called molecular motors. They are protein complexes that convert the chemical energy in fuels (ATP, GTP) or electrical energy into mechanical work to perform their designated tasks [2, 3]. These machines range from DNA and RNA polymerases that drive the replication of the nucleotide strands to transmembrane pumps involved in the transit of ions and small molecules across the plasma membrane. These machines collectively take over the principal roles in cell division and cell maintenance, including the distribution of vesicles, organelles, and other cargo molecules in the cytoplasm [4, 5].

One of the cellular system's basic needs is the potent transportation of substances from one domain of the cell to another in a specific and controlled manner. Cytoskeletal motors are a class of molecular motors specialized for the efficient and definitive conveyance of various cargoes across the cytoplasm, and they utilize the cytoskeleton network for this purpose [6, 7]. Typically eukaryotic cells consist of actin and microtubule filament networks, and the numerous cytoskeletal motors are classified based on the network they resort to transport. Myosin, kinesin, and dynein are the primary cytoskeletal motors employed by the cell. Myosin is actin-based, while kinesin and dynein use microtubule track for movement. These motors sense the filament's polarity and move unidirectionally either to the plus or minus end of the filaments. Most of the myosin family members, like myosin II, which generates force for muscle contraction or the myosin V involved in the transport of organelles like melanosomes are plus-end directed motors

with few exceptions like myosin VI which is a minus-end directed motor protein [8]. Kinesin is the plus-end directed motor in microtubule track while dynein is the minus directed motor. These microtubule-based motors are usually hired for long-range transport. The role of kinesin ranges from transporting smaller vesicles to supramolecular structures like chromosomes and also in the regulation of microtubule dynamics [9, 10]. Cytoplasmic dynein facilitates the positioning of the mitotic spindle and various organelles in the designated regions within the cell, in addition to the transportation of cargoes crucial for cellular function [11-13]. In the structural and working mode, myosin and kinesin are more comparable to each other; they both contain a smaller catalytic domain that can attach to the filament track and consume fuel ATP to move in a hand over hand mechanism across the cytoskeletal filaments [14-17]. Dynein fashions a more massive structure and use separate domains for ATP binding and filament attachment [11]; but all of the cytoskeletal motors consume only one ATP for each directed step. The deployment of these motors is tightly regulated by robust mechanisms to ensure, they ferry the transport process at the right time to the designated compartment, and they transport only the target cargo from the pool of diverse molecules in the cytoplasm.

1.2. Kinesin superfamily

Ron Vale and his colleagues discovered kinesin in the mid-1980s in the long-range ATP dependent transport of organelles in the neuronal axons [2, 3]. Since the initial discovery of kinesin-1, also known as conventional kinesin, many new genes were found that have been highly conserved to the motor protein, grossing as much as ~45 genes in mammals [9, 18]. All the numerous proteins developed through evolution from these genes and also their isoforms formed from gene duplication and mRNA splicing techniques comprise to form the Kinesin superfamily (KIF). Turning to the domain organization of KIF proteins, each motor subunit comprises three significant elements, the catalytic core, the stalk, and the C-terminal tail domain (Figure 1.1) [15]. The catalytic core domain enables microtubule attachment and force generation for walking across the filament; the stalk domain aids in the dimerization of two polypeptide chains in the motor complex for facilitating processive movement and the tail domain in cargo binding [9]. The dimerization of two such identical or distinct polypeptide chains forms the homodimeric and heterodimeric kinesins.

Kinesins can also be differentiated based on the position of the catalytic head in the amino acid sequence, where motor protein with catalytic domain in the amino-terminal is termed as N-kinesin, middle domain as M-kinesin, and in the carboxyl-terminal as C-kinesins. N-kinesins like Kinesin-1 form the typical microtubule plus end moving motors, C-kinesins are exceptions where they climb towards the minus end of microtubules, and M-kinesins are used to depolymerize microtubules. The *Drosophila* motor Ncd from kinesin-14 family, and Chinese hamster protein MCAK from kinesin-13 family are well-studied examples for C-kinesin and M-kinesins [19].

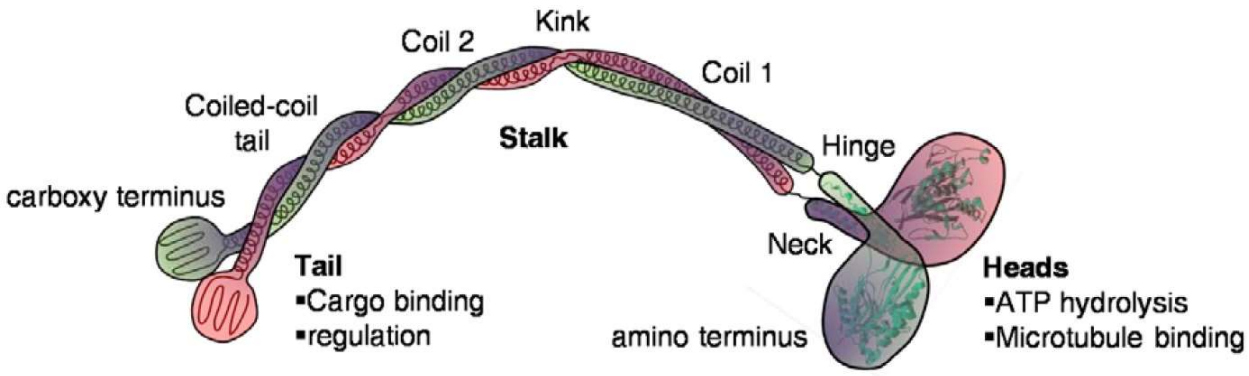

Figure 1.1: Domain organization of conventional kinesin from the kinesin superfamily. The conventional kinesin is constructed from two identical polypeptide heavy chains dimerized together. The domains in the motor can be categorized into the catalytic head domain required for ATP hydrolysis and microtubule attachment; the stalk domain made of coiled-coil structures that enable the efficient and specific dimerization of the polypeptide chains; and the C-terminal tail domain which functions in selective cargo binding and regulatory roles in the motor. The catalytic head domain exploits the chemical energy from ATP hydrolysis to make processive steps on microtubule filaments and the tail domain under the aid from the kink region's flexibility in the stalk domain, regulates such motility to be used only upon cargo attachment. (Adapted from Woehlke and Schliwa, 2000)[15]

Force generation

Molecular motors are practically enzymes that translate chemical energy into mechanical work. Here the active site of the enzyme is located in the catalytic head domain. Kinesin's catalytic core is comparatively smaller to myosins and dyneins, made out of about 350 amino acids, and it consists of a P loop catalytic site (GxxxxGKT/S), which hydrolysis ATP [20]. The domain consumes one ATP to take every 8nm steps (typically) on the microtubules [21]. The chemomechanical cycle in kinesins consists of four biochemical steps; ADP release, ATP binding, ATP hydrolysis, and

inorganic phosphate release [22]. In Kinesin-1, the neck linker (a subdomain in the C-terminal region of the head domain) and cover strand (structural element from the N-terminal region of the catalytic core domain) switches between a free and docked state to the catalytic domain accordingly with the ATPase cycle to introduce conformational changes, which ultimately leads to the forward movement of the motor [23-25].

Processivity and directionality

The ATPase cycle is also regulated by the intramolecular communication between the two catalytic head domains in the motor. This gating mechanism enables the motor to assign one head to remain attached to the microtubule filament at any point in the cycle [26]. Head-to-head coordination also keeps the ATPase cycle of each catalytic domain out of phase, so that the motor can take multiple steps without getting detached from the filament tack. This mechanism enables kinesin motors to take ten to thousands of steps once it gets attached to the filament. This property is known as processivity [22, 27]. The motors must also know where to move in addition to the ability to travel long-distance. Although all kinesin catalytic domain possesses an inherent plus-end direction inclination, the robust movement towards the plus end of microtubules is presented by the corresponding neck and neck linker region [28, 29]. In Ncd, the minus end driving kinesin-14, the neck region is distorted to force the heads domains to stay in a 180° geometry, rather than the 120° asymmetric conformation found in the conventional kinesin [30-32]. Even though the mechanism introducing directionality, to kinesin is unclear, the neck linker region's role remains evident.

Regulation in movement

Autoregulation mechanisms are established to avoid futile ATP hydrolysis and overcrowding of the molecular motors on the microtubule filament. An autoinhibition mechanism inherently restrains the motors unless required for the transport process, improving the kinesin transport efficiency. In the multiple kinesins studied so far, distinct autoinhibition mechanisms have been identified [33-38]. In kinesin-1, direct interaction of the C-terminal tail domain with the catalytic head domain switches off the ATPase activity, while in Kinesin-13 (KIF1), the coiled-coil 1 domain from the stalk region mediates the autoinhibition [34, 39]. The autoinhibition in these motors are relieved by diverse mechanisms such as

Interaction with cargo-adaptor complexes: Kinesin motors are modeled to transport vesicles and other cargoes to destined locations in the cells [19]. So efficient binding with the cargo molecules relieves the motor from its inactivated state. Sometimes, single molecular motors are directed to transport diverse molecules across the cytoplasm. In such cases, specific adaptor proteins or a cascade of adaptor proteins are programmed to effectively activate the motor and also identify a range of cargo molecules [19, 40]. A vast majority of kinesins like KIF5, KIF13A, and KIF-17 adopts this technique for activation. The adaptor proteins can also be further tuned by additional regulation mechanisms like calcium ion signaling [41].

Phosphorylation: The phosphorylation state of kinesin can guide the motor for its binding to cargo molecules and in certain cases also its attachment to microtubule filaments [19]. For instance, Protein Kinase A can regulate KIF5-KLC complexes on its binding to synaptic vesicles, while c-Jun N-terminal kinase (JNK) can regulate the attachment of KIF5 to microtubules [42-44].

Rab GTPase: Various members of the Rab GTPase family can interact with organelles and kinesin motors in a GTP-GDP dependent rule. In the activated GTP form, Rab GTPases can bind to the specific organelles and Rab effector proteins, for its transit across the cytoplasm, and once it reaches the terminal, the Rabs are converted to their GDP form, eventually releasing the organelles. Intra- Golgi transport is a classic example of Rab mediated transport by KIF20A motor protein [45].

Roles in intracellular transport

Kinesin performs a broad array of functions critical for cellular function and morphogenesis. It drives chemical transmitter receptors like AMPA (α-amino-3-hydroxy-5-methyl-4-isoxazole) in the dendrites to membrane organelles, vesicles and synaptic proteins in the axons in neurons [7]. These different transport processes implement the elongation of neurites and polarization of neurons. Also, distinct kinesins have been observed to be crucial for specific functions, like the role of KIF-17 and KIF5 motors in higher brain function; KIF1A, KIF5A, and KIF21A in neuropathies and KIF3 in the building of cilia. In conventional cytoplasmic transport, the lysosomes, endosomes, Golgi apparatus, and other organelles are commuted across the cytoplasm by kinesins [19].

1.3. Kinesn-2 family

kinesin-2 are plus-end directed microtubule motors that have been evolved along with the ciliary compartment for anterograde transport [46]. The motor is specialized for the ciliary organelle in unicellular and smaller order multicellular organisms like *C.elegans* (worm). However, in the higher-order mammals, kinesin-2 emerged to also function as an efficient cytoplasmic transporter. Dispersion of melanosomes from the central domain to the peripheral part in pigment cells; transportation of NMDA receptors, and polarity complex vesicles in neurons; and the conveyance of ribonucleoproteins in *Xenopus* eggs are some of the newly acquired roles by kinesin-2 motors [46].

The motors in the kinesin-2 family can exist as homodimers or as heterodimers with an accessory KAP (kinesin associated protein) subunit. The heterodimer motors are also termed as kinesin-II. The distinct polypeptide chains in the kinesin-II motors have opposing charge residues in their stalk domain to facilitate efficient dimerization. The accessory KAP subunit is proposed to stabilize the C-terminal region of the motor subunits and to establish interaction with the cargo molecules or adaptor proteins for intracellular transport [47-50]. However few exceptions also exist, like the cytoplasmic protein RNF33, which can attach to kinesin-2 motor KIF3A/3B in the absence of KAP3 [51]. The homodimeric motors are significantly faster and comparable to conventional kinesin than the heterodimeric motors. An autoinhibition mechanism regulates Kinesin-2 motors, and the direct attachment of appropriate adaptor protein or cargo molecules is thought to relieve this autoinhibition [52]. Nevertheless, much remains to be learned regarding how the adaptor proteins recruit kinesin-2 for active transport, and it is intriguing how these motors have transformed themselves from a ciliary motor to a cytoplasmic motor.

1.4. Intraflagellar transport (IFT) as a model for studying kinesin-2 mediated transport

The structural components of the primary cilia organelle in eukaryotes cannot be built in the cytoplasm. They must be assembled at the periphery of the cell, emerging from a structural element (a modified form of centriole) called the basal body. Intraflagellar transport is a specialized transport designed to build and maintain primary cilia (Figure 1.2) [53-57]. The

mechanism has been highly conserved from unicellular organisms like *C.reinhardtii* to mammals. Kinesin-2 and cytoplasmic dynein motor proteins implement IFT in sensory cilia. Removal of kinesin-2 from IFT at any time point suspends the transport, eventually leading to the loss of cilia making the motors vital for the transport process [55].

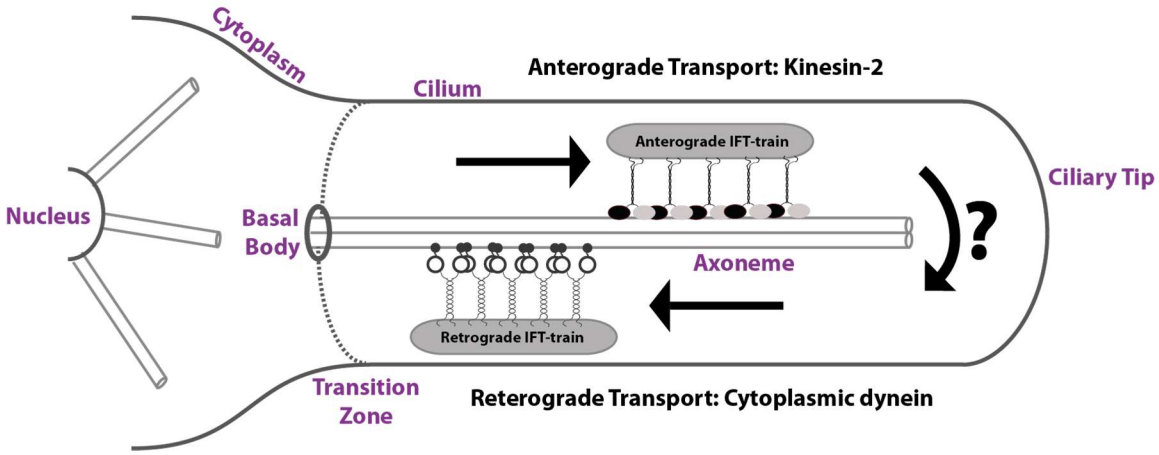

Figure 1.2: Intraflagellar transport process in cilia. The primary cilium is a sensory organelle that is differentiated from the cytoplasm through a lipid gated structure called the transition zone. The cilium consists of a central axoneme emanating from a modified centriolar structure called the basal body. The complex and dynamic structure is built and maintained by a unique bidirectional transport process called Intraflagellar transport. The cilium precursors required for erecting and preserving the cilia are assembled into large adaptor complexes to form supramolecular structures termed as IFT-trains and are carried from the ciliary base to the tip by a group of Kinesin-2 motors. After delivering the necessary components, the anterograde IFT-trains are disassembled and remodeled at the ciliary tip in an enigmatic process, and new retrograde IFT-trains are assembled to be transported back to the base by cytoplasmic dynein motors. The kinesin-2 and dynein motors are inactive and part of the IFT-trains when they are not involved in active transport. The frequency of the IFT-trains is controlled based on the developmental stage of the cilium.

Ciliary structure

Cilia or flagella (used reciprocally) are hair-like structures radiating from the surface of the cell body, several micrometers long. The ciliary membrane is continuous with the plasma membrane, and it encompasses a central axoneme structure nucleating from the basal body. The axoneme consists of '9 + 2' doublet microtubule structure in motile cilia and '9 + 0' arrangement in non-motile primary cilia. The tubules are named as A and B tubules in the doublet structure [58]. The ciliary organelle is separated from the cytoplasm by a gateway at the base called the transition

zone, which controls the entry and exit of proteins into the ciliary compartment (Figure 1.2). The ciliary tip serves as an antenna for signaling pathways and has significant roles in ciliary assembly and disassembly [59].

Intraflagellar transport

Cilium is built at the tip rather than at the base of the structure. So the components necessary for erecting the structure like tubulin and other axonemal proteins, must be transported from the base to the ciliary tip. IFT employs large complexes made from more than 20 protein subunits to assemble supramolecular structures called IFT-trains (Figure 1.2) [60]. The primary protein subcomplexes in the IFT trains are called IFT-A, IFT-B, and BBSome, and these complexes are stacked in multiple numbers to form these trains. Manifold kinesin-2 motors together ferry these trains to the tip in anterograde transport. A structural rearrangement occurs at the tip of the cilia, including the delivery of cargo molecules, and new smaller trains are formed at the apex to be brought back to the base by dynein 1-b motors. During anterograde transport, dynein-1b motors are transported in an autoinhibited form, positioning them away from the microtubules to avoid a tug of war situation with the kinesin-2 motors [55, 61]. Similarly, kinesin-2 motors are also thought to be inactivated in retrograde transport. The anterograde and retrograde trains have been programmed to travel separately on B- and A-tubules to avoid collisions in *C.reinhardtii* flagella [62].

Physiological relevance of IFT

Primary cilia facilitate various signaling pathways such as G protein-coupled receptors, receptor tyrosine kinases, Hedgehog, Wnt, and transforming growth factor-β pathways by transmitting signals from the cell body to extracellular space and vice versa to regulate cell and developmental processes [59]. Defect in IFT can lead to a wide range of diseases, commonly known as ciliopathies [6, 59, 63-65]. Mutating the subunit IFT88, also known as Tg737 from the IFT trains in mouse and human proved lethal to the formation of cilia and caused conditions like polycystic kidney disease, retinal degeneration, defect in left-right axis determination, and various human disease syndromes [66-68].

Why IFT is an ideal model for studying kinesin-2 mediated transport?

- The transport occurs in a closed compartment in uni-direction, providing a simple model with limited players to dissect the transport.
- The specialized transport offers intriguing features like the reversal of roles of kinesin-2 from an active transporter to passenger in the anterograde and retrograde transport.
- The strong evolutionary conservation in the IFT system from the unicellular organisms to humans allows us to compare and study the kinesin-2 based transport process from one species to another.

1.5. Kinesin-2 motors in intraflagellar transport

Since the discovery of IFT by the Rosenbaum lab in 1993 [69], various models have been studied to dissect and explain the intriguing features of this peculiar bidirectional transport [55]. Among them, research is extensively conducted on the unicellular green algae *Chlamydomonas reinhardtii*, multicellular worm *Caenorhabditis elegans*, and mammalian mouse to investigate IFT [69-72]. Despite IFT being highly conserved, there are radical changes in how kinesin-2 motors are distributed and functioned inside the cilia. The analysis of kinesin-2 deployment in these organisms also exhibits how the motors have equipped themselves to perform additional roles in the cytoplasm than IFT through evolution [46].

Chlamydomonas reinhardtii

FLA8/10/KAP

The flagella of *C.reinhardtii* is built and sustained by heterotrimeric kinesin-2 motor FLA8/10/KAP (Figure 1.4 top panel) [73-75]. In the anterograde traffic, an average of ten kinesin-2 motors move 300nm long IFT trains at a velocity of ~2000 nm/s from the ciliary base to the tip [38, 73]. The kinesin-2 motor's area of activity is restricted to the flagellar compartment in the organism, and the absence of the motor leads to the complete loss of organelle. In temperature-sensitive *fla10* mutant, the switch from permissive to restrictive temperature led to the shortening and gradual loss of flagella [75]. The formation of new flagella or regeneration after deflagellation was not possible in the restricted temperature. KAP subunit is an essential component of the motor that relieves the native FLA8/10 motor from its autoinhibited state to the active form and serves as

an adaptor between the kinesin-2 motor and the cargo complex [38]. It is also responsible for directing kinesin-II motors from the nucleus to the flagellar assembly site near the basal body [74].

The FLA8/10/KAP motor docks to the IFT-B subcomplex during the anterograde IFT, and this interaction is regulated by a calcium-dependent kinase. CrCDPK1 phosphorylates FLA8 in the conserved S663 residue to inactivate the motor and disrupt its interaction with the IFT-B complex. Breaking from the IFT-B complex assist kinesin-2 in unloading the IFT cargo in the ciliary tip [76]. Interestingly in *C.reinhardtii* flagella, FLA8/10/KAP motors diffuse back to the base once it delivers its cargo at the tip instead of being conveyed back by the dynein motors (Figure 1.4 top panel) [77]. As the length of the flagella increases, the motors take more time to return to the ground of the anterograde train assembly. *C.reinhardtii* utilizes this feedback mechanism to control the length of the flagellum [78].

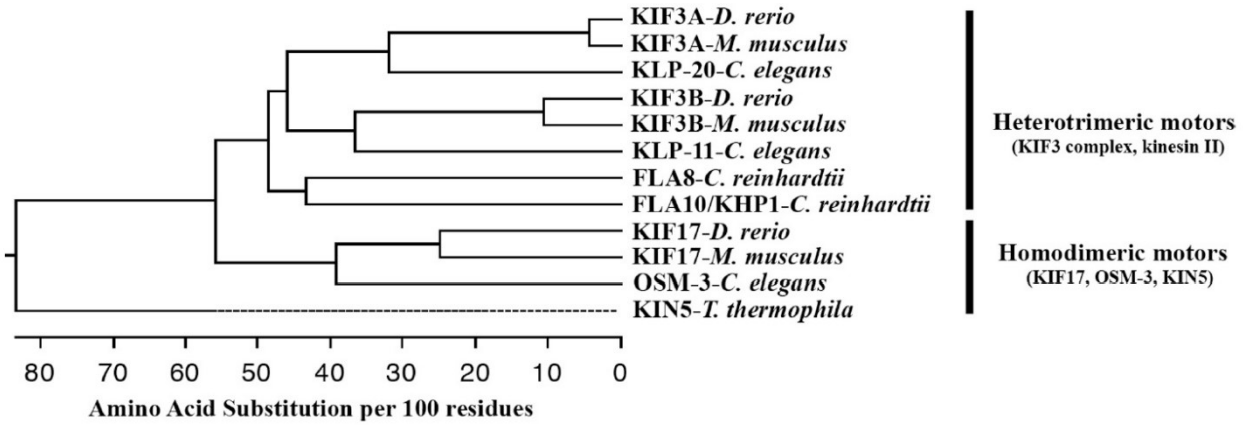

Figure 1.3: Phylogenetic tree of the Kinesin-2 family. The heterotrimeric and homodimeric kinesin-2 members of the kinesin-2 family have evolved separately, initially, as seen in the first branching of the phylogenetic tree. The distinct polypeptide chains in the Kinesin-II proteins have then diversified further in the next steps; however, the FLA8 and FLA10 subunits from *C.reinhardtii* have evolved independently from the other subunits of kinesin-II motor subunits. (Adapted from Wong-Riley and Besharse, 2012) [79]

FLA8/10/KAP boasts an unnaturally high speed compared to the heterotrimeric motors in *Drosophila*, mouse, and *C.elegans*. The phylogenetic analysis predicts FLA8 and FLA10 share more homogeneity between each other than to the subunits from other heterodimeric motors and are proposed to be developed from a separate gene duplication during evolution [80] (Figure 1.3).

However, independent *in vitro* studies are yet missing to verify whether this atypical high speed comes from individual motors or through the coordination from multiple motors.

Caenorhabditis elegans

In *C.elegans*, a significant number (60) of the neurons express non-motile sensory cilium at their dendritic ends [81]. Primary cilia in the worm are classified into amphid and phasmid cilia based on their localization in the body's anterior and posterior region. An additional homodimeric OSM-3 cooperates along with the heterotrimeric KLP11/20/KAP1 motor to build these sensory cilia in neurons (Figure 1.4 middle panel) [82, 83]. KLP11/20/KAP1 does processive IFT at 500nm/s, while OSM-3 is comparatively faster and deliver cargoes in speed ranging from 1300-1700nm/s [52, 83-85]. The heterodimeric and homodimeric motors can exert stall forces of 5 and 6 pN, respectively, when measured *in vitro* [37, 47]. Like in *C.reinhardtii*, the kinesin-2 motors are active only inside the ciliary compartment [82].

KLP11/20/KAP1

In *C.elegans*, the axoneme exhibits a bipartite structure. The nine doublet microtubule architecture of the axoneme is extended only till the middle portion of the cilium, termed the middle segment, from which nine singlet microtubules proceed towards the distal end of the cilium [81]. The heterotrimeric KLP11/20/KAP1 motor specializes in transporting IFT-trains from the cytoplasm through the transition zone into the ciliary compartment [85]. These transition zones are roadblocks that prevent the entry of other proteins into the cilia. OSM-3 gradually replaces the KLP11/20/KAP1 motors once the IFT complexes enter the cilia by employing a conserved MAP kinase DYF-5 [86]. Its activity undocks the kinesin II from the IFT-trains and allows OSM-3 to take over the transport. By the time IFT trains reach the middle segment, all the heterotrimeric motors are replaced from the anterograde trains, and they are transported back to the base by the retrograde trains as passengers. Thereby the localization of the kinesin II is more concentrated at the base and transition zone of the cilium [82]. In *C.elegans*, the removal of KAP1 leads to the functional loss of the KLP11/20 motors. In *kap1* mutants, OSM-3 was able to reconstruct full-length cilia but faced difficultly in crossing the transition zone [85, 87]. During anterograde IFT, KLP11/20/KAP1 docks to the IFT-trains through the IFT-A subcomplex,

contrasting to the heterotrimeric FLA8/10/KAP, which binds through the IFT-B complex in *C.reinhardtii* [76, 84].

Significant studies have also been done to dissect the KLP11/20 motor *in vitro* [47, 88-91]. The findings include; heteromerization of KLP11/20 relies on the two heptad repeats at the C-terminal end of the stalk domain, which function as a nucleation source for heterodimerization. The heterodimerization of the distinct motor subunits facilitates KAP1 binding to the motor. The wild type heteromeric kinesin-II exists in a convoluted autoinhibited state that is made active through cargo binding. In KLP11/20, the tail domain of KLP11 interacts with the catalytic head domain to inhibit ATPase activity. The exact positioning of the KLP11 head domain in the motor is essential for autoinhibition as the swapped head chimera where the KLP11 head domain is replaced with the KLP20 and vice versa have shown to relieve autoinhibition [47]. The autoinhibition can also be resolved by introducing point mutations in the 'kink region' of the KLP11/20 to form an extended coiled-coil conformation in the stalk domain.

OSM-3

OSM-3 performs the significant portion of the long-range anterograde transport in cilia and is solely responsible for building cilia's distal segment [55, 85]. It is also capable of building the full length of the cilium in the absence of KLP11/20/KAP1 motor. However, in the absence of OSM-3, the heterotrimeric motor can only build the middle segment of the cilium. The double mutant of homodimeric and heterotrimeric motor results in the complete loss of axoneme/cilium [87]. The speed of OSM-3 inside the ciliary compartment has been an intriguing feature. In IFT, along with KLP11/20/KAP1, the IFT-trains speed gradually increases to 1100-1300nm/s once it reaches the distal segment, but studies with the heterotrimeric mutant show that OSM-3 can speed up to more than 1500nm/sec inside the cilia [84, 85].

OSM-3 docks to the DYF-1 subunit in the IFT-B subcomplex during anterograde IFT [52, 84]. The motor turns around at the distal end, at the end of anterograde IFT. Nevertheless, information on how the motor gets detached during the remodeling process in the ciliary tip and how it is brought back inactivated in retrograde transport is still missing.

The homodimeric motor is autoinhibited *in vitro* and is suggested to exist in a folded conformation where the tail domain interacts with the head domain [37, 52]. The autoinhibition can be relieved by introducing point mutations in the helix breaker region of the stalk domain or deleting the area to avoid the folding back of the coiled-coil region. However, the activated point mutant OSM-3 G444E motor was severely impaired in delivering processive IFT *in vivo*, illustrating the importance of regulation in motors for IFT [92]. *In vitro* studies suggest OSM-3 displays two activation states, a basal activation state when it attaches to DYF-1 alone and an allosterically activated state provided by the additional presence of DYF-6, OSM-5, and OSM-6 subunits represented by differing velocities at ~1300 and ~1700nm/s [52]. It remains unclear if the allosterically activated state represents the motor's full activation or whether it can be activated further.

Mouse (*Mus musculus*)

Nearly all mammalian cells sport a single nonmotile primary cilium for sensory functions [93]. Mouse also exploits the heteromeric kinesin II KIF3A/3B/KAP3 and homodimeric KIF-17 for various objectives surrounding its primary cilium. Unlike *C.reinhardtii* and *C.elegans*, the kinesin-2 motors in mouse are also deployed outside the cilium for various objectives [46].

KIF3A/3B/KAP3

Like *C.elegans* kinesin II, KIF3A/3B/KAP3 also displays a slower velocity of ~400nm/s during IFT. It is the sole active anterograde transporter of IFT-trains inside the cilium, and cilium biogenesis is entirely dependent on this motor (Figure 1.4 lower panel) [55, 94]. Deleting the motor from the cilium results in the reduction and inevitable loss of cilia. The homodimeric KIF-17 in mouse cannot rescue ciliogenesis like in *C.elegans* in the absence of kinesin II motor [94]. The kinesin-II motor is also employed outside the cilium in various roles, from positioning cellular organelles to steering intercompartmental transport. For example, in neurons, KIF3A/3B/KAP3 ferry fodrin associated vesicles along the axon [46].

KIF-17

KIF-17 exhibits a velocity of 800-1200nm/s during intracellular trafficking [79]. The role of KIF-17 inside the cilium is contrasting from all the kinesin motors mentioned so far. KIF-17 is present

inside the cilium but does not participate as an active transporter of IFT-trains during anterograde IFT (Figure 1.4 lower panel). *In vivo* studies on KIF-17 explicitly demonstrated that the motor is dispensable for ciliogenesis [95]. As aforementioned, in the absence of KIF3A/3B/KAP3, KIF-17 cannot build or maintain cilia, unlike the homodimeric OSM-3 from *C.elegans*. The most intriguing feature is that KIF-17 can enter the cilium, even in the absence of its catalytic head domain [96]. The motor protein utilizes the conserved amino acid sequence immediately upstream of its nuclear localization signal to interact with the IFT-trains to enter the cilium [95]. A Ran GTPase, together with nuclear import protein importin-β2, also displays a regulatory role in the entry of KIF-17 into the cilia [97]. The Ran GTPase separates the motor/importin complex once it traverses the ciliary barrier and frees KIF-17 to carry its functional roles inside the cilium. Delivery of cyclic nucleotide-gated channels (CNGs) to the ciliary membrane of olfactory sensory neurons by functioning as an adaptor protein is one of the known functions of KIF-17 inside sensory cilia [98].

Similar to the heterotrimeric motor, KIF-17 is also used exceptionally outside the cilium [79]. In neuronal dendrites, KIF-17 transport multiple cargoes like kainate receptors (GluR5), potassium Kv4.2 channels, and mRNA. The transport of the NMDA receptor subunits by KIF-17 in the brain is essential for higher cognitive functions, including learning and memory [79, 99]. KIF-17 is also an excellent example of how the motor recognize their cargoes utilizing adaptor proteins, as the adaptors LIN10, LIN2, and LIN7 help the motor to attach to its cargo, the NR2B receptor protein [46]. What has changed the KIF-17 motor to become a robust cytoplasmic trafficker than a ciliary transporter remains obscure.

The Verhey lab explored the autoinhibition mechanism in KIF-17. They propose that a dual molecular mechanism autoinhibits KIF-17 [33] in which; A) the C-terminal tail domain binds the catalytic head domain to prevent the latter's interaction with the microtubules, and b) a coiled-coil region in the stalk domain interacts with the catalytic domain to shut down motor motility.

Evolution of kinesin-2 deployment in model organisms

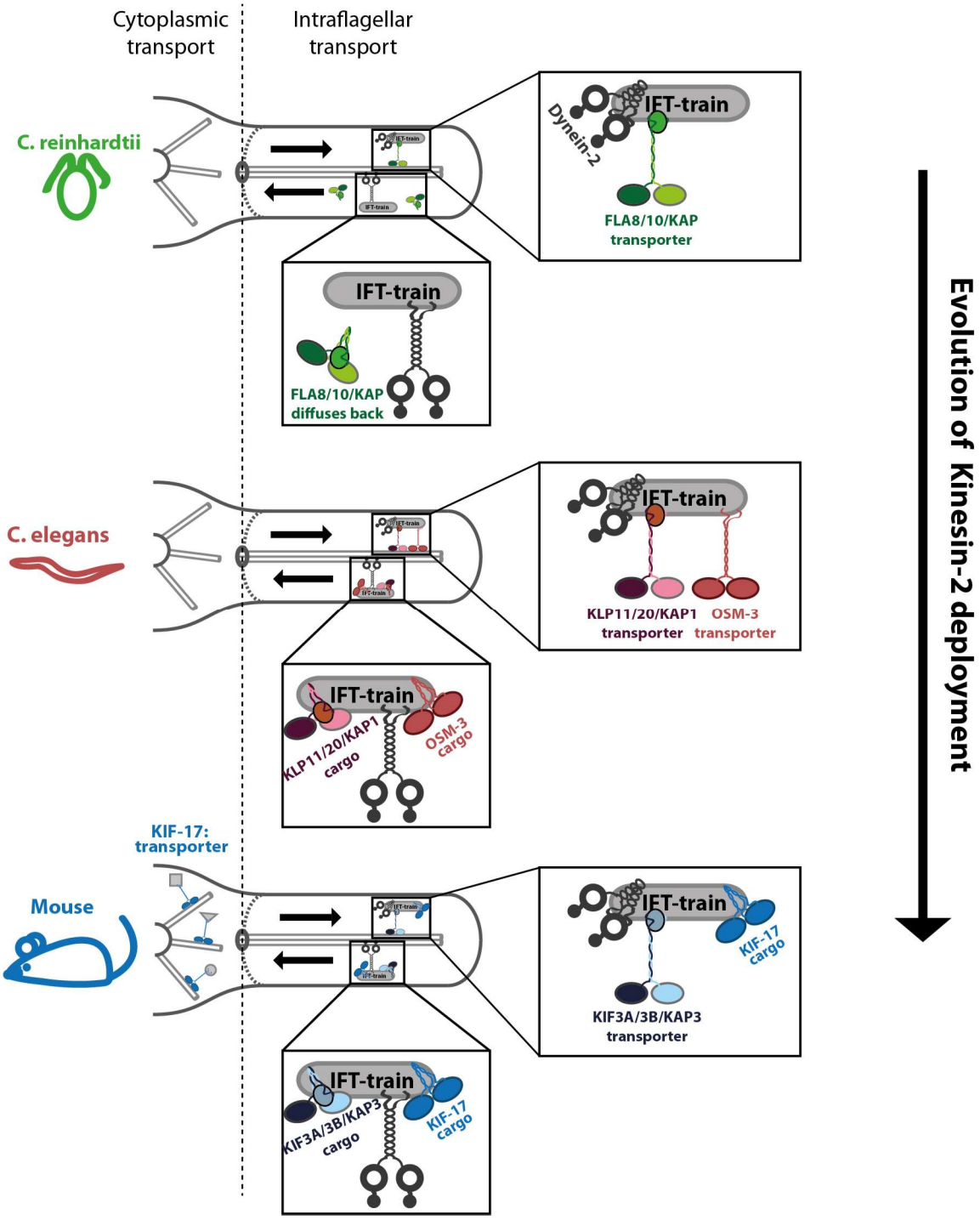

Figure 1.4: Distribution of kinesin-2 motors in *C.reinhardtii, C.elegans,* and mouse. The Kinesin-2 family has been specifically deployed for the transit of IFT-trains across the cilium. The kinesin-2 family consists of heterotrimeric and homodimeric motors, and they have been diversely employed in the cilium across the evolution. (**Top panel**) In unicellular *C.reinhardtii*, heterotrimeric FLA8/10/KAP is lonely expressed in

the organism, and it performs the anterograde transport in flagella. The motor diffuses back to the ciliary base once it disengages from the anterograde IFT-trains. (**Middle panel**) The heterotrimeric KLP11/20/KAP1 and homodimeric OSM-3 is rigorously employed for the efficient anterograde conveyance of IFT-trains in worm *C.elegans*. Unlike *C.reinhardtii*, both the motors are carried as cargo/passengers on its return in the retrograde transport. (**Lower panel**) The mouse sensory cilia also employ both heterotrimeric KIF3A/3B/KAP3 and homodimeric KIF-17 inside the cilia. However, only the Kinesin-II take part in processive IFT, while KIF-17 is ferried inactively during the IFT process. In mouse, KIF-17 transport numerous compounds in the cytoplasm, making it an efficient cytoplasmic transporter than a ciliary transporter.

The kinesin-2 family has been selectively employed from the large pool of kinesin motors for the transport processes inside the ciliary compartment. However, the deployment of the kinesin-2 motors, for constructing the organelle has varied extensively (Figure 1.4) [55]. In *C.reinhardtii*, heterotrimeric Kinesin-II is solely used for IFT. In the next steps of evolution, i.e., when it came to worm *C.elegans*, both heterotrimeric and homodimeric kinesin-2 participate in processive IFT. Finally, when we arrived in mammalian mouse, the homodimeric motor has lost its ability to function as an active transporter, and the efficient conveyance is conducted again by the heterotrimeric motor alone. It should be noted that in *C.reinhardtii* and *C.elegans*, kinesin-2 is adopted for processive transport only inside the ciliary compartment. Nevertheless, in mouse, both heteromeric and homodimeric motors are operated for multiple cytoplasmic transport processes too. It is conceivable that in the course of evolution, as organisms became more complex, cells required kinesin-2 to perform multiple tasks outside IFT, and the variation in the deployment of kinesin-2 inside cilia must be resulting from the new skills achieved.

1.6. IFT subcomplexes in intraflagellar transport

The core IFT-train is composed of multiple units of IFT subcomplexes IFT-A, IFT-B, and BBSome. In the numerous studies conducted so far, the IFT-B subcomplex has been predicted to navigate the Kinesin-2 mediated IFT [55]. In *C.elegans*, where the heteromeric and homodimeric motors are actively involved in processive IFT, they have distinct binding sites on the IFT-trains as Kinesin-II attaches to IFT-A while OSM-3 binds to IFT-B subcomplex. The BBSome functions in connecting the IFT-A and IFT-B subcomplex and as an adaptor complex, where axoneme precursors and other cargo molecules can stick to and travel during the anterograde and retrograde transport [84, 100]. The architecture of IFT-A and IFT-B complexes are well characterized in *C.reinhardtii* by

Lorentzen Lab, and recently much information is also produced on these complexes from mouse [53, 60, 101-103].

IFT-A complex.

The IFT-A subcomplex consists of six subunits: IFT144, 140, 122, 121, 139, and 43 (Table 1.1). Four of the six subunits, IFT 144, 140, 122, and 121, share common domain organizations; amino-terminal WD40 propellers and solenoid carboxy-terminal tail that is naturally found in membrane coat proteins from bioinformatic analysis, suggesting that these subunits might have evolved from an early protocoatomer protein [104]. IFT144, 140, and 122 subunits form a stable subcomplex within IFT-A, independent of the other subunits called the IFT-A core complex (Figure 1.5). The existence of the IFT-A core complex has been independently observed in human cell lines and *C.reinhardtii* [105, 106]. IFT121 can also interact with IFT139 and IFT43 to form a stable tripartite complex (Figure 1.5) [106]. Functional roles seem to be diverse for the core, and non-core subunits in the IFT-A complex as the IFT-A core can travel to the ciliary tip independent of its non-core proteins, but the non-core subunits are essential for its return back to the ciliary base [105, 107]. The IFT-A core also facilitates the entry of G-protein coupled receptors into the ciliary compartment by cooperating with the Tubby family protein TULP3 [105].

In *C.reinhardtii*, *C.elegans*, mouse*, T.thermophila and D.melanogaster*, mutations in IFT-A subunits results in a stumpy flagella phenotype that precipitates IFT-B proteins at the tip. Mutants that lack the IFT dynein motor or its accessory subunits also display a similar phenotype suggesting the IFT-A complex might be directly involved in the retrograde transport [108-114]. The BBSome complex is proposed to be the connecting link between the IFT-A and IFT-B complex. The *bbs-7/bb-8* mutant studies on *C.elegans* showed the two subcomplexes exhibiting two distinct velocities during anterograde IFT [84]. IFT-A moved at the speed of Kinesin-II while IFT-B with the speed of OSM-3. The BBSome complex's wreckage plus the tension caused by two motors of contrasting speed led to the splitting of IFT-A and IFT-B complexes. These results confirm that the kinesin-II motor specifically docks to the IFT-A complex for anterograde IFT in *C.elegans*. However, more detail is missing on the mechanism or subunit/ subcomplex within IFT-A, which is required for kinesin-II recruitment to IFT.

Table 1.1: Nomenclature of IFT subunits in model organisms. The subunits from *C.reinhardtii* and mammals are typically mentioned in their generic names in literature while the specified nomenclature is used in the case of *C.elegans*.

	General Name	***C.reinhardtii***	***C.elegans***	***Mammals***
IFT-A	IFT144	-	DYF-2	WDR19
	IFT140	-	CHE-11	WDTC2
	IFT122	FAP80	DAF-10	WDR10
	IFT139	-	ZK328.7a	THM1/TTC21B
	IFT121	-	IFTA-1	WDR35
	IFT43	-	C25H3.12	C14ORF179
IFT-B	IFT88	-	OSM-5	Polaris/Tg737
	IFT81	-	-	-
	IFT74	-	-	-
	IFT70	FAP259	DYF-1	TTC30A/B
	IFT56	DYF-13	DYF-13	TTC26
	IFT52	BLD1	OSM-6	NGD5
	IFT46	-	DYF-6	-
	IFT27	-	Absent	RabL4
	IFT25	FAP232	Absent	HSPB11
	IFT22	FAP9	IFTA-2	RabL5
	IFT172	-	OSM-1	SLB
	IFT80	-	CHE-2	WDR56
	IFT57	-	CHE-13	Hippi
	IFT54	FAP116	DYF-11	Traf3IP1/MIP-T3
	IFT38	FAP22	DYF-3	Claup1
	IFT20	-	-	-

IFT-B complex

The IFT-B complex comprises 16 subunits, which are classified to form two subcomplexes, the core complex, and peripheral complex. The core subunits are IFT88, 81, 74, 52, 46, 27, 70, 25, 22, 56 and peripheral subunits are IFT172, 80, 57, 20, 54 and 38 (Table 1.1, Figure 1.5) [60]. Yeast two-hybrid based interaction, as well as pull-down assays, displayed the interactome between these subunits. IFT27/25, IFT70/52, IFT70/46, IFT88/52/46, and IFT56/46 complexes can display direct interactions between themselves, but some complexes require a preformed assembly to form a stable complex such as the formation of tetramer IFT81/74/52/46 requires preformed IFT81/74 and IFT52/46 complexes. These subunits utilize hydrophobic surfaces well, to establish stable contacts between each other. Lorentzen and his colleagues were successful in building the

nonameric IFT-B core complex in *C.reinhardtii*, and this complex was highly stable with the hydrophobic interplay such that, it can resist >2 molar NaCl concentration (Figure 1.5) [101]. The six peripheral subunits can also form a stable complex *in vitro* in the absence of the core complex. IFT57/38 is the key to this complex, which can directly interact with IFT54/20, IFT80, and IFT172 [102].

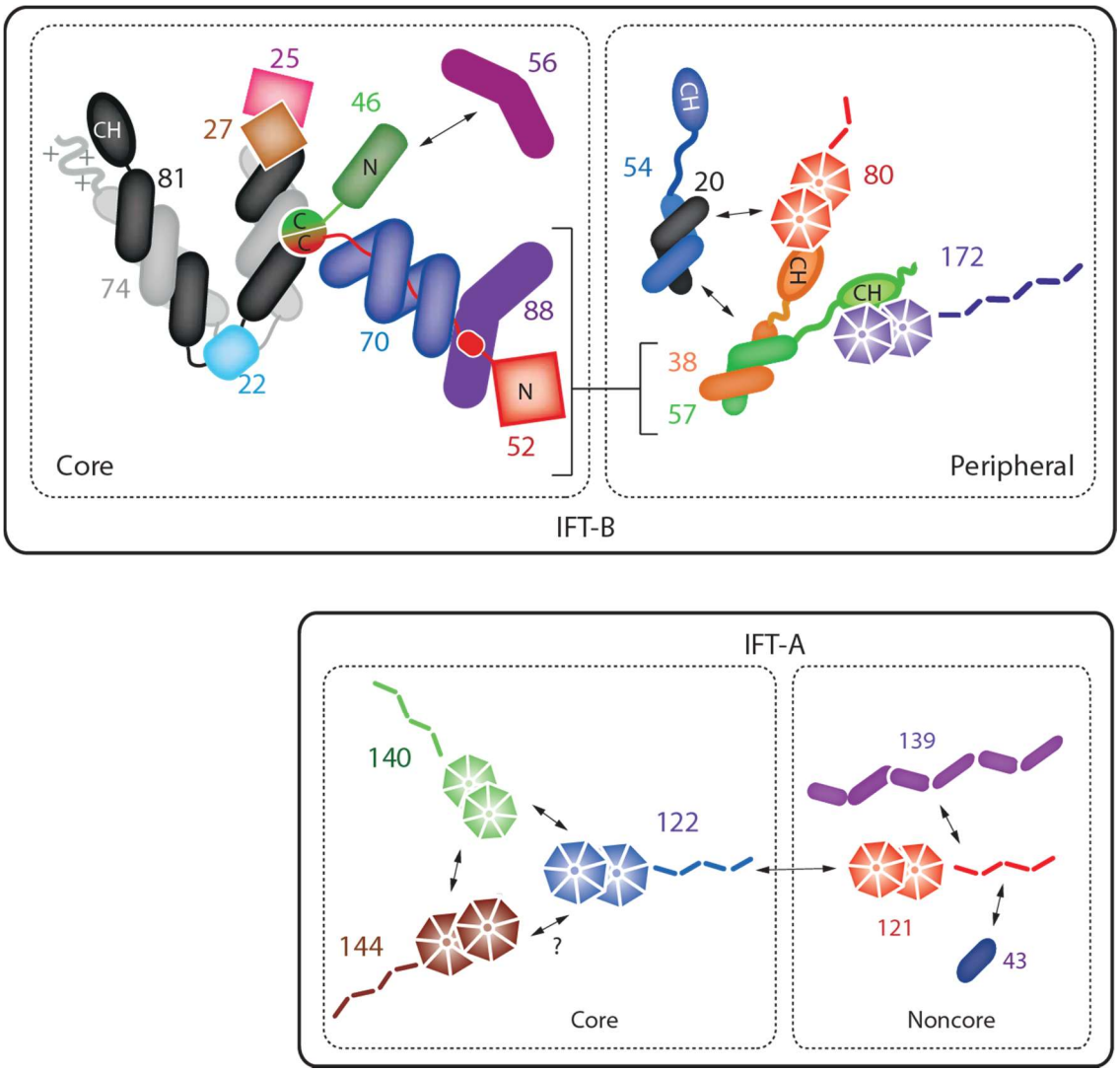

Figure 1.5: Interaction mapping of the IFT subunits in IFT-A and IFT-B subcomplexes from *C.reinhardtii*. The individual subunits in IFT interact with multiple subunits to form a complex array of compounds. These attachments lead to the formation of core, noncore, and peripheral complexes, finally leading to the creation of IFT-A and IFT-B subcomplexes. (Adapted from Taschner and Lorentzen, 2016) [60]

IFT-B complex is extremely crucial for the cilia as loss in single subunits within the complex can lead to the complete loss of cilium from the cells. Absence of the subunits IFT52, IFT70 and IFT88, which are central for the IFT-B core complex, can lead to the partial or complete loss of the organelle in all organisms studied so far [104]. Individual subunits or subcomplexes have also been found to perform specific functions inside the flagella [60]. Some of them are

- Outer and inner dynein arms in *C.reinhardtii* are associated with the subunits IFT46 and IFT56 correspondingly for their ciliary transport. In *C.elegans*, DYF-13, the homolog for IFT56, is required for the delivery of CHE-3 into the cilium.
- The subunits IFT27 and IFT25 operates in the transport of BBSome and also function in regulating the Hedgehog signaling pathway.
- The remodeling process at the ciliary tip is severely affected in the absence of IFT172.

1.7. IFT subcomplexes are responsible for recruiting kinesin-2 motors during IFT

As aforementioned, kinesin gets ready for processive movement by binding to its cargo complexes. The motor can directly interact with the cargo, or the coupling is mediated through adaptor proteins and other regulatory mechanisms such as phosphorylation and Rab GTPases [115]. Even though phosphorylation and other unknown factors may play a critical role in the attachment and detachment of kinesin-2 motors at specific junctions and time points in IFT, the binding to the IFT complexes (IFT-A/ IFT-B) is paramount for motors to take part in the transport. The kinesin must function as active transporter during anterograde transport and as an inactive cargo in the retrograde transport [55]. Hence distinct adaptors must also be employed for these diverse roles.

Much detail is missing regarding the interaction between IFT complexes and kinesin-2 motor. However, IFT-B mutant phenotypes show similarity with the kinesin-2 mutant phenotypes, i.e., general ciliary disassembly, leading to the speculation these motors might interact with IFT-B for anterograde transport [73, 116]. The mouse KIF3A/3B/KAP3 displayed a direct interaction with IFT20 in yeast two-hybrid assay, but this could not be repeated in an independent study [117, 118]. The only promising information available as of now in the motor recruitment is from the

C.elegans OSM-3 motor. OSM-3 directly docks to the IFT-train through the DYF-1(IFT70) subunit from the IFT-B complex [52, 84]. In *dyf-1* mutants, cilia fail to form the distal segment, and the kinesin-II motors transport the IFT-trains till the middle segment. In a recent independent *in vitro* study, the homodimeric motor was activated from its autoinhibited state by DYF-1. However, additional subunits DYF-6, OSM-5, and OSM-6 from the IFT-B core complex proved necessary to introduce an allosteric activation in the OSM-3 motor [52]. It is unknown how the coupling of DYF-1 with other subunits introduces this second activation.

Turning to structural studies for more details on the subunits, IFT70/52 (homolog of DYF-1/OSM-6) dimer in *C.reinhardtii* forms a compelling structural framework from these subunits. IFT70 maintains a tetratricopeptide repeat (TPR) superhelical structure to wrap around a conserved proline-rich sequence in IFT52 in the crystal structure of IFT70/52$^{330\text{-}370}$ complex (Figure 1.6) [101]. Six conserved tyrosine residues (Y55, 58, 59, 70, 83, 86) of IFT70 creates an aromatic field around the tetra-proline sequence (354-PPPP-358) of IFT52 through hydrophobic and CH/π contacts between them to form one of the main interaction junctions between these two subunits. The tight stacking of proline residues between the aromatic residues of IFT70 stabilizes the dimer structure.

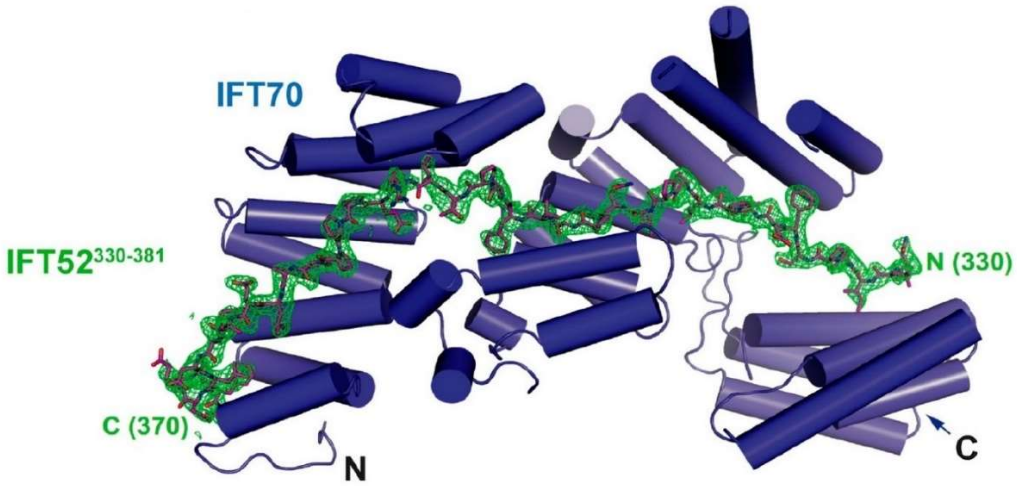

Figure 1.6: Crystal structure of IFT70/52$^{330\text{-}381}$ in *C.reinhardtii*. IFT70 forms a solenoid structure around a conserved proline-rich domain (330-370 amino acids) in IFT52. The α-helices in IFT70 are depicted as blue cylinders. IFT70 and IFT52 are highly conserved across species suggesting that the dimer structure might also remain conserved across various organisms. (Adapted from Taschner et.al, JCB 2014)[101]

Strikingly, for the mouse KIF-17, the IFT-B subunits IFT56/46 proved essential for its ciliary entry [95]. In *ift56* knock out cell lines, KIF-17 was unable to localize within the cilia. KIF-17 interacted with the IFT56/46 dimer through a short conserved C-terminal sequence. Notably, KIF-17 is not active inside the cilium and travels as a passenger during the whole IFT. Autoinhibited motors can get activated for robust movement after binding to non-specific beads in optical trapping bead assays [37]. Hence specific mechanisms must also be kept to keep the motor inactive after attaching to adaptor proteins. It would be fascinating if the interactions between IFT56/46 and KIF-17 can provide insights on how kinesin-2 motors can be kept inactive inside the cilium.

2. Aims of this thesis

1. Dissecting the recruitment of OSM-3, for anterograde transport in *C.elegans*

The homodimeric OSM-3 is the principal long-range anterograde transport motor in *C.elegans* cilia [85]. The motor uses the IFT-B subunit DYF-1 as a key for getting activated and for connecting to the anterograde trains for processive IFT [52, 84]. This mechanism has been validated *in vivo* and *in vitro* studies, making OSM-3 an ideal candidate for studying kinesin based transport. However, the allosteric activation observed in the motor, when coupled to the quadripartite complex DYF-1/OSM-5/OSM-6/DYF-6, indicates that the motor recruitment mechanism for anterograde transport is much more complicated. It is perplexing if OSM-3 had attained its complete activation state with the quadripartite complex, or can it display a higher velocity with the addition of more subunits. So the first objective would be to find the maximum velocity that could be displayed by OSM-3. It is highly probable that DYF-1 does not require all the three additional subunits for allosterically activating OSM-3, but less. Further, the tightly packed structure of IFT70/52 from *C.reinhardtii* lets out a curiosity whether the *C.elegans* homolog DYF-1/OSM-6, which might also follow a similar framework, has a direct role in the activation of the motor. Therefore the next steps should be in the direction of dissecting the quadripartite complex to uncover the minimum deterrent required for activating the OSM-3 motor. Finally, it is essential to understand the physiological relevance of such allosteric activation.

2. Retracing the evolution of kinesin-2 deployment from mouse to worm

During the evolution from worm to mice, the homodimeric motor has lost its ability to work as an active transporter inside the cilium. The mouse KIF-17 is inactive inside the cilium, while OSM-3 is a robust transporter. Nevertheless, KIF-17 learned to perform numerous roles outside the cilium [79]. It means the homodimeric kinesin-2 motor has altered into a cytoplasmic transporter from ciliary transporter over time. So how did KIF-17 lost its ability to convey the IFT-trains during IFT? OSM-3 attaches to DYF-1 subunit for its efficient docking into the anterograde IFT-trains. It is conceivable that in mouse, the connection between the IFT70 (mouse homolog of DYF-1) and KIF-17 is lost. If the interaction between IFT70 and KIF-17 is broken, how did it occur? Did KIF-17

failed to recognize IFT70 or vice versa? It can also appear that IFT70 can bind to KIF-17 but could not activate it for processive IFT. So the first objective is to unmask why KIF-17 failed to perform as a processive motor inside the cilia.

OSM-3 identifies a specific set of adaptor proteins from the large pool of proteins to enable IFT. As IFT has been highly conserved across the spectrum, can OSM-3 recognize the corresponding adaptor proteins in mouse to activate itself? Or have the adaptors been modified to avoid the homodimeric kinesin-2 motor? If the adaptor proteins have significantly changed between *C.elegans* and mouse, does KIF-17 use this variation to adapt to form the cytoplasmic motor rather than a ciliary transporter?

IFT56/46 dimer is essential for the entry of KIF-17 into cilia, and the motor has been kept as an inactive cargo inside the cilium in mouse [95]. During the IFT process, it is also essential to keep the kinesin-2 motors dormant during retrograde transport. Does this specific interaction between IFT56/46 and KIF-17 offer a cue for the mechanism on how to keep the kinesin motors inactive, when it is not required for processive transport? Is it also possible to retrace this connection back to the corresponding *C.elegans* homodimeric motor and adaptor proteins? Acknowledging these questions will direct us to dissect how these motors differ from each other. Moreover, investigating the disparity in the deployment and function of OSM-3 and KIF-17 allows uncovering the multifarious means cells have employed to incorporate existing tools for multiple roles within the system.

3. Generating a tool box for investigating kinesin-II mediated anterograde transport in *C.elegans*

Despite being known, where the kinesin-II motors attach to the trains (IFT-A/IFT-B subcomplexes) during anterograde transport, the definitive interaction points between the complexes and motor is still unknown [55]. Further, the kinesin-II motor has switched between IFT-B and IFT-A complexes in different organisms for anterograde transport. To gain insight into the kinesin-II mediated transport in IFT, a toolbox consisting of the heterotrimeric motor and relevant adaptor proteins is necessary.

Even after more than two decades of IFT discovery in *C.reinhardtii*, no significant study has been conducted to learn the mechanistic properties of its kinesin-II motor. The atypical high speed of kinesin-II motor in *C.reinhardtii* presents an interest in dissecting the motor. So the first objective is to inspect the kinesin-II motors in *C.elegans* and *C.reinhardtii* to study how these motors behave *in vitro*, the role of their structural domains in motility, and their autoregulation features.

In *C.elegans*, the Kinesin-II motors, directly interact with the IFT-A for anterograde transport, but the absence of stable IFT-A complexes *in vitro* restricted the reconstitution of motor-adaptor complex formation till now. Building the *C.elegans* IFT-A complex from its subunits will make it viable to explore and compare the kinesin-II mediated transport in *C.elegans* and *C.reinhardtii*. Studying the anterograde transport in a bottom-up approach utilizing such a toolbox of kinesin-II motors and associated adaptor proteins will also open new doors for assessing kinesin-II based transport in other domains outside the cilia.

3. Materials

3.1. Chemicals and other consumables

Name	Company/Location
Acetic Acid	Roth, Karlsruhe
Adenosine 5'-triphosphate disodium salt hydrate (ATP)	Sigma-Aldrich, Taufkirchen
Agarose	Roth, Karlsruhe
Ammonium bicarbonate	Sigma-Aldrich, Taufkirchen
Ammonium persulfate	Roth, Karlsruhe
Ampicillin	Roth, Karlsruhe
ANTI-FLAG® M2 Affinity Gel	Sigma-Aldrich, Taufkirchen
Atto 550 NHS ester	Sigma-Aldrich, Taufkirchen
Biotin-Conjugated BSA	Sigma-Aldrich, Taufkirchen
Bluo-gal (halogenated indolyl-β-galactoside)	Thermo Fisher Scientific, Darmstadt
Bovine Serum Albumin	Sigma-Aldrich, Taufkirchen
Brilliant Blue R-250	Thermo Fisher Scientific, Darmstadt
Bromophenol Blue	Sigma-Aldrich, Taufkirchen
β-Mercaptoethanol	Sigma-Aldrich, Taufkirchen
cOmplete™, EDTA-free Protease Inhibitor Cocktail	Roche, Penzberg
Coomassie® Brilliant blue R 250	Sigma-Aldrich, Taufkirchen
Dimethyl sulfoxide (DMSO)	Roth, Karlsruhe
Dithiothreitol (DTT)	Sigma-Aldrich, Taufkirchen
Ethanol	Roth, Karlsruhe
Ethylenediaminetetraacetic acid (EDTA)	Sigma-Aldrich, Taufkirchen
Ethylene glycol-bis(β-aminoethyl ether)-N,N,N',N'-tetraacetic acid (EGTA)	Sigma-Aldrich, Taufkirchen
EZ-Link ™ NHS-PEG 4 biotin	Thermo Fisher Scientific, Darmstadt

FLAG® Peptide	Sigma-Aldrich, Taufkirchen
Glucose	Roth, Karlsruhe
Glutamate	Sigma-Aldrich, Taufkirchen
Glycerol	Roth, Karlsruhe
Glycine	Sigma-Aldrich, Taufkirchen
Guanidium-HCl	Sigma-Aldrich, Taufkirchen
Guanosine-5'-triphosphate (GTP)	Sigma-Aldrich, Taufkirchen
HEPES	Sigma-Aldrich, Taufkirchen
Imidazole	Sigma-Aldrich, Taufkirchen
Isopropyl-β-D-thiogalactoside (IPTG)	Sigma-Aldrich, Taufkirchen
Kanamycin Monosulfate	Sigma-Aldrich, Taufkirchen
LB Agar (Lennox)	Sigma-Aldrich, Taufkirchen
LB Broth (Lennox)	Sigma-Aldrich, Taufkirchen
Magnesium chloride hexahydrate	Sigma-Aldrich, Taufkirchen
Methanol	Roth, Karlsruhe
Ni-NTA agarose	Qiagen, Hilden
2-Propanol	Roth, Karlsruhe
peqGOLD prestained Protein-Marker IV	PeqLab, Erlangen
peqGOLD Protein-Marker II	PeqLab, Erlangen
Paclitaxel from *Taxus brevifolia*	Sigma-Aldrich, Taufkirchen
PIPES	Sigma-Aldrich, Taufkirchen
Potasium acetate	Sigma-Aldrich, Taufkirchen
Potasium hydroxide	Sigma-Aldrich, Taufkirchen
Rotiphorese® Gel 30	Roth, Karlsruhe
Sodium azide (NaN_3)	Roth, Karlsruhe
Sodium chloride	Roth, Karlsruhe
Sodium dodecyl sulphate (SDS)	Roth, Karlsruhe
Sodium hydroxide	Sigma-Aldrich, Taufkirchen

Streptavidin from *Streptomyces avidinii*	Sigma-Aldrich, Taufkirchen
Tetracycline	Sigma-Aldrich, Taufkirchen
Tetramethylethylenediamine (TEMED)	Roth, Karlsruhe
Tris (hydroxylmethyl) aminomethane	Roth, Karlsruhe
Triton™ X-100	Sigma-Aldrich, Taufkirchen
Tween® 20	Sigma-Aldrich, Taufkirchen

3.2. Cell culture consumables and reagents

Name	Company/Location
Cellfectin™ II Reagent	Thermo Fisher Scientific, Darmstadt
Fetal Bovine Serum (FBS)	Sigma-Aldrich, Taufkirchen
Filtropur S 0.2	Sarstedt AG, Nümbrecht
Gentamicin (50mg/ml)	Sigma-Aldrich, Taufkirchen
Serological pipettes (1,2,5, 10, 25, and 50ml)	Sarstedt AG, Nümbrecht
Sf-900 II SFM medium	Thermo Fisher Scientific, Darmstadt
Sterile syringes	B. Braun, Melsungen

3.3. Plasmids and vectors

Name	Company/Location
pFastBac TM Dual	Life Technologies, Darmstadt
pFastBac TM 1	Life Technologies, Darmstadt
pFBDM	Life Technologies, Darmstadt

3.4. Reagents kits and enzymes

Kit/Enzyme	Company/Location
Antarctic Phosphatase	New England Biolabs, Frankfurt a. Main
Bac-to-Bac® Baculovirus Expression System	Thermo Fisher Scientific, Darmstadt
Catalase from bovine liver	Sigma-Aldrich, Taufkirchen

Glucose Oxidase Type VII from *Aspergillus niger*	Sigma-Aldrich, Taufkirchen
Halo Tag® Alexa Fluor® 488 and 660	Promega, Mannheim
Platinum™ *Pfx* DNA polymerase	Thermo Fisher Scientific, Darmstadt
Qiaquick ® Gel Extraction kit	Qiagen, Hilden
QIAprep® Miniprep Kit	Qiagen, Hilden
Restriction enzymes	New England Biolabs, Frankfurt a. Main
SNAP-Surface® Alexa Fluor® 488 and 647	New England Biolabs, Frankfurt a. Main
T4 DNA Ligase kit	New England Biolabs, Frankfurt a. Main

3.5. Stock solutions

Buffer	Recipe
Ampicillin solution	100 mg/ml Ampicillin in H_2O
APS solution (100X)	10% (w/v) Ammonium per sulfate in H_2O
Biotin-BSA solution (1X)	1mg/ml Biotin-BSA in PBS (1X)
Catalase solution (50X)	170000 U/ml Catalase in O_2 Quench buffer (1X), 50% (v/v) Glycerol
Glucose Oxidase solution (50X)	2600 U/ml Glucose Oxidase in O_2 quench buffer (1X), 50% (v/v) Glycerol
Glucose solution (50X, 1 ml)	500 mg Glucose in 1 ml water
EGTA solution (pH 7.0)	200mM EGTA in TAE buffer (50X)
FLAG® Peptides	5 mg/ml FLAG® Peptides in 1X TBS
Gentamicin solution	0.50 mg/ml Gentamicin in H_2O
GTP solution (pH 7.0)	0.1 M GTP in H_2O
Kanamycin solution	0.50 mg/ml Kanamycin monosulfate in H_2O
O_2 Quench buffer (1X)	24mM PIPES, 4mM $MgCl_2$, 4mM EGTA
Paclitaxel solution	4mM in DMSO
PBS (1X, pH 7.4)	140mM NaCl, 2.7mM KCl, 1.8mM KH_2PO_4, 10mM Na_2HPO_4

S.O.C medium	10mM $MgCl_2$, 2.5mM KCl, 10mM Glucose in LB medium
Streptavidin solution	1 mg/ml Streptavidin in PBS (1X)
TAE Buffer (50X, pH 8.0)	2 M Tris, 0.57% acetic acid, 50mM EDTA,
TBS buffer (1X, pH 7.2)	20mM Tris Base, 150mM NaCl
Tetracycline solution	0.50 mg Tetracycline in H_2O

3.6. Buffers

The buffers used during each experiments were prepared from the reagents listed above and their content is described in the respective method section

3.7. Microorganisms

Cell strain	Company/Location
MAX Efficiency™ DH10Bac Competent Cells	Thermo Fisher Scientific, Darmstadt
Stellar™ Competent Cells	Thermo Fisher Scientific, Darmstadt
XL1-Blue Subcloning-Grade Competent Cell	Stratagene, La Jolla (U.S.A.)

3.8. Oligonucleotides (sequencing primers)

Primer name	Sequence
PH	5’-cctataaatattccggattattcataccg-3’
P10	5’-cggacctttaattcaaccc-3’
Seq_Che-11_01	5’-gtcgggcacgatc-3’
Seq_Che-11_02	5’-ggctgccatccag-3’
Seq_Che-11_03	5’-cgatgccgtgag-3’
Seq_Che-11_04	5’-gtccgcggtgcac-3’
Seq_Che-11_05	5’-gcgcaatccgcc-3’
Seq_Che-11_06	5’-ggacatcgagacc-3’
Seq_Daf-10_01	5’-cccgcgactcac-3’

Seq_Daf-10_02	5’-ggtcacccacgg-3’
Seq_Daf-10_03	5’-gctgaggatcgc-3’
Seq_Daf-10_04	5’-cggcctggcgag-3’
Seq_Daf-10_05	5’-cgaactcgatggcc-3’
Seq_Dyf-2_01	5’-cggcgagcccacc-3’
Seq_Dyf-2_02	5’-cctcacgcagg-3’
Seq_Dyf-2_03	5’-ccgtgggctccag-3’
Seq_Dyf-2_04	5’-gctggagtggccg-3’
Seq_Dyf-2_05	5’-gccgtgcgcgtgg-3’
Seq_Dyf-2_06	5’-gtcgctgatggc-3’

3.9. Software for data acquisition and analysis

Software	Company/Location
ASTRA 6	Wyatt Technology
ImageJ Versions 1.44p and 1.50i	NIH, Bethesda (U.S.A.)
ImageJ plugin Particle Tracker 2D/3D	NIH, Bethesda (U.S.A.)
MATLAB R2016b	MathWorks, Natick (U.S.A.)
Origin Pro 9.1G 64-bit	Origin Lab, Northampton (U.S.A.)

4. Methods

4.1. Generation of constructs

Nearly all of the constructs have been custom designed, subject to the requirement, and synthesized from Genscript Biotech (New Jersey, United States) into pFastBac1 TM plasmid. In the case of IFT-A subunits, cloning was employed to incorporate multiple genes in a single vector plasmid for efficient expression in insect cells (Sf9). The list of all constructs used in this thesis with their respective amino acid sequences is reported in the Supporting information 8.3 section.

4.2. Cloning of IFT-A subunits

Cloning was done to combine multiple gene constructs into a single pFBDM vector plasmid by using specific restriction enzymes to take out the insert DNA sequence from the parent vector and stitching them into the multiple cloning sites of pFBDM vector [119]. The original constructs used for the cloning were procured from Genscript Biotech (New Jersey, United States) with specific restriction sites in the 5' and 3' end. pFBDM vector has dual multiple cloning sites and a multiplication module, which enables it to add more genes of interest to a single vector. Double digests were conducted on the insert, and vector and each gene construct were added sequentially one after the other.

4.2.1. Restriction digestion of DNA plasmids

Restriction digestion was imposed using the restriction enzymes (New England Biolabs Inc) according to the manufacturer's guidelines. 3-6µg of DNA was used during the digestion of vector and insert. The digestion mix was incubated at 37°C for 90 minutes to ensure complete cleavage of all DNA plasmids. After the digestion, the restriction enzymes were deactivated by incubation at 70°C for 5 minutes. All constructs subjected to restriction digestion were analyzed by agarose gel electrophoresis afterward.

4.2.2. Agarose gel electrophoresis

The size/length of DNA fragments was determined through agarose gel electrophoresis by separating the negatively charged DNA in agarose gels by exercising an electric field. The agarose gels were prepared by dissolving 1% Agarose (Sigma) in 1X TAE buffer and casting it into custom

gel cassettes. After digestion, the DNA fragments were mixed with EZ-VISION™ DNA dye (6X loading buffer) in the ratio, 5:1 for visualization during and after the run. 1X TAE buffer was again used as the running buffer during electrophoresis. Electrophoresis was carried out at 80mV for 30 to 60 minutes. A standard 1kb ladder was always run adjacent to the samples to determine the size of the DNA bands. After the run, the gel was kept under UV illumination to observe the bands and were documented using the Eagle Eye II CCD camera system (Stratagene, Heidelberg).

4.2.3. Isolation of DNA from agarose gels

The target DNA bands from agarose gels were carefully excised using a scalpel and were transferred to a 2ml microcentrifuge tube. The DNA fragments were extracted from the excised gel pieces using the Qiaquick ® Gel Extraction kit (Qiagen) according to the manufacturer's protocol. Final elution of DNA fragments was done in 30-50 µl of Qiagen elution buffer, based on the strength of the DNA bands observed under UV illumination on the agarose gels. The concentration of extracted DNA fragments was determined using Spectrophotometry (Nanodrop 1000). The instrument calculated the sample's concentration by measuring the absorbance of the sample at a wavelength (λ) of 260nm (E 260).

4.2.4. Dephosphorylation of the 5' –ends of DNA

The vector DNA was dephosphorylated at the 5' –ends by Antarctic Phosphatase (AP, New England Biolabs Inc). This step helped to avoid the religation of linearized vector DNA to itself during ligation. The vector DNA (1 µg) was dephosphorylated with 5 U of AP in AP-Buffer (10 x, New England Biolabs Inc) for 60 minutes at 37°C. The AP enzyme in the solution was later deactivated by heat shock at 65°C for 20 minutes.

4.2.5. Ligation of DNA fragments

The vector and insert DNA were ligated using T4 DNA Ligase (New England Biolabs Inc, Frankfurt) in specific ligase buffer given from the manufacturer. In the typical 10µl reaction, vector and insert were mixed in equal concentration (50ng each at least) to 40 U of T4 DNA Ligase. The reaction was carried overnight at 16°C.

4.2.6. Transformation of ligated constructs into chemically competent *E.coli* cells

Chemically competent *E.coli* stellar cells used for the transformation were stored as 200µl aliquots at -80°C. After the initial thawing on ice, cells were mixed with the 10µl ligation. The ligated constructs were allowed to settle with the cells for 20 minutes at 4°C. Then a heat shock at 42°C was given for 1 minute and was immediately kept in ice for another 5 minutes. The cells were then enriched with 300µl of S.O.C. medium and were incubated for 60 minutes at 37°C in a shaker. The cells were finally plated on an LB Agar plate with an ampicillin resistance marker and were allowed to grow overnight in a 37°C incubator.

LB-Ampicillin agar: 3.5% (w/v) LB Agar Lennox, 0.1% (v/v) Ampicillin solution (100 mg/ml)

4.2.7. Identification of transformed *E.coli*

The plates used for transformation were checked for white, isolated, and round colonies after overnight incubation. 2-6 colonies from them were picked using a pipette tip and were transferred to separate 3ml LB-Ampicillin medium containing tubes, which were allowed to grow overnight at 37°C with constant shaking. The transformed cells grew on the medium overnight and were pelleted at 2,500 x g for 10 min at 4°C, the next day. The Mini-plasmid from the cells was isolated using the QIAprep ® Miniprep kit (Qiagen), according to the manufacturer's protocol. The final plasmid DNA was eluted in 30µl of elution buffer (Qiagen). The purified plasmid DNA was then cleaved using respective restriction enzymes and was run on agarose gels. The samples which identity with the expected DNA sizes were taken as stocks of successfully transformed plasmid DNA and were stored at -20°C.

LB-Ampicillin medium: 2.0% (w/v) LB Broth Lennox, 0.1% (v/v) Ampicillin solution (100 mg/ml)

4.2.8. Sequencing of cloned constructs

The genome sequence of each construct after cloning was reviewed through DNA sequencing to confirm that the successive steps in cloning did not introduce any point mutations or other changes. Sequencing was conducted by MWG Eurofins (Ebersberg) for the study. Samples of 100 ng/µl purified DNA was mixed with 15 pmol of sequencing primer in a total reaction volume of 15µl. The sequences provided by the company were cross-checked with the parent sequence by DNA sequence alignment (Multalin, Florence corpet) [120].

4.2.9. Amplification of plasmid DNA

Due to the low volume of holy stocks of plasmid DNA after cloning, they were amplified for further steps. The plasmid was transformed into XL-Blue *E.coli* cells using the same protocol that was used for transformation during the cloning method. Instead of plating to the LB-Agar plates, 100µl from the transformed cells were used to inoculate 6ml of LB-Amp medium and were allowed to grow overnight at 37°C with constant shaking. After overnight incubation, the cells were pelleted by centrifuging at 2,500 x g for 10 min at 4°C. The plasmid from the cells were purified using the QIAprep ® Miniprep kit (Qiagen) according to the manufacturer's protocol, and the final DNA was eluted in 100µl of elution buffer (Qiagen). The quality of DNA amplification was analyzed through restriction digestion of plasmid DNA using restriction endonucleases followed by checking on agarose gels. The amplified Mini- plasmid was later used for protein expression.

4.3. Protein expression using the baculovirus expression system

The baculovirus expression system is ideal for eukaryotic protein expression due to its facility of protein-folding and post-translational modification after protein translation, ultimately capacitating the protein for its intended biological functions in functional characterization studies [121, 122]. The system also showcases advantages in higher rate of soluble protein recovery and in translating larger protein complexes. For protein overexpression from insect cell line Sf9, I used the eukaryotic Bac-to-Bac baculovirus expression system (Invitrogen).

4.3.1. Generation of the baculovirus transfer vector (bacmids) for protein expression

The gene of interest from donor plasmid (pFastBac1 TM, pFBDM) must be transferred to intermediate baculovirus shuttle vectors or bacmids for ultimate protein expression. The transposition was done by transformation into competent MAX Efficiency ® DH10Bac TM *E.coli* cells by heat shock. The *E.coli* strain contains two plasmids, one being a helper plasmid coding a transposase with a tetracycline resistance marker and the other, the Autographa californica nuclear polyhedrosis virus (AcNPV) bacmid with a kanamycin resistance marker. There is a mini-attTn7 cassette planted in between the LacZα gene within the bacmid [123]. Site-specific transposition between the mini-Tn7 element of the pFastBac1 TM donor vector and the mini-

attTn7 attachment site on the bacmid disrupts the lacZα gene. Cells with successfully recombinant bacmids appear as white colonies during the blue-white screening while the failed ones produced blue colonies.

In this method, 200µl aliquots of MAX Efficiency ® DH10Bac TM *E.coli* cells were used to transform each construct and were maintained at 4°C on ice. 100-200ng of the donor plasmid containing the gene of interest was incubated in the cells for 30 minutes. Heat shock was given for one minute at 42 °C followed by immediate cooling on ice for 5 minutes. The cells were then supplied with 800 µl of S.O.C medium and were incubated at 37°C with constant shaking for 4 hours. After incubation, the transformed cells were plated onto blue-white plates at three different dilutions: 50 µl, 15 µl, and 1.5 µl. The plates were then kept at 37°C incubator for three days. Typically, numerous cell colonies are formed on the plates during this period of time, from which four white colonies were restreaked into a new blue-white plate and were grown overnight to affirm colony color. The resulting white cell colonies were picked again and suspended in 6ml of blue-white medium to be incubated at 37°C with constant shaking overnight. The grown cells after incubation were pelleted by centrifugation with Rotanta 460R swinging bucket centrifuge (Hettich) at 2,500 x g for 15 minutes at 4°C for isolation of bacmids.

Blue-white agar: 3.5% (w/v) LB agar lennox, 0.1 mg/ml Bluo-gal, 0.04 mg/ml IPTG, 0.05 mg/ml Kanamycin, 7 µg/ml Gentamicin, 0.02 mg/ml Tetracycline

Blue-white medium: 2% (w/v) LB broth lennox, 0.05 mg/ml Kanamycin, 7 µg/ml Gentamicin, 0.02 mg/ml Tetracycline

4.3.2. Isolation of bacmids

Qiagen ® Miniprep kit, solutions P1, P2, and P3 were used for isolating bacmids from cell pellets from the previous step. Each cell pellet was first resuspended in 500µl of P1 buffer and then followed by lysis with 500µl of P2 buffer. The lysed mix was kept for 5 minutes at room temperature. Then the P3 neutralization buffer was mixed into the lysate and incubated at 4°C for 10 minutes. Centrifugation (16900 x g, Eppendorf 5418R) for 30 minutes at room temperature, precipitated the cell debris and other complexes inside cells while the bacmid DNA stayed in the supernatant. The supernatant was transferred to a clean microcentrifuge tube, and 1.5ml of isopropanol was added to the solution. The solution was gently mixed and incubated at

4°C for 30 minutes. The bacmid DNA precipitated in the presence of isopropanol and was isolated by centrifugation at 16900 x g for 30 minutes at room temperature. The bacmid pellets were washed with 300µl of 70% ethanol and were finally suspended in 50-100 µl of autoclaved sterile water.

4.3.3. Transfection of Sf9 cells with recombinant bacmid and generation of recombinant virus particles

Recombinant virus particles specific to each construct were generated through transfecting Sf9 cells with purified recombinant bacmids. Sf9 cells were freshly diluted to a density of 0.5X 10^6 cells/ml in Sf-900 II plus medium (10% serum and 0.2% gentamicin, 50mg/ml). 2ml from this culture was transferred to the five wells of a 6-well tissue culture plate each and were incubated, light protected for 30 minutes at 28°C. The culture in one well was taken as control, while the other four wells were used for infection with each of the four bacmids of a single construct. In the meantime, 15 µl of purified bacmid DNA (25-50µg) was mixed with 10 µl of the cationic lipid Cellfectin ® transfection reagent (Invitrogen) in 200 µl of Sf-900 II serum-free medium (SFM) and was incubated for 30 minutes at room temperature. Cellfectin ® reagent provides a cationic lipid formulation around the bacmid DNA for its efficient transfection into Sf9 cells. 800 µl of SFM was added to this mixture after incubation. The Sf9 cells from the first step, remain affixed to the surface of the cell culture plate after incubation. After the removal of medium, the adherent cells were washed twice with 1ml of SFM in each well. The bacmid DNA mix was then pipetted into the wells and were kept at 28 °C for 5 hours in the dark. The transfection of bacmids to the cells takes place during this period. The mix was then pipetted out from the wells and was supplied with 2ml of fresh Sf-900 II plus medium. The tissue cultures plates were then sealed with parafilm tapes and were incubated for four to five days at 28 °C. Baculoviruses are produced from the bacmids with the aid of Sf9 cell machinery. Synthesis of recombinant virus particles leads to inflation of cells and, ultimately, to its rupture. The cells were examined through a light microscope. Deformed and detached Sf9 cells indicated successful generation of virus particles. The first generation of virus particles (P0) was isolated by filtering the supernatant with a 0.2 µm sterile filter and were stored at 4 °C.

4.3.4. Amplification of baculoviruses

Baculoviruses were amplified to successive generations for protein expression due to the low titer volume of P0 viruses. The second generation of baculoviruses (P1) was formed by infecting 30 ml of Sf9 cells at a density of 0.5X 10^6 cells/ml with 0.7ml of P0 virus in a sterile 26-cm tissue culture dish. The infected cells were then grown at 28 °C for seven days in the dark. A control culture dish was maintained, besides, to check contamination. Baculoviruses were harvested by centrifugation at 5,000 x g (Rotanta 460R swinging bucket centrifuge, Hettich) and room temperature for 20 minutes. The supernatant containing the virus particles was transferred to a sterile 50ml centrifuge tube and stored at 4°C. P1 baculoviruses were used as stock to amplify to P2 generation of baculoviruses. P2 was amplified following the same method as in P1 and was subsequently used for protein expression.

4.3.5. Protein expression in Sf9 cells

Protein expression was carried out in Sf9 insect cells through suspension culture. The cells were diluted to a concentration of 2X 10^6 cells/ml using Sf-900 II plus medium in a sterile Erlenmeyer flask and were infected with 0.5-5% (v/v, of prepared cell suspension) of the virus. The infected cells were then incubated for 48 to 72 hours at 28 °C and 110 rpm in an Innova 43 shaker (Eppendorf, Hamburg). Upon the completion of incubation, the cells were harvested by centrifugation at 2,500 x g (Rotanta 460R swinging bucket centrifuge, Hettich) and room temperature for 15 minutes. The supernatant was discarded, and cell pellets were used for direct protein purification or stored at -20°C.

4.4. Protein purification by affinity chromatography

Nearly all the proteins used in this thesis were fused with either FLAG® or 6x His tags on their N-terminal/ C-terminal to facilitate affinity-based purification. The underlying protocols allowed the purification of required proteins with considerable amount and purity.

Flag purification

The harvested Sf9 cells through cell culture were used for purification. Cells were lysed in 4% Vol. of the initial suspension volume using ice-cold Flag lysis buffer. Lysis was performed through gently pipetting the mixture up and down using a pipetboy (Integra Biosciences, Germany) up to

4 minutes. The homogenate mix was then centrifuged at 65,000 x g for 10min at 4°C (Beckmann L8-M, rotors 70.1 Ti, or Beckmann Optima TL, rotor TLA 100.3). The supernatant containing the protein of interest was then incubated with 4% vol. (lysis solution volume) of anti-FLAG antibody agarose resin for 1.5 hours at 4°C. This step allowed the specific binding of Flag-tagged protein on to the anti-FLAG resin. After incubation, the resin was washed 3 to 4 times with 1 ml of ice-cold Flag washing buffer 1, followed by 3 to 4 times washing with ice-cold Flag washing buffer 2 in microcentrifuge tubes (Eppendorf reaction tube, 1.5ml) with centrifugation steps (16900 x g for 1min, Eppendorf 5418R) in-between, to eliminate unbound protein. The flag tagged proteins were eluted from the flag beads using Flag elution buffer (Wash buffer 2 containing FLAG-peptides). The resin was incubated with a minimum of 1 vol. (resin) of the elution buffer for 45min at 4°C. If required, a second elution step was done with the elution buffer. Eluted proteins were directly used for functional assays or were shock-frozen in liquid nitrogen and stored at -70°C for later experiments.

Flag Lysis buffer: 50mM PIPES pH 6.9, 300mM Potassium Acetate, 1mM Magnesium Chloride , 1% Triton-X 100, protease inhibitor cocktail (complete, Roche) (1 Tablet for 50 ml reaction volume), 1mM DTT , 10% glycerol and 100µM ATP

Washing buffer 1: 80mM PIPES pH 6.9, 500mM Potassium Acetate, 0.1% Tween 20, protease inhibitor cocktail (complete, Roche) (1 Tablet for 50 ml reaction volume), 1mM DTT , 10% glycerol and 100µM ATP

Washing buffer 2: 80mM PIPES pH 6.9, 500mM Potassium Acetate, 1mM Magnesium Chloride, 1mM EGTA, 0.1% Tween 20, protease inhibitor cocktail (complete, Roche) (1 Tablet for 50 ml reaction volume), 1mM DTT , 10% glycerol and 100µM ATP

Elution buffer: Wash buffer 2 with 100 µg/ml FLAG-peptides

Note: ATP was used in the buffers only while purifying motor proteins.

His purification

His purification is specifically designed for proteins with His tag (6x Histidine). The purification is conducted in a similar approach as in flag purification. The target protein's harvested cells were lysed using 4% vol. of the initial suspension volume using ice-cold His lysis buffer. The lysate was

then centrifuged at 65,000 x g for 10min at 4°C (Beckmann L8-M, rotors 70.1 Ti, or Beckmann Optima TL, rotor TLA 100.3). The supernatant was then incubated with 5% vol. (supernatant) of Ni-NTA Agarose for 1.5 hours at 4°C. After incubation, the Ni-NTA beads were washed extensively with ice-cold His washing buffer to eliminate unbound protein. The protein was then eluted by incubating the resin with 1-2 vol. (resin) of His elution buffer for 45 min at 4°C. SDS polyacrylamide gel electrophoresis was carried out to estimate the quality of the purification. The proteins were then either directly used for functional assays or shock-frozen in liquid nitrogen and stored at -70°C for later use.

His Lysis buffer pH 8.0 : 50mM PIPES, 300mM Potassium Acetate, 10mM Imidazole , 1% Triton-X 100, protease inhibitor cocktail (complete, Roche) (1 Tablet for 50 ml reaction volume), 1mM DTT and 10% glycerol.

His washing buffer pH 8.0 : 50mM PIPES, 500mM Potassium Acetate, 40mM Imidazole, protease inhibitor cocktail (complete, Roche) (1 Tablet for 50 ml reaction volume), 1mM DTT and 10% glycerol.

His Elution buffer pH 7.5 : 50mM PIPES, 100mM Potassium Acetate, 500mM Imidazole, 1mM EGTA, protease inhibitor cocktail (complete, Roche) (1 Tablet for 50 ml reaction volume), 1mM DTT and 10% glycerol.

Tandem His-Flag purification

Tandem His-Flag purification is used during co-precipitation assays when one protein is His-tagged while the other is Flag-tagged, to precise pull-down coupled proteins. In this technique, His purification is performed first, as explained above. The purified protein from His purification is then incubated with 0.5 volume (purified protein volume) of anti-FLAG antibody agarose resin (Anti-FLAG M2 ® Affinity Gel, Sigma) for 1.5 hours at 4°C. The resin was then washed 3 to 4 times with 1 ml of ice-cold Flag washing buffer 1, followed by 3 to 4 times washing with Flag washing buffer 2. The coupled proteins were then eluted from the flag beads using flag elution buffer, as described in the flag purification method. This method enables the purification of the coupled proteins in the right stoichiometric form as it is bound to each other.

4.5. Labeling of proteins

The studied proteins were fluorescently labeled through Halo and Snap-tag method (New England BioLabs, Frankfurt a. Main). GFP (green fluorescent protein) –tagged constructs exhibited inherent fluorescence for visualization while Snap/Halo -tagged constructs required additional labeling with subsequent dyes for imaging. These tags are indeed amino acid peptides fused to the target protein either on its N-terminus or C-terminus end. Halo tag (297 A.a., 33 kDa) is a haloalkane dehalogenase that serves as a hydrolase to specifically bind reactive chloroalkane linkers, which are bound with fluorescent dyes (HaloTag® Alexa Fluor® 488 or 660). SNAP-tag (182 A.a., 19.4 kDa) is evolved from mammalian O6 -alkylguanine-DNA-alkyltransferase, which reacts with derivatives of benzylguanines and benzyl chloropyrimidines, that are coupled with fluorescent dyes (SNAP-Surface® Alexa Fluor® 488 or 647). The respective protein with these tags are purified using the standard protein purification method, and before elution, it was labeled with 10µM Halo/Snap-tag substrate in the wash buffer2 (Flag/His) for 45mins at 4°C in the dark on a rotator. The beads were then extensively washed with wash buffer2 (Flag/His) to remove excess dye.

4.6. Sodium dodecyl sulfate-polyacrylamide gel electrophoresis (SDS-PAGE)

SDS-PAGE is the standard technique for analyzing the quality of protein expression after purification [124]. This method separates proteins based on its mass in a polyacrylamide based discontinuous gel. The polyacrylamide concentration controls the pore sizes in the gels, and the respective gels are made following the protein of study. In this thesis, 10% and 7% acrylamide gels were used for SDS-PAGE analysis. The gels were prepared in two stacks, resolving gel at the bottom and a stacking gel above it in a Bio-rad gel cassette. The resolving gel is employed to separate the protein while stacking gel for loading and making sure all the samples across the gel start running for separation simultaneously. The resolving gel was prepared and filled to 75% of the gel chamber and was allowed to solidify for 20 minutes. A thin layer of 70% ethanol was pipetted on top of the resolving gel to remove bubbles from pipetting and to form a straight stretch on the gel. Once the resolving gel is solidified, the stacking gel is prepared fresh and added on top of the resolving gel after removing the 70% ethanol.

The protein samples were prepared by mixing the proteins with SDS loading buffer (6X) and heating to 95°C for 5 minutes. The denaturation breaks their secondary and tertiary structure and applies a negative charge along the protein's length. The proteins are then allowed to run towards a positive electrode in an applied electric field of 80 mA for 40 to 60 minutes with a standard protein marker by the side. The protein with lower mass runs further into the gel rather than protein with a larger mass. After the electrophoresis, the proteins in the gel were immediately fixed and stained using Coomassie Brilliant Blue for 30 minutes. The gel was later destained using the freshly prepared destaining buffer for 30 minutes. The destained gels were then digitalized for further analysis

Separating gel (10%, 10 ml): 3.3 ml Rotiphorese Gel 30, 2.5 ml Separating gel buffer, 4.2 ml H_2O, 10 µl TEMED, 100 µl APS

Separating gel buffer (10X): 0.5M Tris Base pH 6.8, 0.4% (w/v) SDS

Stacking gel (10 ml): 1.3 ml Rotiphorese Gel 30, 2.5 ml Stacking gel buffer, 6.2 ml H_2O, 10 µl TEMED, 100 µl APS

Stacking gel buffer (10X): 1.5 M Tris Base pH 8.8, 0.4% (w/v) SDS

Electrophoresis buffer (10X, pH 8.8): 3% (w/v) Tris Base, 1% (w/v) SDS, 14% (w/v) Glycine

SDS protein sample buffer (6X): 300mM Tris Base pH 6.8, 15mM EDTA, 12% (w/v) SDS, 30% (v/v) Glycerol, 0.06% (v/v) Bromophenol Blue, 15% (v/v) β-Mercaptoethanol

Coomassie Brilliant Blue solution: 0.25% (w/v) Brilliant Blue R-250, 50% (v/v) Methanol, 10% (v/v) Glacial acetic acid

Destain solution: 10% Glacial acetic acid, 25% Isopropyl alcohol

4.7. Determination of protein concentration

Protein concentrations were estimated by running SDS-PAGE of the samples along with a series of known BSA dilutions (0.1; 0.2; 0.3, and 0.4 mg/ml). The intensity of protein bands from BSA samples after staining was used to generate a standard concentration calibration curve using the ImageJ software. The calibration curve was then used to calculate the concentration of the target protein by correlating with the intensity of its gel band.

4.8. Size exclusion chromatography – Multiple angle light scattering (SEC-MALS)

Tandem Flag-His purification combined with SDS-PAGE analysis, can predict the interactome between multiple proteins, but we are limited in understanding the oligomeric nature and stability of the complexes. SEC-MALS combines size exclusion chromatography with multiple angle light scattering method to precisely measure the molar mass of protein complexes and, hence, predict the robustness and hetero-oligomeric nature of such complexes. In this thesis, I used Superose® 6 Increase 10/300 GL (GE Healthcare, UK) columns with a bed volume of 24ml to separate protein complexes based on their size. The separation was carried out at a flow rate of 0.5ml/min maintained by an injector pump (Agilent 1260 Infinity series) for 1hr. The columns were attached to the pump and were calibrated with two volumes of running buffer. Highly pure BSA (Sigma) was used to calibrate the system. Protein complexes for analysis were freshly purified and were eluted in the running buffer. Samples were manually loaded into the sample loop and injected into the column at the start of the run. The elution from the column was connected to the UV absorbance monitor (Agilent 1260 Infinity series) at 280 nm wavelength and MALS detector (DAWN8 + Wyatt Technology) inflow. The final eluent was collected to separate 0.5ml fractions in a fraction collector (Agilent 1260 Infinity series). The sample concentration was inferred from the UV-signal and molar mass from the MALS detector through the ASTRA 6 software (Wyatt Technology). The molar mass was calculated by setting the dn/dc value to 0.185 ml/g.

Running buffer: 25mM PIPES, 200mM Sodium Chloride, 1mM Magnesium Chloride, 1mM EGTA, 1mM DTT, 0.02% Sodium azide

4.9. ATP purification using ion-exchange chromatography

Commercially bought ATP (Adenosine 5'-triphosphate disodium salt hydrate) could not sufficiently activate the OSM-3 wild type motor in single-molecule TIRF microscopy experiments. Hence ATP (sigma) was purified in the lab by Ion exchange chromatography technique using the Mono QTM 10/100 GL (GE Healthcare, UK) column with a bed volume of 8ml. The purification was performed by passing the ATP in a concentration gradient of NH_4HCO_3 through the column. At lower concentrations of NH_4HCO_3 (150mM), the ATP attached and remained bound to the

column and did elute when the concentration of NH_4HCO_3 was gradually raised to higher concentrations. ATP typically elutes in the range of 300-400mM of NH_4HCO_3. The elution from the column was connected in line to the UV absorbance detector (Agilent 1260 Infinity series) and the Fraction collector. The wavelength of the UV detector was set at 290nM to prevent saturation of the detector.

Table 4.1: Percentage distribution of 1M NH_4HCO_3 and autoclaved water in the course of ATP purification.

Volume (ml)	*1M NH_4HCO_3 (%)*	*Autoclaved Water (%)*
0	15	85
10	15	85
30	55	55
32	100	0
40	100	0
42	15	85
45	15	85

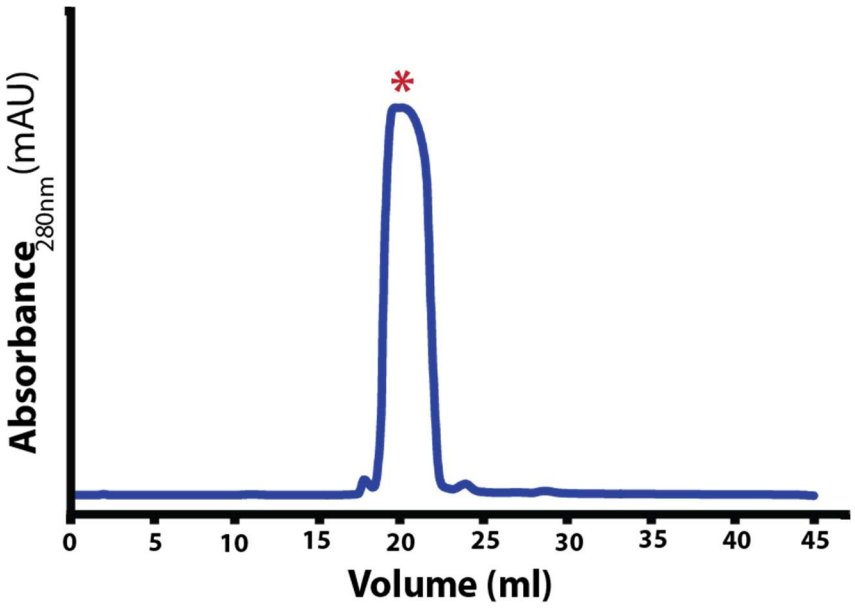

Figure 4.1: Elution profile for ATP purification. The purification was conducted using Mono QTM 10/100 GL column by running ATP across a concentration gradient of NH_4HCO_3. Clean ATP eluted in between 150mM and 550mM of NH_4HCO_3. The fraction under the dominant peak (red asterisk) was solely collected and pooled together for the further steps.

For the purification, 500ml of 1M NH_4HCO_3 and 1litre of autoclaved cold water was prepared fresh and was attached to the column using a pump (Agilent 1260 Infinity series). The pump was

programmed, as shown in Table 4.1, for maintaining the gradient. The sample for purification was prepared by dissolving 1gram of ATP in autoclaved ice water to a concentration of 250mM and pH 7.0. The columns were calibrated with 150mM of NH_4HCO_3 before the run. The calibration and purification were carried at a flow rate of 1.2ml/min. 100µl of ATP was injected into the column and allowed to bind to the column for 1 volume of the column. Any unbound ATP in the column was flushed out during this time. Then the gradient was steadily raised to 550mM over three volumes of the column (20 minutes). ATP was eluted during this time, which could be observed from the UV plot in the ASTRA 6 software (Wyatt Technology) (Figure 4.1). The gradient was then increased to 1M NH_4HCO_3 and was run for one column volumes to remove any ATP trace, still bound to the column. The column was then recalibrated to a gradient of 150mM NH_4HCO_3 for the next run. The eluted samples from each run were collected in separate 0.6ml fractions in the fraction collector. Around 15 runs were done, and all the fractions under the UV peak were pooled together. The concentration of the pool mix was determined using Spectrophotometry (Nanodrop 1000) and was subsequently mixed with 1.3 molar equivalents of NaOH from 10M NaOH stock. The samples were then shell froze using liquid nitrogen and were lyophilized overnight. The lyophilized ATP was dissolved in ice-cold autoclaved water to a concentration of 100mM at pH 7.0 and was aliquoted to smaller volumes (20, 50µl) and finally stored at -80°C after flash freezing in liquid nitrogen.

4.10. Purification of tubulin from porcine brain

Microtubule dynamics is tightly regulated by temperature that allows tubulin to polymerize at a higher temperature (35°C) and depolymerize at lower temperature (4°C) [125]. This property was exploited for the purification of tubulin from the porcine brain tissue. 800-1000g of porcine brain halves were used for purification and were maintained on ice. The blood and connective tissues were carefully excised from the surface of the brain halves. Around 700g of brain tissue was mixed with an equal volume of Buffer A to be homogenized in a blender (Braun, Germany) and was centrifuged at 26,000 x g for 70 min at 4°C (J2-21M/E centrifuge and JA-14 Rotor, Beckman-Coulter). The supernatant containing the depolymerized tubulin was gently transferred to a new flask containing pre-warmed 25% glycerol (final concentration v/v, Roth) and 2mM Na_2 ATP. The protein was allowed to polymerize by keeping the mix in a shaking water bath for 30 min at 35°C.

The polymerized tubulin was extracted through centrifugation at 200,000 x g for 45 min at 35°C (L8-70M Ultracentrifuge and 45Ti Rotor, Beckman-Coulter). Microtubules were then depolymerized by homogenizing the pellets with 10ml of Buffer C using Dounce homogenizers (Wheaton) in ice for 30 minutes. After ensuring the tubulin mix is then a fine homogenate, centrifugation was carried out at 150,000 x g for 30 minutes at 4°C (L8-70M Ultra-centrifuge and 42Ti Rotor, Beckman-Coulter). The supernatant containing the depolymerized tubulin is allowed to polymerize again by supplementing with 2mM Na_2 ATP and incubating at 35°C for 30 minutes. Polymerized tubulin was precipitated by centrifugation at 125,000 x g for 30 min at 35°C (pre-warmed L8-70M Ultracentrifuge and 42.1Ti Rotor, Beckman-Coulter). The next homogenization of the tubulin pellets was conducted in Buffer B of higher ionic strength to remove elements of microtubule-associated proteins (MAPs) attached to the tubulin. Microtubules were dissolved to a final volume of 50ml at 4°C and centrifuged at 150,000 x g for 30 min at 4°C (L8-70M Ultracentrifuge and 42.1Ti Rotor, Beckman-Coulter). The tubulin monomers were again taken for a final polymerization step with 10% DMSO and 2mM Na_2ATP at 35°C for 30 minutes. Microtubules were sedimented by centrifugation at 125,000 x g for 60 min at 35°C (L8-70M Ultracentrifuge and 42.1Ti Rotor, Beckman-Coulter). The pellets are then dissolved in 10ml of Buffer D like in earlier steps by homogenization on ice for 30 minutes and centrifuged afterward at 135,000 x g for 30 min at 4°C (L8-70M Ultracentrifuge and 42.1Ti Rotor, Beckman-Coulter). The isolated tubulin is then passed through a gravity-flow phosphocellulose P11 column, pre-equilibrated with 100 ml of Buffer D. Tubulin was accurately collected by continually checking the concentration of the eluent throughout the elution using Bradford reagent [126]. Purified tubulin was supplemented with 0.1mM GTP and was shock-frozen in liquid nitrogen and stored at -80°C.

Buffer A pH 6.9: 0.1M PIPES (NaOH), 2mM EGTA, 1mM $MgSO_4$, 1mM DTT, 100µM ATP

Buffer B pH 6.9: 0.5M PIPES (NaOH), 1mM EGTA, 1mM $MgSO_4$, 1mM DTT, 1mM ATP

Buffer C pH 6.9: 0.1M PIPES (NaOH), 1mM EGTA, 1mM $MgSO_4$, 1mM DTT, 1mM ATP

Buffer D pH 6.9: 0.1M PIPES (NaOH), 1mM EGTA, 1mM $MgSO_4$, 1mM DTT, 50µM ATP

4.11. Determination of tubulin concentration

Tubulin concentration was estimated by spectrophotometry. Purified protein was diluted to 0.1 and 0.2 part volume with 6.6 M guanidium-HCl, for sample preparation. The absorbance was measured at E280 against a blank prepared from 0.1 part volume of tubulin buffer with 6.6 M guanidium-HCl. Tublin concentration was then calculated from the absorbance value by using the following formula

$$(E\ 280 / 1.03) \times \text{Final dilution of MT (100 or 50)} = x\ \mu M\ MT$$

The molecular weight of tubulin dimer was taken as 100,000 g/mol for calculation.

4.12. Functionalization of tubulin

Biotin-functionalized tubulin facilitates single-molecule assays by allowing the microtubule filaments to attach on the glass surface through the Biotin-Streptavidin conjugation method [127]. Also, visualization of microtubules on fluorescent microscopes requires tubulin functionalized with fluorescent dyes. I functionalized tubulin with biotin and fluorescent dyes for these critical needs.

For each functionalization step, 8 ml of 15-20 mg/ml purified tubulin was used. The volume was supplemented with 5mM $MgCl_2$ and 1mM GTP and was allowed to polymerize in a constant shaking water bath for 15 minutes at 35°C. The protein polymerized to form a white jelly-like mixture. It was then diluted with 1/3 volume of pre-warmed glycerol and was again kept on the water bath for another 10 minutes at 35°C. The polymerized tubulin was then carefully transferred, on the top of high pH cushion buffer in ultracentrifuge tubes such that the lower 20% volume of the tube is filled with the buffer while the protein occupies the upper volume. Centrifugation was carried out at 38500 rpm for 50 minutes at 35°C (Beckmann Optima TL, rotor TLA 100.3) to sediment the protein. After centrifugation, the supernatant is discarded, and the pellet is gently washed with Labeling buffer for 3-4 times. The pellet is then dissolved in 5ml of labeling buffer containing EZ-Link™ NHS-PEG 4 biotin/ Atto 550 NHS ester (2-4 molar excess over tubulin) on ice. The NHS-esters group in the biotin/fluorescent dye readily reacts with the amino groups of proteins. At pH 8.0 – 9.0 range, the ε-amino groups of lysines and other amino acids in tublin are unprotonated to a higher degree and are highly reactive towards the -NHS-ester group.

The reaction is carried out in the water bath at 35°C for 30 minutes and stopped after adding 1 volume of pre-warmed Quench buffer. The functionalized tubulin is then pipetted slowly on the top of low pH cushion buffer in ultracentrifuge tubes and centrifuged at 45000 rpm for 30 minutes at 35°C (Beckmann Optima TL, rotor TLA 100.3).

The pellets were then washed with 1X BRB80 buffer 3-4 times and were suspended in equal volume (pellet) of Inversion buffer supplemented with 1mM of GTP at 4°C. The homogenate is centrifuged at 80,000 rpm at 2°C for 30 minutes (Beckmann Optima TL, rotor TLA 100.3). The supernatant containing the depolymerized tubulin is polymerized again by mixing it with 1/5 volume 5X BRB80, 1/3 volume glycerol, and 4mM $MgCl_2$ and incubating on the water bath at 35°C for 30 minutes. Polymerized tubulin was recovered after centrifugation at 70,000 rpm at 35°C for 30 minutes (Beckmann Optima TL, rotor TLA 100.3). The final pellet was dissolved in an equal volume of Inversion buffer at 4°C. The homogenous mix is centrifuged again at 80,000rpm at 2°C for 20 minutes (Beckmann Optima TL, rotor TLA 120.3). The supernatant is then aliquoted and shock-frozen in liquid nitrogen for storage at -80°C.

High pH Cushion: 100mM HEPES (NaOH) (pH- 8.6), 1mM $MgCl_2$, 1mM EGTA, 60% glycerol

Labeling Buffer: 100mM HEPES (NaOH) (pH- 8.6), 1mM $MgCl_2$, 1mM EGTA, 40% glycerol

5X BRB80: 400mM PIPES (KOH) (pH- 6.9), 5mM $MgCl_2$, 5mM EGTA

Quench Buffer: 2X BRB80, 100mM Glutamate (KOH) (pH- 7), 40% glycerol

Low pH Cushion: 1X BRB80, 60% glycerol

10X Inversion Buffer: 500mM Glutamate (KOH) (pH- 7), 5mM $MgCl_2$

4.13. Polymerization of tubulin

Microtubule filaments are prepared by polymerizing tubulin dimers above a critical concentration and critical temperature utilizing GTP. Biotinylated tubulin and Atto550-labeled tubulin was mixed with purified tubulin in the ratio 1:50 and were polymerized in 1X BRB80 with 1mM GTP at 35°C. After 45 minutes, 5µM taxol was added to the mix, and polymerization was extended overnight at 35°C. The next day, microtubules were diluted using BRB80/Tax depending

on the quality of polymerization and were maintained at 35°C. The filaments remain stable for 2-3 weeks.

BRB80/Tax: 80mM PIPES pH 6.9, 1mM $MgCl_2$, 1mM EGTA, 5mM DTT, 5µM Taxol

4.14. Total internal reflection fluorescence (TIRF) microscopy

Total internal reflection fluorescence microscopy is an advanced form of fluorescence microscopy that allows the visualization of fluorophores with a high signal to noise ratio [128]. In theory, light rays gets refracted or reflected while traveling from one surface to another at the interface, depending on the two surfaces' refractive indices (n) and incident angle (θ). At higher incident angles than the critical angle (Equation 1), when the light sails from a transparent cover glass (n2) to an aqueous solution containing the sample of study (n1), it gets totally internally reflected at its interface with the liquid sample, to generate an electromagnetic field termed evanescent wave in the sample's solid-liquid interface. The evanescent wave's depth (d) depends on the incident lights wavelength (λ), illumination angle, and refractive index differences of the surfaces (Equation 2); and the intensity of the electromagnetic field (I_z) decays exponentially with distance from the interface (Equation 3) [128]. Hence the evanescent wave could only excite fluorophores that are within a few hundred nanometers from the coverslip. The selective excitation of a thin axial section of the sample significantly reduces the background and out of focus fluorescence, observed in epifluorescence microscopy to provide a high signal to background ratio. The samples are also subjected to a lower amount of light to avoid unnecessary photobleaching events in this method.

$$\theta critical = \sin^{-1}(n_1/n_2) \quad \text{Equation 1}$$

$$d = \lambda_o/4\pi\,(n_2^{\,2}\,sin^2\theta - n_1^{\,2})^{1/2}$$

$$\text{Rearranging, } d = \lambda_o/(4\pi\, n_2) \times ((sin^2\theta/\, sin^2\theta critical) - 1)^{1/2} \quad \text{Equation 2}$$

$$I_z = I_o e^{z/d} \quad \text{Equation 3}$$

TIRF experiments regarding the study were conducted using Leica DMi8 fluorescent microscope system. The microscope boasted three excitation channels at 488, 561, and 647 nm wavelength, which allowed us to visualize differently labeled multiple proteins simultaneously with a notably

lower delay time. A 100x objective with numerical aperture 1.47 and an immersion oil suspension was used to transmit light from the laser source to the fluorescently labeled protein samples. The transmitted light from the samples is then captured using an Andor iXon Ultra EMCCD camera (Andor Technology, Belfast, UK) and were analyzed with the microscope software AF 6000 (Leica microsystems, Wetzlar, Germany).

4.14.1. Multiple motor gliding filament assay

Molecular motors, especially Kinesins, tend to stay autoinhibited without its activation partners inside the cell to provide specialized transport and avoid the futile hydrolysis of ATP. Filament gliding assay is conducted by utilizing the property of non-specific binding of the globular C-terminal region of the molecular motors to the glass surface of coverslip in a glass slide-coverslip chamber, thereby discharging its autoinhibition [129]. Upon flushing of microtubule filaments with ATP, the bed of multiple motors on the glass surface can power the gliding of filaments across the surface. In most cases, the maximum velocity of the motors can be measured from the velocity of gliding fluorescently labeled filaments.

Flow chambers were constructed with a glass coverslip, glass slide, and custom cut parafilm for binding them and also to introduce the 5µl volume in chambers for the assay. Gliding assays were performed following standard methods in BRB80 buffer. Briefly, 10µl of purified motor protein was flown into the chamber and incubated for 3 minutes. The unbound motors were removed, and the unbound regions were blocked by washing with 30µl of BRB80- BSA. After the washing step, 50µl of motility buffer containing Atto550-labeled microtubules, an oxygen scavenger system, and ATP were flushed into the system. The fluorescent microtubules were immediately monitored on the TIRF microscope (DMi8, Leica) over time, and multiple videos were recorded on different positions of the slide. The velocity of filaments was calculated using the distance tool in the manufacturer's software (Leica, Germany)

BRB80-BSA: 80mM Pipes pH-6.9, 2mM $MgCl_2$, 1mM EGTA, 1mg/ml BSA, 5mM DTT

Motility Buffer: 80mM Pipes pH-6.9, 2mM $MgCl_2$, 1mM EGTA, 2mM ATP, 5mM DTT, Atto550-labeled microtubules, 0.4% Glucose, 0.18 mg/ml glucose-oxidase, and 0.06 mg/ml catalase.

4.14.2. Single molecule motility assay

In single-molecule assays, microtubules are attached to the glass surface, and motor proteins are allowed to walk across them, replicating the process as inside cells. The assay was accomplished using the protocol from Vale et al. (1996)[130]. In brief, 8 µl of Biotin-BSA were initially pipetted into the chamber and allowed to bind to the coverslip for 2 minutes. After incubation, the chamber was washed with 30 µl of BRB80-BSA and was incubated with 8 µl of streptavidin for two minutes. Washing was repeated using 30 µl of BRB80-BSA, and sufficient dilution of polymerized, biotinylated Atto550-labeled microtubules was allowed to attach to the surface for 2 minutes. Motility buffer was prepared freshly containing the fluorophore-labeled motor proteins or subunits and was then flown into the flow chamber. The slide is immediately mounted on to the microscope for visualization and data capture.

The videos were analyzed using multiple in-house written programs in MATLAB software, as described in Stepp et al. (2017) [89]. Briefly, the fluorescent signals from labeled proteins (data points) were picked in accordance with their relative brightness to the background in each frame. Consecutive runs with a minimum run length of 1 µm were considered processive and data points were fit to a single exponential distribution. Velocity runs were calculated as distance over time from data points that show displacement for at least six frames. The velocity data points were fit to a Gaussian distribution with r^2-values >95%.

Motility Buffer: 80mM Pipes pH-6.9, 2mM $MgCl_2$, 1mM EGTA, 2mM ATP, 5mM DTT, Atto 488/Atto647 labeled motor proteins/IFT subunits, 0.4% Glucose, 0.18 mg/ml glucose-oxidase, and 0.06 mg/ml catalase.

4.14.3. Bleaching experiment on labeled proteins

Bleaching experiments were rendered to validate if the fluorophore-labeled protein that is visualized in TIRF microscopy exists in a dispersed state or an aggregated form. In this assay, the proteins are exposed at high laser power without any oxygen scavenger system support and are allowed to bleach over time, until all the fluorophore signals from the field of exposure disappear. The movie is then analyzed over an in-house written MATLAB program to measure if the

fluorophore signal vanished in a single step or multiple steps. Single-step bleaching indicated dispersed and stable proteins while longer steps implied of protein aggregation.

4.14.4. Colocalization experiments

The strength of interaction between multiple proteins can be evaluated by fluorophore labeling them differently (Alexa 488/647) and checking the number of pairwise colocalized proteins to uncolocalized proteins in a TIRF microscope. In the assay, the proteins are labeled separately and mixed in equal ratio and were incubated overnight for binding. Multiple images were collected for each binding assay and were analyzed using in-house written MATLAB program to calculate the percentage of colocalization from the ratio of pairwise colocalized proteins to the total number of labeled proteins (Alexa 488/647) on the surface.

5. Results

5.1. Method of approach used for the study

In this thesis, I focused on understanding the kinesin-2 motors' properties by studying them on the single-molecule level. We fluorescently labeled motor proteins and IFT subunits individually to address their characteristics. Single-molecule TIRF assays were conducted with motor proteins alone or in coupling with adaptor proteins for the study. Velocity and run length data were calculated from the analysis of videos from motors walking over the microtubule filaments. Velocity data were fitted to a Gaussian (± width of distribution) distribution, and the run length was obtained from a single exponential fit (± confidence interval). Data were obtained from three independent protein preparations for the study. The observed differences in the velocity data in comparative studies were analyzed through t-test to confirm the significance of such variation (Supporting information 8.2 for chapters 5.2 & 5.3). In Colocalization assays, pairwise colocalization was calculated between two subunits to analyze the interaction pattern between them. Proteins that interacted significantly showed a colocalization percentage of 60-80%, while the ones that did not interact showed a colocalization percentage of 5-20%. Data were analyzed from fifteen images of three independent protein preparations each. The amino acid sequences of all proteins used for the study are featured in the supporting information section 8.3. The SDS-PAGE analysis of the corresponding proteins are exhibited in the supporting information section 8.1, unless they are mentioned in the respective results chapters.

5.2. Dissecting the recruitment of OSM-3, for anterograde IFT in *C.elegans*

5.2.1. OSM-3 displays maximum velocity at 1700nm/s in the absence of its stalk and tail domains

Even though both KLP11/20/KAP1 and OSM-3 motors participate in the anterograde transport of IFT-trains from the base to the tip of the cilia in *C.elegans*, OSM-3 have been inferred as the principal transporter [85]. OSM-3 administer this transport through a highly regulated autoinhibition mechanism, which dictates the motor when and where to get switched ON and OFF [37]. It is intriguing that the homodimeric motor can also exhibit activation at different levels. *In vitro* reconstitution of the OSM-3 with DYF-1 subunit activated the motor from its

autoinhibited state to a robust motor displaying movement at a velocity of ~1300nm/s, while the quadripartite (OSM-6, DYF-6, OSM-5, DYF-1) core complex; (QCC) can allosterically activate the motor up to 1700nm/sec [52]. Similarly, the point mutation G444E in the kink region of OSM-3 can switch the motor 'On', only to a speed of 1100nm/sec, but the attachment of the tail domain of the motor to carboxylated latex beads in an optical trapping bead assay can relieve autoinhibition to the velocity of ~1700nm/s [37]. From these studies, it is unclear what is the real velocity of OSM-3 motor is. It is indeed possible that OSM-3 can exhibit much higher velocities than 1700nm/s. In order to attain the maximum velocity in OSM-3, the motor must be devoid of any factors that can cause autoinhibition. Various models have been proposed for the autoinhibition motor regulation in kinesins, the classic one being the direct binding of the C-terminal tail domain to the catalytic head domain in Kinesin-1 [34]. In KIF-17, the homolog of OSM-3 in mouse, the coiled coil stalk domain along with the C-terminal tail domain engage in a dual autoinhibition mechanism [33]. Therefore I designed the construct OSM-3 GCN4 merely with the catalytic head domain & neck linker region from the wild type motor and a GCN4 zipper motif was used to dimerize the motor as shown in the Figure 5.1 (Supporting Information 8.3). In functional single molecule TIRF assays, OSM-3 GCN4 produced the velocity of ~1700nm/s (Figure 5.1). So in the absence of any inhibitory factors, the velocity of the motor can attain only up to 1700nm/s which can thus be considered to be the maximum velocity of OSM-3. Hence it also proves that the quadripartite core complex can sufficiently activate the OSM-3 motor to its maximum capacity.

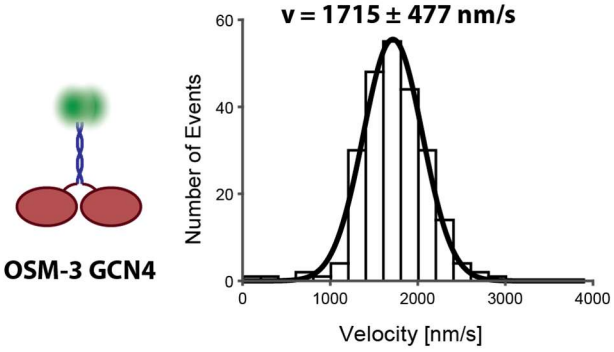

Figure 5.1: The velocity of OSM-3 GCN4 concludes the upper speed limit of OSM-3 wild type motor to 1700nm/s. OSM-3 GCN4^{GFP} motor, created without any known autoinhibition causing factors (stalk and tail domains) from the OSM-3 wild type motor, is processive on microtubules in single molecule TIRF

assays with velocity 1715 ± 477nm/s and run length 2.4 ± 0.3µm (Number of events, N = 237). Hence we can conclude that the maximum velocity that could be exhibited by OSM-3 is around 1700nm/s.

5.2.2. OSM-6/DYF-1 complex from QCC is sufficient to recapitulate OSM-3 to its maximum velocity

DYF-1 subunit is essential to dock the OSM-3 motor to the IFT-B core complex. But the attachment to DYF-1 alone introduces barely a basal activation of ~1300nm/s in OSM-3. Incorporation of DYF-1 subunit into the QCC complex is essential for the full activation of the motor [52]. The capability of QCC complex to speed up OSM-3 from ~1300nm to ~1700nm/s draws attention. How does the QCC allosterically activate OSM-3 or what are the factors in the QCC complex that introduce this trigger are questions worth pursuing. DYF-1 shows direct interactions with OSM-6, DYF-6, and OSM-5 subunits in the QCC complex, but it is possible that that all the three additional subunits may not be involved in the full activation of the OSM-3 motor. Therefore I decided to break down the QCC complex to decipher the minimum factors responsible for the maximum activation. In a 2014 JCB study, Lorentzen and his colleagues developed the crystal structure for the complex IFT70/52 which is the corresponding homolog for DYF-1/OSM-6 in *C.reinhardtii* [101]. In this high resolution structure, the whole IFT70 subunit wraps around a short unstructured proline-rich region of IFT52 (330-370) to form a stable complex. Since the IFT subunits have been highly conserved throughout the evolution, it is acceptable to assume that such a stabilized structure also exist in between the DYF-1 and OSM-6 subunits. Also OSM-6 was found to serve as an essential component in ciliogenesis in all the organisms studied so far [104]. So the next question is whether the formation of DYF-1/OSM-6 complex would reproduce the allosteric activation as observed with the QCC complex. In order to answer this question, I did functional single molecule TIRF assays by dual labeling the subunits OSM-6 with 2x superfolder GFP and DYF-1 with $SNAP^{647}$ and tracked both of them simultaneously to confirm the data is collected from the OSM-6/DYF-1 complex. Strikingly OSM-6/DYF-1 recapitulated OSM-3 wild type motor to its maximum velocity confirming our hypothesis (Figure 5.2 A; Movie S1 top right panel). However OSM-5/DYF-1 which is another complex made from within the QCC could not reproduce the full activation of OSM-3 motor reiterating that the OSM-

6 is the critical component in QCC that directs this allosteric activation (Figure 5.2 B; Movie S1 bottom left panel).

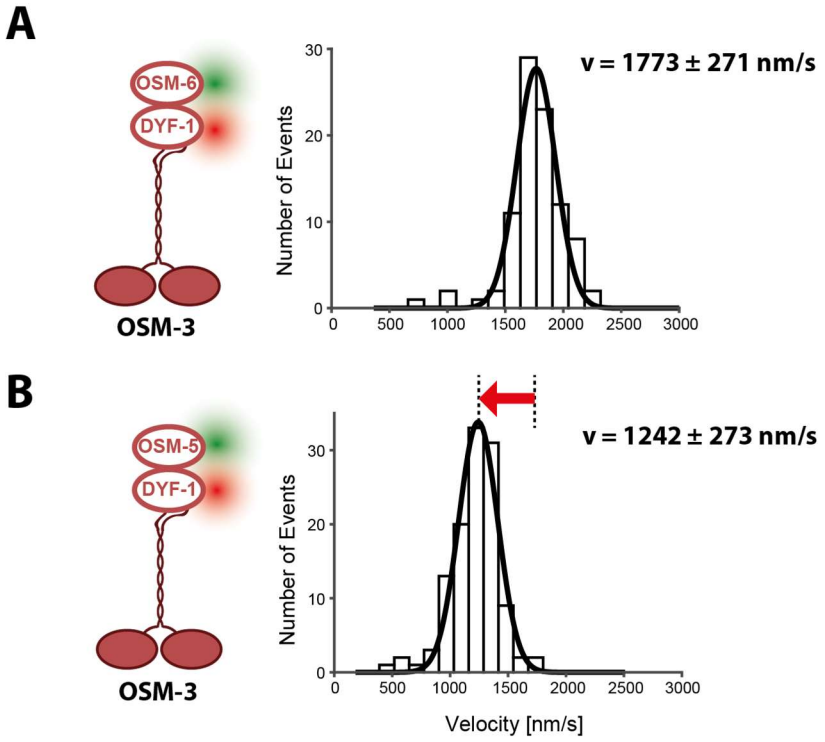

Figure 5.2: OSM-6 along with DYF-1 administers the allosteric activation of OSM-3 motor in QCC complex. (A vs B) OSM-6^{GFP} enables the complete activation of OSM-3 by forming a complex with DYF-$1^{SNAP647}$ (velocity= 1773 ± 271 nm/s, run length= 3.9 ± 0.8 µm, N = 91). However the OSM-5^{GFP}/DYF-$1^{SNAP647}$ complex, made out of the QCC, is unable to introduce the full activation in OSM-3 motor (velocity= 1242 ± 273 µm/s, run length= 3.2 ± 0.6 µm, N= 117) [131].

5.2.3. The middle domain of OSM-6 (N322-380) along with DYF-1 is responsible for generating the complete activation in OSM-3

As mentioned before, the whole IFT70 subunit fold around the short proline-rich region (amino acids 330-370) of IFT52 subunit in *C.reinhardtii*. We have seen that the formation of a complex with OSM-6 empowers DYF-1 to activate OSM-3 to its maximal activity in *C.elegans*. It is absorbing to dissect whether the equivalent region corresponding to the unstructured region in IFT52 is responsible for the secondary activation put forward by OSM-6 together with DYF-1 to OSM-3? To test this hypothesis, I designed the new OSM-6 DEL construct by deleting the corresponding region (322-380 amino acids) in OSM-6 that is involved in passing across the IFT70/DYF-1 subunit. Interestingly deleting this middle domain from OSM-6 did not hinder in its

binding capability to DYF-1 (not shown). I then wondered whether the OSM-6 DEL along with DYF-1 subunit is also capable of fully activating OSM-3. For this study, I did functional single molecule assays for the complex OSM-6 DEL/DYF-1 with OSM-3 G444E activated motor. Notably OSM-3 G444E also showcases similar activation pattern like wild type motor with OSM-6/DYF-1 and OSM-5/DYF-1. Curiously, the deletion of the middle domain of OSM-6 in OSM-6 DEL/DYF-1 brought the OSM-3 motor from its completely activated state to its basal activation level of velocity ~1300nm/s, demonstrating that the middle domain of OSM-6 is essential for the activation of the homodimeric motor (Figure 5.3 B).

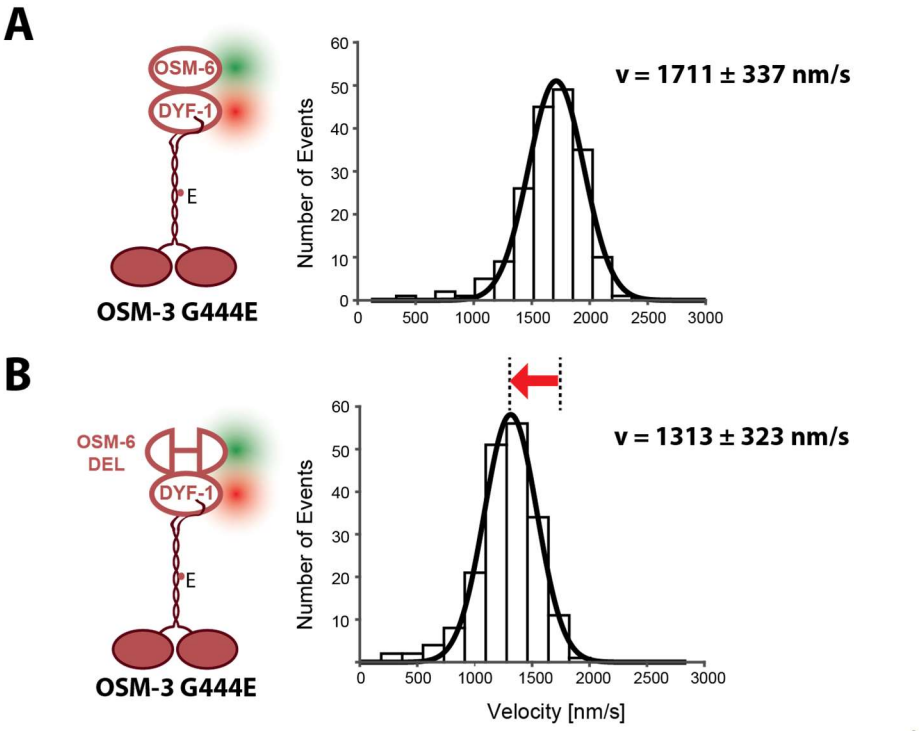

Figure 5.3: Deleting the middle domain of OSM-6 (N322-380) in OSM-6 DEL/DYF-1 complex takes OSM-3 back from its fully activated state to basal activation level. (A vs B) DYF-1^{SNAP647} fully activates the OSM-3 G444E motor in the presence of OSM-6^{GFP} (velocity= 1711 ± 337 nm/s, run length= 3.8 ± 0.6 µm, N = 184) but deleting the middle domain of OSM-6(N322-380) in OSM-6 DEL^{GFP}/DYF-1^{SNAP647} complex made it fail to reproduce the allosteric activation in OSM-3 motor (velocity= 1313 ± 323 nm/s, run length= 3.1 ± 0.4 µm, N = 190).

But this arises another query whether the middle domain of OSM-6 alone is sufficient for this property. A new construct was made; OSM-6 Trunc with only the middle domain of OSM-6 (N322-380 amino acids) and a SNAP tag on its N-terminal for fluorescent labeling. OSM-6 Trunc also

efficiently interacted with DYF-1 and in functional single molecule assays OSM-6 Trunc/DYF-1 could foster the wild type OSM-3 motor to its maximum velocity like the OSM-6/DYF-1 complex (Figure 5.4). The experiments in this study is also conducted by dual labeling the OSM-6 and DYF-1 constructs. From these studies, we can conclude the binding of middle domain corresponding to the short unstructured proline-rich region in IFT52, to DYF-1 is in charge of the full activation of OSM-3 motor.

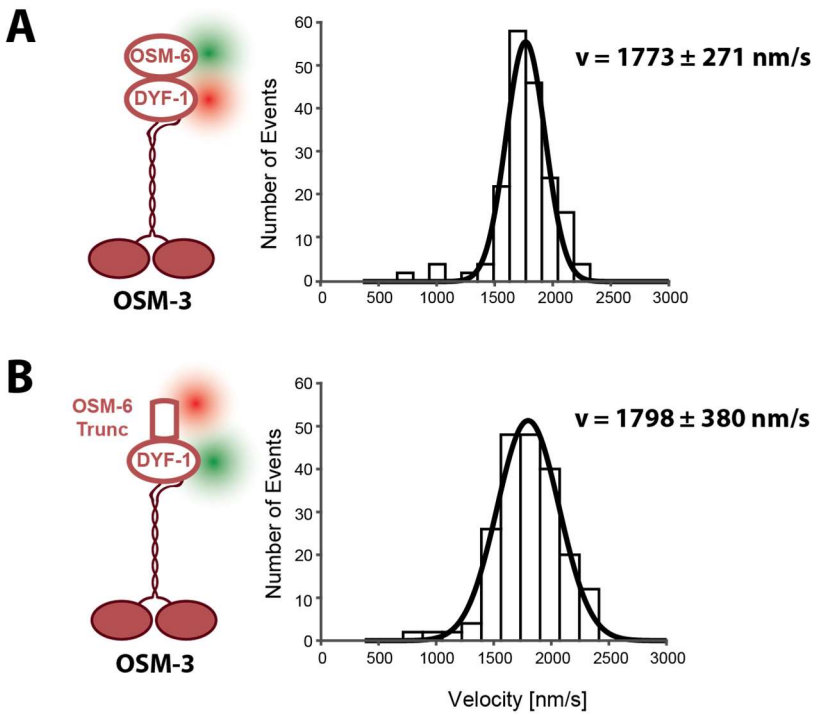

Figure 5.4: The middle domain of OSM-6 (N322-380) along with DYF-1 adaptor is adequate enough to fully activate OSM-3. (A vs B) The complex OSM-6 Trunc^{SNAP647}/DYF-1^{GFP} can activate OSM-3 motor to its fully activated state (velocity= 1798 ± 380 nm/s, run length= 2.3 ± 0.4 µm, N = 102) identical to that of the OSM-6/DYF-1 complex (replotted from Figure 5.2 A for direct comparison to the truncated complex).

5.2.4. A strictly conserved tyrosine-motif in the DYF-1 subunit retained throughout evolution is key to the full activation of OSM-3 motor.

Unmasking the significance of the middle domain in OSM-6 encouraged us to question if it possible to determine the bottom line of this cargo based motor activation. Examining the crystal structure of IFT52/70 complex in *C.reinhardtii* expose that the short unstructured region of IFT52

penetrating through the IFT70 subunit is a proline rich region which forms a stacking arrangement with the tyrosine residues from IFT70 inside the groove [101]. The aromatic rings of the tyrosine residues in IFT70 tightly stack against the proline rings of IFT52 in this high-resolution structure. Notably one such tyrosine motif in IFT70 have been highly conserved across the species from single celled to multicellular organisms (Figure 5.5). These conserved tyrosines enclose and interact with a conserved proline motif (354-PPPP-358) in IFT52. It is evident from the single molecule data of OSM-6 Trunc/DYF-1 that the effective wrapping of the proline rich region in OSM-6 by DYF-1 is essential for the activation of OSM-3. I then wondered if disrupting the tyrosine motif in DYF-1 (Y51, 53, 54, 55) would in any way break the hydrophobic interface between DYF-1 and OSM-6 and if so, can this disarray of the organization of the subunits would impact the adaptor based activation mechanism in OSM-3.

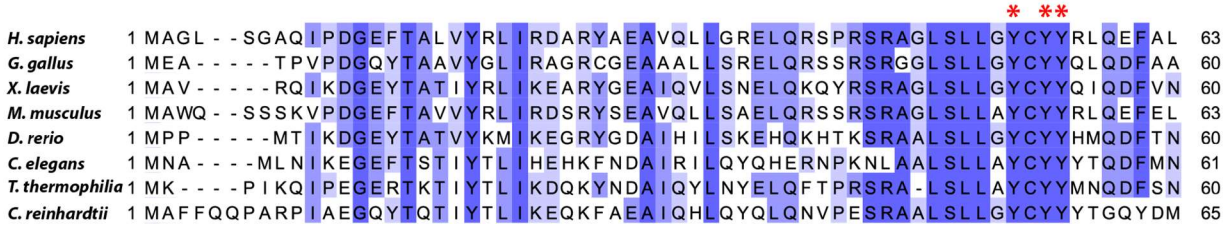

Figure 5.5: Protein sequence alignment of DYF-1 subunit's N-terminal region with its corresponding homologs. The amino acid sequence alignment of DYF-1 from multiple organisms from single-celled to mammals demonstrates the presence of a highly conserved tyrosine patch (highlighted by red asterisks) [131].

In order to answer this question, I generated two point mutation constructs; DYF-1^{Ala} (Y51, 53, 54, 55A) and DYF-1^{Phe} (Y51, 53, 54, 55F). In DYF-1^{Ala,} the repetitive tyrosine residues are mutated to alanines and in DYF-1^{Phe} the corresponding residues were mutated to phenylalanines (Figure 5.6 A). Phenylalanine is structurally identical to tyrosine, except for the hydroxyl group (-OH) on the aromatic ring while alanines lacks the whole aromatic ring and hydroxyl group. In functional single molecule TIRF assays the complex of OSM-6 with DYF-1^{Ala} could not reproduce the full activation of OSM-3 motor like the OSM-6/DYF-1 complex, and was only able to switch the motor to its basal activation level of ~1300nm/s (Figure 5.6 B vs C; Movie S2 left panel). However, OSM-6/DYF-1^{Phe} complex could efficiently rescue the OSM-3 motor back to its fully activated state (Figure 5.6 D; Movie S2 right panel).

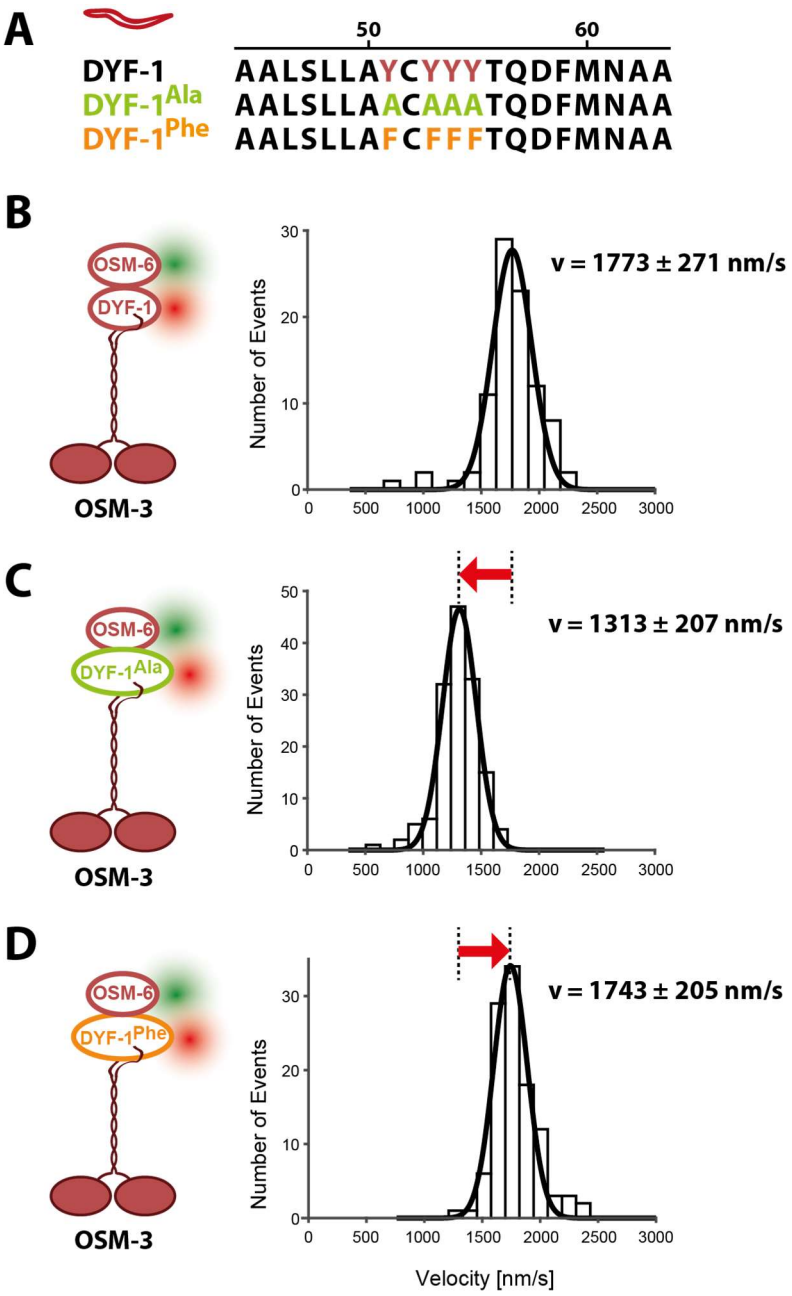

Figure 5.6: The allosteric activation in the OSM-3 motor is regulated by an evolutionary conserved tyrosine motif in DYF-1 subunit. (A) Sequence alignment of the conserved tyrosine motif from the wild type DYF-1 (top lane) to the DYF-1^{Ala} mutant Y51/53/54/55A (green) and DYF-1^{Phe} mutant Y51/53/54/55F (orange). **(B)** Wild type DYF-1/OSM-6 adaptors can completely activate the OSM-3 motor (replotted from Figure 5.2 A for direct comparison to the mutant DYF-1 adaptors). **(C)** Reconstituting the OSM-3 wild type motor with OSM-6^{GFP}/DYF-$1^{Ala,\ SNAP647}$ mutant complex failed to yield the motor's full activation (velocity= 1313 ± 207 nm/s, run length= 2.4 ± 0.4 µm, N = 145). **(D)** However, the allosteric activation of OSM-3 was restored with OSM-6^{GFP}/DYF-$1^{Phe,\ SNAP647}$ adaptor complex (velocity= 1743 ± 205 µm/s, run length= 3.3 ± 0.6 µm, N = 109) [131].

DYF-1^{Ala} lacking the aromatic ring groups of Phenylalanine/tyrosine seems to abolish the hydrophobic interface with OSM-6 losing its ability to allosterically activate OSM-3 motor, while the phenylalanine residues in DYF-1^{Phe} can efficiently substitute the function of tyrosine residue in wild type DYF-1 for motor activation. Thus the hydrophobic stacking between the aromatic rings of phenylalanine/tyrosine residues in DYF-1 and the proline residues in OSM-6 proves to be fundamental for the complete activation of OSM-3.

5.2.5. What is the significance of evolutionary conserved tyrosine motif *in vivo*?

The sensory cilia in *C.elegans* features single-rod, pair of rods, and wing-shaped ciliary structure in distinct neurons [81]. The expression and necessity of individual IFT subunits have been shown to vary in these different cilia types. For example, the IFT-A complex subunit ZK328.7a is a crucial component for IFT transport in AWC neurons but seems trivial for amphid and phasmid channel neurons. However, the C25H3.12 subunit is dispensable in all the cilia studied so far [132]. It suggests that the different cilia types have modulated the IFT machinery depending on their specific needs.

Curiously, in the case of DYF-1, two isoforms exist in the *C.elegans* genome. While the full-length DYF-1 (used in this study) contains the conserved tyrosine-motif, the DYF-1b isoform is truncated right after this motif. Since DYF-1b lacks the tyrosine motif, it is highly probable, that it is incapable of powering the full activation of OSM-3. It is also uncertain if the DYF-1b subunit can at least introduce the basal activation in OSM-3 motor. As expected from our previous functional dissection, this particular isoform lacking the tyrosine-motif also failed to activate the OSM-3 motor fully (Figure 5.7 B). However, DYF-1b retained the capacity to activate OSM-3 from its autoinhibited to its basal activation state (Figure 5.7 C). It is worth noting that in previous *in vivo* studies, the velocity of IFT-trains in the distal segment, where it is carried solely by the OSM-3 motors, has always remained in the range of 1100-1300nm/s [84]. As mentioned earlier, only in a recent study, it was shown that the velocity of IFT-trains could increase higher than 1500nm/s in the absence of KLP11/20/KAP1 motors in phasmid cilia [85]. Therefore it is tempting to speculate that there can be neurons that express DYF-1b isoform in its cilia to carry out IFT.

The huge IFT-trains may also supposedly produce enough drag on the OSM-3 motors forcing them to reduce the velocity by considerable margin; can also be another reason for the observed low *in vivo* velocity. It is unclear regarding the type of DYF-1 isoform present in different cilia types studied *in vivo*. It would be interesting if the corresponding isoforms of DYF-1 in the different cilia types could be unmasked and learn how the OSM-3 activity is balanced accordingly.

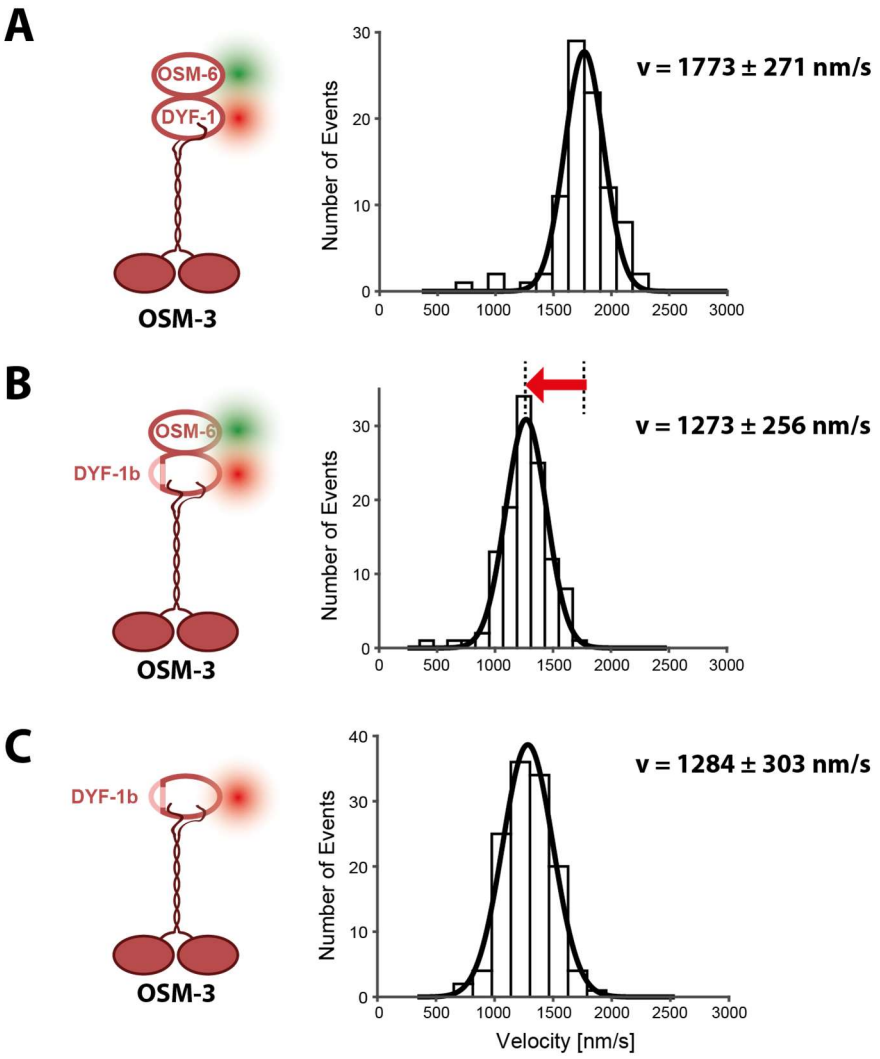

Figure 5.7: The loss of the conserved tyrosine motif in DYF-1b isoform prevents OSM-6/DYF-1b from fully activating the OSM-3 motor *in vitro* **(A)** The allosteric activation of the OSM-3 wild type motor by the DYF-1/OSM-6 complex replotted from Figure 5.2 for direct comparison to the OSM-6/DYF-1b adaptor. **(B)** DYF-1b^{SNAP647} isoform was unsuccessful in fully activating OSM-3 in the presence of OSM-6^{GFP} (Velocity= 1273 ± 256 nm/s, run length= 2.3 ± 0.4 µm, N = 117). **(C)** However, DYF-1b^{SNAP647} could still activate OSM-3 to its basal activation level. (Velocity= 1284 ± 303 nm/s, run length= 2.3 ± 0.4 µm, N = 126) similar to full length DYF-1 [52].

5.3. Evolution of kinesin-2 deployment from worm to mouse

The heterotrimeric KIF3A/3B/KAP3 and homodimeric KIF-17 actively participate in the intraflagellar transport in mice and other mammals [46]. Though KIF3A/3B/KAP3 has been characterized as the functional transporter of IFT-trains, the role of KIF-17 in the IFT process has been highly obscure. Despite KIF-17, been found to involve in specific chemosensory transduction purposes inside the cilium, it is not an essential component for ciliogenesis [79]. Knowing its worm homolog OSM-3 as robust transporter inside cilia, it intrigues how does KIF-17 lost its ability to be an active transporter even after having the ability to enter the cilium? In this second chapter of the thesis, I address how the homodimeric Kinesin-2 motors evolved in its deployment from worm to the mouse.

5.3.1. KIF-17 is an autoinhibited motor *in vitro*

In order to dissect how KIF-17 differs from OSM-3 in its role in the ciliary compartment, it is vital to express functional motors *in vitro* for the study. I designed a full-length KIF-17 motor with an N-terminal SNAP-tag for fluorescent labeling. The motor expressed well in eukaryotic Sf9 cells (Figure 8.1.2 A), but in functional single-molecule assays, the motors were inactive. They were either diffusing on the microtubule filament or stuck on the glass surface (Movie S3 left panel). KIF-17 was in-turn, predicted to be an autoinhibited motor through a dual intramolecular mechanism in a previous study [33]. Moreover, relieving the autoinhibitory domains from their partners in microtubule gliding assay activated the motor, delivering a gliding velocity of ~1000nm/s, comparable to its *in vivo* velocity of KIF-17 (Figure 5.8 A; Movie S4) [133, 134]. Another construct was also made, the SNAP KIF-17 $^{1\text{-}747}$, leaving out the inhibitory coiled-coil and C-terminal tail domains involved in the autoinhibition mechanism of KIF-17. The new construct displayed ~1200nm/sec in functional single-molecule assays, which is also in the range of its *in vivo* speed of 800-1200nm/s (Figure 5.8 B; Movie S3 right panel) [79]. From these experiments, it is evident, the motors expressed in the Sf9 system are functional, and the inactivity of the full-length KIF-17 in single-molecule assays is only due to the inherent autoinhibition prevailing within the motor. The native autoinhibition behavior of KIF-17 well collides with its worm homolog, OSM-3, which also stays autoinhibited *in vitro* when studied alone [52].

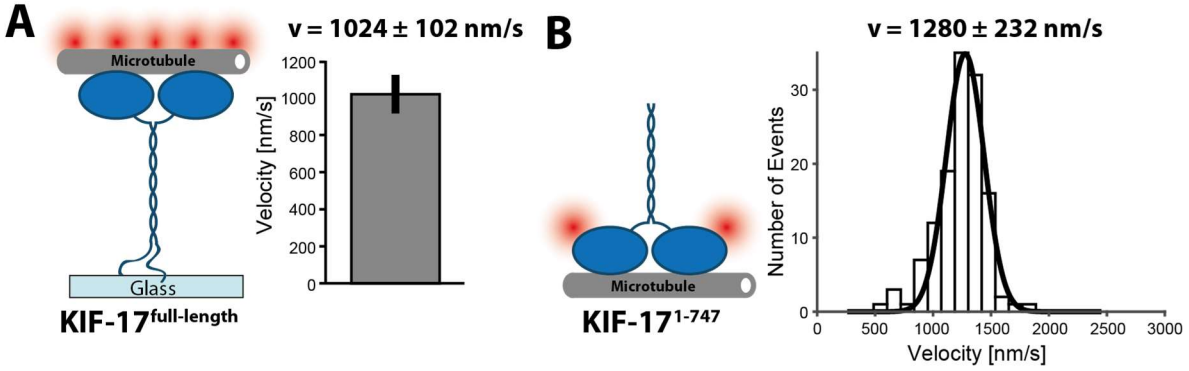

Figure 5.8: The inherent autoinhibition in native KIF-17 motor can be eliminated by surface-attachment or by the elimination of its C-terminus. (A) Attaching the full-length, native KIF-17 motors to the glass surface through its C-terminal region in microtubule gliding assays relieved the autoinhibition in the motor and powered the gliding of ATTO^{550} labeled microtubules across the surface with velocity 1024 ± 102 nm/s (N = 24; Error bars indicate the standard deviation (S.D.) from two separate protein preparations). **(B)** The removal of autoinhibition causing C-termini from KIF-17 enabled SNAP^{647} labeled KIF-17$^{1-747}$ motor to processively move across the microtubules with velocity 1280 ± 232 nm/s (N = 130) [131].

5.3.2. The mouse adaptor protein IFT70 has lost its ability to interact with its kinesin-2 motor KIF-17 but can connect to the *C.elegans* motor OSM-3

OSM-3 was activated for intraflagellar transport by anchoring on to the DYF-1 subunit in *C.elegans* [52, 84]. The disability of KIF-17 to be the active transporter in mouse cilium would doubt the capability of KIF-17 to interact with the adaptor protein IFT70, which is the mouse homolog for DYF-1. Colocalization assays were used to check the interactome between the motors and the adaptor proteins, as described in the methods 4.14.4 section. Curiously the full-length KIF-17 and the truncated KIF-17 $^{1-747}$ were unable to interact with the mouse adaptor protein IFT70 (Figure 5.9, first and second lane). So the interaction between the motor and its respective adaptor protein is broken. Now the loss of interaction can be due to multiple reasons; both KIF-17 and IFT70 might have lost their function to recognize each other, or the loss in function only happened from the adaptor protein's side or vice versa. If it is only the adaptor protein that has lost its power to interact with the kinesin-2 motor while evolving from the worm to the mouse, the KIF-17 motor must have retained its ability to interact with DYF-1. However, in the binding assays, KIF-17 also failed to interact with DYF-1, signifying that the motor definitely lost its function to interact with the corresponding adaptor protein destined for its activation to

participate in IFT (Figure 5.9, third lane). Strikingly OSM-3 very well interacted with mouse IFT70, meaning the adaptor protein has preserved its property to interact with the OSM-3 motor (Figure 5.9, fourth lane). In summary, the adaptor proteins IFT70/DYF-1 has remained strictly conserved in its binding property to the homodimeric kinesin-2 motor that work as a functional transporter in IFT. However, through evolution, KIF-17 has been reshaped to lose its function to interact with its essential adaptor protein.

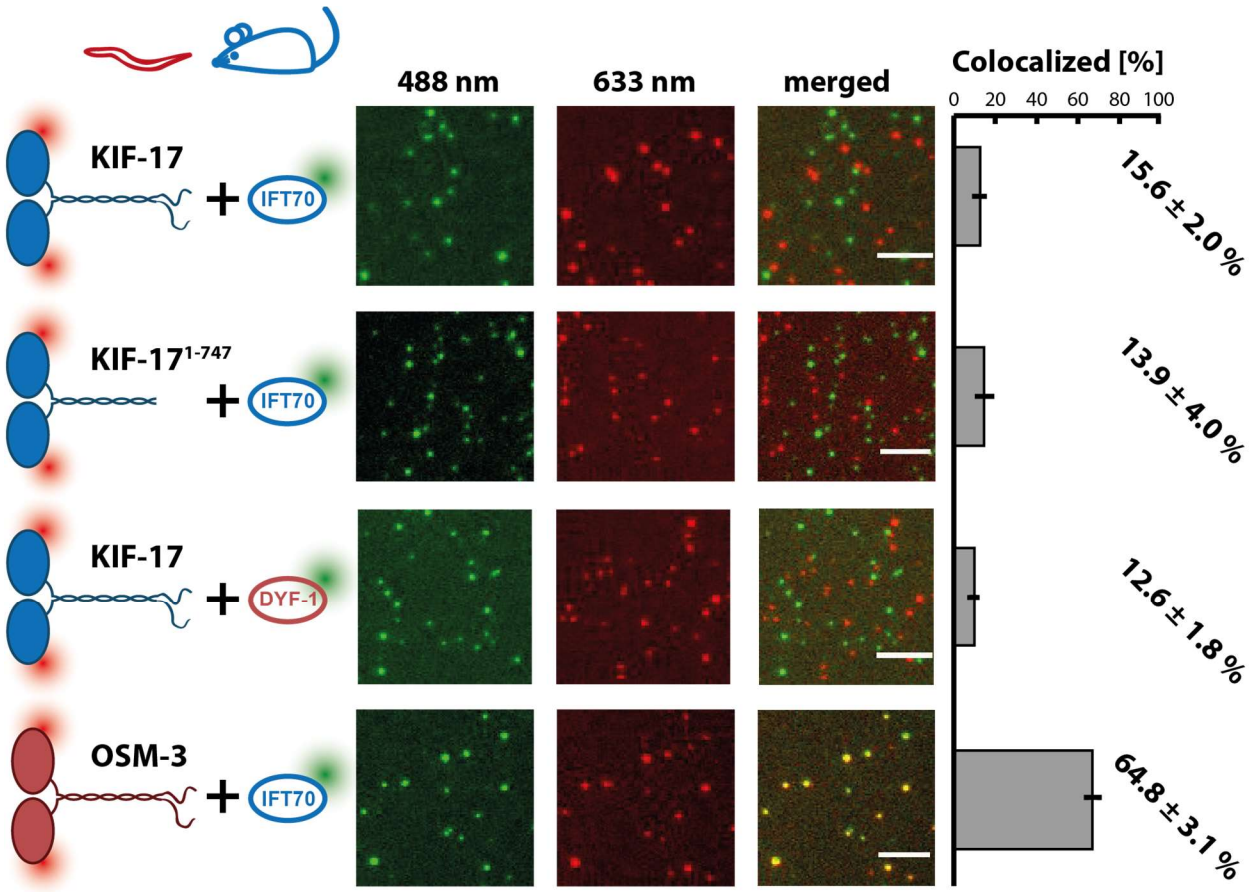

Figure 5.9: KIF-17 fails to recognize mouse IFT70 adaptor. (First and second lanes) The KIF-17 motors, full-length KIF-17^{SNAP647}, and truncated KIF-17$^{(1-747)\ SNAP647}$ (633 nm channel) did not effectively interact with the mouse adaptor IFT70^{SNAP488} (488 nm channel) as indicated by their colocalization percentages (merged channel and quantification on the right). **(Third lane)** The mouse KIF-17^{SNAP647} motor was also unsuccessful in interacting with the *C.elegans* adaptor DYF-1^{SNAP488}. **(Fourth lane)** However, the OSM-3^{SNAP647} motor efficiently interacted with the mouse IFT70^{SNAP488} adaptor. The capacity of OSM-3 to attach with IFT70 confirms that it is KIF-17 that has lost the ability to interact with mouse IFT70. The error bars in the colocalization percentage quantification, represents the standard deviation (S.D.) from three independent protein preparations with ten images each. Scale bar = 5 µm [131].

5.3.3. The mouse adaptor protein IFT70, along with IFT52, can switch OSM-3 to activation identical to the *C.elegans* OSM-6/DYF-1 complex

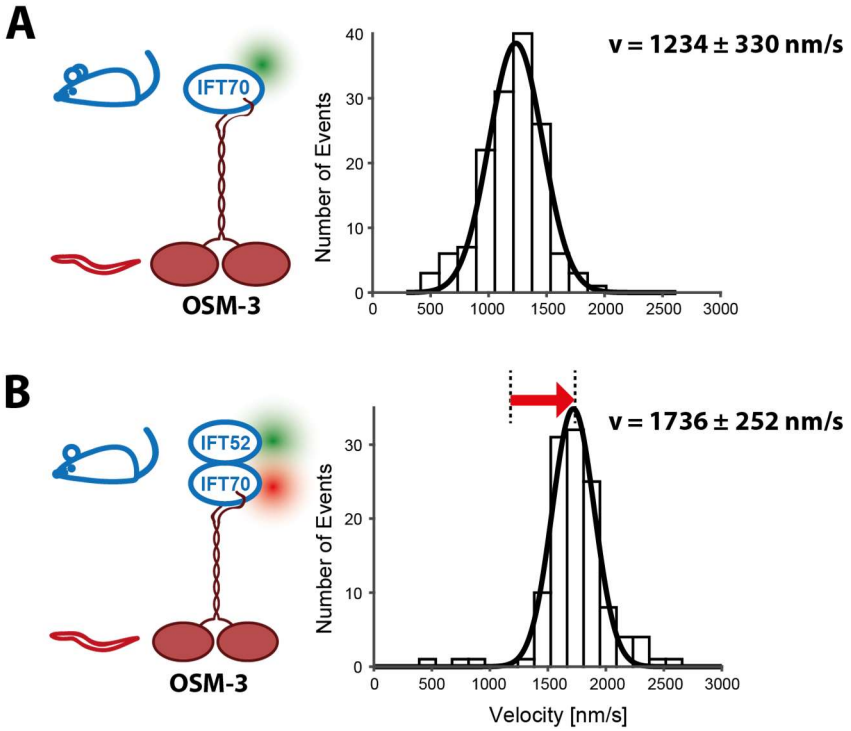

Figure 5.10: Mouse adaptor complex IFT52/70 can fully activate OSM-3 motor *in vitro* (A) IFT70^{SNAP488} can activate OSM-3 to its basal activation state (velocity= 1234 ± 330 nm/s; run length= 2.2 ± 0.4 µm, N = 145) **(B)** Moreover the presence of IFT52^{GFP} with IFT70^{SNAP647} can allosterically activate the motor to a velocity of 1736 ± 252nm/s and run length 3.0 ± 0.5 µm (N = 120) similar to that of *C.elegans* OSM-6/DYF-1 complex [131].

The interaction of IFT70 with OSM-3 invites the next obvious question if the adaptor protein is also capable of activating the motor out of its native autoinhibition state. As seen previously with the DYF-1 subunit, mouse IFT70 adaptor also relieved the autoinhibited immobile state and brought the motor to its basal activation level in functional single-molecule assays (Figure 5.10 A; Movie S5 top right panel). Now it became inquisitive, whether the OSM-3 can also be fully activated by utilizing the corresponding subunits from the mouse IFT-train. In mouse, IFT52 is the homolog for OSM-6, and as suspected, IFT70 could fully activate OSM-3 in the presence of IFT52 (Figure 5.10 B; Movie S5 bottom panels). From the functional, single-molecule assays, it becomes clear that the IFT52/70 complex had strictly retained its ability to activate the homodimeric

kinesin-2 motor. From these results, it becomes clear that the loss of function happened within KIF-17, ceding its capability to function as an active transporter in the IFT process. Since KIF-17 is an active transporter of the NMDA receptors, GluR5, and other cargoes in dendrites and also in other domains of the cytoplasm, the failure to recognize these "On-Switch" (IFT52/70 & OSM-6/DYF-1) may be the nature's way of deploying the motor for cytoplasmic transport rather than ciliary transport.

5.3.4. The "On-Switch" adaptor proteins have been highly conserved across the evolution such that swapping the adaptors did not affect the activation of OSM-3

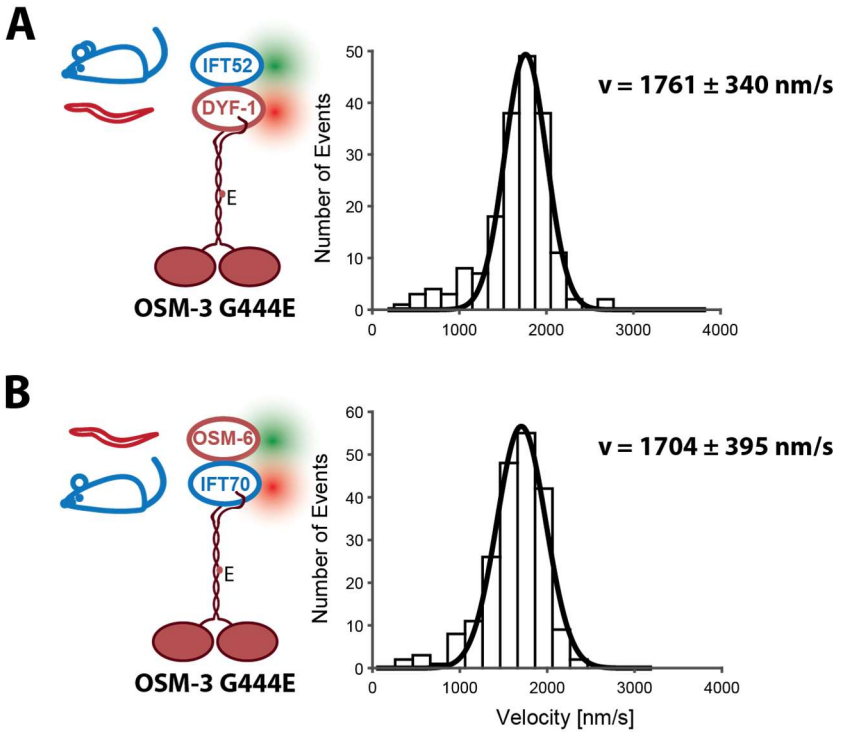

Figure 5.11: Mouse and *C.elegans* 'On –Switch' adaptor proteins are flexible in substituting for each other in functional activation of OSM-3 *in vitro*. (A) DYF-1^{SNAP647} can activate OSM-3 G444E to its fully activated state in the presence of mouse IFT52^{GFP} (velocity= 1761 ± 340 nm/s; run length= 3.4 ± 0.4 µm, N = 185) **(B)** Similarly, mouse IFT70 ^{SNAP647} could also fully activate OSM-3 G444E in the presence of *C.elegans* OSM-6^{GFP} (velocity= 1704 ± 395 nm/s; run length= 2.9 ± 0.4 µm, N = 207).

The replication of OSM-3 motor activation by the On-Switch adaptor proteins in *C.elegans* and mouse made it keen to validate the extent of the observed strict conservation between the

adaptor proteins in the functional activation of the motor. I wondered if it is possible to substitute mouse IFT52 with *C.elegans* OSM-6 in a complex with mouse IFT70 and replace OSM-6 with IFT52 in complex with DYF-1 to activate the OSM-3 motor fully. The sequence alignment of IFT70 and DYF-1 has shown the tyrosine residues critical for motor activation have been rightfully placed in the correct position, making this swapping most probable to function (Figure 5.5). As in previous experiments, I dual labeled the subunits to confirm adaptor protein's attachment during data acquisition. The complexes IFT52/DYF-1 and OSM-6/IFT70 were reconstituted with the OSM-3 G444E in functional single-molecule assays. The OSM-3 G444E motor showed the same activation pattern with mouse IFT70 and IFT52/70 as the wild type motor and since was easier in handling, was used for this assay. Remarkably as expected, IFT52/DYF-1 and OSM-6/IFT70 could efficiently activate OSM-3 to fully activation (Figure 5.11 A & B). These data explain the absolute conservation between these adaptor proteins in the functional role of activating the OSM-3 motor.

5.3.5. The functional conservation in the On-switch adaptor proteins can be retraced even back to *Chlamydomonas reinhardtii*

In *C.reinhardtii*, the homodimeric kinesin-2 motor is absent in its genome, and the heterotrimeric FLA8/10/KAP motor singularly carries out the whole IFT [73]. However, its genome expresses the conserved IFT52 and IFT70 subunits. It should be noted, that the dissection of motifs in *C.elegans* OSM-6/DYF-1 responsible for OSM-3 activation was entirely constructed from the structural data from *C.reinhardtii* IFT52/IFT70 complex [101]. The presence of the On-switch adaptors in *C.reinhardtii* invoked the curiosity of whether these corresponding adaptor proteins can also replicate the OSM-3 activation. As expected, the *C.reinhardtii* proteins could mirror the two-step activation of OSM-3 with IFT70 and IFT52/IFT70 (Figure 5.12). These results explain two aspects of IFT. The functional role of adaptor proteins in OSM-3 activation can be recalled even back to single cellular organisms. Also, IFT utilized already existing adaptor proteins in the system to craft the homodimeric OSM-3 for processive IFT in *C.elegans*.

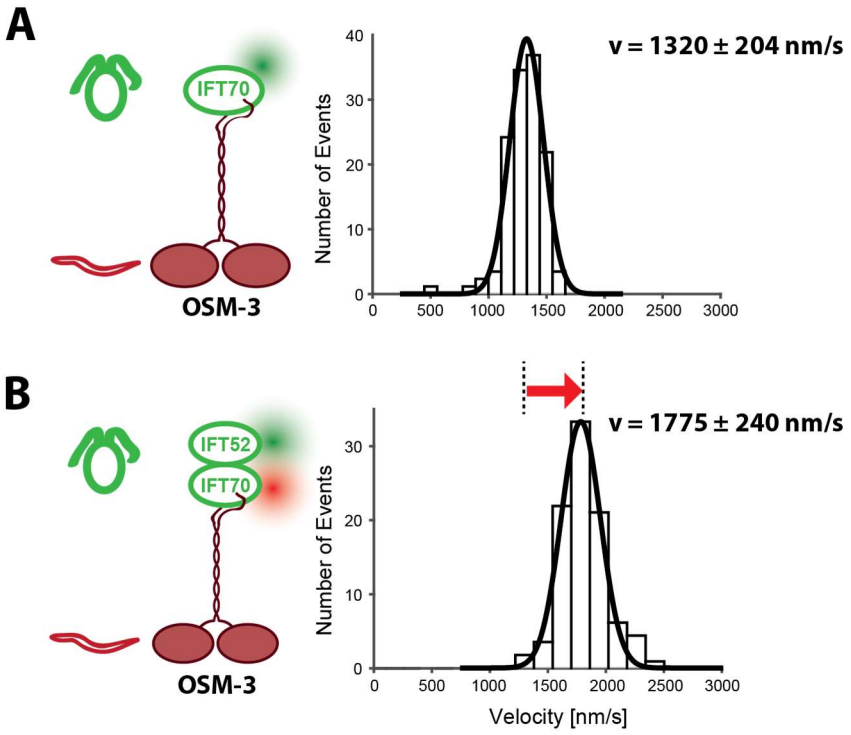

Figure 5.12: The 'On –Switch' adaptor proteins from *C.reinhardtii* can replicate the activation of OSM-3 motor equivalent to the adaptor proteins from worm and mouse. (A) *C.reinhardtii* IFT70^{SNAP488} can activate OSM-3 to its basal activation level (velocity= 1320 ± 204 nm/s; run length= 2.8 ± 0.4 µm, N = 112) **(B)** In addition, the presence of *C.reinhardtii* IFT52^{GFP} with IFT70^{SNAP647} can fully activate the motor to a velocity of 1775 ± 240nm/s and run length 3.4 ± 0.7 µm (N = 106).

5.3.6. DYF-13/DYF-6 and IFT56/46 serve as the "Off-Switch" adaptors for homodimeric kinesin-2 motors in *C.elegans* and mouse IFT

It is clear from our functional assays that the mouse KIF-17 has lost its ability to interact with IFT70, but multiple *in vivo* studies suggest that KIF-17 can enter and circulate across the cilium by the anterograde and retrograde transport [79, 97]. Even deleting the catalytic head domains did not prevent KIF-17 from entering and traveling across the mouse cilium [96]. In a recent co-immunoprecipitation study, the IFT56/46 subunits within the IFT trains were found to be critical in the entry of KIF-17 into the ciliary compartment [95]. From these cues, I decided to check the significance and relation between IFT56/46 complex and KIF-17 motor through our *in vitro* experiments. Strikingly, KIF-17 produced robust binding with IFT56/46 in colocalization assays

with a high colocalization percentage >60% (Figure 5.13 first lane). However, the interaction could not transform KIF-17 into an activated motor in single-molecule assays. After attaching to the complex, the motor remained inactive/diffusive on the microtubule surface in functional assays (Movie S6 top left panel).

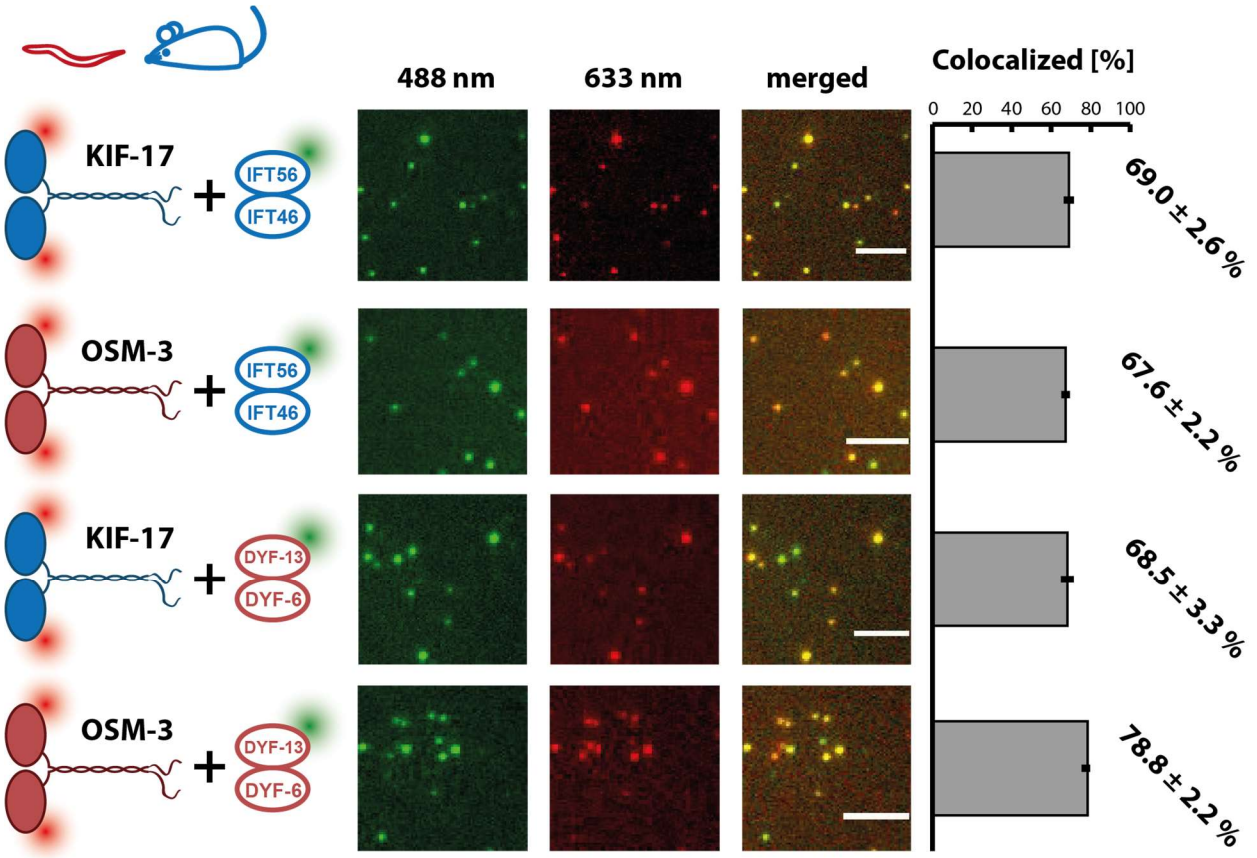

Figure 5.13: The 'Off-switch' adaptors, mouse IFT56/IFT46 and *C.elegans* DYF-13/DYF-6 efficiently interact with the homodimeric kinesin-2 motors, KIF-17 and OSM-3. (First and second lanes) Mouse KIF-17^{SNAP647} and *C.elegans* OSM-3^{SNAP647} motors (633 nm channels) bind actively with the mouse IFT46/IFT56^{Halo488} adaptor (488 nm channel) as represented by their colocalization percentages (merged channel and quantification on the right). **(Third and fourth lanes)** Similarly, both mouse KIF-17^{SNAP647} and *C.elegans* OSM-3^{SNAP647} motors (633 nm channels), interact efficiently with the *C.elegans* DYF-6/DYF-13^{SNAP488} adaptor (488 nm channel). The error bars represent the standard deviation (S.D.) from three repetitions with ten images each. Scale bar = 5 µm [131].

Remarkably, OSM-3 also inherits the conserved C-terminal amino acid sequence that grants the potent attachment between KIF-17 and IFT56/46 [95]. Hence, we asked the question, how OSM-

3 will operate with these new subunits? Notably, IFT56/46 also showed efficient binding to OSM-3 but failed to activate the motor similar to KIF-17 (Figure 5.13 second lane; Movie S6 top right panel). The *C.elegans* subunits DYF-13/DYF-6, the homologs for IFT56/46, also reproduced the same behavior as they could effectively interact with the Kinesin-2 motors (Figure 5.13 third and fourth lane) KIF-17 and OSM-3, but failed to activate them from their autoinhibited stature (Movie S6 bottom panels). In IFT, OSM-3 stays autoinhibited in its retrograde transport from the tip to the ciliary base and is carried as a passenger during the process. In the case of KIF-17, it has been in the passenger's role all along in the ciliary length. Such motor conduct means there has to be a time, where the motor should stay inactivated but remains attached to the IFT-trains. The discovery of the new exercises of OSM-3 and KIF-17 with complexes IFT-56/46 and DYF-13/DYF-6 proposes that these subunits are ideal candidates for "Off-Switch" adaptors that allow the motor to remain dormant and attached to the IFT-trains. The functional conservation existing between these subunits in *C.elegans* and mouse makes it compelling to nominate these adaptors proteins as responsible for facilitating the retrograde transport of homodimeric kinesin-2 motors in cilia.

5.4. Dissection of heterotrimeric kinesin-2 motor and subsequently generating a toolbox for investigating kinesin-II mediated conveyance in intraflagellar transport

The functional studies with OSM-3 have now given a substantial insight on to how the motor is turned on to facilitate cargo transport during the anterograde transport and how it is turned off during the retrograde transport. But major evidence in the heterotrimeric Kinesin-II mediated transport is still lacking. As mentioned earlier the heterotrimeric Kinesin-II is the sole transporter of IFT-trains in *C.reinhardtii* and mouse, but have been found to function redundantly with OSM-3 in *C.elegans* [46, 55]. Recent studies have argued that the Kinesin-II mediated transport in *C.reinhardtii* have been carried out through the IFT B complex, but intriguingly when it comes to *C.elegans* it is over the IFT A complex.

In this last part of my thesis, I tried to dissect the heteromeric motor KLP11/20 from *C.elegans* and also FLA8/10 from *C.reinhardtii* to learn the specific nature of these motors. I used TIRF single molecule assays to measure the velocity and run length to study these motors. The velocity data were fitted to a Gaussian (± width of distribution) distribution and the run length data to a single exponential fit (± confidence interval). Data were obtained from three independent protein preparations each for the study. Finally, I turned to eukaryotic expression and building of the IFT-A subcomplex in *C.elegans* by employing colocalization and SEC-MALS technique. The dissection of the heteromeric Kinesin-II and building the IFT A complex provides a new platform to unlock the intricacies in the Kinesin-II mediated IFT transport.

5.4.1. The heterotrimerization of *C.elegans* kinesin-II, KLP11/20 with KAP1 *in vitro* does not fully activate the motor to *in vivo* velocity, like its homolog in *C.reinhardtii*

The heteromeric KLP11/20/KAP1 along with OSM-3 motor build and maintain the cilia in *C.elegans* [55]. The Kinesin-II motors dock to the IFT-trains to ferry essential components from the base to the middle segment of the cilia. In previous *in vitro* studies KLP11/20 operated as an autoinhibited motor when studied alone, and mutations were required to transform it in to a robust walker [47]. Two glycine residues in the kink region of the KLP11 and KLP20 subunit were replaced with glutamate residues to eliminate the autoinhibition in the motor. It is alluring how

the autoinhibition observed in the optical trap assays for the native motor will translate on TIRF single molecule assays, which can give a sense into the kinetic parameters of the wild type motor like its velocity and run length.

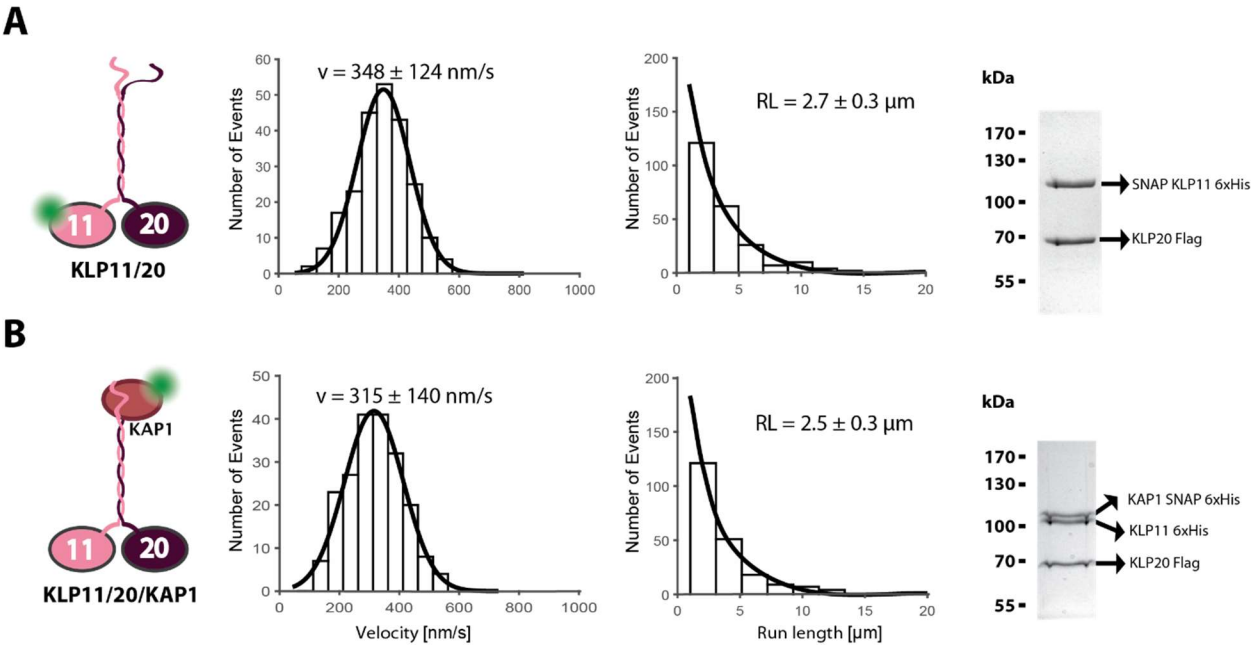

Figure 5.14: Heterotrimerization of KAP1 with KLP11/20 *in vitro* is not adequate for achieving maximum velocity as *in vivo*. (A) The wild type KLP11$^{N\text{-}SNAP488}$/20 exhibited processive movement on microtubules in single molecule TIRF assays with a velocity of 348 ± 124nm/s and run length of 2.7 ± 0.3µm (N = 229). **(B)** The heterotrimeric motor KLP11/20/KAP1^{SNAP488} also showcased a similar velocity of 315 ± 140nm/s and run length 2.5 ± 0.3µm (N = 315). The addition of KAP1 to KLP11/20 was not sufficient in lifting the velocity to its *in vivo* speed of ~500nm/s. (Right panel; A&B) The SDS-PAGE analysis of the proteins indicate efficient and stoichiometric expression of the motor proteins.

In order to have a mechanistic understanding on the autoinhibition and other characteristics, I co-expressed the motor subunits in Sf9 insect cells and did TIRF single molecule assays on the wild type motor. Fluorescent labeling was done through the SNAP tag as described in the experiments before. The KLP11/20 motors showed robust processive movement, but exhibited a lesser velocity of 348nm/sec in comparison to its *in vivo* velocity of ~500nm/sec (Figure 5.14 A). This in turn shows that KLP11/20 is unable to achieve full speed due to autoinhibition, unlike its homolog in mouse, the KIF3A/3B motor which displays maximum velocity *in vitro* even in the wild type state [89]. In *C.reinhardtii*, the heterotrimerization with the accessory KAP subunit proved to be pivotal in dissolving the autoinhibition exhibited in Kinesin-II motor FLA8/10 [38]. However

the heterotrimerization of KAP1 with KLP11/20 did not raise the velocity to ~500nm/sec but continued to stay at the lower velocity of 315nm/sec (Figure 5.14 B). It is highly possible that in the case of KLP11/20/KAP1, additional partners from the IFT-train may be necessary to attain the observed maximum velocity *in vivo*.

5.4.2. KLP11 and KLP20 catalytic domain have distinct but similar kinetic profiles

Two distinct polypeptides KLP11 and KLP20 heterodimerize to form KLP11/20 to facilitate intraflagellar transport at a velocity of ~500nm/sec *in vivo* [46]. This raises the question of whether these distinct proteins share similar kinetic properties, or do they differ significantly from each other? Similar kinetic profiles can lead to efficient coordination between the motors, while distant profiles can mean that one motor head domain is moving faster than the other, ultimately generating a limping motor. KLP11/20 did not exhibit any prominent limping behavior in optical trap assays as well as the ATP hydrolysis rate of the motor head domain of KLP11 and KLP20 have been comparable [47]. However, a recent study found that the distinct subunits display disparate dwell times in its stepping behavior when measured individually [135]. Even though this difference has been attributed to the motor's autoinhibition property, it still offers doubt whether the subunits' kinetic properties also exhibit any role in the limping behavior. Therefore it is important to get a clear-cut understanding of how these subunits behave individually.

I generated new constructs, KLP11-GCN4, and KLP20-GCN4 to investigate these motors independently. The molecular zipper GCN4 was used to dimerize the respective motor domains to eliminate any possible self-inhibitory effects conveyed by the wild-type stalk. To probe any steric hindrance arising from the dimerization, the GCN4 motif was stitched to the sequence after an additional eight wild type residues from the neck-linker region. Superfolder GFP tags were introduced in the C-terminal region for fluorescence (The design of these constructs are specified in the Supporting information 8.3). In TIRF single-molecule assays, KLP11-GCN4 moved a par with KLP20-GCN4 with comparable velocities (Figure 5.15 A vs B), indicating that both subunits display similar kinetic properties. The shorter run length of these constructs also indicates the importance of the stalk and tail domain in the motor's processivity. Thus, in compromise with the previous studies, I propose that KLP11 and KLP20 catalytic domains are equivalent in their kinetic

properties and the inherent limping displayed by the heterodimeric motor is exclusively due to the autoinhibition feature of the motor

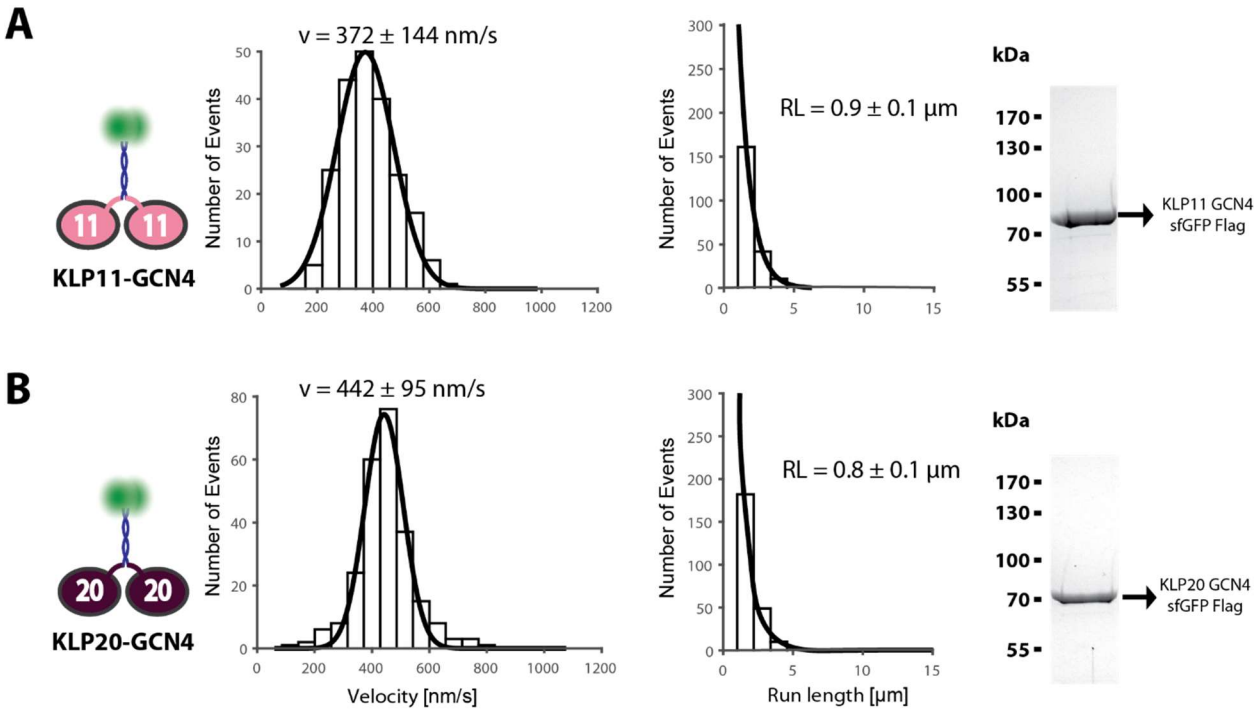

Figure 5.15: KLP11 and KLP20 are equivalent in their kinetic properties. (A) KLP11-GCN4^{sfGFP} was active in single molecule TIRF assays but aired shorter runs. The motor had a velocity of 372 ± 144nm/s and run length 0.9 ± 0.1µm (N = 217). **(B)** KLP20-GCN4^{sfGFP} too displayed a similar behavior with velocity 442 ± 95nm/s and run length 0.8 ± 0.1µm (N = 244). (Right panel; A&B) Proteins were expressed at high purity in Sf9 cells and were characterized through SDS-PAGE analysis.

Table 5.1: t- test analysis. P-values are calculated from two sample t –tests for KLP11-GCN4 against KLP20-GCN4 for velocity and run length parameters. Both velocity and run length data exhibited no significant difference between the two data sets (green) (Value >0.01).

	KLP11 GCN4 Vs KLP20 GCN4
Velocity	0.0178
Run length	0.8972

5.4.3. The autoinhibition in KLP11/20 can be due to a direct inhibitory effect of the motor's C-terminal domain, interacting with the KLP11 catalytic domain.

Brunnbauer et al. (2010) [47] have ratified that the autoinhibition in KLP11/20 will function only when motors' catalytic domains are rightfully placed in the wild type position. Switching the head domains relieves the autoinhibition. Moreover, the KLP20/20 chimera, generated from replacing the KLP11 head domain with the KLP20 catalytic domain, is a robust motor while the KLP11/11 chimera, synthesized from replacing the KLP20 head domain with the KLP11 head domain is a non-processive motor. This indicates that the presence of KLP11 in its correct position is essential for building up a regulatory function in KLP11/20. Stepp.et.al (2019) [135] shows that even in the activated $KLP11^{EE}/20^{EE}$ motor, the KLP11 subunit is subjected to autoinhibitory effects as its dwell time distribution in optical trapping assays is formed from merging of two exponential fits rather than a single exponential distribution as observed in KLP20. I wondered whether the activated motor's autoinhibitory effect could also be replicated in TIRF single-molecule assays.

For this purpose, I did single-molecule assays on distinct kinesin-II motor chimeras, as illustrated in Figure 5.16 (Supporting information 8.3). All the motor subunits were in the activated stalk domain form with point mutations in KLP11 on G451, 452E, and in KLP20 with G444, 445E to observe noticeable effects. The chimeras were constructed as in the previous study, and fluorescent labeling was done through SNAP tags. The activated $KLP11^{EE}/20^{EE}$ motor displayed a velocity of ~415nm/sec, comparable to *in vivo* velocity (Figure 5.16 A). In stark contrast, the $KLP11^{EE}/11^{EE}$ chimera moved with a reduced velocity of ~279nm/sec, and even the run length of the motor crashed down to ~1µm/sec (Figure 5.16 B). On the other hand, the $KLP20^{EE}$ $/20^{EE}$, as well as $KLP20^{EE}$ $/11^{EE}$ SW chimera, produced similar velocity and run length profiles to the $KLP11^{EE}$ $/20^{EE}$ motor (Figure 5.16 C, D). The drop in velocity and run length of $KLP11^{EE}$ $/11^{EE}$ to $KLP11^{EE}/20^{EE}$ has been significant in t-tests analysis (Table 5.2)

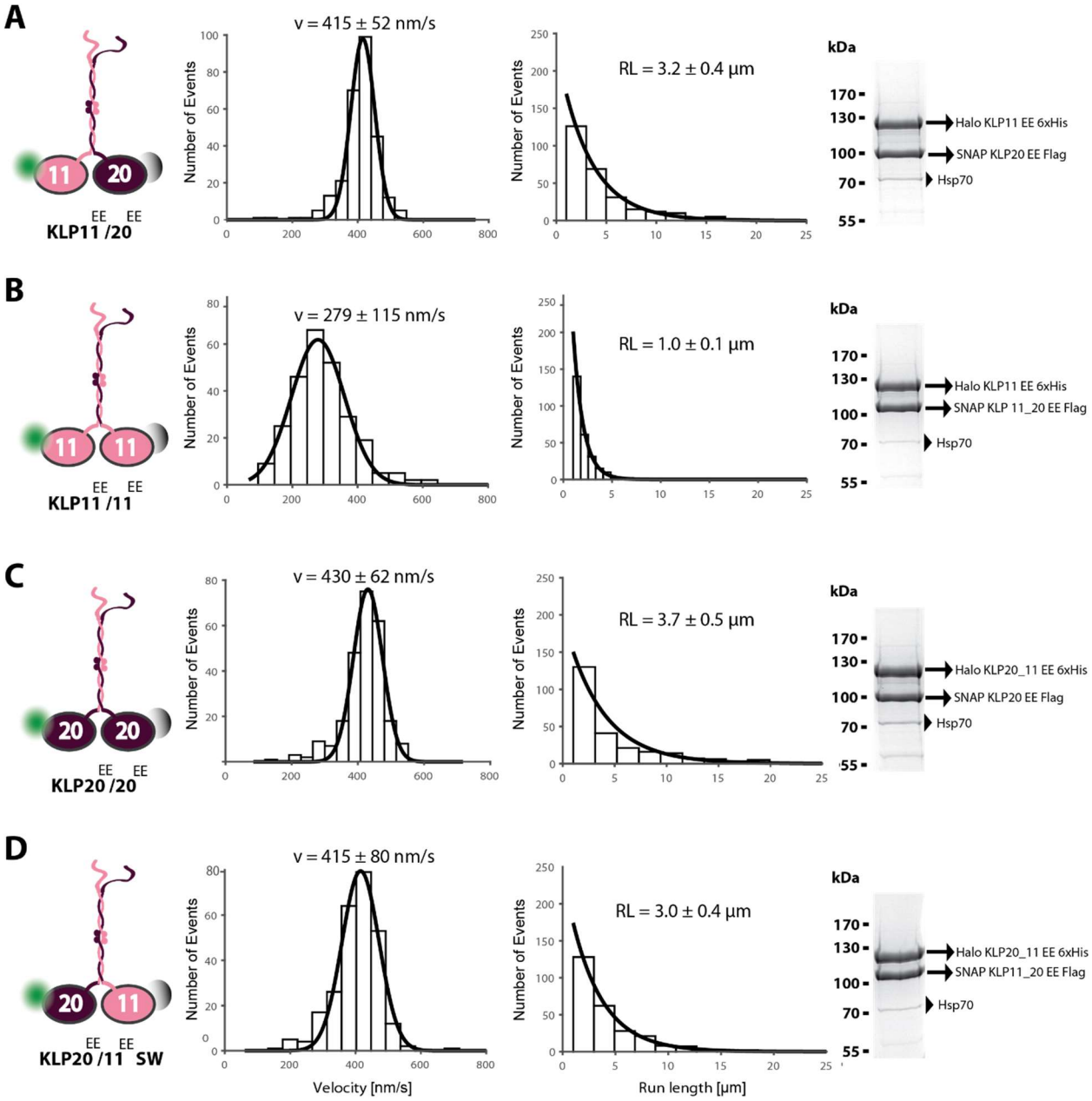

Figure 5.16: The presence of the second KLP11 head domain in KLP11^{EE}/11^{EE} chimera diminishes the activation provided by point mutations. (A) The activated KLP11$^{EE\ N\text{-}Halo488}$/20$^{EE\ N\text{-}SNAPunlabeled}$ was able to achieve a velocity of 415 ± 52nm/s which is comparable to the *in vivo* velocity and displayed run length of 3.2 ± 0.4µm (N = 274) as observed in previous studies. **(B)** However the KLP11$^{EE\ N\text{-}Halo488}$/11$^{EE\ N\text{-}SNAPunlabeled}$ chimera showcased a restrained processive movement with velocity 279 ± 115nm/s and run length 1.0 ± 0.1µm (N = 261). **(C)**, **(D)** The KLP20$^{EE\ N\text{-}Halo488}$/20$^{EE\ N\text{-}SNAPunlabeled}$ and KLP20$^{EE\ N\text{-}Halo488}$/11$^{EE\ N\text{-}SNAPunlabeled}$ SW chimeras were active and expressed similar kinetic behavior to the control KLP11^{EE}/20^{EE} motor with velocities 430 ± 62 nm/s & 415 ± 80 nm/s and run lengths 3.7 ± 0.5µm & 3.0 ± 0.4µm (N = 243;260) respectively. (Right panel; A, B, C & D) The SDS-PAGE analysis of the purified proteins demonstrates

efficient and stoichiometric expression of the motor proteins. HSP70 protein was commonly expressed along with the target proteins due to the overexpression in Sf9 cells.

Earlier, it was hypothesized that the loss of processivity in the KLP11^{EE}/11^{EE} chimera might be due to a specific steric effect between the catalytic head domains, which prevents the motor from swinging past each other or perhaps a result of direct inhibitory interaction between the two KLP11 heads [47]. The KLP11-GCN4 data from Figure 5.15A disapprove these theories. Strikingly there is a possibility that this decreased inactivity results from inhibitory binding of the C-terminal region of the motor protein to the KLP11 head domain. Indeed the C-terminal domain of KLP20 motor subunit interacts with the catalytic head domain of KLP11 in co-expression pull-down assays [91]. The proper positioning of KLP11 in the heterodimeric motor is essential for regulatory autoinhibition, but the presence of a second KLP11 head domain can produce an added effect to the degree of auto-inhibition. Here in KLP11^{EE}/20^{EE}, the KLP11 head domain is in its wild type position, but we have eliminated the autoinhibition by introducing point mutations. The second KLP11 head domain in the KLP11^{EE}/11^{EE} chimera effectively screened the activation brought forward by these point mutations. This additional effect of autoinhibition can be observed in the TIRF experiments. Therefore, I propose that the autoinhibition observed in KLP11/20 is a direct inhibitory effect of the motor's C-terminal domain, interacting with the KLP11 catalytic domain. Also taking in to account the functional data of KLP11-GCN4, we can affirm that KLP11 is not a non-processive motor as viewed earlier but the non-processivity observed in KLP11^{EE}/11^{EE} chimera is a repercussion of the inhibition by the C-terminal domains of KLP11/20.

Table 5.2: t- test analysis. P-values are calculated from two sample t –tests for KLP11^{EE} /11^{EE}, KLP20^{EE} /20^{EE} and KLP20^{EE} /11^{EE} SW in comparison with the KLP11^{EE} /20^{EE} for both velocity and run length. KLP11^{EE} /11^{EE} data showed statistically significant variation from the control (orange) (value <0.01) while P- values of KLP20^{EE} /20^{EE} and KLP20^{EE} /11^{EE} SW exhibited no significant difference between the two data sets (green).

	KLP11^{EE}/11^{EE}	KLP20^{EE}/20^{EE}	KLP20^{EE}/11^{EE} SW
Velocity	3.2873e-11	0.0156	0.4368
Run length	1.5097e-09	0.0141	0.6937

5.4.4. Neck linker does not have a decisive impact on the processivity of heterodimeric KLP11/20 in comparison to Kinesin-1

Kinesin motors' catalytic domain is attached to the coiled-coil stack domain through a short stretch of amino acids called the neck linker. Neck linker sequences are highly conserved across the Kinesin superfamily, and they play a significant role in converting the chemical energy released through ATP hydrolysis into processive steps [20]. They have been found to act as a lever, which generates force upon ATP binding to the catalytic domain, in the Kinesin-1(hereafter, Kin-1) motor.

The primary role of KLP11/20 in the intraflagellar transport of *C.elegans* has been proposed to carry the IF-trains from the cytoplasm across the transition zone to the ciliary compartment [85]. In such a case, KLP11/20 must be programmed to specialize in navigating roadblocks and other obstacles across the microtubule surface. Besides, the neck linker region plays a critical role in surpassing microtubule-associated protein (MAPS) in kinesins [136]. The longer neck linker provides an advantage to Kinesin-2 in tackling these obstructions compared to Kin-1. Also, the length of the neck linker has been optimized for maximum processivity. Extension of the neck linker leads to reduced processivity, which has been proposed to resulting from the lag in the strain-dependent detachment of the rear head and a decrease in the strain-dependent inhibition of ATP binding [137]. In Kin-1, extending the neck linker by one residue can hamper the motor's processivity to a great extent. Hence, I asked how the heterodimeric KLP11/20 will adapt to an extension in neck linker length. Will, there be an effect on the velocity and run length of the motor, and even if there is a difference, what is the degree of the impact of such extension.

I introduced 8x GS repeats (16 amino acid residues) directly after the neck linker (Figure 5.17; Supporting information 8.3) in KLP11 and KLP20. Fluorescent labeling was done through corresponding N-terminal Halo tags in the KLP11 subunit. TIRF single-molecule assays were carried in different combinations, as shown in Figure 5.17, to study the neck linker's influence in KLP11/20. All constructs were in the activated stalk form as done previously, with KLP11^{EE}/20^{EE} as a control for these experiments. In all three constructs; KLP11^{EE} 8xGS /20^{EE}, KLP11^{EE} /20^{EE} 8xGS, and KLP11^{EE} 8xGS/20^{EE} 8xGS the velocity got reduced to ~320nm/sec from 415nm/sec, but did

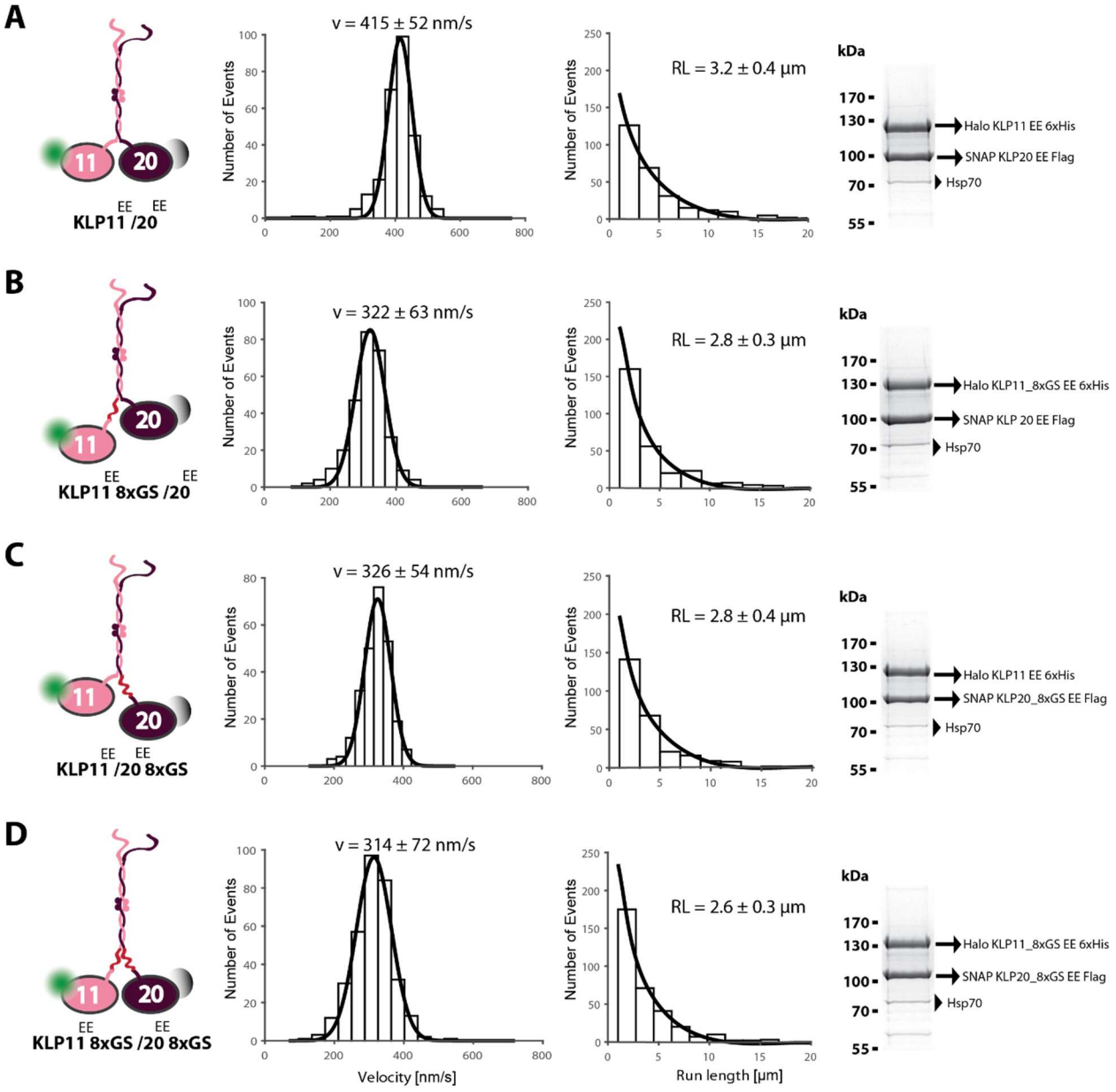

Figure 5.17: The extension of neck linker in Kinesin-2; KLP11/20 have minor effect on its processivity. **(A)** The control KLP11$^{EE\ N\text{-}Halo488}$/20$^{EE\ N\text{-}SNAPunlabeled}$ moved with a velocity of 415 ± 52nm/s and run length 3.2 ± 0.4µm (N = 274) again. **(B)** & **(C)** KLP11$^{EE\ N\text{-}Halo488}$ 8xGS/20$^{EE\ N\text{-}SNAPunlabeled}$ and KLP11$^{EE\ N\text{-}Halo488}$/20$^{EE\ N\text{-}SNAPunlabeled}$ 8xGS, where the neck linker of only one of the subunit in the motor complex was extended by a insertion of 8xGS, the velocity of the motor dropped to 322 ± 63 nm/s and 326 ± 54 nm/s respectively, but the run length remained close to the control value at 2.8 ± 0.3µm and 2.8 ± 0.4µm (N = 279; 266). **(D)** Even in the case of KLP11$^{EE\ N\text{-}Halo488}$ 8xGS/20$^{EE\ N\text{-}SNAPunlabeled}$ 8xGS, where there is addition of residues on both the subunits, the motor continued to express equivalent run length of 2.6 ± 0.3 µm, while the velocity remained at 314 ± 72 nm/s (N = 332). (Right panel; A, B, C & D) SDS-PAGE analysis of the motor proteins show efficient pull down of His-tagged proteins by flag-tagged proteins through flag purification. HSP70

protein was commonly expressed along with the target proteins because of the overexpression in Sf9 cells.

not have any significant effect on the run length of the motors (Figure 5.17. A vs B, C & D). Even though there is a considerable reduction in the velocity, the decrease is only by ~25% upon adding 16 amino acid residues on each subunit (Table 5.3, Figure 5.17). Moreover, there was no effect on these constructs' run length, while the run length of Kin-1 succumbed to less than 50% upon adding a single residue [137]. These results imply that heterodimeric KLP11/20 is a more stable motor compared to Kin-1 in maintaining the strain-dependent co-ordination in the chemo-mechanical ATPase cycle. The capacity to adapt to the increase in neck linker length might be an evolutionary advantage that Kinesin-2 has acquired along to aid in crossing the obstacles efficiently across the microtubule surface.

Table 5.3: t- test analysis. P-values are calculated from two sample t –tests for KLP11^{EE} 8xGS /20^{EE}, KLP11^{EE}/20^{EE} 8xGS and KLP11^{EE} 8xGS /20^{EE} 8xGS in comparison with the KLP11^{EE} /20^{EE} for both velocity and run length parameters. All the three construct showed significant variation from the control in the velocity data (orange) (value <0.01), while the run length data exhibited no significant difference between the two data sets (green).

	KLP11^{EE} 8xGS/ 20^{EE}	KLP11^{EE}/ 20^{EE} 8xGS	KLP11^{EE} 8xGS/ 20^{EE} 8xGS
Velocity	2.3392e-09	4.8231e-05	7.7854e-07
Run length	0.3774	0.3201	0.1748

5.4.5. The stability in strain dependent co-ordination between the KLP11 and KLP20 motor subunit in KLP11/20 is independent of its neck linker

The striking difference in the ability to respond, to the strain-dependent co-ordination between the motor heads in Kin-1 and KLP11/20, can be due to the inherent property of their catalytic domain or a function of their neck linker. From the previous study, it is known that manipulating the neck-linker in KLP11/20 did not produce an extensive impact on its processivity. Now it is intriguing if this response is because of its innate ability of the head domain or due to the specialization developed by the neck linker in corresponding with its ability to transverse blocks smoothly on the microtubule surface.

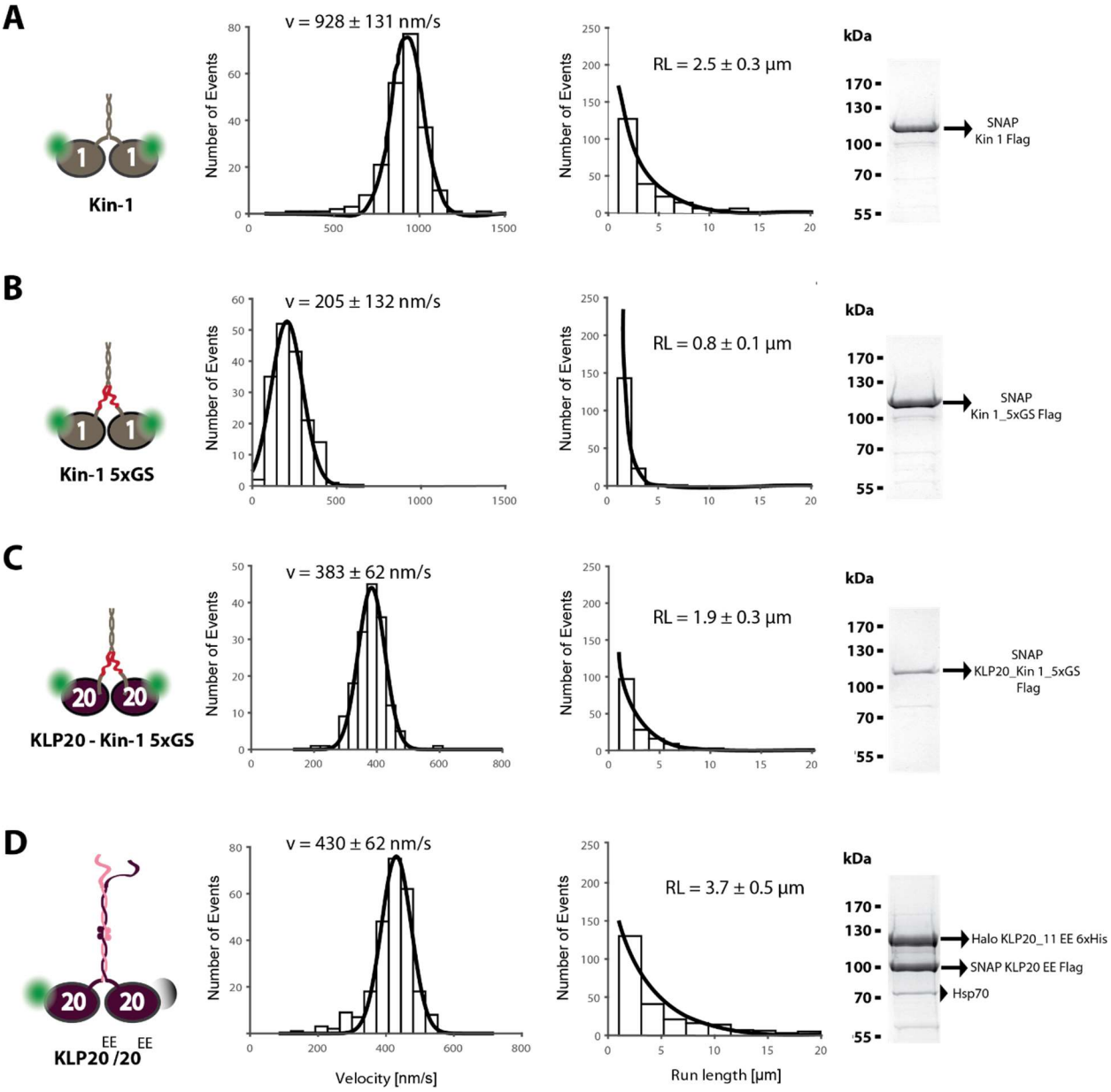

Figure 5.18: The processivity of KLP20 is unaltered by replacing the wild type neck linker with the neck linker from Kin-1. (A) vs **(B)** Kin-1 processivity is greatly hindered by changes in the neck linker. The wild type kin-1 was highly processive with a velocity of 928 ± 131nm/s and run length 2.5 ± 0.3µm. The insertion of 5x GS to Kin-1 suppressed its ATPase activity and abated the velocity to 205 ± 132nm/s and run length to 0.8 ± 0.1µm (N = 218; 170). **(C)** vs **(D)** The replacement of KLP20 neck linker with the stretched Kin-1 neck linker in KLP20-Kin-1 5xGS did not hamper the processivity of KLP20, and was able to sustain a velocity of 383 ± 62nm/s and run length 1.9 ± 0.3µm (N = 160) when compared to the $KLP20^{EE\ N\text{-}Halo488}/20^{EE\ N\text{-}SNAPunlabeled}$ chimera (velocity = 430 ± 62 nm/s; run length = 3.7 ± 0.5µm; N = 243 replotted from Figure 5.16 C for direct comparison). (Right panel; A, B, C & D) The SDS-PAGE analysis of the purified proteins showcased efficient expression of motor proteins in Sf9 cells.

To answer this question, I developed a chimera with the KLP20 head domain followed by the Kin-1 neck linker and stalk domain with an insertion of 5xGS right after the neck linker, (Figure 5.18 C; supporting information 8.3) As a control for the study, Kin-1 and Kin-1 5xGS constructs were made similar for direct comparison. The Kin-1 constructs were truncated (1-560 amino acid residues) following past studies [17]. TIRF experiments were conducted via fluorescent labeling of the constructs through SNAP tags. Kin-1 motor was active and showed processive movement with a velocity of ~928nm/s and a run length of ~2.5µm while the addition of 5xGS to the neck linker in Kin-1 5xGS curtailed the velocity and run length by almost 4X to ~205nm/s and 0.8µm (Figure 5.18 A & B, Table 5.4). In stark contrast, the velocity of KLP20-Kin-1 5xGS was equivalent to that of the $KLP20^{EE}/20^{EE}$ construct at ~383nm/sec (Figure 5.18 C vs D, Table 5.4). It would not be possible to directly compare the run length, since the wild type C-terminal domain of KLP20 is replaced with the Kin-1 C-terminal domain. Still, a direct one to one comparison can be made in terms of the velocity data, which means that even replacing the neck linker from Kin-1 to KLP20 did not diminish its activity, justifying the hypothesis that the neck linker is not a major factor in determining the processivity of the KLP11/20 motor. Otherwise, KLP11/20 has achieved an evolutionary advantage over Kin-1, which helps it to overcome severe alterations made in the neck linker domain.

Table 5.4: t- test analysis. P-values are calculated from two sample t –tests for Kin-1 against Kin-1 5XGS and for KLP20- Kin-1 5xGS against $KLP20^{EE}/20^{EE}$ regarding their kinetic parameters. Both velocity and run length data exhibited significant difference between the two data sets (orange) (Value <0.01) of Kin-1 and Kin-1 5xGS. However, KLP20- Kin-1 5xGS and $KLP20^{EE}/20^{EE}$ did not display any significant difference in the velocity data in their respective sample t-tests.

	Kin-1 Vs Kin-1 5xGS	**KLP20- Kin-1 5xGS Vs $KLP20^{EE}/20^{EE}$**
Velocity	3.5672e-15	0.0236
Run length	2.3572e-07	

5.4.6. The C-terminal tail domain of KLP11 and KLP20 subunits does not play a major role in ensuring the processivity of KLP11/20

The C-terminal tail domain has been widely speculated in handling a primary role in the processivity of Kinesins. From the previous experiments itself, we have seen the KLP20-GCN4 construct had a low processivity while the KLP20/20, which contains the wild type stalk and C terminal tail domain, showcased greater processivity. In the *X.laevis* KIF3A/3B, the C-terminal tail domain of KIF3A is directly responsible for the attachment of KAP3 to the heterodimeric motor, while the KIF3B polypeptide is dispensable for KAP3 binding (unpublished data from Georg Merck). Nonetheless, KIF3B's tail is vital in establishing the processivity in KIF3A/3B, although KIF3A does not play any role in it [89]. This differential property in the KIF3A/3B tails makes it intriguing to investigate if typical features are also present in its *C.elegans* homolog KLP11/20. In *C.elegans*, notably, the C-terminal regions of both KLP11 and KLP20 are crucial for KAP1 binding to the KLP11/20 motor. Removing the tail domain of KLP11 or KLP20 can disengage the KAP subunit from the KLP11/20 motor [47].

To unmask the tails' features in KLP11/20, I made truncation constructs by chopping off the KLP11 and KLP20 tails after a highly conserved 'FIP' motif (Figure 5.19, supporting information 8.3). TIRF experiments were conducted with different combinations with the made constructs. Curiously, there were no recommendable changes in the velocity or run length, when the tails of KLP11 and KLP20 were removed separately or in conjugation (Figure 5.19). T-test analysis signified the minimal decrease in the run length observed in the constructs to be trivial (Table 5.5). Thus we can witness one more differential characteristic in the functions of tail domains of KLP11/20 and KIF3A/3B, where one of the tail domain in KIF3A/3B, is central in ensuring the processivity, while none of the tail domains in KLP11/20 is primarily essential for the processivity of the motor. These studies explain how these motors have evolved to be highly conserved in their domain of action, still extremely different in their properties.

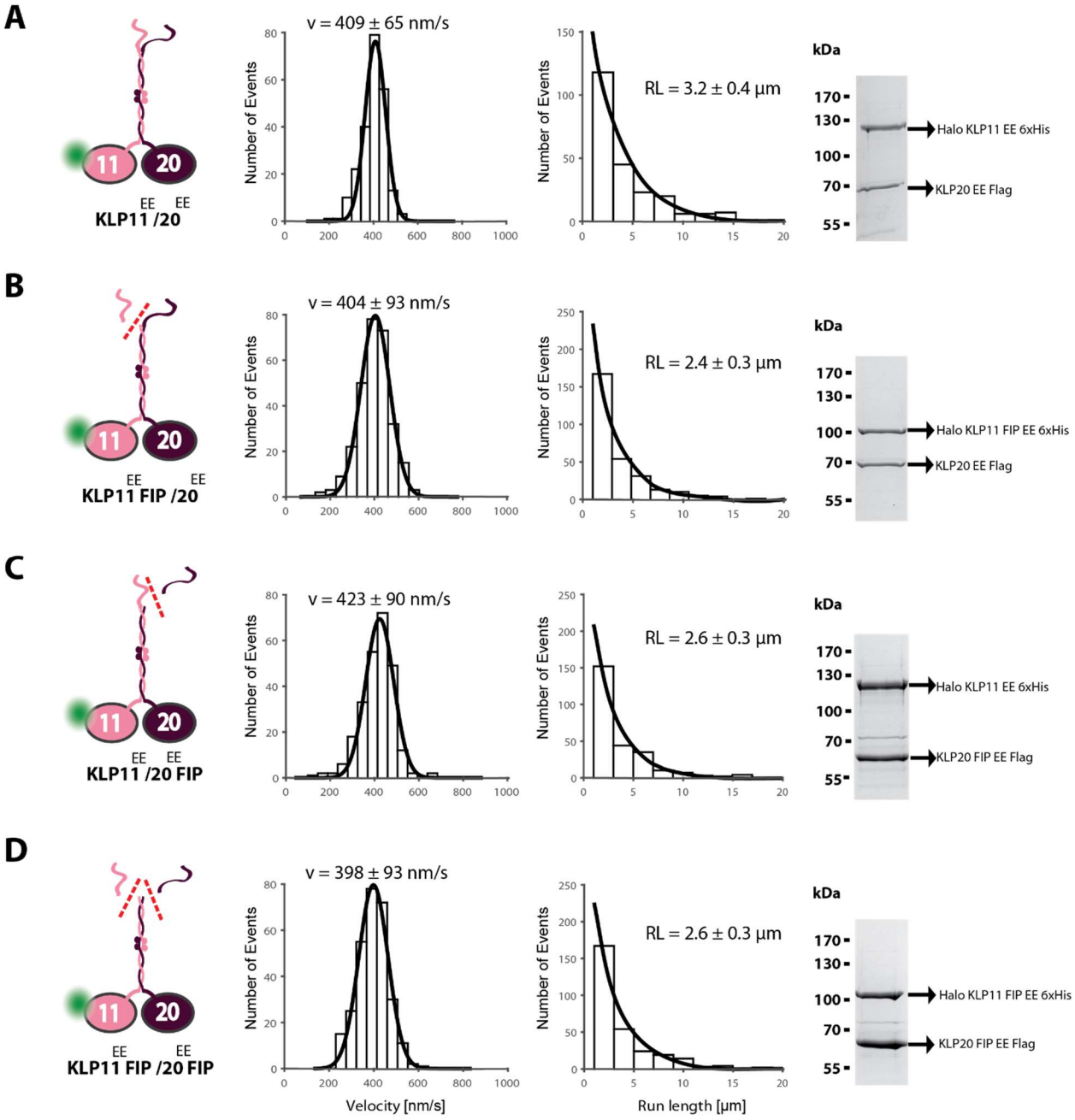

Figure 5.19: The processivity of KLP11/20 is independent of its C-terminal tail domains. (A) The control KLP11$^{EE\ N\text{-}Halo488}$/20^{EE} was active in TIRF single molecule assays with velocity 409 ± 65 nm/s and run length 3.2 ± 0.4µm (N = 224). **(B), (C)** & **(D)** The truncation constructs made by eliminating the tail domains were equivalent in their kinetic action to the KLP11$^{EE\ N\text{-}Halo488}$/20^{EE} motor. Their velocity and run length figures are 1) KLP11$^{EE\ N\text{-}Halo488}$ FIP/20^{EE}: 404 ± 93 nm/s & 2.4 ± 0.3µm (N = 285); 2) KLP11$^{EE\ N\text{-}Halo488}$/20^{EE} FIP: 423 ± 90nm/s & 2.6 ± 0.3µm (N = 257); 3) KLP11$^{EE\ N\text{-}Halo488}$ FIP/20^{EE} FIP: 398 ± 93 nm/s & 2.6 ± 0.3 µm (N = 287). (Right panel; A, B, C & D) The SDS-PAGE analysis of the purified proteins reveals robust and stoichiometric expression of the motor proteins.

Table 5.5: t- test analysis. P-values are calculated from two sample t –tests for KLP11^{EE} FIP/20^{EE}, KLP11^{EE}/20^{EE} FIP and KLP11^{EE} FIP /20^{EE} FIP in comparison with the KLP11^{EE} /20^{EE} motor for both velocity and run length data. Both velocity and run length parameters exhibited no significant difference between the two data sets for all the three constructs analyzed (green) (Value >0.01).

	KLP11^{EE} FIP/ 20^{EE}	KLP11^{EE}/ 20^{EE} FIP	KLP11^{EE} FIP/ 20^{EE} FIP
Velocity	0.5447	0.369	0.1642
Run length	0.030	0.124	0.096

5.4.7. Kinesin-2 from *C.reinhardtii* is an atypically fast and autoinhibited motor

Despite the early discovery of intraflagellar transport in *C.reinhardtii*, no significant studies have been done *in vitro* to understand the mechanistic properties of heterodimeric Kinesin-2: FLA8/10 that is involved in ferrying the IFT trains from the ciliary base to the tip. The IFT-trains in *C.reinhardtii* have been observed to be travel at a velocity of ~2000nm/sec in the anterograde transport [69]. Intriguingly all the heterodimeric kinesin-2 motors studied so far from diverse model organisms move 4-fold slower, both *in vivo* and *in vitro* except the case *Trypanosoma brucei* which displays an anterograde velocity of 2-3µm/sec [55]. In such case, it is essential to verify if this high velocity observed in the anterograde IFT of *C.reinhardtii*, is coming from the inherent velocity of FLA8/10 or a result of the combined effects of the multiple motors in the IFT-train.

I coexpressed FLA8 and FLA10 subunits using flag purification in this regard. In functional single-molecule assays, the heterodimeric FLA8/10 motors were processive on microtubule filaments but exhibited two velocity populations at ~2000nm/sec and ~750nm/sec (Figure 5.20 A). The higher velocity in the distribution is comparable to the *in vivo* velocity of *C.reinhardtii* anterograde IFT-trains, implying that the heterodimeric FLA8/10 motors can singularly attain the atypically fast speed as displayed *in vivo*. However, most of the native FLA8/10 motors exist in the slower velocity distribution, hinting that an autoinhibition might also exist in the *C.reinhardtii* Kinesin-II, restricting the motors from utilizing its full ATPase capacity [38].

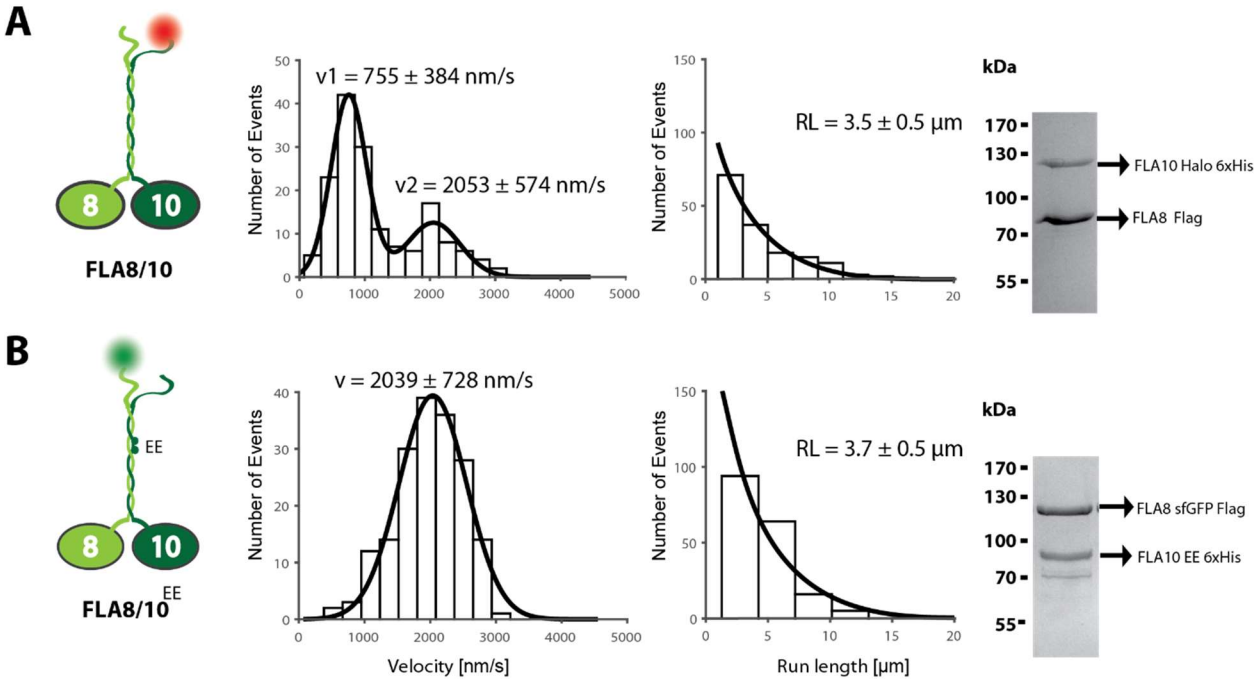

Figure 5.20: The autoinhibition in FLA8/10 can be resolved by introducing point mutations G515E/G516E in the FLA10 subunit. (A) The wild type FLA8/10^{Halo647} is autoinhibited and displayed two Gaussian distributions for velocity, one at 755 ± 384nm/sec and the other at 2053 ± 574 nm/s and run length of 3.5 ± 0.5µm (N = 158). **(B)** Introduction of point mutations G515E/G516E in the FLA10 stalk domain eliminated the lower velocity population of FLA8/10, to feature a single Gaussian distribution for velocity at 2039 ± 728 nm/sec in FLA8^{sfGFP}/10^{EE} (run length = 3.7 µm) (N = 179). (Right panel; A & B) SDS-PAGE analysis of the *C.reinhardtii* motor proteins indicate efficient heterodimerization of the distinct subunits [38].

From the studies conducted so far on the autoinhibition mechanism in the kinesin motors, it is highly probable the autoinhibition in FLA8/10 results from the folding back of the C-terminal tail domain on to the catalytic head domains in the motor. In *C.elegans* Kinesin-2 motors, KLP11/20 and OSM-3, the inherent autoinhibition could be eliminated by replacing the flexible glycine residues in the kink region with glutamates, which subsequently activates the motors *in vitro*. The glutamate residues are proposed to prevent the tails from folding back to the head domain. Examining the amino acid sequences of the FLA8 and FLA10 subunits revealed that they also possess these conserved glycine residues. But in coiled-coil predictions, the glycine residues can install prominent helix breakers in the coiled-coil domain of FLA10 alone but not to the FLA8 subunit. Still, the replacement of glycine residues at 515 & 516 to glutamates in FLA10 reduces the propensity to form a helix breaker in FLA10 and forms a continuous coiled-coil [38]. In functional single-molecule TIRF assays, this replacement was enough to remove the slow-velocity

population of the wild-type FLA8/10 (Figure 5.20 B). Considering the similar nature of FLA8/10 to KLP11/20 and OSM-3, I propose that the respective motor is also autoinhibited through the autoinhibitory folding of tail/stack domains to the head domain similar to other kinesin family motors [38].

5.4.8. The kinetic properties of FLA8/10 is encoded in the catalytic head domain of the motor

The catalytic head domains of Kinesin-2 motors have been well conserved across the kinesin superfamily. However, there is a striking difference in the speed of single-celled *C.reinhardtii* (2,000 nm/s) and multicellular organisms like mouse and *C.elegans* (~500 nm/s) [55]. In order to obtain a mechanistic explanation for this difference, I tried to find the domain responsible for the observed kinetic differences in the Kinesin-2 motor, between the individual model organisms. For the study, different chimeras were made wherein one, the head domains of the slower KLP11/20 heterodimer was replaced with the corresponding faster FLA10 and FLA8 head domains (FLA8/10$^{KLP\ tails}$), and in second, the FLA8 and FLA10 catalytic domains in FLA8/10 were substituted with the slower KLP11 and KLP20 head domains (KLP11/20$^{FLA\ tails}$). In others, only one of the head domain of KLP11/20 was replaced with FLA8 or FLA10 (FLA10/KLP20$^{KLP\ tails}$ & KLP11/FLA8$^{KLP\ tails}$) (Figure5.21, supporting information 8.3). The constructs were designed with SNAP tags for fluorescent labeling.

The chimera Fla8/10$^{KLP\ tails}$ were able to display robust processive movement in functional single molecule assay with a velocity greater than 1850 nm/s (Figure 5.21 A). Similarly, in the KLP11/20$^{FLA\ tails}$ chimera, where the faster FLA8 and FLA10 catalytic domains are replaced with the slower KLP11 and KLP20 head domains, the velocity distribution was identical to that of wild type KLP11/20 motor (Figure 5.21 B). Moreover, FLA10/KLP20$^{KLP\ tails}$ & KLP11/FLA8$^{KLP\ tails}$ chimeras exhibited intermediate velocities rather than maintaining slow (~300 nm/s) or fast (~2,000 nm/s) velocities (Figure 5.21 C & D). From these results, we can infer that the catalytic heads and not the stalk or tail domains are the sole responsible factor in providing the atypically fast velocity in *C.reinhardtii* IFT-trains [38].

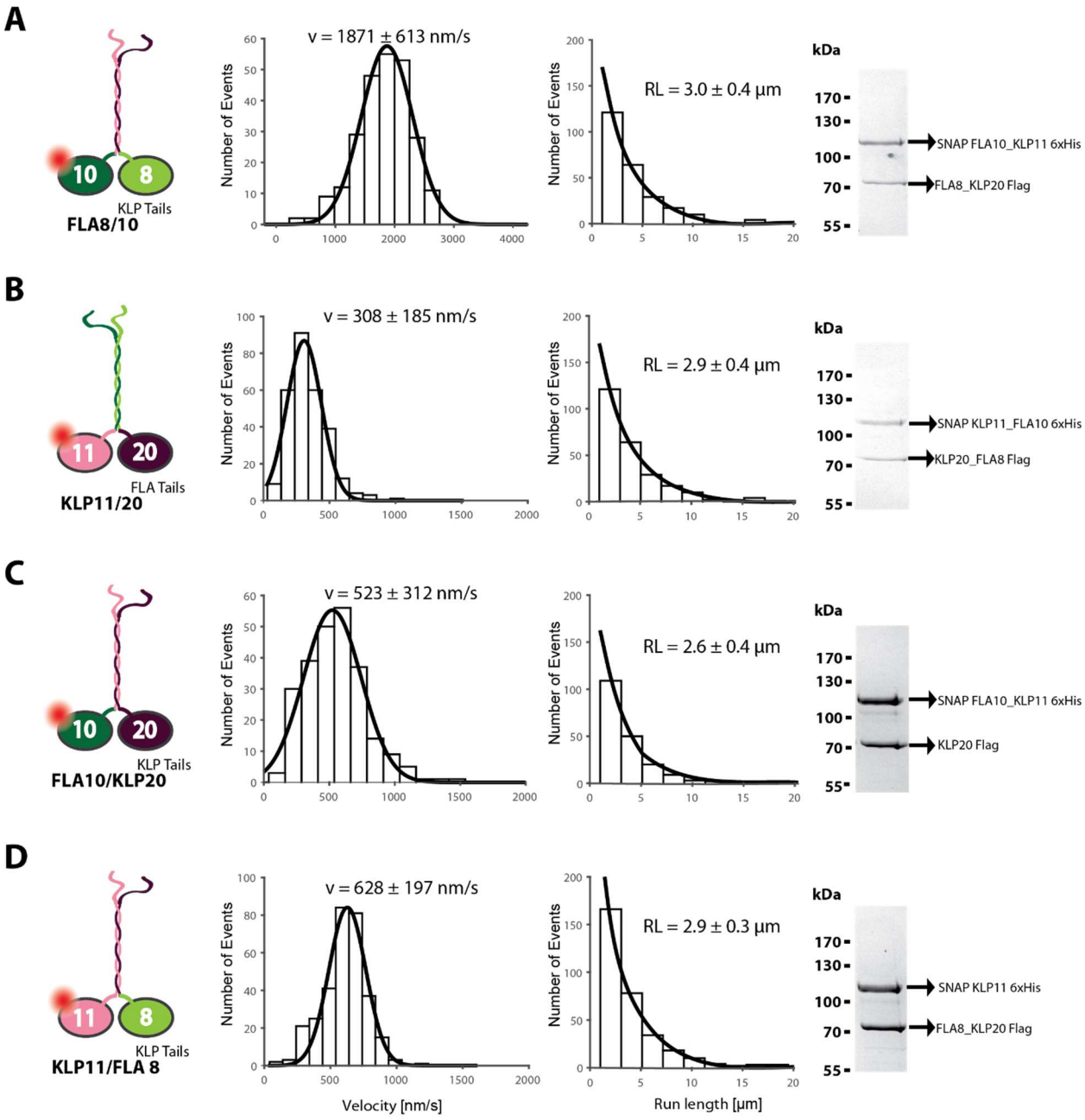

Figure 5.21: The catalytic head domains dictate the velocity parameter in heterodimeric kinesin-2 motors, KLP11/20 and FLA8/10. (A) FLA8/10$^{N\ SNAP647}$ (KLP tails) was able to showcase maximum velocity after being forced to travel with the stalk and tail domains from KLP11/20 (Velocity = 1871 ± 613 nm/s; run length = 3.0 ± 0.4 µm; N = 248) **(B)** Nevertheless, even after earning the stalk and tail domain from the fast FLA8/10 motor did not increase the velocity of KLP11$^{N\ SNAP647}$/20 (FLA tails) from its wild type velocity (Velocity = 308 ± 185nm/s, run length = 2.9 ± 0.4µm; N = 279). **(C)** & **(D)** Intermediate chimeras, FLA10$^{N\ SNAP647}$/KLP20 (KLP tails) and KLP11$^{N\ SNAP647}$/FLA8 (KLP tails) moved with parameters; Velocity = 523 ±

312nm/s, run length = 2.6 ± 0.4µm and Velocity = 628 ± 197nm/s, run length = 2.9 ± 0.3µm (N = 196; 318), proposing that when a slow and fast head walks together, they both compromise to provide an intermediary velocity. (Right panel; A, B, C & D) The SDS-PAGE analysis of the purified proteins indicates robust and stoichiometric expression of the motor proteins.

5.4.9. The autoinhibition in FLA8/10 is abolished by replacing the FLA10 head domain with the FLA8 head domain

The latest results from dissecting the KLP11/20 motor prompted us to analyze whether any specific characteristics displayed by the *C.elegans* Kinesin-II motor can also be showcased by the FLA8/10 motor from *C.reinhardtii* [47]. For instance, the autoinhibition in the native KLP11/20 motor was eliminated by substituting the KLP11 catalytic head domain with the KLP20 head domain in the chimeric KLP20/20 motor. However, the KLP11/11 chimera resulted in a stricter autoinhibited motor. Accordance with these results, I asked whether a similar feature is also present in the wild type FLA8/10 by which its inherent autoinhibition can also be surpassed. To answer this challenge, I utilized the chimeras; FLA8/8 by replacing the catalytic head domain of FLA10 with FLA8 and FLA10/10 by changing the FLA8 head domain with FLA10 in FLA8/10 (Figure 5.22, supporting information 8.3).

In functional single-molecule assays, FLA8/8 displayed a single Gaussian distribution for velocity >2000nm/s, eliminating the slower population at ~760nm/s in wild type FLA8/10 (Figure 5.22 A). Interestingly, the FLA10/10 chimera also exhibited a single velocity distribution but in a lower range at ~1590nm/s than the FLA8/8 motor (Figure 5.22 B). Nevertheless, the speed of FLA10/10 is considerably higher than the velocity of kinesin-2 motors from *C.elegans* and other multicellular organisms. Disengaging the C-terminal domain by attaching to the glass surface in microtubule gliding assays also presented similar velocity parameters for FLA8/8 and FLA10/10 [38], showing that the fast speeds are indeed the property of the individual head domains. Taken together, replacement of FLA10 head domain with FLA8 recapitulated the motor's velocity to *in vivo* speed similar to KLP20/20 chimera, but the FLA10/10 chimera did not result in an autoinhibited motor like KLP11/11 chimera, meaning the autoinhibition mechanism in FLA8/10 is comparatively different from that of KLP11/20 [38].

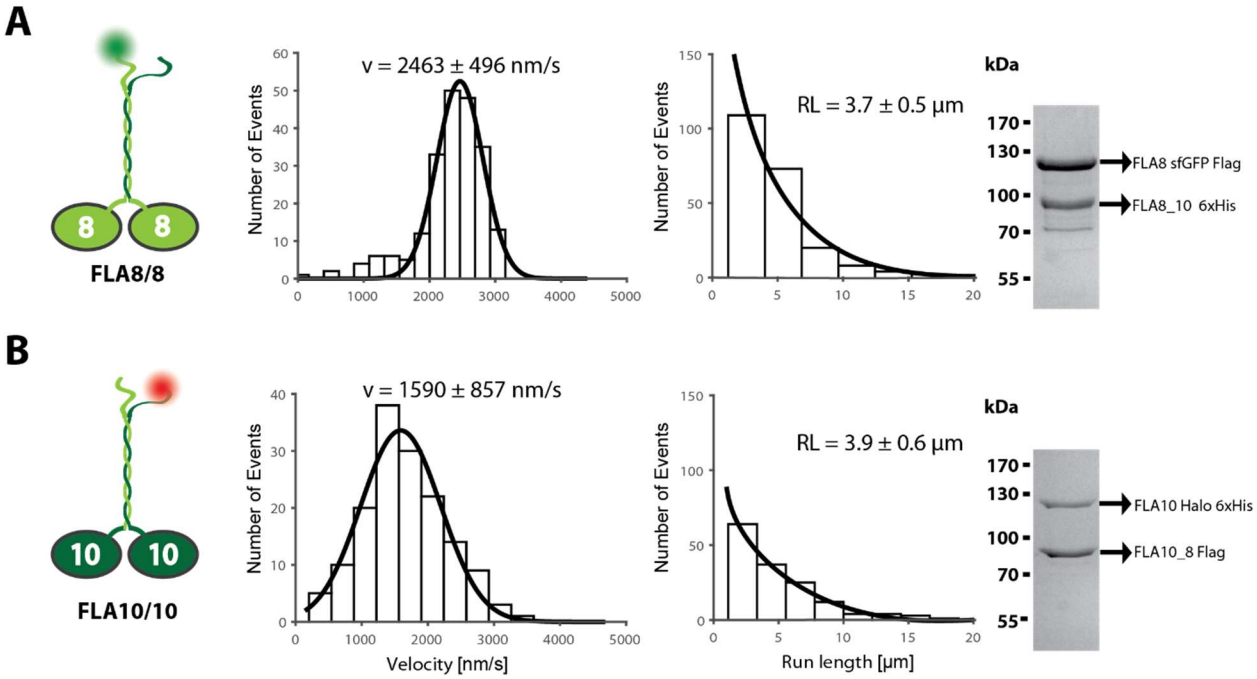

Figure 5.22: The higher velocity in FLA8/10 motor is a result of the individual fast speeds of FLA8 and FLA10 subunits (A) The replacement of FLA10 head domain with FLA8 catalytic domain in FLA8^{sfGFP}/8 chimera resolved the autoinhibition element to display a velocity of 2463 ± 496 nm/s and run length 3.7 ± 0.5µm (N = 214). **(B)** The FLA10/10^{Halo647} chimera could also display a substantially higher velocity of 1590 ± 857 nm/s and run length 3.9 ± 0.6µm (N = 150). The single molecule data along with microtubule gliding assays prove that these fast speeds are result of the individual high speeds of FLA8 and FLA10 subunit [38]. (Right panel; A, B, C & D) The SDS-PAGE analysis of the purified proteins indicates robust and stoichiometric expression of the motor proteins.

5.4.10. Expression and analysis of IFT-A subunits

The IFT-trains are composed of more than distinct 20 proteins, which assemble in to separate specialized complexes with defined functions in most of the cases (Table 1.1) [60]. These complexes serve as the adaptors by which kinesin-2 and dynein-2 motors transport diverse cargoes across the cilium. The IFT-A complex is one of the well-defined complex in the IFT-trains of particular significance. Ou.et.al Nature (2005) [84], proposed that KLP11/20/KAP1 mediated IFT transport in *C.elegans* is directed through the IFTA complex making it very compelling to dissect this complex. IFT-A complex in *C.elegans* consist of six subunits: CHE-11, DAF-10, DYF-2, IFTA-1, ZK328.7a and C25H3.12. Except C25H3.12, rest of the subunits enjoy a larger molecular weight >120 kDa (Figure 5.23). The large size of the IFT-A subunits had made recombinant based

studies on it a challenging task. Here I used Sf9 cells for eukaryotic expression of the IFT-A subunits rather than bacterial expression as used in earlier studies. IFT-A subunits expressed very well in Sf9 cells and was purified using Flag affinity purification. SDS-PAGE analysis after purification confirms that the subunits have been expressed well with high protein recovery and solubility (Figure 5.23). The efficient expression of IFT-A subunits facilitate the functional studies with IFT-A complex.

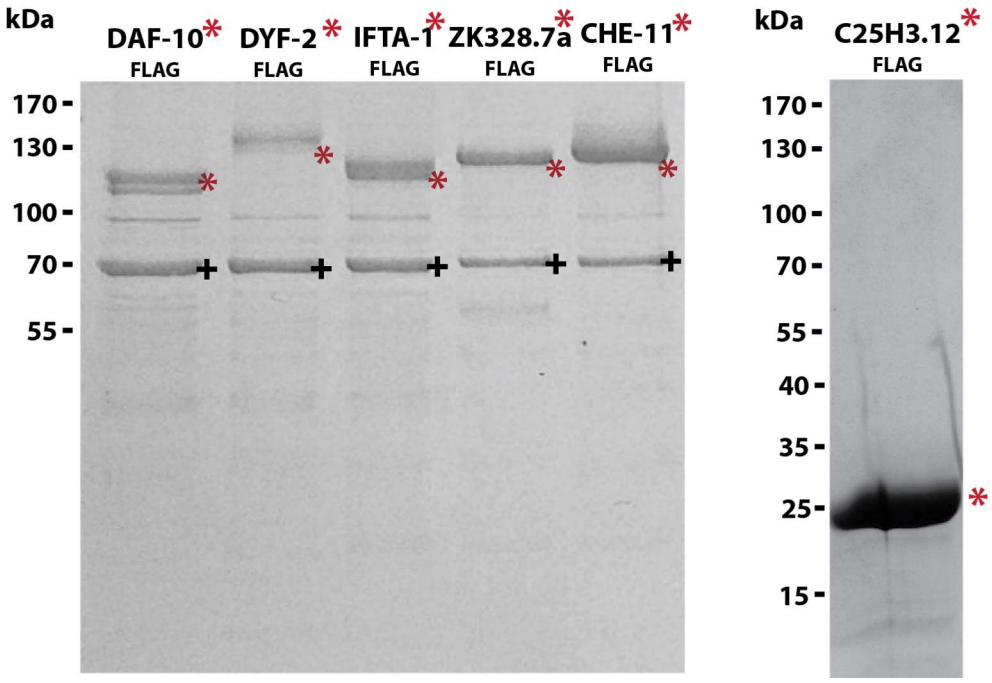

Figure 5.23: Expression of IFT-A subunits in Sf9 cells. All the six subunits of IFT-A subcomplex was successfully expressed in Sf9 cells. The SDS-PAGE analysis of FLAG-affinity purified subunits; DAF-10 Flag (137kDa), DYF-2 Flag (156kDa), IFTA-1 Flag (143 kDa), ZK328.7a Flag (152 kDa), CHE-11 Flag (164 kDa), and C25H3.12 Flag (24 kDa) that are used in this study (red asterisks indicate the coomassie stained bands of the respective proteins and the black cross indicates the HSP70 protein that is commonly observed due the overexpression in Sf9 cells).

5.4.11. CHE-11, DAF-10 and DYF-2 subunits form a stable core complex in IFT-A

Through the various studies conducted on mapping the protein-protein interactions in the IFT subunits in *C.reinhardtii*, an architecture have been developed on the structure of the IFT-A complex. Subunits IFT144 (CHE-11), IFT140 (DYF-2) and IFT122 (DAF-10) formed the core complex, while IFT139 (ZK328.7a), IFT121 (IFTA-1) and IFT43 (C25H3.12) formed the peripheral

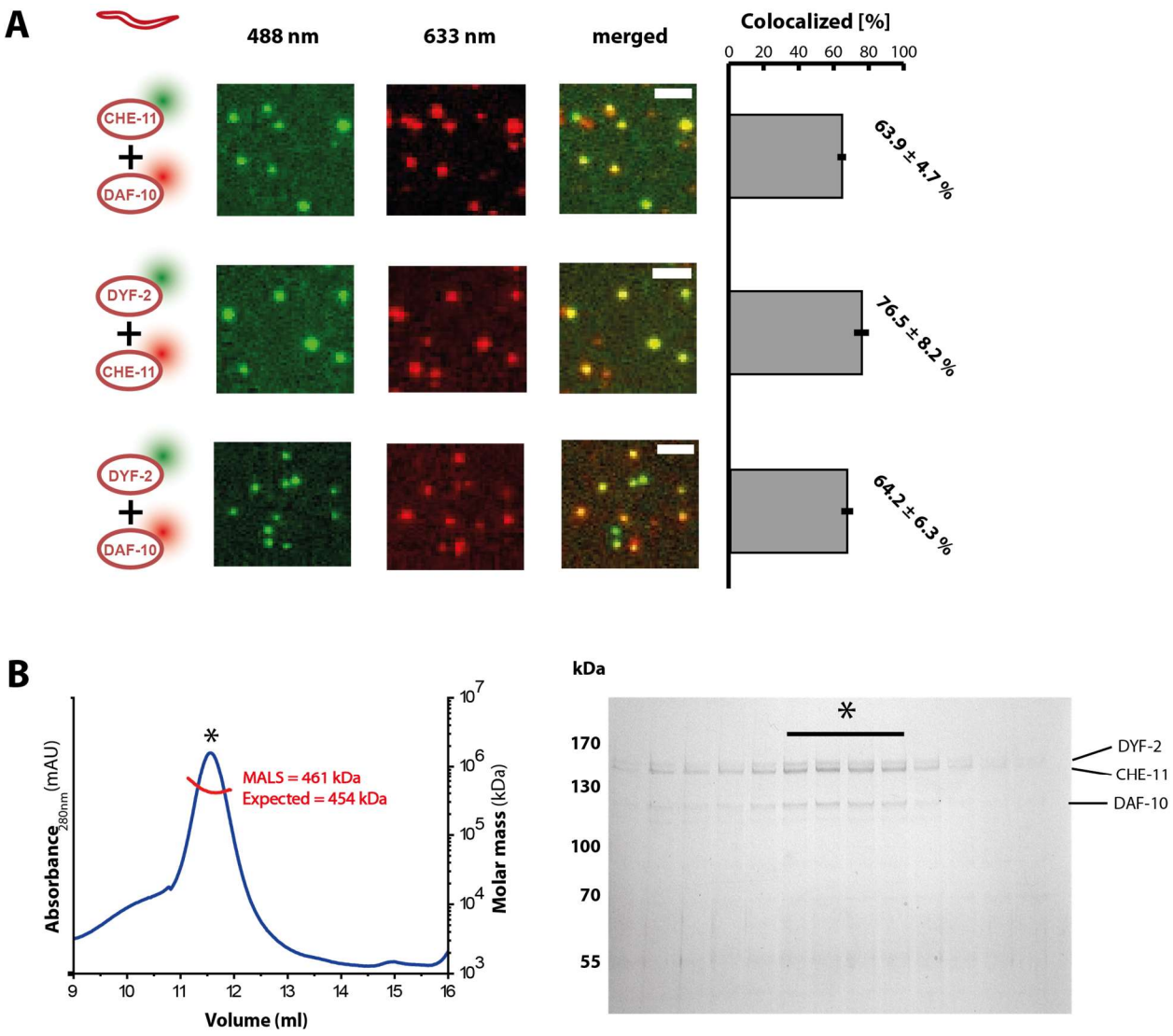

Figure 5.24: CHE-11, DAF-10 and DYF-2 make a stable core complex in IFT-A. (A) The IFT-A subunits from *C.elegans* display direct one to one binding in colocalization assays. **(First lane)** CHE-11^{SNAP488} (488 channel) interacts efficiently with DAF10^{Halo647} (633 channel) with a colocalization percentage of 63.9 ± 4.7. **(Second lane)** CHE-11^{SNAP647} (633 channel) can also bind effectively with DYF-2^{GFP} (488 channel) with a colocalization percentage of 76.5 ± 8.2. **(Third lane)** DYF-2^{GFP} (488 channel) too colocalize readily with DAF10^{Halo647} (633 channel) with percentage of colocalization 64.2 ± 6.3. **(B)** SEC-MALS analysis of CHE-11, DAF-10 and DYF-2 subunits establish them as forming a stable core complex (Column: Superose® 6 Increase 10/300 GL (GE Healthcare, UK)). **(Left panel)** The MALS molar mass was calculated from the peak (black asterisk) in the elution profile of the core complex. MALS predicted a molar mass of 461 kDa which is close to the expected molar mass value of 454 kDa (when the subunits are present in the ratio 1:1:1). **(Right panel)** The eluted fractions of the core complex from SEC-MALS was analyzed on SDS-PAGE. The IFT-A subunits eluted rightly under the single peak.

region of IFT-A [60]. Protein-protein interaction databases like STRING have predicted an interactome mapping for the IFT-A complex [138], but vital information on the architecture of the complex is still missing in *C.elegans*. The IFT machinery has been highly conserved across the evolution. So it fitting to assume that CHE-11, DAF-10 and DYF-2, which are the homologs for IFT144, IFT140 and IFT122 might also form a stable core complex.

It is also crucial to understand the path of binding between these subunits, whether there is a direct case of binding between these subunits or do they undergo sequential binding? I used colocalization assays to interpret the binding between these subunits by employing SNAP, Halo and GFP tags (Figure 5.24 A, supporting information 8.1.1 C & 8.3). All three subunits showed direct one to one binding between each other with a colocalization percentage of >60%. The next question would then be if these subunits can also exist as a stable complex. I used size exclusion chromatography combined with multiple angle light scattering technique (SEC-MALS) to detect the nature of the complex. Proteins were purified and concentrated to 0.8-1mg/ml for the technique. In SEC-MALS analysis, CHE-11, DAF-10 and DYF-2 existed as a steady complex with a MALS molar mass of 460kDa (Figure 5.24 B). Assuming the complex is built from the subunits CHE-11, DAF-10 and DYF-2 present in the ratio 1:1:1, it would give a molecular weight of 454kDa, which is in unanimity with the MALS molar mass value. The MALS value also confirms, that the complex does not undergo any further oligomerization or aggregation. The establishment of IFT-A core complex gives new tools for exploring the KLP11/20/KAP1 based transit in *C.elegans*.

6. Discussion

Dissecting the recruitment of OSM-3 for anterograde transport in *C.elegans*

Kinesin motors have consistently applied an autoinhibition mechanism to regulate the necessary transport processes. A unique adaptor protein or a cascade of proteins is set to utilize the motors for specialized functions in adaptor mediated motor activation techniques [19]. In IFT, the Kinesin-2 motors have to interact with specific proteins in the IFT core complexes to manage the transport. These adaptor proteins either keeps the motor active for processive IFT or hold them inactive to be transported as cargo on the return to the ciliary base. One of the most well characterized transport process, is the homodimeric kinesin-2 OSM-3 mediated anterograde transport in *C.elegans* sensory cilia. The motor attaches to the IFT-B subcomplex for the long-range transport in cilia [84].

However, the grasp on the mechanism of OSM-3 mediated processive transport still contains many missing links. The DYF-1 subunit from IFT-B could activate the motor to a basal level of velocity ~1300nm/s, while the quadripartite complex DYF-1/OSM-6/OSM-5/DYF-6 was required to introduce an allosteric activation, to produce the velocity ~1700nm/s [52]. It is unclear whether this new activation state represents the full capacity of the motor. In previous multimotor-filament gliding assays, which is supposed to relieve the motor from its autoinhibition state due to the assays geometry, the motor switched between velocities of 900-1300nm/s [37, 139], only to introduce more confusion. To measure the motor's real, complete activation level, removal of all the domains that are capable of producing any hindrance to the motor's motility is crucial. The OSM-3 GCN4 construct created solely with the head domains, avoiding the stalk and tail domain known for possible auto-inhibition roles, displayed a similar velocity of 1700nm/s as the allosteric activated OSM-3 by the quadripartite complex, substantiating the four subunit complex can generate the full activation in OSM-3 and this velocity indeed is the maximum velocity that can be produced by the motor. This full activation of OSM-3 also corresponds to the *in vivo* velocity of motor in the absence of heterotrimeric kinesin-II motor [85].

The functional reconstitution of OSM-3 with the subunits from the quadripartite complex revealed that DYF-1/OSM-6 dimer is enough and necessary for the complete activation of the kinesin-2 motor. IFT70 styles a super helical structure to wrap around a conserved proline-rich sequence motif of IFT52 in *C.reinhardtii* (Figure 1.6) [101]. I found that the corresponding conserved proline-rich sequence motif of OSM-6 is essential for OSM-3 activation as its elimination from the OSM-6/DYF-1 dimer brought back the activation of the motor to its basal level. It is also fascinating that the corresponding OSM-6 sequence motif is not only essential but enough to produce full activation in OSM-3 together with DYF-1. In the tight stacking between the residues in the DYF-1/OSM-6 complex, a conserved tyrosine motif in DYF-1 (Y51, 53, 54, 55) is fundamental for OSM-3 activation. These tyrosines sandwich around a conserved proline motif in OSM-6. Mutating the conserved tyrosines to alanines diminished OSM-3 to its basal activation level while mutating the alanines to phenylalanines could rescue the motor's full activation. The mutants testify that the hydrophobic contacts established from the aromatic pocket of the conserved tyrosine residues of DYF-1 around the prolines in OSM-6 powers the OSM-3 activity. Thus the minimum elements required for adaptor based activation of OSM-3 can be pointed out to the amino acid residue level in this study.

In the *C.elegans* genome, there is a second isoform for DYF-1, termed DYF-1b which lacks the N-terminal region and translates directly after the conserved tyrosine motif. On the contrary, DYF-1b isoform could also switch the motor on to its basal activation state but fails to complete the full activation in the presence of OSM-6 as expected. *C.elegans* incorporate diverse cilia types in their sensory neurons, and these distinct cilia types regulate IFT by redistributing IFT genes differentially [132]. It is reasonable that neurons might deploy DYF-1b too for anterograde transport as it can also bind and activate OSM-3. However, it is unknown what other functional roles than anterograde IFT are specified for the N-terminal region of DYF-1, which is absent in the DYF-1b isoform.

Although there is an extensive library on kinesin-cargo based studies in the *in vivo* field, significant studies of any kinesin family motor with its corresponding cargoes in the *in vitro* front are considerably less to nil. The *in vitro* reconstitution methods are better suited to decisively explain the motor-cargo complexes' interactome and features, which are challenging to attain in

in vivo studies. Our study gives an in-depth understanding of how specific adaptor proteins can impose activation at different levels on the kinesin-2 motor. The amino acid residue level dissection of the motifs in DYF-1/OSM-6 adaptor required for OSM-3 activation is a major advancement in understanding how motor proteins are incorporated into processive transport in intracellular processes.

Retracing the evolution of kinesin-2 deployment from mouse to worm

The motors from the Kinesin-2 family are explicitly deployed for assembling and maintaining the ciliary structure. During evolution, more tasks got assigned for kinesin-2 motors outside the cilium. In the meantime, the characteristics of these motor's duties also varied significantly inside the cilium. When the heterotrimeric Kinesin-II has been a consistent carrier of IFT cargoes inside the cilia in all the organisms studied so far, the homodimeric kinesin-2 switched from being an active transporter to dormant and even being absent in some [55]. The case of homodimeric kinesin-2 is particularly compelling especially on what has caused the mouse KIF-17 to be inactive inside the cilium while *C.elegans* OSM-3 operate as a functional transporter.

DYF-1 was the key to incorporate OSM-3 to IFT-B complex for anterograde transport [84]. Considering the evolutionary conservation in IFT, KIF-17 must also interact with its equivalent adaptor protein to take part in IFT. In functional reconstitution of KIF-17 with mouse IFT70, the adaptor protein neither activated nor interacted with the motor, conceding that the connection between the motor and its corresponding adaptor protein is broken. The mouse IFT70 was able to bind and activate the *C.elegans* OSM-3 motor but could not recognize its motor KIF-17, which underlies, it is KIF-17 who has lost its ability to identify its adaptor protein and not vice versa. The mouse IFT70/52, the homologs of DYF-1/OSM-6, could switch OSM-3 to full activation, confirming that the adaptor proteins have retained their capacity for motor activation. The functional conservation of the adaptor proteins can be even retraced back to the single-celled green algae *C.reinhardtii*, which even lacks the homodimeric kinesin-2 in its genome as the *C.reinhardtii* IFT70/52 is also capable of activating OSM-3 to its fully activated state. The strongly conserved adaptor proteins DYF-1/OSM-6 and its homologs can thus be called the 'On-Switch,' which can activate the motor for IFT. The On-Switch proteins are functionally conserved among

themselves that it is indeed possible to replace DYF-1 or OSM-6 subunits from one organism to another and still activate the OSM-3 motor. Thus, the cells have utilized a conserved set of proteins to facilitate the conveyance of cargo, and modification is done on motor proteins according to necessity.

The amino acid sequence of KIF-17 and OSM-3 is significantly divergent apart from the catalytic motor domain. However, both of them possess a conserved C-terminal sequence, which allows KIF-17 to enter the cilia through interaction with the IFT56/46 dimer [95]. After arriving inside the ciliary compartment, KIF-17 remains inactive and migrate across the length as a cargo. The art of remaining inactive is also important for OSM-3 as it has to be transported as a passenger in the retrograde trains by dynein-1b motors [55]. In our bottom-up approach, we found that KIF-17 can interact with IFT56/46 *in vitro*, but the binding does not activate the motor. In most *in vitro* experiments, attaching any motors' C-terminal region to any non-specific surface or tool relieves its autoinhibition and activates them [37]. Hence interaction of KIF-17 with IFT56/46 provides a candidate for the mechanism by which motors can be kept passive when not in use. Strikingly mouse IFT56/46 could also interact with OSM-3 but failed to activate the motor and the *C.elegans* homologs of these adaptor proteins DYF-13/DYF-6 also replicated the same behavior with KIF-17 and OSM-3. Thereby the conserved adaptor proteins IFT56/46 and DYF-13/DYF-6 can be termed as 'Off-Switch' utilized to transport the motors as passengers when not required for active IFT.

From the adaptor proteins studied, I am proposing a model in which organisms employ distinct conserved proteins for specific functions inside the cilia (Figure 6.1). The homodimeric kinesin-2 must recognize and bind to on-switch proteins DYF-1/OSM-6 or mouse IFT70/52 to be incorporated for processive IFT. Failing to attach to the on-switch deprives the motor of taking part in the anterograde transport. The ciliary machinery has also allocated specific proteins DYF-13/DYF-6 and IFT56/46 as off-switch adaptors that interact and carry the motors across the cilia without activating them. However, it is not possible to exclude that other proteins from the IFT-train won't interact with the homodimeric kinesin-2 motors. In the case of KIF-17, it is possible that in the enigmatic remodeling and restructuring of IFT-trains at the ciliary tip, the motor might

exchange its adaptor proteins. Nevertheless, in the highly complicated IFT process, IFT56/46 remains a solid candidate for keeping the motors inactive based on our direct interaction and previous *in vivo* studies [95].

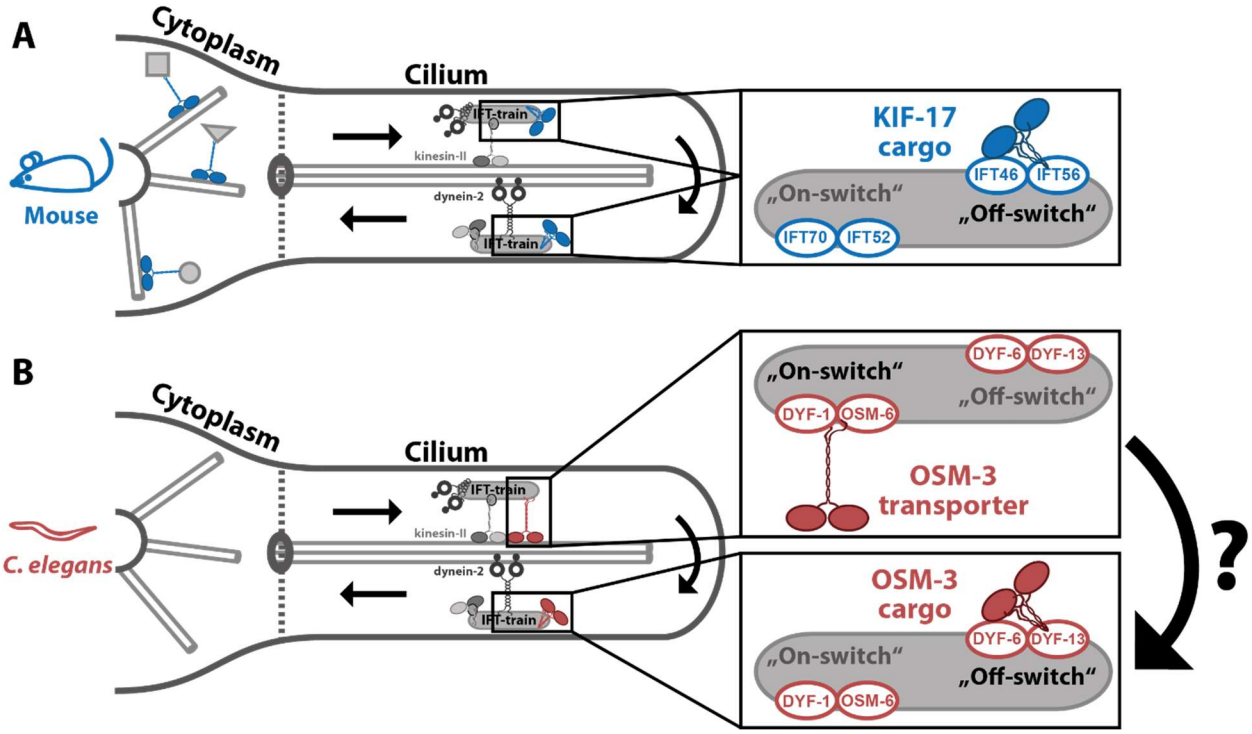

Figure 6.1: Proposed model of kinesin-2 deployment in mouse and *C.elegans*. (A) The intraflagellar transport machinery has crafted conserved adaptor proteins to serve as 'On-switch' and 'Off-switch' to regulate kinesin-2 motors' deployment inside the cilia. The On-switch activates and integrates the motor for processive IFT, while the Off-switch allows it to be transported as an inactive cargo. This function has been conserved between mouse and worm. Strikingly, for the mouse, the KIF-17 motor lost the ability to exploit the ciliary On-switch, IFT52/70, in the course of evolution and hence failed to take part in processive IFT. Still, the motor retained its capacity to interact with the Off-switch adaptors IFT56/46 for its transportation inside the cilium. However, KIF-17 reclaimed the opportunity to work as a functional transporter by readapting to recognize multiple cytoplasmic 'On-switches' to transport diverse cargo types in the cytoplasm through unknown mechanisms. **(B)** The *C.elegans* OSM-3 can effectively employ both the ciliary on- and off-switches, hence can be utilized as a regulatable transport motor in the cilium. I propose that, after actively transporting the IFT-trains to the ciliary tip, OSM-3 motors detaches from the On-switch adapter OSM-6/DYF-1 in the enigmatic remodeling process and attaches to the Off-switch adapter DYF-13/DYF-6 in an autoinhibited dormant form to be transported back as an inactive cargo to the ciliary base. (Adapted from Cleetus et.al, 2020)[131]

Generating a tool box for investigating kinesin-II mediated anterograde transport in *C.elegans*

The heterotrimeric kinesin-2 had occupied the constant transporter role for IFT-trains in the anterograde transport [55]. However, in *C.elegans*, the KLP11/20/KAP1 has a constricted act of helping the large IFT molecules cross the transition zone, which serves as a roadblock for the traffic [85]. The innate capability of KLP11/20/KAP1 to effectively navigate barriers has been shown in independent studies; and in a different *in vivo* study, in the single *kap1* mutant cilia, the OSM-3 motors takes longer time to attain its maximum velocity than the motors in double mutant *kap1, mksr-1* mutant cilia [85]. The homodimeric OSM-3 faces difficulty in crossing the transition zone with MSKR-1 present, a well-studied protein that acts as a roadblock in the IFT transport; indicating, between KLP11/20/KAP1 and OSM-3, the kinesin-II motor is more abled in crossing the transition zone. The IFT-trains are transferred to OSM-3 motors once they enter the cilia for long-range transport. Hence it is imperative to dissect the kinesin-II motor to learn how the *C.elegans* motor attained such capabilities.

The significant features we learned about the KLP11/20/KAP1 motor from the dissection are 1) the motor's processivity is least dependent on the neck linker subdomain compared to Kinesin-1. Because, the KLP11/20 motors' velocity gets reduced by merely a ~20%, without any drop in the run length parameter, while the Kinesin-1 kinetic parameters, velocity and run length drop by more than 70%, with the addition of flexible repeats after the neck linker domain. 2) The KLP11/20 motors can exhibit significant processive movement in the absence of its C-terminal tail domains. The insensitivity of the motor's processivity towards the neck linker subdomain and tail domains suggests that KLP11/20 has been modeled as a robust motor for large scale cargo delivery. 3) The KLP11 catalytic head domain directly governs the autoinhibition regulation in KLP11/20, and additional placing of the second KLP11 head domain in KLP20's position can inflate the degree of autoinhibition. KLP11/20 displays limping in its processive movement even after having equivalent catalytic activity for both subunit motor domains due to the autoregulation exhibited by the KLP11 motor. 4) It is also significant that the addition of KAP1 to KLP11/20 does not switch the motor to its activated form, as seen in *C.reinhardtii* [38]. From these results, it is clear that the *C.elegans* heteromeric KLP11/20/KAP1 has a strict autoregulation mechanism to

take part in IFT, but the motor does not compromise on other factors to provide any hindrance to its processivity.

In *C.reinhardtii*, the heterotrimeric FLA8/10/KAP alone is present inside the flagella and adroitly carries out the anterograde transport. The absence of any significant *in vitro* dissection of the motor arose many doubts regarding the unusual high velocity displayed by the IFT-trains in the anterograde transport. In this thesis, I could identify that the high ~2000nm/s velocity showcased by the IFT-trains is indeed coming from the individual FLA8/10 motors. However, the wild type motor is autoinhibited and exhibits two velocity populations at ~700nm/s and ~2000nm/s in single molecule TIRF assays, the lower velocity population indicating the autoinhibited state. Strikingly the autoinhibition can be relieved by introducing point mutations on the helix breaker region of the FLA10 subunit. The mutations allow the coiled-coil domain to exist in an extended conformation than the folded autoinhibition state, activating the motor [38]. It is puzzling how the FLA8/10 can exhibit this atypical high velocity, unlike its homologs from other organisms. From multiple catalytic head chimeras from KLP11/20 and FLA8/10, I found that the catalytic head domain alone determines the speed of kinesin-2 motors through its ATPase activity. It is the exclusive ability of the FLA8/10 catalytic domains that allow it to exhibit its four-fold higher velocity than the *C.elegans* motor. In autoinhibition regulation too, FLA8/10 inherited a different mechanism as the FLA8/8 or FLA10/10 did not exhibit lower motility as observed in KLP11/11 chimera from *C.elegans*, but could generate velocities higher than 1500nm/s. Moreover, the physiological relevance of the auxiliary subunit KAP is observed in the case FLA8/10 as its attachment could activate the motor to its maximum velocity, which was not seen in the *C.elegans* motor. The dissection of Kinesin-II motors in *C.elegans* and *C.reinhardtii* helps to identify the specific characteristics of these motors, how they differ from each other on autoregulation and motility, and a sense on how they are utilized for IFT.

The *C.elegans* Kinesin-2 binds to IFT-A subcomplex for transporting the IFT cargoes across the cilia [84]. The expression and functional study of IFT-A proteins is a challenging task due to the large size, and insolubility of the proteins in aqueous solutions because of their hydrophobic nature. The subunits need essential partners to be stable in solution. Hence very few studies are available for the IFT-A subunits *in vitro* compared to the vast library of IFT-B proteins present. In

this thesis, I could adequately express all the subunits of IFT-A complex in *C.elegans* by employing the Sf9 expression system and could also clone fluorescent GFP, Halo, and SNAP tags to the C-terminal region of the core subunits for functional studies. From size exclusion chromatography and colocalization assays, it is clear that *C.elegans* also establish a core complex consisting of CHE-11, DAF-10, and DYF-2 within IFT-A, similar to *C.reinhardtii* through direct one to one interaction between the subunits. The establishment of the IFT-A core complex and the other peripheral subunits through the combination with KLP11/20/KAP1 and FLA8/10/KAP provides a useful tool in mastering the kinesin-II mediated IFT. As FLA8/10/KAP attaches to the IFT-B complex for anterograde transport, the new tools also provide an option to figure the changes that happened between the kinesin-II mediated transport in *C.elegans* and *C.reinhardtii*.

Taken together, the thesis provides the mechanism on how OSM-3 motors can be turned 'ON' for processive movement by recognizing its specific adaptor proteins. The critical site responsible for motor activation in the adaptor protein was found and dissected to the amino acid residue level. Next, the thesis explains how the homodimeric Kinesin-2 motors OSM-3 and KIF-17 have been adapted for divergent roles inside the cilia. The cells employ specific adaptor proteins as master keys to keep the motors ON or OFF during IFT. The on-switch adaptors stimulate the motor for processive transport across IFT, and the Off-switch adaptors keep the motor inactive when not required. The homodimeric Kinesin-2 motors must recognize these master keys for the particular function. The motors which fail to identify the corresponding switch will also miss to carry out the particular function. The existence of the on and off switches finely explains the inability of KIF-17 to take part in active IFT. Finally, the thesis also provides new tools to investigate the Kinesin-II mediated IFT in *C.elegans* and *C.reinhardtii*.

7. Outlook and prospects

The delicate, coordinated circulation of intracellular cargo within cells is carried out through a diverse set of molecular motors. Kinesin motors, in particular, are hired for long-range transport of organelles and multiprotein complexes across microtubule tracks. These motors are challenged on how to organize such transport without traffic jams and waste of energy. In such a case, the kinesins are activated for transport only through effective cargo binding. The attachment of the target molecules to the motors can also be mediated through special set of proteins called adaptor proteins [40].

In this thesis, I focused on how the homodimeric kinesin-2 motor OSM-3, is stimulated for processive IFT inside the cilia. OSM-3 is completely suppressed in the absence of its adaptor proteins. The motor protein identifies a specific motif from the DYF-1 subunit in the OSM-6/DYF-1 to fully activate itself for transport. The study has been successful in establishing the necessary partners for activating the motor. However, the mechanism of interplay between OSM-3 and OSM-6/DYF-1 remains unexplored. It is essential to determine the structural domains in OSM-3 that are responsible for OSM-6/DYF-1 interaction. Subsequently, structural studies can provide a final interpretation of the OSM-6/DYF-1 mediated activation of OSM-3. In kinesins, the motors routinely deactivate themselves by tying their tail domain to their catalytic head domain to inhibit motility. Protein X-ray crystallography technique can be used to analyze the structure of such autoinhibited OSM-3 and the activated motor in complex with the OSM-6/DYF-1 subunits. The dissection of indispensable motifs in DYF-1 and OSM-6 from our study enables the trimming of these subunits to facilitate more facile crystallization of the proteins. The structural studies will then explain how OSM-3 switches between autoinhibited and activated states through maneuvering between autoinhibiting domains and adaptor proteins.

This thesis also investigated how the homodimeric kinesin-2 family proteins, the *C.elegans* OSM-3, and mouse KIF-17 can exhibit contrasting behaviors in its activity inside the ciliary compartment. The inability of the KIF-17 to take part in processive IFT is directed to the evolutionary variation observed in the motor. As proposed earlier on the need to determine the motif in OSM-3 responsible for the On-switch binding, the discovery of the same motif will enable

one to compare with KIF-17 to validate this evolutionary variation directly. We found that Off-switch adaptor proteins exist in the IFT complexes that can interact with the homodimeric kinesin-2 to keep them passive, apart from the on-switch adaptors. In a complete run of IFT, the kinesin-2 motors need to swap between On-switch and Off-switch protein during anterograde and retrograde transport. In the highly convoluted process of IFT, it is unclear how this rearrangement happens. There is a possibility that the Off-switch adaptors are hidden from the motors during anterograde, and the train restructuring reveals them for binding during the return. The *C.elegans* ciliary tip is proposed to be a site of high DYF-18 and DYF-5a kinase activity. Hence it is conceivable that phosphorylation might too play a direct role in the regulation of OSM-3. Therefore it is vital to understand whether the On-switch and Off-switch adaptors plus the OSM-3 motor are phosphorylation targets of these kinases. Besides, determination of the binding affinity/dissociation constant of OSM-3 to On- and Off-switch adaptor proteins with respect to their phosphorylation states can help in grasping how the OSM-3 motors get detached from the On-switch adaptors, surrender to autoinhibition and attaches to Off-switch adaptor to be transported back in the retrograde transport, at the ciliary tip. Since this thesis provides a fully functional yet regulated KIF-17 motor, it allows enormous potential to study how the motor is utilized for cytoplasmic transport *in vitro*. It should be noted that there are rarely any reconstitution studies on KIF-17 transport *in vitro*.

In the last section of the thesis, I generated multiple tools necessary for investigating the Kinesin-II mediated transport in *C.elegans*. The specialized role of KLP11/20/KAP1 in the *C.elegans* poses great interest in the mechanism of its transport. These motor directly attach to the IFT-A subcomplex unlike other Kinesin-II motors for anterograde transport [139]. Nevertheless, it is obscure if the motor attaches through a single docking point, within the IFT-A subcomplex similarly to OSM-3 and DYF-1, or through multiple joints, since their main task is to cross IFT cargoes over the transition zone? The doubt is reasonable since four of the six subunits in IFT-A share similar domain architecture [104]. The new tools from the thesis will allow reconstitution and dissection of the IFT-A – KLP11/20/KAP1 complex in *C.elegans* directly. The availability of the finely established FLA8/10/KAP motor will allow us to compare and learn the disparity in the Kinesin-II mediated transport in *C.reinhardtii* and *C.elegans*

8. Supporting information

8.1. SDS-PAGE analysis of proteins used in the thesis

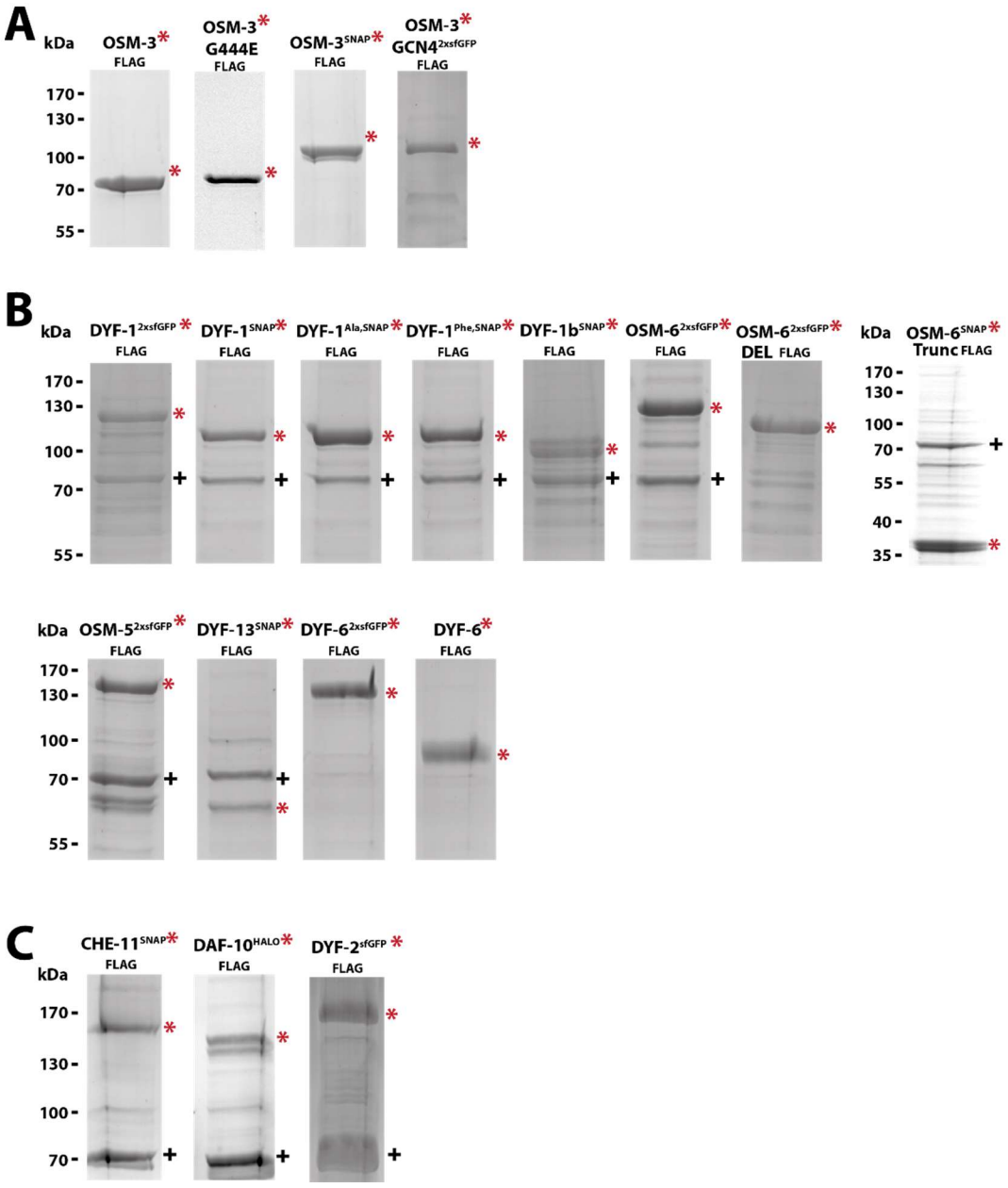

Figure 8.1.1: Protein expression of the *C.elegans* constructs used in this study. SDS-PAGE analysis of the FLAG-affinity purified constructs that are used in this study (red asterisks indicate the Coomassie stained bands of the respective proteins and the black cross indicates the HSP70 protein that is commonly observed by overexpression in Sf9 cells). **(A) Motor proteins**: OSM-3 full-length wild type Flag (80 kDa), OSM-3 full-length G444E Flag (80 kDa), OSM-3 full-length wild type with N-terminal SNAP-tag (100 kDa),

and OSM-3 GCN4 2xsfGFP (97 kDa). **(B) IFT-B subunits**: DYF-1 2xsfGFP FLAG (131 kDa), DYF-1 SNAP Flag (96 kDa), DYF-1^{Ala} SNAP FLAG (96 kDa), DYF-1^{Phe} SNAP FLAG (96 kDa), DYF-1b SNAP Flag (89 kDa), OSM-6 2xsfGFP Flag (108 kDa), OSM-6 DEL 2xsfGFP Flag (102 kDa), Flag SNAP OSM-6 Trunc (28 kDa), OSM-5 2xsfGFP Flag (147 kDa), DYF-13 SNAP Flag (87 kDa), DYF-6 2xsfGFP Flag (108 kDa), and DYF-6 FLAG (55 kDa). **(C) IFT-A subunits:** CHE-11 SNAP Flag (183 kDa), DAF-10 Halo Flag (171 kDa), and DYF-2 sfGFP Flag (183 kDa)

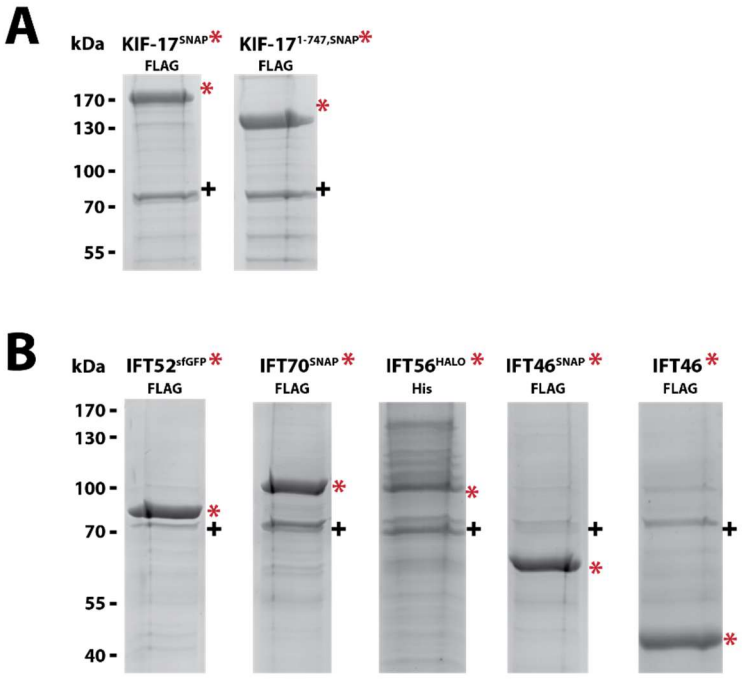

Figure 8.1.2: Protein expression of the mouse constructs used in this study. SDS-PAGE analysis of the FLAG-affinity and 6X-His affinity purified constructs that are used in this study (red asterisks indicate the Coomassie stained bands of the respective proteins and the black cross indicates the HSP70 protein that is commonly observed by overexpression in Sf9 cells). **(A) Motor proteins**: KIF-17 full-length wild type with N-terminal SNAP-tag (138 kDa) and KIF-17$^{1-747}$ with N-terminal SNAP-tag (104 kDa). **(B) IFT subunits**: IFT52 sfGFP Flag (76 kDa), IFT70 SNAP Flag (97 kDa), IFT56 Halo 6xHis (99 kDa), IFT46 SNAP Flag (55 kDa), and IFT46 Flag (36 kDa).

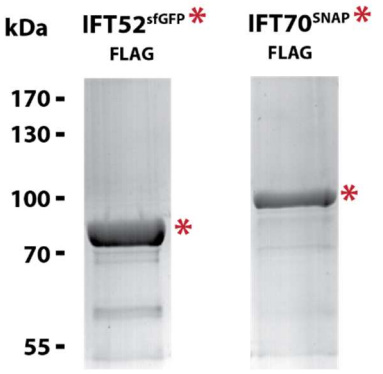

Figure 8.1.3: Protein expression of the *C.reinhardtii* constructs used in this study. SDS-PAGE analysis of the FLAG-affinity purified constructs that are used in this study (red asterisks indicate the Coomassie stained bands of the respective proteins). Subunits expressed were IFT52 sfGFP Flag (78 kDa), and IFT70 SNAP Flag (95 kDa)

8.2. t-test analysis of OSM-3 velocity through activation by various adaptor proteins.

P-values are calculated from two sample t –tests for the velocity data of OSM-3 in correspondence with the adaptor proteins (left column). The data which showed significant difference (Value <0.01) in the analysis is highlighted in orange and those without any significant variation in green (Value >0.01). The figures corresponding to each t-test are mentioned in the right column.

Constructs			P-Value	Related to
OSM-6/DYF-1	*Vs*	*OSM-5/DYF-1*	4.7496e-39	Figure 5.2
OSM-6/DYF-1	*Vs*	*OSM-6 DEL/DYF-1*	6.475e-25	Figure 5.3
OSM-6/DYF-1	*Vs*	*OSM-6 Trunc/DYF-1*	0.8925	Figure 5.4
OSM-6/DYF-1	*Vs*	*OSM-6/DYF-1^{Ala}*	1.7548e-33	Figure 5.6
OSM-6/DYF-1^{Ala}	*Vs*	*OSM-6/DYF-1^{Phe}*	1.3392e-55	Figure 5.6
OSM-6/DYF-1	*Vs*	*OSM-6/DYF-1b*	4.6732e-42	Figure 5.7
Mouse: IFT70	*Vs*	*IFT52/70*	1.2494e-35	Figure 5.10
C.reinhardtii: IFT70	*Vs*	*IFT52/70*	2.7376e-32	Figure 5.12

8.3. Protein sequences of the constructs used in the study

Color-coded protein sequences of all constructs that are used in this study (Accession numbers from NCBI)

1. Motor constructs

OSM-3 Flag (P46873.4)

MAESVRVAVRCRPFNQREKDLNTTLCVGMTPNVGQVNLNAPDGAAKDFTFDGAYFMDSTGEQIYNDIVFPLVENVIE
GYNGTVFAYGQTGSGKTFSMQGIETIPAQRGVIPRAFDHIFTATATTENVKFLVHCSYLEIYNEEVRDLLGADNKQKLEIK
EQPDRGVYVAGLSMHVCHDVPACKELMTRGFNNRHVGATLMNKDSSRSHSIFTVYVEGMTETGSIRMGKLNLVDLA
GSERQSKTGATGDRLKEATKINLSLSALGNVISALVDGKSKHIPYRDSKLTRLLQDSLGGNTKTIMIACVSPSSDNYDETLS
TLRYANRAKNIKNKPTINEDPKDALLREYQEEIARLKSMVQPGAVGVGAPAQDAFSIEEERKKLREEFEEAMNDLRGEYE
REQTSKAELQKDLESLRADYERANANLDNLNPEEAAKKIQQLQDQFIGGEEAGNTQLKQKRMKQLKEAETKTQKLAAA
LNVHKDDPLLQVYSTTQEKLDAVTSQLEKEVKKSKGYEREIEDLHGEFELDRLDYLDTIRKQDQQLKLLMQIMDKIQPIIK
KDTNYSNVDRIKKEAVWNEDESRWILPEMSMSRTILPLANNGYMQEPARQENTLLRSNFDDKLRERLAKSDSENLANS
YFKPVKQINVINKYKSDQKLSTSKSLFPSKTPTFDGLVNGVVYTDALYERAQSAKRPPRLASLNPKGGDYKDDDDK

OSM-3 G444E Flag

MAESVRVAVRCRPFNQREKDLNTTLCVGMTPNVGQVNLNAPDGAAKDFTFDGAYFMDSTGEQIYNDIVFPLVENVIE
GYNGTVFAYGQTGSGKTFSMQGIETIPAQRGVIPRAFDHIFTATATTENVKFLVHCSYLEIYNEEVRDLLGADNKQKLEIK
EQPDRGVYVAGLSMHVCHDVPACKELMTRGFNNRHVGATLMNKDSSRSHSIFTVYVEGMTETGSIRMGKLNLVDLA
GSERQSKTGATGDRLKEATKINLSLSALGNVISALVDGKSKHIPYRDSKLTRLLQDSLGGNTKTIMIACVSPSSDNYDETLS
TLRYANRAKNIKNKPTINEDPKDALLREYQEEIARLKSMVQPGAVGVGAPAQDAFSIEEERKKLREEFEEAMNDLRGEYE
REQTSKAELQKDLESLRADYERANANLDNLNPEEAAKKIQQLQDQFIEGEEAGNTQLKQKRMKQLKEAETKTQKLAAA
LNVHKDDPLLQVYSTTQEKLDAVTSQLEKEVKKSKGYEREIEDLHGEFELDRLDYLDTIRKQDQQLKLLMQIMDKIQPIIK
KDTNYSNVDRIKKEAVWNEDESRWILPEMSMSRTILPLANNGYMQEPARQENTLLRSNFDDKLRERLAKSDSENLANS
YFKPVKQINVINKYKSDQKLSTSKSLFPSKTPTFDGLVNGVVYTDALYERAQSAKRPPRLASLNPKGGDYKDDDDK

OSM-3_ GCN4 2x_superfolder GFP Flag

MAESVRVAVRCRPFNQREKDLNTTLCVGMTPNVGQVNLNAPDGAAKDFTFDGAYFMDSTGEQIYNDIVFPLVENVIE
GYNGTVFAYGQTGSGKTFSMQGIETIPAQRGVIPRAFDHIFTATATTENVKFLVHCSYLEIYNEEVRDLLGADNKQKLEIK
EQPDRGVYVAGLSMHVCHDVPACKELMTRGFNNRHVGATLMNKDSSRSHSIFTVYVEGMTETGSIRMGKLNLVDLA
GSERQSKTGATGDRLKEATKINLSLSALGNVISALVDGKSKHIPYRDSKLTRLLQDSLGGNTKTIMIACVSPSSDNYDETLS
TLRYANRAKNIKNKPTINEDPKDALLREYQEEIGPRMKQLEDKVEELLSKNYHLENEVARLKKLVGEGAPGGGSGGSMS
KGEELFTGVVPILVELDGDVNGHKFSVRGEGEGDATNGKLTLKFICTTGKLPVPWPTLVTTLTYGVQCFARYPDHMKQH
DFFKSAMPEGYVQERTISFKDDGTYKTRAEVKFEGDTLVNRIELKGIDFKEDGNILGHKLEYNFNSHNVYITADKQKNGIK
ANFKIRHNVEDGSVQLADHYQQNTPIGDGPVLLPDNHYLSTQSVLSKDPNEKRDHMVLLEFVTAAGITHGMDELYKG
GGSGGSKGEELFTGVVPILVELDGDVNGHKFSVRGEGEGDATNGKLTLKFICTTGKLPVPWPTLVTTLTYGVQCFARYP
DHMKQHDFFKSAMPEGYVQERTISFKDDGTYKTRAEVKFEGDTLVNRIELKGIDFKEDGNILGHKLEYNFNSHNVYITA
DKQKNGIKANFKIRHNVEDGSVQLADHYQQNTPIGDGPVLLPDNHYLSTQSVLSKDPNEKRDHMVLLEFVTAAGITHG
MDELYKDYKDDDDK

Flag SNAP OSM-3

MDYKDDDDKGGMDKDCEMKRTTLDSPLGKLELSGCEQGLHEIKLLGKGTSAADAVEVPAPAAVLGGPEPLMQATAW
LNAYFHQPEAIEEFPVPALHHPVFQQESFTRQVLWKLLKVVKFGEVISYQQLAALAGNPAATAAVKTALSGNPVPILIPC

HRVVSSSGAVGGYEGGLAVKEWLLAHEGHRLGKPGLGAPGGGSGGSMAESVRVAVRCRPFNQREKDLNTTLCVGMT
PNVGQVNLNAPDGAAKDFTFDGAYFMDSTGEQIYNDIVFPLVENVIEGYNGTVFAYGQTGSGKTFSMQGIETIPAQR
GVIPRAFDHIFTATATTENVKFLVHCSYLEIYNEEVRDLLGADNKQKLEIKEQPDRGVYVAGLSMHVCHDVPACKELMT
RGFNNRHVGATLMNKDSSRSHSIFTVYVEGMTETGSIRMGKLNLVDLAGSERQSKTGATGDRLKEATKINLSLSALGNV
ISALVDGKSKHIPYRDSKLTRLLQDSLGGNTKTIMIACVSPSSDNYDETLSTLRYANRAKNIKNKPTINEDPKDALLREYQE
EIARLKSMVQPGAVGVGAPAQDAFSIEEERKKLREEFEEAMNDLRGEYEREQTSKAELQKDLESLRADYERANANLDNL
NPEEAAKKIQQLQDQFIGGEEAGNTQLKQKRMKQLKEAETKTQKLAAALNVHKDDPLLQVYSTTQEKLDAVTSQLEKE
VKKSKGYEREIEDLHGEFELDRLDYLDTIRKQDQQLKLLMQIMDKIQPIIKKDTNYSNVDRIKKEAVWNEDESRWILPEM
SMSRTILPLANNGYMQEPARQENTLLRSNFDDKLRERLAKSDSENLANSYFKPVKQINVINKYKSDQKLSTSKSLFPSKTP
TFDGLVNGVVYTDALYERAQSAKRPPRLASLNPK

Flag SNAP KIF-17 (NP_034753.1)

MDYKDDDDKGGMDKDCEMKRTTLDSPLGKLELSGCEQGLHEIKLLGKGTSAADAVEVPAPAAVLGGPEPLMQATAW
LNAYFHQPEAIEEFPVPALHHPVFQQESFTRQVLWKLLKVVKFGEVISYQQLAALAGNPAATAAVKTALSGNPVPILIPC
HRVVSSSGAVGGYEGGLAVKEWLLAHEGHRLGKPGLGGGSGGSGAPMASESVKVVVRCRPMNKRERELSCQSVVTV
DSARGQCFIQNPGAADEPPKQFTFDGAYYIEHFTEQIYNEIAYPLVEGVTEGYNGTIFAYGQTGSGKSFTMQGLPDPPC
QRGIIPRAFEHVFESVQCAENTKFLVRASYLEIYNEDVHDLLGADTKQRLELKEHPEKGVYVKGLSMHTVHNVAQCERV
METGWKNRAVGYTLMNKDSSRSHSIFTINIEIYAVDERGKDHLRAGKLNLVDLAGSERQSKTGATGERLKEATKINLSLS
ALGNVISALVDGRCKHIPYRDSKLTRLLQDSLGGNTKTLMVACLSPADNNYDETLSTLRYANRAKNIKNKPRINEDPKDA
LLREYQEEIKRLKAILAQQMGPGNLSALLSTQTPPGPVQSEEKLLSPTTVQQDTEAEKQLIREEYEERLARLKADYEAEQE
SRVRLQEDITAMRNSYDVKLSTLQENLRKEKETEAILKAEVLCKTEVMSRAELASGPEYSPPLQYETAVKPTILSMPDMPP
SGKVTKSQAPLAFEEPHGETSRSEFSFESNECSTLEDSATSEAFPGPEEFSNMEFSMAAALTESRYLPEEYLGGQEAAASP
LEAERYVQENEPSLEPLRILASLQDPFAEVEAKLARLSSTVAMSDSSQTVVPQIPKQPSSADLLEPSDTKSEADVAVADNV
VLGTEPDVNLRVAEEVVSEAETGVWMESEAQVAHVAQVSEEAQPQPLLAMVSVRRESVGVEVAVLTEEELQPVDQQ
QVLARLQLLEQQVVGGEQAKNKDLREKHKRRKRYADERKKQLVAALQNSDEDGGDWVLLNVYDSIQEEVRAKSKLLE
KMQRKLRAAEVEIKDLQSEFQLEKIDYLATIRRQERDSMLFQQLLEQVQPLIRRDCNYSNLEKIRRESSWDEDNGFWKIP
DPIILKTSLPVVPTGTQNKPARKTSAVDSGEPHMQEEDRYKLMLSRSDSENIASNYFRSKRASQILSTDPMKSLTYHNSP
PGLNSSLSNNSALPPTQTPEMPQPRPFRLESLDIPFSKAKRKKSKNSFGGEPL

Flag SNAP KIF-17$^{1-747}$

MDYKDDDDKGGMDKDCEMKRTTLDSPLGKLELSGCEQGLHEIKLLGKGTSAADAVEVPAPAAVLGGPEPLMQATAW
LNAYFHQPEAIEEFPVPALHHPVFQQESFTRQVLWKLLKVVKFGEVISYQQLAALAGNPAATAAVKTALSGNPVPILIPC
HRVVSSSGAVGGYEGGLAVKEWLLAHEGHRLGKPGLGGGSGGSGAPMASESVKVVVRCRPMNKRERELSCQSVVTV
DSARGQCFIQNPGAADEPPKQFTFDGAYYIEHFTEQIYNEIAYPLVEGVTEGYNGTIFAYGQTGSGKSFTMQGLPDPPC
QRGIIPRAFEHVFESVQCAENTKFLVRASYLEIYNEDVHDLLGADTKQRLELKEHPEKGVYVKGLSMHTVHNVAQCERV
METGWKNRAVGYTLMNKDSSRSHSIFTINIEIYAVDERGKDHLRAGKLNLVDLAGSERQSKTGATGERLKEATKINLSLS
ALGNVISALVDGRCKHIPYRDSKLTRLLQDSLGGNTKTLMVACLSPADNNYDETLSTLRYANRAKNIKNKPRINEDPKDA
LLREYQEEIKRLKAILAQQMGPGNLSALLSTQTPPGPVQSEEKLLSPTTVQQDTEAEKQLIREEYEERLARLKADYEAEQE
SRVRLQEDITAMRNSYDVKLSTLQENLRKEKETEAILKAEVLCKTEVMSRAELASGPEYSPPLQYETAVKPTILSMPDMPP
SGKVTKSQAPLAFEEPHGETSRSEFSFESNECSTLEDSATSEAFPGPEEFSNMEFSMAAALTESRYLPEEYLGGQEAAASP
LEAERYVQENEPSLEPLRILASLQDPFAEVEAKLARLSSTVAMSDSSQTVVPQIPKQPSSADLLEPSDTKSEADVAVADNV
VLGTEPDVNLRVAEEVVSEAETGVWMESEAQVAHVAQVSEEAQPQPLLAMVSVRRESVGVEVAVLTEEELQPVDQ

***C.elegans* KAP-1 SNAP 6xHis (NP_001367739.1)**

MNQVSIDAHPSDQAIIVRFEQSPSSSAGISIKKRASSANVESLGHQKIIHLKEMSLDVDIRALSNVILQKCLFIPATSRSQLE
QVLFYIQKRGNQRISARSRSSSAVSFDRRPIHSPTISAELGKIDEYIECFYGETSVEKNKGAVALYELSKNPQNLTQLVNNE
TLMMALARVFREDWKKHFEVGTNIMNLFVNISKFSCLHGILLHHKIGTLCVNAMEHETKRYDFWIAEMKKTDQETLRK
LKTAIRKQAMLLAACVTFLTNLATDISVELKMVRRNLVALLVKCLQMSSESTSSLTTATIKFLLKLSIFDENKIVMEQNGTIE
KLLKLFPIQDPELRKAVIMLLFNFSFDSKNLPKMVNGGLVPHMASLLDSDTKALNMMMYLLSCNDDAKAMLAYTDAIKLL
MKDVLSGTGSEVTKAVLLNICLEKRNAQLVCGQRGQGLDLLMEMSINSRDLMLIKVVRAISSHEGATQNMFLKWIETLI
GIAKNEGADNSESKSSFGLECMGTVAELKVAPWAKIIQSENLVPWMKTQLQEGIDESEEVTVLRDIKPLQLQIVIACGT
MARQLDAARLLAPLIDTFVQLLQSCQIDDEFVVQLLYVFLQFLKHKELSARLMTQDSALGAHMIDLMHDANAVVREVC
DNALLIMGEHSKEWAKRIAGERFKWHNAQWLEMVERDDSEFVDYDDEDFGADLKFDHYDDGFDMNEPLFGAPMD
KDCEMKRTTLDSPLGKLELSGCEQGLHEIKLLGKGTSAADAVEVPAPAAVLGGPEPLMQATAWLNAYFHQPEAIEEFPV
PALHHPVFQQESFTRQVLWKLLKVVKFGEVISYQQLAALAGNPAATAAVKTALSGNPVPILIPCHRVVSSSGAVGGYEG
GLAVKEWLLAHEGHRLGKPGLHHHHHH

SNAP KLP11 6XHis (NP_001369897.1)

MDKDCEMKRTTLDSPLGKLELSGCEQGLHEIKLLGKGTSAADAVEVPAPAAVLGGPEPLMQATAWLNAYFHQPEAIEE
FPVPALHHPVFQQESFTRQVLWKLLKVVKFGEVISYQQLAALAGNPAATAAVKTALSGNPVPILIPCHRVVSSSGAVGG
YEGGLAVKEWLLAHEGHRLGKPGLGAPMVEIMKKSSKQETVKVIVRCRPLSSQEIANNYSKIVHMRPQRGQIELKNPKE
QDEPSKDFTFDAIYDENSTQSDLYEETFRDLVDSVLNGYNATIFAYGQTGTGKTHTMEGKSSDPEQRGVIYKCIDHIFEH
MAASHNQEYLVRASYLEIYQEELRDLLEAESNKKLEIKERPDGGVYVKDLTSKLTRTVGEIHEVMIRGNGHRSVGRTNM
NEHSSRSHAIFIITVECSRIGEDGESHITVGRLNLVDLAGSERQSKTGATGERFKEATKINLSLSALGNVISALVDAKSAHIP
YRDSKLTRLLQDSLGGNSKTVMVACIGPASYNFEETLGTLRYANRAKNIKNQPKINEDPKDALLREFQEEIEMLREQLKQ
RKTRSRDGATQSFYDAERAKLEDDIEAIQKDDSLIKHEKDRLIREIQEKHDLLEKERIEQARVAERIANIQSRLIVGSEEDGR
LESRTKEQHAQLEKKRRELAEQKRREREMVEALERQEEDTVDLKQTFSDLRTEVEAKTKKLKKMLIKLRQARNEIRDVSG
AYSDERQDLDQTIAEVSKELKLKLLIVENFIPRDVSERIKERAEWNEDSFEWNVNAFQSTSSNSSTPLNNTIEVNEDGVFT
RSSGADSGVSVSGGNGTPATSQFLDKRLVATPGCRRPMSMCERMLVETAREQFGAQRRPPISGSGSFVEATIPEETIRF
CGENVVVFSALERFVPEVTDSDPSTFSNSMMMSARRPSIENLTIDASKVLVPILNQSTMILKNSKNGQARNDTMPPNG
SMRRSQNHHHHHH

Halo KLP11 EE 6xHis

MEIGTGFPFDPHYVEVLGERMHYVDVGPRDGTPVLFLHGNPTSSYVWRNIIPHVAPTHRCIAPDLIGMGKSDKPDLGY
FFDDHVRFMDAFIEALGLEEVVLVIHDWGSALGFHWAKRNPERVKGIAFMEFIRPIPTWDEWPEFARETFQAFRTTDV
GRKLIIDQNVFIEGTLPMGVVRPLTEVEMDHYREPFLNPVDREPLWRFPNELPIAGEPANIVALVEEYMDWLHQSPVPK
LLFWGTPGVLIPPAEAARLAKSLPNCKAVDIGPGLNLLQEDNPDLIGSEIARWLSTLEISGGGSGGSGAPMVEIMKKSSK
QETVKVIVRCRPLSSQEIANNYSKIVHMRPQRGQIELKNPKEQDEPSKDFTFDAIYDENSTQSDLYEETFRDLVDSVLNG
YNATIFAYGQTGTGKTHTMEGKSSDPEQRGVIYKCIDHIFEHMAASHNQEYLVRASYLEIYQEELRDLLEAESNKKLEIKE
RPDGGVYVKDLTSKLTRTVGEIHEVMIRGNGHRSVGRTNMNEHSSRSHAIFIITVECSRIGEDGESHITVGRLNLVDLAG
SERQSKTGATGERFKEATKINLSLSALGNVISALVDAKSAHIPYRDSKLTRLLQDSLGGNSKTVMVACIGPASYNFEETLG
TLRYANRAKNIKNQPKINEDPKDALLREFQEEIEMLREQLKQRKTRSRDGATQSFYDAERAKLEDDIEAIQKDDSLIKHEK
DRLIREIQEKHDLLEKERIEQARVAERIANIQSRLIVEEEEDGRLESRTKEQHAQLEKKRRELAEQKRREREMVEALERQEE
DTVDLKQTFSDLRTEVEAKTKKLKKMLIKLRQARNEIRDVSGAYSDERQDLDQTIAEVSKELKLKLLIVENFIPRDVSERIKE
RAEWNEDSFEWNVNAFQSTSSNSSTPLNNTIEVNEDGVFTRSSGADSGVSVSGGNGTPATSQFLDKRLVATPGCRRP
MSMCERMLVETAREQFGAQRRPPISGSGSFVEATIPEETIRFCGENVVVFSALERFVPEVTDSDPSTFSNSMMMSARR
PSIENLTIDASKVLVPILNQSTMILKNSKNGQARNDTMPPNGSMRRSQNHHHHHH

SNAP KLP11(Head) _KLP20(Tail) EE Flag

MDKDCEMKRTTLDSPLGKLELSGCEQGLHEIKLLGKGTSAADAVEVPAPAAVLGGPEPLMQATAWLNAYFHQPEAIEE
FPVPALHHPVFQQESFTRQVLWKLLKVVKFGEVISYQQLAALAGNPAATAAVKTALSGNPVPILIPCHRVVSSSGAVGG
YEGGLAVKEWLLAHEGHRLGKPGAPMVEIMKKSSKQETVKVIVRCRPLSSQEIANNYSKIVHMRPQRGQIELKNPKEQ
DEPSKDFTFDAIYDENSTQSDLYEETFRDLVDSVLNGYNATIFAYGQTGTGKTHTMEGKSSDPEQRGVIYKCIDHIFEHM
AASHNQEYLVRASYLEIYQEELRDLLEAESNKKLEIKERPDGGVYVKDLTSKLTRTVGEIHEVMIRGNGHRSVGRTNMNE
HSSRSHAIFIITVECSRIGEDGESHITVGRLNLVDLAGSERQSKTGATGERFKEATKINLSLSALGNVISALVDAKSAHIPYR
DSKLTRLLQDSLGGNSKTVMVACIGPASYNFEETLGTLRYANRAKNIKNQPKINEDPKDALLRKFQLEIEALRKILDEENP
GDDENQEEAWEAKMQEREVEMEKKRKILEERVNSAVNDEETHRLVKEMMENEAELKKARSEHEKLRSKLEKIEKKLIV
EEENLLEKVEEQAKLLEVNNKELEQSKFQEAHLRTQLEERTAVKVEIEERYSSLQEEAFVKSKKIKKVSNELKDARAELKDL
EEDHQRQVEAMLDDIRQLRKELLLNIAIIDEYIPVEHVELIEKYVSWSEEHGDWQLKAIAYTGNNMRASAPPAKKEFSN
NNQTVPMYYSYRADLGASTAEHRPRTSSKKHRASIRLQQLLTGGDYKDDDDK

SNAP KLP11(Head) _FLA10(Tail) 6xHis

MDKDCEMKRTTLDSPLGKLELSGCEQGLHEIKLLGKGTSAADAVEVPAPAAVLGGPEPLMQATAWLNAYFHQPEAIEE
FPVPALHHPVFQQESFTRQVLWKLLKVVKFGEVISYQQLAALAGNPAATAAVKTALSGNPVPILIPCHRVVSSSGAVGG
YEGGLAVKEWLLAHEGHRLGKPGLGAPMVEIMKKSSKQETVKVIVRCRPLSSQEIANNYSKIVHMRPQRGQIELKNPKE
QDEPSKDFTFDAIYDENSTQSDLYEETFRDLVDSVLNGYNATIFAYGQTGTGKTHTMEGKSSDPEQRGVIYKCIDHIFEH
MAASHNQEYLVRASYLEIYQEELRDLLEAESNKKLEIKERPDGGVYVKDLTSKLTRTVGEIHEVMIRGNGHRSVGRTNM
NEHSSRSHAIFIITVECSRIGEDGESHITVGRLNLVDLAGSERQSKTGATGERFKEATKINLSLSALGNVISALVDAKSAHIP
YRDSKLTRLLQDSLGGNSKTVMVACIGPASYNFEETLGTLRYANRAKNIKNQPKINEDPKDALLRQFQEEIKKLKEQLAA
RAAGGGGPITMPSGGGSPTQKIVERTEEVDPDIDAIKAQMRAELEAKMKSDISTEALDKAREEAEAAAKKQLQAIIDDQ
GKTEAQKKAARDALKKQAEEARAIAGAIEKEKQEKAVLESRIKEMEGKIVVGGVNMLEKVDELKQKSEDIKREAAIRKRQ
EEEAKRRLEELQAAQVDADAKFASLDEEINVKSRQLKKLFEKYQGKKGELADLQEQFQREREGMLEDYRILTQQIKLKNL
IIACFIPPDYQDKIMQHCHWQDYDSSWNIDCIAYAGNAVRTNQELQAAQEDKEHDAAAENERLKNCFFSYEQFEAAGA
GSKQGGGGGGGGGGAARPGSSAGRAVGSAARRTGGKAGGKDITDIGSLRDSVNWGDDDDKKKGAIPKAKGLVKDT
VDPRLRASKLKGGHHHHHH

Halo KLP11 8xGS EE 6xHis

MEIGTGFPFDPHYVEVLGERMHYVDVGPRDGTPVLFLHGNPTSSYVWRNIIPHVAPTHRCIAPDLIGMGKSDKPDLGY
FFDDHVRFMDAFIEALGLEEVVLVIHDWGSALGFHWAKRNPERVKGIAFMEFIRPIPTWDEWPEFARETFQAFRTTDV
GRKLIIDQNVFIEGTLPMGVVRPLTEVEMDHYREPFLNPVDREPLWRFPNELPIAGEPANIVALVEEYMDWLHQSPVPK
LLFWGTPGVLIPPAEAARLAKSLPNCKAVDIGPGLNLLQEDNPDLIGSEIARWLSTLEISGAPMVEIMKKSSKQETVKVIV
RCRPLSSQEIANNYSKIVHMRPQRGQIELKNPKEQDEPSKDFTFDAIYDENSTQSDLYEETFRDLVDSVLNGYNATIFAYG
QTGTGKTHTMEGKSSDPEQRGVIYKCIDHIFEHMAASHNQEYLVRASYLEIYQEELRDLLEAESNKKLEIKERPDGGVYV
KDLTSKLTRTVGEIHEVMIRGNGHRSVGRTNMNEHSSRSHAIFIITVECSRIGEDGESHITVGRLNLVDLAGSERQSKTGA
TGERFKEATKINLSLSALGNVISALVDAKSAHIPYRDSKLTRLLQDSLGGNSKTVMVACIGPASYNFEETLGTLRYANRAK
NIKNQPKINEDPKDALGSGSGSGSGSGSGSGSLREFQEEIEMLREQLKQRKTRSRDGATQSFYDAERAKLEDDIEAIQKD
DSLIKHEKDRLIREIQEKHDLLEKERIEQARVAERIANIQSRLIVEEEEDGRLESRTKEQHAQLEKKRRELAEQKRREREMV
EALERQEEDTVDLKQTFSDLRTEVEAKTKKLKKMLIKLRQARNEIRDVSGAYSDERQDLDQTIAEVSKELKLKLLIVENFIP
RDVSERIKERAEWNEDSFEWNVNAFQSTSSNSSTPLNNTIEVNEDGVFTRSSGADSGVSVSGGNGTPATSQFLDKRLV
ATPGCRRPMSMCERMLVETAREQFGAQRRPPISGSGSFVEATIPEETIRFCGENVVVFSALERFVPEVTDSDPSTFSNS
MMMSARRPSIENLTIDASKVLVPILNQSTMILKNSKNGQARNDTMPPNGSMRRSQNHHHHHH

Halo KLP11 EE FIP 6xHis

MEIGTGFPFDPHYVEVLGERMHYVDVGPRDGTPVLFLHGNPTSSYVWRNIIPHVAPTHRCIAPDLIGMGKSDKPDLGY
FFDDHVRFMDAFIEALGLEEVVLVIHDWGSALGFHWAKRNPERVKGIAFMEFIRPIPTWDEWPEFARETFQAFRTTDV
GRKLIIDQNVFIEGTLPMGVVRPLTEVEMDHYREPFLNPVDREPLWRFPNELPIAGEPANIVALVEEYMDWLHQSPVPK
LLFWGTPGVLIPPAEAARLAKSLPNCKAVDIGPGLNLLQEDNPDLIGSEIARWLSTLEISGGGSGGSGAPMVEIMKKSSK
QETVKVIVRCRPLSSQEIANNYSKIVHMRPQRGQIELKNPKEQDEPSKDFTFDAIYDENSTQSDLYEETFRDLVDSVLNG
YNATIFAYGQTGTGKTHTMEGKSSDPEQRGVIYKCIDHIFEHMAASHNQEYLVRASYLEIYQEELRDLLEAESNKKLEIKE
RPDGGVYVKDLTSKLTRTVGEIHEVMIRGNGHRSVGRTNMNEHSSRSHAIFIITVECSRIGEDGESHITVGRLNLVDLAG
SERQSKTGATGERFKEATKINLSLSALGNVISALVDAKSAHIPYRDSKLTRLLQDSLGGNSKTVMVACIGPASYNFEETLG
TLRYANRAKNIKNQPKINEDPKDALLREFQEEIEMLREQLKQRKTRSRDGATQSFYDAERAKLEDDIEAIQKDDSLIKHEK
DRLIREIQEKHDLLEKERIEQARVAERIANIQSRLIVEEEEDGRLESRTKEQHAQLEKKRRELAEQKRREREMVEALERQEE
DTVDLKQTFSDLRTEVEAKTKKLKKMLIKLRQARNEIRDVSGAYSDERQDLDQTIAEVSKELKLKLLIVENFIPHHHHHH

KLP11 GCN4 superfolder GFP Flag

MVEIMKKSSKQETVKVIVRCRPLSSQEIANNYSKIVHMRPQRGQIELKNPKEQDEPSKDFTFDAIYDENSTQSDLYEETF
RDLVDSVLNGYNATIFAYGQTGTGKTHTMEGKSSDPEQRGVIYKCIDHIFEHMAASHNQEYLVRASYLEIYQEELRDLLE
AESNKKLEIKERPDGGVYVKDLTSKLTRTVGEIHEVMIRGNGHRSVGRTNMNEHSSRSHAIFIITVECSRIGEDGESHITV
GRLNLVDLAGSERQSKTGATGERFKEATKINLSLSALGNVISALVDAKSAHIPYRDSKLTRLLQDSLGGNSKTVMVACIGP
ASYNFEETLGTLRYANRAKNIKNQPKINEDPKDALLREFQEEIGPRMKQLEDKVEELLSKNYHLENEVARLKKLVGEGAP
GGGSGGSMSKGEELFTGVVPILVELDGDVNGHKFSVRGEGEGDATNGKLTLKFICTTGKLPVPWPTLVTTLTYGVQCFA
RYPDHMKQHDFFKSAMPEGYVQERTISFKDDGTYKTRAEVKFEGDTLVNRIELKGIDFKEDGNILGHKLEYNFNSHNVYI
TADKQKNGIKANFKIRHNVEDGSVQLADHYQQNTPIGDGPVLLPDNHYLSTQSVLSKDPNEKRDHMVLLEFVTAAGIT
HGMDELYKDYKDDDDK

KLP20 Flag (NP_497178.1)

MEGAEKVKVVVRCRPISTTEKLQGHKIAVTCNDEEKAVNIKSLSQEDPPRTFYFDAVFSPNTDQMTVYNVAARPIVENV
LKGYNGTIFAYGQTGTGKTFTMAGDLEPVEMRGIIPNSFAHIFDHIAKCQHDTTFLVRVSYLEIYNEEIRDLLSKDHNGNL
EIKERPDVGVYVRNLSNPTVENASKMQALMEFGSKNRKVGATAMNLESSRSHAMFTVTIESCRNGLVTQGKLQLVDL
AGSERQSKTGAQGERLKEAAKINLSLSTLGNVISSLVDGKSTHIPYRNSKLTRLLQDSLGGNSKTVMIANVGPATYNYDET
LSTLRYANRAKNIQNVAKINEDPKDAQLRKFQLEIEALRKILDEENPGDDENQEEAWEAKMQEREVEMEKKRKILEERV
NSAVNDEETHRLVKEMMENEAELKKARSEHEKLRSKLEKIEKKLIVGGENLLEKVEEQAKLLEVNNKELEQSKFQEAHLR
TQLEERTAVKVEIEERYSSLQEEAFVKSKKIKKVSNELKDARAELKDLEEDHQRQVEAMLDDIRQLRKELLLNIAIIDEYIPV
EHVELIEKYVSWSEEHGDWQLKAIAYTGNNMRASAPPAKKEFSNNNQTVPMYYSYRADLGASTAEHRPRTSSKKHRA
SIRLQQLLTGGDYKDDDDK

KLP20 EE Flag

MEGAEKVKVVVRCRPISTTEKLQGHKIAVTCNDEEKAVNIKSLSQEDPPRTFYFDAVFSPNTDQMTVYNVAARPIVENV
LKGYNGTIFAYGQTGTGKTFTMAGDLEPVEMRGIIPNSFAHIFDHIAKCQHDTTFLVRVSYLEIYNEEIRDLLSKDHNGNL
EIKERPDVGVYVRNLSNPTVENASKMQALMEFGSKNRKVGATAMNLESSRSHAMFTVTIESCRNGLVTQGKLQLVDL
AGSERQSKTGAQGERLKEAAKINLSLSTLGNVISSLVDGKSTHIPYRNSKLTRLLQDSLGGNSKTVMIANVGPATYNYDET
LSTLRYANRAKNIQNVAKINEDPKDAQLRKFQLEIEALRKILDEENPGDDENQEEAWEAKMQEREVEMEKKRKILEERV
NSAVNDEETHRLVKEMMENEAELKKARSEHEKLRSKLEKIEKKLIVEENLLEKVEEQAKLLEVNNKELEQSKFQEAHLRT
QLEERTAVKVEIEERYSSLQEEAFVKSKKIKKVSNELKDARAELKDLEEDHQRQVEAMLDDIRQLRKELLLNIAIIDEYIPVE
HVELIEKYVSWSEEHGDWQLKAIAYTGNNMRASAPPAKKEFSNNNQTVPMYYSYRADLGASTAEHRPRTSSKKHRASI
RLQQLLTGGDYKDDDDK

Flag SNAP KLP20 EE

MDYKDDDDKGGMDKDCEMKRTTLDSPLGKLELSGCEQGLHEIKLLGKGTSAADAVEVPAPAAVLGGPEPLMQATAW
LNAYFHQPEAIEEFPVPALHHPVFQQESFTRQVLWKLLKVVKFGEVISYQQLAALAGNPAATAAVKTALSGNPVPILIPC
HRVVSSSGAVGGYEGGLAVKEWLLAHEGHRLGKPGLGGGSGGSMEGAEKVKVVVRCRPISTTEKLQGHKIAVTCNDE
EKAVNIKSLSQEDPPRTFYFDAVFSPNTDQMTVYNVAARPIVENVLKGYNGTIFAYGQTGTGKTFTMAGDLEPVEMRG
IIPNSFAHIFDHIAKCQHDTTFLVRVSYLEIYNEEIRDLLSKDHNGNLEIKERPDVGVYVRNLSNPTVENASKMQALMEFG
SKNRKVGATAMNLESSRSHAMFTVTIESCRNGLVTQGKLQLVDLAGSERQSKTGAQGERLKEAAKINLSLSTLGNVISSL
VDGKSTHIPYRNSKLTRLLQDSLGGNSKTVMIANVGPATYNYDETLSTLRYANRAKNIQNVAKINEDPKDAQLRKFQLEI
EALRKILDEENPGDDENQEEAWEAKMQEREVEMEKKRKILEERVNSAVNDEETHRLVKEMMENEAELKKARSEHEKL
RSKLEKIEKKLIVEEENLLEKVEEQAKLLEVNNKELEQSKFQEAHLRTQLEERTAVKVEIEERYSSLQEEAFVKSKKIKKVSNE
LKDARAELKDLEEDHQRQVEAMLDDIRQLRKELLLNIAIIDEYIPVEHVELIEKYVSWSEEHGDWQLKAIAYTGNNMRAS
APPAKKEFSNNNQTVPMYYSYRADLGASTAEHRPRTSSKKHRASIRLQQLLT

Halo KLP20_KLP11 EE 6xHis

MEIGTGFPFDPHYVEVLGERMHYVDVGPRDGTPVLFLHGNPTSSYVWRNIIPHVAPTHRCIAPDLIGMGKSDKPDLGY
FFDDHVRFMDAFIEALGLEEVVLVIHDWGSALGFHWAKRNPERVKGIAFMEFIRPIPTWDEWPEFARETFQAFRTTDV
GRKLIIDQNVFIEGTLPMGVVRPLTEVEMDHYREPFLNPVDREPLWRFPNELPIAGEPANIVALVEEYMDWLHQSPVPK
LLFWGTPGVLIPPAEAARLAKSLPNCKAVDIGPGLNLLQEDNPDLIGSEIARWLSTLEISGAPMEGAEKVKVVVRCRPIST
TEKLQGHKIAVTCNDEEKAVNIKSLSQEDPPRTFYFDAVFSPNTDQMTVYNVAARPIVENVLKGYNGTIFAYGQTGTGK
TFTMAGDLEPVEMRGIIPNSFAHIFDHIAKCQHDTTFLVRVSYLEIYNEEIRDLLSKDHNGNLEIKERPDVGVYVRNLSNP
TVENASKMQALMEFGSKNRKVGATAMNLESSRSHAMFTVTIESCRNGLVTQGKLQLVDLAGSERQSKTGAQGERLKE
AAKINLSLSTLGNVISSLVDGKSTHIPYRNSKLTRLLQDSLGGNSKTVMIANVGPATYNYDETLSTLRYANRAKNIQNVAKI
NEDPKDAQLREFQEEIEMLREQLKQRKTRSRDGATQSFYDAERAKLEDDIEAIQKDDSLIKHEKDRLIREIQEKHDLLEKE
RIEQARVAERIANIQSRLIVEEEEDGRLESRTKEQHAQLEKKRRELAEQKRREREMVEALERQEEDTVDLKQTFSDLRTEV
EAKTKKLKKMLIKLRQARNEIRDVSGAYSDERQDLDQTIAEVSKELKLKLLIVENFIPRDVSERIKERAEWNEDSFEWNVN
AFQSTSSNSSTPLNNTIEVNEDGVFTRSSGADSGVSVSGGNGTPATSQFLDKRLVATPGCRRPMSMCERMLVETAREQ
FGAQRRPPISGSGSFVEATIPEETIRFCGENVVVFSALERFVPEVTDSDPSTFSNSMMMSARRPSIENLTIDASKVLVPILN
QSTMILKNSKNGQARNDTMPPNGSMRRSQNGPHHHHHH

Flag SNAP KLP20 8xGS EE

MDYKDDDDKGGMDKDCEMKRTTLDSPLGKLELSGCEQGLHEIKLLGKGTSAADAVEVPAPAAVLGGPEPLMQATAW
LNAYFHQPEAIEEFPVPALHHPVFQQESFTRQVLWKLLKVVKFGEVISYQQLAALAGNPAATAAVKTALSGNPVPILIPC
HRVVSSSGAVGGYEGGLAVKEWLLAHEGHRLGKPGLGGAPMEGAEKVKVVVRCRPISTTEKLQGHKIAVTCNDEEKA
VNIKSLSQEDPPRTFYFDAVFSPNTDQMTVYNVAARPIVENVLKGYNGTIFAYGQTGTGKTFTMAGDLEPVEMRGIIPN
SFAHIFDHIAKCQHDTTFLVRVSYLEIYNEEIRDLLSKDHNGNLEIKERPDVGVYVRNLSNPTVENASKMQALMEFGSKN
RKVGATAMNLESSRSHAMFTVTIESCRNGLVTQGKLQLVDLAGSERQSKTGAQGERLKEAAKINLSLSTLGNVISSLVD
GKSTHIPYRNSKLTRLLQDSLGGNSKTVMIANVGPATYNYDETLSTLRYANRAKNIQNVAKINEDPKDAQGSGSGSGSG
SGSGSLRKFQLEIEALRKILDEENPGDDENQEEAWEAKMQEREVEMEKKRKILEERVNSAVNDEETHRLVKEMMENEA
ELKKARSEHEKLRSKLEKIEKKLIVEEENLLEKVEEQAKLLEVNNKELEQSKFQEAHLRTQLEERTAVKVEIEERYSSLQEEAF
VKSKKIKKVSNELKDARAELKDLEEDHQRQVEAMLDDIRQLRKELLLNIAIIDEYIPVEHVELIEKYVSWSEEHGDWQLKAI
AYTGNNMRASAPPAKKEFSNNNQTVPMYYSYRADLGASTAEHRPRTSSKKHRASIRLQQLLTGP

KLP20 FIP EE Flag

MEGAEKVKVVVRCRPISTTEKLQGHKIAVTCNDEEKAVNIKSLSQEDPPRTFYFDAVFSPNTDQMTVYNVAARPIVENV
LKGYNGTIFAYGQTGTGKTFTMAGDLEPVEMRGIIPNSFAHIFDHIAKCQHDTTFLVRVSYLEIYNEEIRDLLSKDHNGNL
EIKERPDVGVYVRNLSNPTVENASKMQALMEFGSKNRKVGATAMNLESSRSHAMFTVTIESCRNGLVTQGKLQLVDL

AGSERQSKTGAQGERLKEAAKINLSLSTLGNVISSLVDGKSTHIPYRNSKLTRLLQDSLGGNSKTVMIANVGPATYNYDET
LSTLRYANRAKNIQNVAKINEDPKDAQLRKFQLEIEALRKILDEENPGDDENQEEAWEAKMQEREVEMEKKRKILEERV
NSAVNDEETHRLVKEMMENEAELKKARSEHEKLRSKLEKIEKKLIVEEENLLEKVEEQAKLLEVNNKELEQSKFQEAHLRT
QLEERTAVKVEIEERYSSLQEEAFVKSKKIKKVSNELKDARAELKDLEEDHQRQVEAMLDDIRQLRKELLLNIAIIDEYIPGG
DYKDDDDK

KLP20(Head)_FLA8(Tail) Flag

MEGAEKVKVVVRCRPISTTEKLQGHKIAVTCNDEEKAVNIKSLSQEDPPRTFYFDAVFSPNTDQMTVYNVAARPIVENV
LKGYNGTIFAYGQTGTGKTFTMAGDLEPVEMRGIIPNSFAHIFDHIAKCQHDTTFLVRVSYLEIYNEEIRDLLSKDHNGNL
EIKERPDVGVYVRNLSNPTVENASKMQALMEFGSKNRKVGATAMNLESSRSHAMFTVTIESCRNGLVTQGKLQLVDL
AGSERQSKTGAQGERLKEAAKINLSLSTLGNVISSLVDGKSTHIPYRNSKLTRLLQDSLGGNSKTVMIANVGPATYNYDET
LSTLRYANRAKNIQNVAKINEDPKDAQLREFQDEIARLKAALEAEGGALPEGFATGPGGEIIVEKVVQVPKALDASFLEQ
MRKDMEEQMKKELASQQAAALNDEQLQKVKEEAAAKAKAEAARLEEEKKKAEEEAARMQRKQQKIKAEMDKKSLD
AEQIRAEKEALAKKLKAMESKILKGDQAGGLAEVTKKKEEELKRKEQELERRRKEEEEQRKKIQVMEEQQLAMEDKYKD
KADEADQKTKKLKKLWKKFQEVNAEVEDMYKEFQREKEDLLESIRMLQDQMQLKDMVIEAFIPPEEVQKVMKRAHW
DDEREVWVLERLSDIGKRETAQGASRRPVSASGQRRPTSDFAKLANAMGDMNPRFKSENILNLELDLPERTTYDYEGP
GVDPRVQAAINAAFAEDGELIFVGSEQNVHLGDASAAAARPDSAKKRPASARKGTKKGGDYKDDDDK

KLP20 GCN4 superfolder GFP Flag

MEGAEKVKVVVRCRPISTTEKLQGHKIAVTCNDEEKAVNIKSLSQEDPPRTFYFDAVFSPNTDQMTVYNVAARPIVENV
LKGYNGTIFAYGQTGTGKTFTMAGDLEPVEMRGIIPNSFAHIFDHIAKCQHDTTFLVRVSYLEIYNEEIRDLLSKDHNGNL
EIKERPDVGVYVRNLSNPTVENASKMQALMEFGSKNRKVGATAMNLESSRSHAMFTVTIESCRNGLVTQGKLQLVDL
AGSERQSKTGAQGERLKEAAKINLSLSTLGNVISSLVDGKSTHIPYRNSKLTRLLQDSLGGNSKTVMIANVGPATYNYDET
LSTLRYANRAKNIQNVAKINEDPKDAQLRKFQLEIGPRMKQLEDKVEELLSKNYHLENEVARLKKLVGEGAPGGGSGGS
MSKGEELFTGVVPILVELDGDVNGHKFSVRGEGEGDATNGKLTLKFICTTGKLPVPWPTLVTTLTYGVQCFARYPDHM
KQHDFFKSAMPEGYVQERTISFKDDGTYKTRAEVKFEGDTLVNRIELKGIDFKEDGNILGHKLEYNFNSHNVYITADKQK
NGIKANFKIRHNVEDGSVQLADHYQQNTPIGDGPVLLPDNHYLSTQSVLSKDPNEKRDHMVLLEFVTAAGITHGMDEL
YKDYKDDDDK

Flag SNAP Kin-1$^{1\text{-}560}$ (P33176.1)

MDYKDDDDKGGMDKDCEMKRTTLDSPLGKLELSGCEQGLHEIKLLGKGTSAADAVEVPAPAAVLGGPEPLMQATAW
LNAYFHQPEAIEEFPVPALHHPVFQQESFTRQVLWKLLKVVKFGEVISYQQLAALAGNPAATAAVKTALSGNPVPILIPC
HRVVSSSGAVGGYEGGLAVKEWLLAHEGHRLGKPGLGGGSGGSGAPMADLAECNIKVMCRFRPLNESEVNRGDKYIA
KFQGEDTVVIASKPYAFDRVFQSSTSQEQVYNDCAKKIVKDVLEGYNGTIFAYGQTSSGKTHTMEGKLHDPEGMGIIPRI
VQDIFNYIYSMDENLEFHIKVSYFEIYLDKIRDLLDVSKTNLSVHEDKNRVPYVKGCTERFVCSPDEVMDTIDEGKSNRHV
AVTNMNEHSSRSHSIFLINVKQENTQTEQKLSGKLYLVDLAGSEKVSKTGAEGAVLDEAKNINKSLSALGNVISALAEGST
YVPYRDSKMTRILQDSLGGNCRTTIVICCSPSSYNESETKSTLLFGQRAKTIKNTVCVNVELTAEQWKKKYEKEKEKNKILR
NTIQWLENELNRWRNGETVPIDEQFDKEKANLEAFTVDKDITLTNDKPATAIGVIGNFTDAERRKCEEEIAKLYKQLDDK
DEEINQQSQLVEKLKTQMLDQEELLASTRRDQDNMQAELNRLQAENDASKEEVKEVLQALEELAVNYDQKSQEVEDK
TKEYELLSDELNQKSATLASIDAELQKLKEMTNHQKKRAAEMMASLLKGP

Flag SNAP Kin-1_ 5xGS

MDYKDDDDKGGMDKDCEMKRTTLDSPLGKLELSGCEQGLHEIKLLGKGTSAADAVEVPAPAAVLGGPEPLMQATAW
LNAYFHQPEAIEEFPVPALHHPVFQQESFTRQVLWKLLKVVKFGEVISYQQLAALAGNPAATAAVKTALSGNPVPILIPC
HRVVSSSGAVGGYEGGLAVKEWLLAHEGHRLGKPGLGGGSGGSGAPMADLAECNIKVMCRFRPLNESEVNRGDKYIA
KFQGEDTVVIASKPYAFDRVFQSSTSQEQVYNDCAKKIVKDVLEGYNGTIFAYGQTSSGKTHTMEGKLHDPEGMGIIPRI

VQDIFNYIYSMDENLEFHIKVSYFEIYLDKIRDLLDVSKTNLSVHEDKNRVPYVKGCTERFVCSPDEVMDTIDEGKSNRHV
AVTNMNEHSSRSHSIFLINVKQENTQTEQKLSGKLYLVDLAGSEKVSKTGAEGAVLDEAKNINKSLSALGNVISALAEGST
YVPYRDSKMTRILQDSLGGNCRTTIVICCSPSSYNESETKSTLLFGQRAKTIKNTVCVNVELGSGSGSGSGSTAEQWKKKY
EKEKEKNKILRNTIQWLENELNRWRNGETVPIDEQFDKEKANLEAFTVDKDITLTNDKPATAIGVIGNFTDAERRKCEEEI
AKLYKQLDDKDEEINQQSQLVEKLKTQMLDQEELLASTRRDQDNMQAELNRLQAENDASKEEVKEVLQALEELAVNY
DQKSQEVEDKTKEYELLSDELNQKSATLASIDAELQKLKEMTNHQKKRAAEMMASLLKGP

Flag SNAP KLP20_ 5xGS_Kin-1

MDYKDDDDKGGMDKDCEMKRTTLDSPLGKLELSGCEQGLHEIKLLGKGTSAADAVEVPAPAAVLGGPEPLMQATAW
LNAYFHQPEAIEEFPVPALHHPVFQQESFTRQVLWKLLKVVKFGEVISYQQLAALAGNPAATAAVKTALSGNPVPILIPC
HRVVSSSGAVGGYEGGLAVKEWLLAHEGHRLGKPGLGGGSGGSGAPMEGAEKVKVVVRCRPISTTEKLQGHKIAVTC
NDEEKAVNIKSLSQEDPPRTFYFDAVFSPNTDQMTVYNVAARPIVENVLKGYNGTIFAYGQTGTGKTFTMAGDLEPVE
MRGIIPNSFAHIFDHIAKCQHDTTFLVRVSYLEIYNEEIRDLLSKDHNGNLEIKERPDVGVYVRNLSNPTVENASKMQAL
MEFGSKNRKVGATAMNLESSRSHAMFTVTIESCRNGLVTQGKLQLVDLAGSERQSKTGAQGERLKEAAKINLSLSTLG
NVISSLVDGKSTHIPYRNSKLTRLLQDSLGGNSKTVMIANVGPATYNYDETLSTLRYANRAKTIKNTVCVNVELGSGSGS
GSGSTAEQWKKKYEKEKEKNKILRNTIQWLENELNRWRNGETVPIDEQFDKEKANLEAFTVDKDITLTNDKPATAIGVI
GNFTDAERRKCEEEIAKLYKQLDDKDEEINQQSQLVEKLKTQMLDQEELLASTRRDQDNMQAELNRLQAENDASKEEV
KEVLQALEELAVNYDQKSQEVEDKTKEYELLSDELNQKSATLASIDAELQKLKEMTNHQKKRAAEMMASLLKGP

FLA8 Flag (XP_001697037.1)

MASGGECVKVAVRCRPLNGKEKGDNRATIVEVDNKTGQVTLNNPKGDEPPKTFTFDNAFDWNVTQRDVY
DVVARPIVNSVMDGYNGTIFAYGQTGTGKTHTMEGFPTPELQGIIPNCFDHVFETVNSSTGKQWMVRASYL
EIYNEEVRDLLSKDPKNKLELKEHKDSGVYVKGLNAFVVKGVPELKNVLEVGKKNRSVGATLMNQDSSRSHSI
FTITIETIEQTQAQPEGHIRVGKLNLVDLAGSERQSKTGATGDRLKEATKINLSLSALGNVISALVDGKSGHVPY
RDSKLTRLLQDSLGGNTKTIMCANMGPADWNYDETLSTLRYANRAKNIKNKPKINEDPKDAMLREFQDEIA
RLKAALEAEGGALPEGFATGPGGEIIVEKVVQVPKALDASFLEQMRKDMEEQMKKELASQQAAALNDEQL
QKVKEEAAAKAKAEAARLEEEKKKAEEEAARMQRKQQKIKAEMDKKSLDAEQIRAEKEALAKKLKAMESKIL
KGDQAGGLAEVTKKKEEELKRKEQELERRRKEEEEQRKKIQVMEEQQLAMEDKYKDKADEADQKTKKLKKL
WKKFQEVNAEVEDMYKEFQREKEDLLESIRMLQDQMQLKDMVIEAFIPPEEVQKVMKRAHWDDEREVW
VLERLSDIGKRETAQGASRRPVSASGQRRPTSDFAKLANAMGDMNPRFKSENILNLELDLPERTTYDYEGPG
VDPRVQAAINAAFAEDGELIFVGSEQNVHLGDASAAAARPDSAKKRPASARKGTKKGAPDYKDDDDK

FLA8 superfolder GFP Flag

MASGGECVKVAVRCRPLNGKEKGDNRATIVEVDNKTGQVTLNNPKGDEPPKTFTFDNAFDWNVTQRDVY
DVVARPIVNSVMDGYNGTIFAYGQTGTGKTHTMEGFPTPELQGIIPNCFDHVFETVNSSTGKQWMVRASYL
EIYNEEVRDLLSKDPKNKLELKEHKDSGVYVKGLNAFVVKGVPELKNVLEVGKKNRSVGATLMNQDSSRSHSI
FTITIETIEQTQAQPEGHIRVGKLNLVDLAGSERQSKTGATGDRLKEATKINLSLSALGNVISALVDGKSGHVPY
RDSKLTRLLQDSLGGNTKTIMCANMGPADWNYDETLSTLRYANRAKNIKNKPKINEDPKDAMLREFQDEIA
RLKAALEAEGGALPEGFATGPGGEIIVEKVVQVPKALDASFLEQMRKDMEEQMKKELASQQAAALNDEQL
QKVKEEAAAKAKAEAARLEEEKKKAEEEAARMQRKQQKIKAEMDKKSLDAEQIRAEKEALAKKLKAMESKIL
KGDQAGGLAEVTKKKEEELKRKEQELERRRKEEEEQRKKIQVMEEQQLAMEDKYKDKADEADQKTKKLKKL
WKKFQEVNAEVEDMYKEFQREKEDLLESIRMLQDQMQLKDMVIEAFIPPEEVQKVMKRAHWDDEREVW
VLERLSDIGKRETAQGASRRPVSASGQRRPTSDFAKLANAMGDMNPRFKSENILNLELDLPERTTYDYEGPG

VDPRVQAAINAAFAEDGELIFVGSEQNVHLGDASAAAARPDSAKKRPASARKGTKKGAPMSKGEELFTGVVPI
LVELDGDVNGHKFSVRGEGEGDATNGKLTLKFICTTGKLPVPWPTLVTTLTYGVQCFARYPDHMKQHDFFKSAMPEG
YVQERTISFKDDGTYKTRAEVKFEGDTLVNRIELKGIDFKEDGNILGHKLEYNFNSHNVYITADKQKNGIKANFKIRHNVE
DGSVQLADHYQQNTPIGDGPVLLPDNHYLSTQSVLSKDPNEKRDHMVLLEFVTAAGITHGMDELYKDYKDDDDK

FLA8_KLP20 Flag

MASGGECVKVAVRCRPLNGKEKGDNRATIVEVDNKTGQVTLNNPKGDEPPKTFTFDNAFDWNVTQRDVY
DVVARPIVNSVMDGYNGTIFAYGQTGTGKTHTMEGFPTPELQGIIPNCFDHVFETVNSSTGKQWMVRASYL
EIYNEEVRDLLSKDPKNKLELKEHKDSGVYVKGLNAFVVKGVPELKNVLEVGKKNRSVGATLMNQDSSRSHSI
FTITIETIEQTQAQPEGHIRVGKLNLVDLAGSERQSKTGATGDRLKEATKINLSLSALGNVISALVDGKSGHVPY
RDSKLTRLLQDSLGGNTKTIMCANMGPADWNYDETLSTLRYANRAKNIKNKPKINEDPKDAMLRKFQLEIEA
LRKILDEENPGDDENQEEAWEAKMQEREVEMEKKRKILEERVNSAVNDEETHRLVKEMMENEAELKKARSE
HEKLRSKLEKIEKKLIVGGENLLEKVEEQAKLLEVNNKELEQSKFQEAHLRTQLEERTAVKVEIEERYSSLQEEAF
VKSKKIKKVSNELKDARAELKDLEEDHQRQVEAMLDDIRQLRKELLLNIAIIDEYIPVEHVELIEKYVSWSEEHG
DWQLKAIAYTGNNMRASAPPAKKEFSNNNQTVPMYYSYRADLGASTAEHRPRTSSKKHRASIRLQQLLTGT
GAPDYKDDDDK

FLA8_FLA10 6xHis

MASGGECVKVAVRCRPLNGKEKGDNRATIVEVDNKTGQVTLNNPKGDEPPKTFTFDNAFDWNVTQRDVY
DVVARPIVNSVMDGYNGTIFAYGQTGTGKTHTMEGFPTPELQGIIPNCFDHVFETVNSSTGKQWMVRASYL
EIYNEEVRDLLSKDPKNKLELKEHKDSGVYVKGLNAFVVKGVPELKNVLEVGKKNRSVGATLMNQDSSRSHSI
FTITIETIEQTQAQPEGHIRVGKLNLVDLAGSERQSKTGATGDRLKEATKINLSLSALGNVISALVDGKSGHVPY
RDSKLTRLLQDSLGGNTKTIMCANMGPADWNYDETLSTLRYANRAKNIKNKPKINEDPKDAMLRQFQEEIK
KLKEQLAARAAGGGGPITMPSGGGSPTQKIVERTEEVDPDIDAIKAQMRAELEAKMKSDISTEALDKAREEA
EAAAKKQLQAIIDDQGKTEAQKKAARDALKKQAEEARAIAGAIEKEKQEKAVLESRIKEMEGKIVVGGVNML
EKVDELKQKSEDIKREAAIRKRQEEEAKRRLEELQAAQVDADAKFASLDEEINVKSRQLKKLFEKYQGKKGELA
DLQEQFQREREGMLEDYRILTQQIKLKNLIIACFIPPDYQDKIMQHCHWQDYDSSWNIDCIAYAGNAVRTN
QELQAQEDKEHDAAAENERLKNCFFSYEQFEAAGAGSKQGGGGGGGGGGAARPGSSAGRAVGSAARRTG
GKAGGKDITDIGSLRDSVNWGDDDDKKKGAIPKAKGLVKDTVDPRLRASKLKGGHHHHHH

FLA10 Halo 6xHis (XP_001701510.1)

MPPAGGGSESVKVVVRCRPLNGKEKADGRSRIVDMDVDAGQVKVRNPKADASEPPKAFTFDQVYDWNC
QQRDVFDITARPLIDSCIEGYNGTIFAYGQTGTGKSHTMEGKDEPPELRGLIPNTFRYVFEIIARDSGTKEFLVR
SSYLEIYNEEVRDLLGKDHSKKMELKESPDRGVYVKDLSQFVCKNYEEMNKVLLAGKDNRQVGATLMNQDS
SRSHSIFTITIECIEKLESAAAQKPGAKKDDSNHVRVGKLNLVDLAGSERQDKTGATGDRLKEGIKINLSLTALG
NVISALVDGKSGHIPYRDSKLTRLLQDSLGGNTKTVMVANIGPADWNYDETMSTLRYANRAKNIQNKPKINE
DPKDAMLRQFQEEIKKLKEQLAARAAGGGGPITMPSGGGSPTQKIVERTEEVDPDIDAIKAQMRAELEAKM
KSDISTEALDKAREEAEAAAKKQLQAIIDDQGKTEAQKKAARDALKKQAEEARAIAGAIEKEKQEKAVLESRIK
EMEGKIVVGGVNMLEKVDELKQKSEDIKREAAIRKRQEEEAKRRLEELQAAQVDADAKFASLDEEINVKSRQ
LKKLFEKYQGKKGELADLQEQFQREREGMLEDYRILTQQIKLKNLIIACFIPPDYQDKIMQHCHWQDYDSSW
NIDCIAYAGNAVRTNQELQAQEDKEHDAAAENERLKNCFFSYEQFEAAGAGSKQGGGGGGGGGGAARPG

SSAGRAVGSAARRTGGKAGGKDITDIGSLRDSVNWGDDDDKKKGAIPKAKGLVKDTVDPRLRASKLKGAPG
GGSGGSMEIGTGFPFDPHYVEVLGERMHYVDVGPRDGTPVLFLHGNPTSSYVWRNIIPHVAPTHRCIAPDLI
GMGKSDKPDLGYFFDDHVRFMDAFIEALGLEEVVLVIHDWGSALGFHWAKRNPERVKGIAFMEFIRPIPTW
DEWPEFARETFQAFRTTDVGRKLIIDQNVFIEGTLPMGVVRPLTEVEMDHYREPFLNPVDREPLWRFPNELPI
AGEPANIVALVEEYMDWLHQSPVPKLLFWGTPGVLIPPAEAARLAKSLPNCKAVDIGPGLNLLQEDNPDLIG
SEIARWLSTLEISGGHHHHHH

FLA10 EE 6xHis

MPPAGGGSESVKVVVRCRPLNGKEKADGRSRIVDMDVDAGQVKVRNPKADASEPPKAFTFDQVYDWNC
QQRDVFDITARPLIDSCIEGYNGTIFAYGQTGTGKSHTMEGKDEPPELRGLIPNTFRYVFEIIARDSGTKEFLVR
SSYLEIYNEEVRDLLGKDHSKKMELKESPDRGVYVKDLSQFVCKNYEEMNKVLLAGKDNRQVGATLMNQDS
SRSHSIFTITIECIEKLESAAAQKPGAKKDDSNHVRVGKLNLVDLAGSERQDKTGATGDRLKEGIKINLSLTALG
NVISALVDGKSGHIPYRDSKLTRLLQDSLGGNTKTVMVANIGPADWNYDETMSTLRYANRAKNIQNKPKINE
DPKDAMLRQFQEEIKKLKEQLAARAAGGGGPITMPSGGGSPTQKIVERTEEVDPDIDAIKAQMRAELEAKM
KSDISTEALDKAREEAEAAAKKQLQAIIDDQGKTEAQKKAARDALKKQAEEARAIAGAIEKEKQEKAVLESRIK
EMEGKIVVEEVNMLEKVDELKQKSEDIKREAAIRKRQEEEAKRRLEELQAAQVDADAKFASLDEEINVKSRQL
KKLFEKYQGKKGELADLQEQFQREREGMLEDYRILTQQIKLKNLIIACFIPPDYQDKIMQHCHWQDYDSSWN
IDCIAYAGNAVRTNQELQAQEDKEHDAAAENERLKNCFFSYEQFEAAGAGSKQGGGGGGGGGGAARPGSS
AGRAVGSAARRTGGKAGGKDITDIGSLRDSVNWGDDDDKKKGAIPKAKGLVKDTVDPRLRASKLKGAPGG
GSGGSHHHHHH

SNAP FLA10_ KLP11 6xHis

MDKDCEMKRTTLDSPLGKLELSGCEQGLHEIKLLGKGTSAADAVEVPAPAAVLGGPEPLMQATAWLNAYFHQPEAIEE
FPVPALHHPVFQQESFTRQVLWKLLKVVKFGEVISYQQLAALAGNPAATAAVKTALSGNPVPILIPCHRVVSSSGAVGG
YEGGLAVKEWLLAHEGHRLGKPGLGGGSGGSGTMPPAGGGSESVKVVVRCRPLNGKEKADGRSRIVDMDVDAGQV
KVRNPKADASEPPKAFTFDQVYDWNCQQRDVFDITARPLIDSCIEGYNGTIFAYGQTGTGKSHTMEGKDEPPELRGLIP
NTFRYVFEIIARDSGTKEFLVRSSYLEIYNEEVRDLLGKDHSKKMELKESPDRGVYVKDLSQFVCKNYEEMNKVLLAGKDN
RQVGATLMNQDSSRSHSIFTITIECIEKLESAAAQKPGAKKDDSNHVRVGKLNLVDLAGSERQDKTGATGDRLKEGIKIN
LSLTALGNVISALVDGKSGHIPYRDSKLTRLLQDSLGGNTKTVMVANIGPADWNYDETMSTLRYANRAKNIQNKPKINE
DPKDAMLREFQEEIEMLREQLKQRKTRSRDGATQSFYDAERAKLEDDIEAIQKDDSLIKHEKDRLIREIQEKHDLLEKERIE
QARVAERIANIQSRLIVGSEEDGRLESRTKEQHAQLEKKRRELAEQKRREREMVEALERQEEDTVDLKQTFSDLRTEVEA
KTKKLKKMLIKLRQARNEIRDVSGAYSDERQDLDQTIAEVSKELKLKLLIVENFIPRDVSERIKERAEWNEDSFEWNVNAF
QSTSSNSSTPLNNTIEVNEDGVFTRSSGADSGVSVSGGNGTPATSQFLDKRLVATPGCRRPMSMCERMLVETAREQFG
AQRRPPISGSGSFVEATIPEETIRFCGENVVVFSALERFVPEVTDSDPSTFSNSMMMSARRPSIENLTIDASKVLVPILNQS
TMILKNSKNGQARNDTMPPNGSMRRSQNGTGAPHHHHHH

FLA10_FLA8 Flag

MPPAGGGSESVKVVVRCRPLNGKEKADGRSRIVDMDVDAGQVKVRNPKADASEPPKAFTFDQVYDWNCQQRDVF
DITARPLIDSCIEGYNGTIFAYGQTGTGKSHTMEGKDEPPELRGLIPNTFRYVFEIIARDSGTKEFLVRSSYLEIYNEEVRDLL
GKDHSKKMELKESPDRGVYVKDLSQFVCKNYEEMNKVLLAGKDNRQVGATLMNQDSSRSHSIFTITIECIEKLESAAAQ

KPGAKKDDSNHVRVGKLNLVDLAGSERQDKTGATGDRLKEGIKINLSLTALGNVISALVDGKSGHIPYRDSKLTRLLQDS
LGGNTKTVMVANIGPADWNYDETMSTLRYANRAKNIQNKPKINEDPKDAMLREFQDEIARLKAALEAEGGALPEG
FATGPGGEIIVEKVVQVPKALDASFLEQMRKDMEEQMKKELASQQAAALNDEQLQKVKEEAAAKAKAEAA
RLEEEKKKAEEEAARMQRKQQKIKAEMDKKSLDAEQIRAEKEALAKKLKAMESKILKGDQAGGLAEVTKKKE
EELKRKEQELERRRKEEEEQRKKIQVMEEQQLAMEDKYKDKADEADQKTKKLKKLWKKFQEVNAEVEDMY
KEFQREKEDLLESIRMLQDQMQLKDMVIEAFIPPEEVQKVMKRAHWDDEREVWVLERLSDIGKRETAQGA
SRRPVSASGQRRPTSDFAKLANAMGDMNPRFKSENILNLELDLPERTTYDYEGPGVDPRVQAAINAAFAED
GELIFVGSEQNVHLGDASAAAARPDSAKKRPASARKGTKKGGDYKDDDDK

2. IFT-B subunits

Mouse IFT52 superfolder GFP Flag (NP_742162.2)

MEKELRSTILFNAYKKEVFTTNTGYKSLQKRLRSNWKIQSLKDEITSEKLIGVKLWITAGPREKFTAAEFEVLKKYLDSGGDI
LVMLGEGGESRFDTNINFLLEEYGIMVNNDAVVRNVYYKYFHPKEALVSDGVLNREISRAAGKAVPGVIDEENSGNNA
QALTFVYPFGATLSVMKPAVAVLSTGSVCFPLNRPILAFYHSKNQGFGKLAVLGSCHMFSDQYLDKEENSKIMDVVFQ
WLTTGDIHLNQIDAEDPEISDYTMVPDTATLSEQLRVCLQEGDENPRDFTTLFDLSIYQLDTTCLPKVIKAHEELNVKHEP
LQLVQPQFEMPLPALQPAVFPPSFRELPPPPLELFDLDETFSSEKARLAQITNKCTDEDLEFYVRKCGDILGVTSKLPKDQ
QDAKHILEHIFFQVVEFKKLNQEAHGAPMSKGEELFTGVVPILVELDGDVNGHKFSVRGEGEGDATNGKLTLKFICTTG
KLPVPWPTLVTTLTYGVQCFARYPDHMKQHDFFKSAMPEGYVQERTISFKDDGTYKTRAEVKFEGDTLVNRIELKGIDF
KEDGNILGHKLEYNFNSHNVYITADKQKNGIKANFKIRHNVEDGSVQLADHYQQNTPIGDGPVLLPDNHYLSTQSVLSK
DPNEKRDHMVLLEFVTAAGITHGMDELYKDYKDDDDK

Mouse IFT70 (TTC30A1) SNAP Flag (NP_084464.3)

MAWQSSSKVPDGEFTAVVYRLIRDSRYSEAVQLLSAELQRSSRSRAGLSLLAYCYYRLQEFELAAECYEQLSQMHPELEQ
YRLYQAQALYKACLYPEATRVTFLLDNPAYQTRVLRLQAAIKYSEGDLPGARSLVEQLLSGEAGEDSGGENDPDGLVNM
GCLLYKEGHYEAACSKFLAALQASGYQPDLSYNLALAYYSSRQYAPALKHIADIIERGIRQHPELGVGMTTEGIDVRSVGN
TVVLHQTALIEAFNLKAAIEYQLRNFEVAQETLTDMPPRAEEELDPVTLHNQALMNMDAKPTEGFEKLQFLLQQNPFP
PETFGNLLLLYCKYEYFDLAADVLAENAHLTYKFLTPYLYDFLDAMITCQTAPEEAFIKLDGLAGMLTEQLRRLTKQVQEA
RHNRDDEIIKKAMNEYDETLEKYIPVLMAQAKIYWNLENYPMVEKIFRKSVEFCNDHDVWKLNVAHVLFMQENKYKE
AIGFYEPIVKKNYDNILSVSAIVLANLCVSYIMTSQNEEAEELMRKIEKEEEQLSYGDPDKKIYHLCIVNLVIGTLYCAKGNY
DFGISRVIKSLEPYHKKLGTDTWYYAKRCFLSLLENMSKHMIVLCDGVVQECVQFLEYCELYGRNIPAVLEQPLEEERIHT
GKNTVTYESRLLKALIYEVIGWNMGAPMDKDCEMKRTTLDSPLGKLELSGCEQGLHEIKLLGKGTSAADAVEVPAPAAV
LGGPEPLMQATAWLNAYFHQPEAIEEFPVPALHHPVFQQESFTRQVLWKLLKVVKFGEVISYQQLAALAGNPAATAAV
KTALSGNPVPILIPCHRVVSSSGAVGGYEGGLAVKEWLLAHEGHRLGKPGLDYKDDDDK

Mouse IFT46 SNAP Flag (NP_076320.2)

MADNSSDEYEEDNKEKKKPSQLTPQQGFSENDDDDDDDSSETDSDDDDDDEEHGAPLEGAYDPADYEHLPVSAEIKE
LFEYISRYTPQLIDLDHKLKPFIPDFIPAVGDIDAFLKVPRPDGKPDHLGLLVLDEPSTKQSDPTVLSLWLTENSKQHNITQ
HMKVKSLEDAEKNPKAIDTWIESISELHRSKPPATVHYTRPMPDIDTLMQEWSPEFEELLGKVSLPTVEIDCSLAEYIDMI
CAILDIPFYKSRIQSLHLLFSLYSEFKNSQHFKALAEGKKVFTPPPNSASQAGDAETLTFIGAPMDKDCEMKRTTLDSPLGK
LELSGCEQGLHEIKLLGKGTSAADAVEVPAPAAVLGGPEPLMQATAWLNAYFHQPEAIEEFPVPALHHPVFQQESFTR
QVLWKLLKVVKFGEVISYQQLAALAGNPAATAAVKTALSGNPVPILIPCHRVVSSSGAVGGYEGGLAVKEWLLAHEGH
RLGKPGLDYKDDDDK

Mouse IFT46 Flag (NP_076320.2)

MADNSSDEYEEDNKEKKKPSQLTPQQGFSENDDDDDDDSSETDSDDDDDDEEHGAPLEGAYDPADYEHLPVSAEIKE
LFEYISRYTPQLIDLDHKLKPFIPDFIPAVGDIDAFLKVPRPDGKPDHLGLLVLDEPSTKQSDPTVLSLWLTENSKQHNITQ
HMKVKSLEDAEKNPKAIDTWIESISELHRSKPPATVHYTRPMPDIDTLMQEWSPEFEELLGKVSLPTVEIDCSLAEYIDMI
CAILDIPFYKSRIQSLHLLFSLYSEFKNSQHFKALAEGKKVFTPPPNSASQAGDAETLTFIGAPDYKDDDDK

Mouse IFT56 Halo 6X-His (NP_705828.2)

MMLSRAKPAVGGESPHTDKRKKKGRKIPKLEDLLSQRDFTGAITLLEFKRHVGEQEDDTNLWIGYCAFHLGDYKRALEE
YENATKEENCNPEVWVNLACTYFFLGMYKQAEAAGFKAPKSRLQNRLLFHLAHKFNDEKKLMNFHQNLQDIKEDQLS
LASIHYMRSHYQEAIDIYKRILLDNREYLALNVYYVALCYYKLDYYDVSQEVLAVYLQQIPDSTIALNLKACNHFRLYNGKAA
EAELKSLMDNASSPFEFAKELIRHNLVVFRGGEGALQVLPPLVDVIPEARLNLVIYYLRQDDVQEAYNLIKDLEPTTPQEYI
LKGVVNAALGQEMGSRDHMKIAQQFFQLVGGSASECDTIPGRQCMASCFFLLKQFDDVLIYLNSFKSYFYNDDIFNFN
YAQAKAATGNTSEGEEVFLLIQSEKLKNDYIYLSWLARCYIMNKKPRLAWELYLKMETSGESFSLLQLIANDCYKMGQFY
YSAKAFDVLERLDPNPEYWEGKRGACVGIFQMILAGREPKETLREVLHLLRSTGNTQVEYIIRIMKKWAKENRVPIGAP
MEIGTGFPFDPHYVEVLGERMHYVDVGPRDGTPVLFLHGNPTSSYVWRNIIPHVAPTHRCIAPDLIGMGKSDKPDLGY
FFDDHVRFMDAFIEALGLEEVVLVIHDWGSALGFHWAKRNPERVKGIAFMEFIRPIPTWDEWPEFARETFQAFRTTDV
GRKLIIDQNVFIEGTLPMGVVRPLTEVEMDHYREPFLNPVDREPLWRFPNELPIAGEPANIVALVEEYMDWLHQSPVPK
LLFWGTPGVLIPPAEAARLAKSLPNCKAVDIGPGLNLLQEDNPDLIGSEIARWLSTLEISHHHHHH

DYF-1 2x_superfolder GFP Flag (CCD67546.1)

MNAMLNIKEGEFTSTIYTLIHEHKFNDAIRILQYQHERNPKNLAALSLLAYCYYYTQDFMNAADCYSQLSYNFPQYSQYK
LYHAQSLYNAFRPADALAVVSMIQDENLLNESVKLEAAIKYQEDDLVNCRILVEQLPENDAAVIINTACIDYKEGNYEEAL
KKFNEATEFSGYQSGLAYSIALCHYRRGDYDSALKLISEIINRGVKDHPEFNIGMVTEGIDVNFIQNTQKLHESALIEAFNL
KFAIYYRTKDFKAAKESLTDMPPRNEHDADPITLHNLAISNANSDFGDSSAKLQFLLGINPFPQETFANLLFLYCKNDYFG
LAADVLAENPSHTFYCLNEYQFNLLEALIYMPTNPEESLKKLEKLEKECLDRLRKTAIEIQIKKEQKTTDSDDSLEMRNLIES
YDDSLEMYLPVLMTYAKYYWDKRDYQAVEKLFRNSVDYCKEHDTWKLNVAHTIFMQEKKYKDAAAFYEPIVHKKYDD
GILEVPAMILANLVVCYIMTNQTDEAELILKAVENEEEAALMMKPNEKFFHNSIISLVIGSLYCSKGNFEFGISRVVKALEP
PEKKLGVDTWYYAKRCIVAAIELMAKNLLVMRDSVVMEVIQFLTSCEVPGRNIYTVPDDLFEQAGESKVKCNVTYEAR
MIKAALLMVFNDGAPMSKGEELFTGVVPILVELDGDVNGHKFSVRGEGEGDATNGKLTLKFICTTGKLPVPWPTLVTTL
TYGVQCFARYPDHMKQHDFFKSAMPEGYVQERTISFKDDGTYKTRAEVKFEGDTLVNRIELKGIDFKEDGNILGHKLEY
NFNSHNVYITADKQKNGIKANFKIRHNVEDGSVQLADHYQQNTPIGDGPVLLPDNHYLSTQSVLSKDPNEKRDHMVLL
EFVTAAGITHGMDELYKGGGSGGSKGEELFTGVVPILVELDGDVNGHKFSVRGEGEGDATNGKLTLKFICTTGKLPVPW
PTLVTTLTYGVQCFARYPDHMKQHDFFKSAMPEGYVQERTISFKDDGTYKTRAEVKFEGDTLVNRIELKGIDFKEDGNIL
GHKLEYNFNSHNVYITADKQKNGIKANFKIRHNVEDGSVQLADHYQQNTPIGDGPVLLPDNHYLSTQSVLSKDPNEKR
DHMVLLEFVTAAGITHGMDELYKGGDYKDDDDK

DYF-1 SNAP Flag

MNAMLNIKEGEFTSTIYTLIHEHKFNDAIRILQYQHERNPKNLAALSLLAYCYYYTQDFMNAADCYSQLSYNFPQYSQYK
LYHAQSLYNAFRPADALAVVSMIQDENLLNESVKLEAAIKYQEDDLVNCRILVEQLPENDAAVIINTACIDYKEGNYEEAL
KKFNEATEFSGYQSGLAYSIALCHYRRGDYDSALKLISEIINRGVKDHPEFNIGMVTEGIDVNFIQNTQKLHESALIEAFNL
KFAIYYRTKDFKAAKESLTDMPPRNEHDADPITLHNLAISNANSDFGDSSAKLQFLLGINPFPQETFANLLFLYCKNDYFG
LAADVLAENPSHTFYCLNEYQFNLLEALIYMPTNPEESLKKLEKLEKECLDRLRKTAIEIQIKKEQKTTDSDDSLEMRNLIES
YDDSLEMYLPVLMTYAKYYWDKRDYQAVEKLFRNSVDYCKEHDTWKLNVAHTIFMQEKKYKDAAAFYEPIVHKKYDD
GILEVPAMILANLVVCYIMTNQTDEAELILKAVENEEEAALMMKPNEKFFHNSIISLVIGSLYCSKGNFEFGISRVVKALEP
PEKKLGVDTWYYAKRCIVAAIELMAKNLLVMRDSVVMEVIQFLTSCEVPGRNIYTVPDDLFEQAGESKVKCNVTYEAR

MIKAALLMVFNDGAPMDKDCEMKRTTLDSPLGKLELSGCEQGLHEIKLLGKGTSAADAVEVPAPAAVLGGPEPLMQA
TAWLNAYFHQPEAIEEFPVPALHHPVFQQESFTRQVLWKLLKVVKFGEVISYQQLAALAGNPAATAAVKTALSGNPVPI
LIPCHRVVSSSGAVGGYEGGLAVKEWLLAHEGHRLGKPGLDYKDDDDK

DYF-1^{Ala} SNAP Flag

MNAMLNIKEGEFTSTIYTLIHEHKFNDAIRILQYQHERNPKNLAALSLLAACAAATQDFMNAADCYSQLSYNFPQYSQY
KLYHAQSLYNAFRPADALAVVSMIQDENLLNESVKLEAAIKYQEDDLVNCRILVEQLPENDAAVIINTACIDYKEGNYEEA
LKKFNEATEFSGYQSGLAYSIALCHYRRGDYDSALKLISEIINRGVKDHPEFNIGMVTEGIDVNFIQNTQKLHESALIEAFN
LKFAIYYRTKDFKAAKESLTDMPPRNEHDADPITLHNLAISNANSDFGDSSAKLQFLLGINPFPQETFANLLFLYCKNDYF
GLAADVLAENPSHTFYCLNEYQFNLLEALIYMPTNPEESLKKLEKLEKECLDRLRKTAIEIQIKKEQKTTDSDDSLEMRNLIE
SYDDSLEMYLPVLMTYAKYYWDKRDYQAVEKLFRNSVDYCKEHDTWKLNVAHTIFMQEKKYKDAAAFYEPIVHKKYD
DGILEVPAMILANLVVCYIMTNQTDEAELILKAVENEEEAALMMKPNEKFFHNSIISLVIGSLYCSKGNFEFGISRVVKALE
PPEKKLGVDTWYYAKRCIVAAIELMAKNLLVMRDSVVMEVIQFLTSCEVPGRNIYTVPDDLFEQAGESKVKCNVTYEAR
MIKAALLMVFNDGAPMDKDCEMKRTTLDSPLGKLELSGCEQGLHEIKLLGKGTSAADAVEVPAPAAVLGGPEPLMQA
TAWLNAYFHQPEAIEEFPVPALHHPVFQQESFTRQVLWKLLKVVKFGEVISYQQLAALAGNPAATAAVKTALSGNPVPI
LIPCHRVVSSSGAVGGYEGGLAVKEWLLAHEGHRLGKPGLDYKDDDDK

DYF-1^{Phe} SNAP Flag

MNAMLNIKEGEFTSTIYTLIHEHKFNDAIRILQYQHERNPKNLAALSLLAFCFFFTQDFMNAADCYSQLSYNFPQYSQYK
LYHAQSLYNAFRPADALAVVSMIQDENLLNESVKLEAAIKYQEDDLVNCRILVEQLPENDAAVIINTACIDYKEGNYEEAL
KKFNEATEFSGYQSGLAYSIALCHYRRGDYDSALKLISEIINRGVKDHPEFNIGMVTEGIDVNFIQNTQKLHESALIEAFNL
KFAIYYRTKDFKAAKESLTDMPPRNEHDADPITLHNLAISNANSDFGDSSAKLQFLLGINPFPQETFANLLFLYCKNDYFG
LAADVLAENPSHTFYCLNEYQFNLLEALIYMPTNPEESLKKLEKLEKECLDRLRKTAIEIQIKKEQKTTDSDDSLEMRNLIES
YDDSLEMYLPVLMTYAKYYWDKRDYQAVEKLFRNSVDYCKEHDTWKLNVAHTIFMQEKKYKDAAAFYEPIVHKKYDD
GILEVPAMILANLVVCYIMTNQTDEAELILKAVENEEEAALMMKPNEKFFHNSIISLVIGSLYCSKGNFEFGISRVVKALEP
PEKKLGVDTWYYAKRCIVAAIELMAKNLLVMRDSVVMEVIQFLTSCEVPGRNIYTVPDDLFEQAGESKVKCNVTYEAR
MIKAALLMVFNDGAPMDKDCEMKRTTLDSPLGKLELSGCEQGLHEIKLLGKGTSAADAVEVPAPAAVLGGPEPLMQA
TAWLNAYFHQPEAIEEFPVPALHHPVFQQESFTRQVLWKLLKVVKFGEVISYQQLAALAGNPAATAAVKTALSGNPVPI
LIPCHRVVSSSGAVGGYEGGLAVKEWLLAHEGHRLGKPGLDYKDDDDK

DYF-1b SNAP Flag

MNAADCYSQLSYNFPQYSQYKLYHAQSLYNAFRPADALAVVSMIQDENLLNESVKLEAAIKYQEDDLVNCRILVEQLPE
NDAAVIINTACIDYKEGNYEEALKKFNEATEFSGYQSGLAYSIALCHYRRGDYDSALKLISEIINRGVKDHPEFNIGMVTEG
IDVNFIQNTQKLHESALIEAFNLKFAIYYRTKDFKAAKESLTDMPPRNEHDADPITLHNLAISNANSDFGDSSAKLQFLLGI
NPFPQETFANLLFLYCKNDYFGLAADVLAENPSHTFYCLNEYQFNLLEALIYMPTNPEESLKKLEKLEKECLDRLRKTAIEIQ
IKKEQKTTDSDDSLEMRNLIESYDDSLEMYLPVLMTYAKYYWDKRDYQAVEKLFRNSVDYCKEHDTWKLNVAHTIFMQ
EKKYKDAAAFYEPIVHKKYDDGILEVPAMILANLVVCYIMTNQTDEAELILKAVENEEEAALMMKPNEKFFHNSIISLVIG
SLYCSKGNFEFGISRVVKALEPPEKKLGVDTWYYAKRCIVAAIELMAKNLLVMRDSVVMEVIQFLTSCEVPGRNIYTVPD
DLFEQAGESKVKCNVTYEARMIKAALLMVFNDGAPMDKDCEMKRTTLDSPLGKLELSGCEQGLHEIKLLGKGTSAADA
VEVPAPAAVLGGPEPLMQATAWLNAYFHQPEAIEEFPVPALHHPVFQQESFTRQVLWKLLKVVKFGEVISYQQLAALA
GNPAATAAVKTALSGNPVPILIPCHRVVSSSGAVGGYEGGLAVKEWLLAHEGHRLGKPGLDYKDDDDK

DYF-6 2x_superfolder GFP Flag (CAL36517.1)

MSSETTAPMIINEKSSLPVKSEPGQLGNPISDESSEDEQSQIRALEEDQGIYYNEEVVASPKNESDDDIPLRRIQLSHQTST
QQHPEDSEPQEVIDVNDIELPAGEAQPNMERRRSVRFSGRHDEEEDGRNKHFRTPSPESLRYIQALENPMAANGEFEE
EFNDLADPQVQPPPMGSPPAYTSADEGPKTPPPRASAGSNMRQESMNELIMRKISDPLQNLIRRASRLEDDSSNDDD

DDDDDEDDDYTEDEIAILTYIDAYKTQEVELRPQLRPFTIEYIPAMGDVDLFIKVPRPDEIDDNVGLTQIDEPPSNQSDATI
VDMQIRNATKDAAILDDDVPVKLLERADENPDEIKKWISDIKEFHKSKPAQTVHYRTQLPDVETLMQEWPQKLEEVLKT
TKIPSAELDVSLEKYVEICLNIVDIPVGKSRIEALHLMFSLLNEFNNSQHFRNLAQNNNLGGETGETMDRLELGAPMSKG
EELFTGVVPILVELDGDVNGHKFSVRGEGEGDATNGKLTLKFICTTGKLPVPWPTLVTTLTYGVQCFARYPDHMKQHDF
FKSAMPEGYVQERTISFKDDGTYKTRAEVKFEGDTLVNRIELKGIDFKEDGNILGHKLEYNFNSHNVYITADKQKNGIKA
NFKIRHNVEDGSVQLADHYQQNTPIGDGPVLLPDNHYLSTQSVLSKDPNEKRDHMVLLEFVTAAGITHGMDELYKGG
GSGGSKGEELFTGVVPILVELDGDVNGHKFSVRGEGEGDATNGKLTLKFICTTGKLPVPWPTLVTTLTYGVQCFARYPD
HMKQHDFFKSAMPEGYVQERTISFKDDGTYKTRAEVKFEGDTLVNRIELKGIDFKEDGNILGHKLEYNFNSHNVYITAD
KQKNGIKANFKIRHNVEDGSVQLADHYQQNTPIGDGPVLLPDNHYLSTQSVLSKDPNEKRDHMVLLEFVTAAGITHG
MDELYKGGDYKDDDDK

DYF-6 Flag

MSSETTAPMIINEKSSLPVKSEPGQLGNPISDESSEDEQSQIRALEEDQGIYYNEEVVASPKNESDDDIPLRRIQLSHQTST
QQHPEDSEPQEVIDVNDIELPAGEAQPNMERRRSVRFSGRHDEEEDGRNKHFRTPSPESLRYIQALENPMAANGEFEE
EFNDLADPQVQPPPMGSPPAYTSADEGPKTPPPRASAGSNMRQESMNELIMRKISDPLQNLIRRASRLEDDSSNDDD
DDDDDEDDDYTEDEIAILTYIDAYKTQEVELRPQLRPFTIEYIPAMGDVDLFIKVPRPDEIDDNVGLTQIDEPPSNQSDATI
VDMQIRNATKDAAILDDDVPVKLLERADENPDEIKKWISDIKEFHKSKPAQTVHYRTQLPDVETLMQEWPQKLEEVLKT
TKIPSAELDVSLEKYVEICLNIVDIPVGKSRIEALHLMFSLLNEFNNSQHFRNLAQNNNLGGETGETMDRLELGAPDYKD
DDDK

OSM-5 2x_superfolder GFP Flag (AAK01173.1)

MANSTFREDDDDFYGGFDSYDKAYDIQNITQNPQFQQAVARSSHGRRPTASQMGFRDASSSYGKPPGTMMGNQSR
MGGRTAMANNNEPARPMTAVRGAGYTSFANKVQAAERPLSTENSGENGEEKCRQMENKVMEMLRESMLASEKKK
FKEALDKAKEAGRRERAVVKHREQQGLVEMMNLDLTFTVLFNLAQQYEANDMTNEALNTYEIIVRNKMFPNSGRLKV
NIGNIHFRKREFTKALKYYRMALDQVPSIQKDTRIKILNNIGVTFVRMGSYDDAISTFDHCVEENPNFITALNLILVAFCIQ
DAEKMREAFVKMIDIPGFPDDDYMKEKDDDDVLLNQTLNSDMLKNWEKRNKSDAEKAIITAVKIISPVIAPDYAIGYE
WCLESLKQSVHAPLAIELEMTKAGELMKNGDIEGAIEVLKVFNSQDSKTASAAANNLCMLRFLQGGRRLVDAQQYAD
QALSIDRYNAHAQVNQGNIAYMNGDLDKALNNYREALNNDASCVQALFNIGLTAKAQGNLEQALEFFYKLHGILLNN
VQVLVQLASIYESLEDSAQAIELYSQANSLVPNDPAILSKLADLYDQEGDKSQAFQCHYDSYRYFPSNLETVEWLASYYLE
TQFSEKSINYLEKAALMQPNVSKWQMMIASCLRRTGNYQRAFELYRQIHRKFPQDLDCLKFLVRIAGDLGMTEYKEYK
DKLEKAEKINQLRLQRESDSSQGKRHSANSTHSLPPSGLTGLGSGSGGSSGGGTRQYSAHVPLLLDSGTPFTVAQRDMK
AEDFSYDDPVAISSRPKTGTRKTTTDTNIDDFGDFDDSLLPDGAPMSKGEELFTGVVPILVELDGDVNGHKFSVRGEGE
GDATNGKLTLKFICTTGKLPVPWPTLVTTLTYGVQCFARYPDHMKQHDFFKSAMPEGYVQERTISFKDDGTYKTRAEV
KFEGDTLVNRIELKGIDFKEDGNILGHKLEYNFNSHNVYITADKQKNGIKANFKIRHNVEDGSVQLADHYQQNTPIGDG
PVLLPDNHYLSTQSVLSKDPNEKRDHMVLLEFVTAAGITHGMDELYKGGGSGGSKGEELFTGVVPILVELDGDVNGHK
FSVRGEGEGDATNGKLTLKFICTTGKLPVPWPTLVTTLTYGVQCFARYPDHMKQHDFFKSAMPEGYVQERTISFKDDG
TYKTRAEVKFEGDTLVNRIELKGIDFKEDGNILGHKLEYNFNSHNVYITADKQKNGIKANFKIRHNVEDGSVQLADHYQQ
NTPIGDGPVLLPDNHYLSTQSVLSKDPNEKRDHMVLLEFVTAAGITHGMDELYKGGDYKDDDDK

OSM-6 2x_superfolder GFP Flag (CAA03975.1)

MPPFSDEKMTNRSIGRKVLIDQSKQQQISLISGFRGVARHLKSVLTVEINTEPINLNGLEDVRMLIIPQPKTSFGTGEIEAI
WKFVEEGGSLMILSGEGGERQSLNEMIAKYGITVNKDSVIRTVFLKYFDPKEALVANGVINRAIAVAAKKNVSTEQKHN
SQALSFIYPYGCTLDVNNRMSNVVLSSGSTSFPTSRPVAAFHETKLNEMKKKGRVCVVGSVSMFHDTYIDKEENGKIFD
TFVEFLVNGLELNTIDAAEPEINDYTNIPDHIHMSQQIKVCMYEGELDQAISSDFMKIMDTSLHSFNLKHWPMTIRLYEA
LNLSPPPLTLVEPQFELPMPPFQPAVFPPTFQELPMPPLELFDLDEQFSSPEIQLSQLANRSEEEDLIFFIEKAGEITGISAEL

TRSERTPKKIIELAVSKLMLFKRSMMDGELEVASAFDIGEHDAHHQSFNQGEEMDEQLFSDIDEFDDLGAPMSKGEELF
TGVVPILVELDGDVNGHKFSVRGEGEGDATNGKLTLKFICTTGKLPVPWPTLVTTLTYGVQCFARYPDHMKQHDFFKS
AMPEGYVQERTISFKDDGTYKTRAEVKFEGDTLVNRIELKGIDFKEDGNILGHKLEYNFNSHNVYITADKQKNGIKANFKI
RHNVEDGSVQLADHYQQNTPIGDGPVLLPDNHYLSTQSVLSKDPNEKRDHMVLLEFVTAAGITHGMDELYKGGGSG
GSKGEELFTGVVPILVELDGDVNGHKFSVRGEGEGDATNGKLTLKFICTTGKLPVPWPTLVTTLTYGVQCFARYPDHMK
QHDFFKSAMPEGYVQERTISFKDDGTYKTRAEVKFEGDTLVNRIELKGIDFKEDGNILGHKLEYNFNSHNVYITADKQKN
GIKANFKIRHNVEDGSVQLADHYQQNTPIGDGPVLLPDNHYLSTQSVLSKDPNEKRDHMVLLEFVTAAGITHGMDELY
KGGDYKDDDDK

OSM-6 DEL 2x_superfolder GFP Flag

MPPFSDEKMTNRSIGRKVLIDQSKQQQISLISGFRGVARHLKSVLTVEINTEPINLNGLEDVRMLIIPQPKTSFGTGEIEAI
WKFVEEGGSLMILSGEGGERQSLNEMIAKYGITVNKDSVIRTVFLKYFDPKEALVANGVINRAIAVAAKKNVSTEQKHN
SQALSFIYPYGCTLDVNNRMSNVVLSSGSTSFPTSRPVAAFHETKLNEMKKKGRVCVVGSVSMFHDTYIDKEENGKIFD
TFVEFLVNGLELNTIDAAEPEINDYTNIPDHIHMSQQIKVCMYEGELDQAISSDFMKIMDTSLHSFNLKHWPMTIRLYEA
LPQLANRSEEEDLIFFIEKAGEITGISAELTRSERTPKKIIELAVSKLMLFKRSMMDGELEVASAFDIGEHDAHHQSFNQGE
EMDEQLFSDIDEFDDLGAPMSKGEELFTGVVPILVELDGDVNGHKFSVRGEGEGDATNGKLTLKFICTTGKLPVPWPTL
VTTLTYGVQCFARYPDHMKQHDFFKSAMPEGYVQERTISFKDDGTYKTRAEVKFEGDTLVNRIELKGIDFKEDGNILGH
KLEYNFNSHNVYITADKQKNGIKANFKIRHNVEDGSVQLADHYQQNTPIGDGPVLLPDNHYLSTQSVLSKDPNEKRDH
MVLLEFVTAAGITHGMDELYKGGGSGGSKGEELFTGVVPILVELDGDVNGHKFSVRGEGEGDATNGKLTLKFICTTGKL
PVPWPTLVTTLTYGVQCFARYPDHMKQHDFFKSAMPEGYVQERTISFKDDGTYKTRAEVKFEGDTLVNRIELKGIDFKE
DGNILGHKLEYNFNSHNVYITADKQKNGIKANFKIRHNVEDGSVQLADHYQQNTPIGDGPVLLPDNHYLSTQSVLSKDP
NEKRDHMVLLEFVTAAGITHGMDELYKGGDYKDDDDK

Flag SNAP OSM-6$^{322\text{-}380}$

MDYKDDDDKGGMDKDCEMKRTTLDSPLGKLELSGCEQGLHEIKLLGKGTSAADAVEVPAPAAVLGGPEPLMQATAW
LNAYFHQPEAIEEFPVPALHHPVFQQESFTRQVLWKLLKVVKFGEVISYQQLAALAGNPAATAAVKTALSGNPVPILIPC
HRVVSSSGAVGGYEGGLAVKEWLLAHEGHRLGKPGLGGAPMNLSPPPLTLVEPQFELPMPPFQPAVFPPTFQELPMP
PLELFDLDEQFSSPEIQLSQLAN

***C.elegans* DYF-13 SNAP Flag (NP_741021.1)**

MLNLFRNRKRNGAGPTIKKAQKMPELDDFLSNQDYEGAISLLNHKLKAGNLDREEEDSLQLWLAHCYYRLRNYEEAAN
VYTFLMNKDDAPAELGVYLACCKFYLKQYIEAKSIAEKCPKTPLCIRLMMNVSLRLNDEKRILTFHSSLGDTLEDRLSLAGV
NYSRMHYQDAIEVYTSVLQTSPNLIGLNVNMALCYAKMDYPHVAYNLIKNYLRNFPNSPFAKNLLLSVLYRTITSKTTVD
EKSELARNIDQEGLTMVSDMEALLKQKLYPEIEYICKHNLVLFKNCETALQVLPSLMKHIPEARVNLILYHLNKNNVKDAI
SLCKDFDPVTPYEFLVKALTFLRHGQETNSREHLKIAENFFQMVGESGLVQDTIAGRQSSAAYLFLSFKFDDVITYLKSIEA
YFTNNDDFLLNLAQAYLMYKNYVAAEKLFIRVSGPERDKILYKSMLARCYVRNKKPQSAWDMMLKTNNPSDRMSLLK
VIAQDCYIANEFYYASKAFHEIEISDPTTENWSGKRGACAGLFRQLANHKTDPILISQMREVVHLVAMKPHSNCEFLLKV
VRNWAETHNVNIINGAPMDKDCEMKRTTLDSPLGKLELSGCEQGLHEIKLLGKGTSAADAVEVPAPAAVLGGPEPLM
QATAWLNAYFHQPEAIEEFPVPALHHPVFQQESFTRQVLWKLLKVVKFGEVISYQQLAALAGNPAATAAVKTALSGNP
VPILIPCHRVVSSSGAVGGYEGGLAVKEWLLAHEGHRLGKPGLDYKDDDDK

***C.reinhardtii* IFT52 superfolder GFP Flag (XP_001692161.1)**

MEEPGAEEVRILFSTAKGESHTHKAGFKQLFRRLRSTYRPDKVDKDDFTLDTLRSAHILVLGGPKEKFTAPEVDMLKKFV
KNGGSILILMSEGGEEKAGTNINYFLEQFGMSVNNDAVVRTTHYKYLHPKEVLISDGILNRAVITGAGKSLNSNDDDEFR
VSRGPQAFDGTGLEYVFPFGATLSVQKPAVPVLSSGKIAYPMNRPVGAVWAQPGYGRIAVLGSCAMFDDKWLDKEE
NSKIMDFFFKFLKPHSKIQLNDIDAEEPDVSDLKLLPDTASLADKLKGCLQEIDDVPRDWTSLFDDSLFKFDTGLIPEAVSL

YEKLGVKKGQLNLIPPSFETPLPPLQPAVFPPTIREPPPPALELFDLDESFASETNRLASLTNKCHGEEDLEYYIMEAGHILG
LKLQENANAKHVLSEVFRRIAQYKMGSLGLGQTLDSMGQTLPAANQFGDQFELGAPMSKGEELFTGVVPILVELDGD
VNGHKFSVRGEGEGDATNGKLTLKFICTTGKLPVPWPTLVTTLTYGVQCFARYPDHMKQHDFFKSAMPEGYVQERTIS
FKDDGTYKTRAEVKFEGDTLVNRIELKGIDFKEDGNILGHKLEYNFNSHNVYITADKQKNGIKANFKIRHNVEDGSVQLA
DHYQQNTPIGDGPVLLPDNHYLSTQSVLSKDPNEKRDHMVLLEFVTAAGITHGMDELYKGGDYKDDDDK

***C.reinhardtii* IFT70 SNAP Flag (4UZY_A)**

MAFFQQPARPIAEGQYTQTIYTLIKEQKFAEAIQHLQYQLQNVPESRAALSLLGYCYYYTGQYDMASQMYEQLVTLYPS
NEDYKLYYAQSLYKGGMYPEASKAVVKVEGHQKAVTTLLVACSYEQDDLTGCRRQLDKCAPEDPDTMVNTGCIMFKE
GKFEAARQKFNDAVQALGYQPELLYNIALCYYKTKQFGPALKHLAEIIEKAVREHPELSVGSNTDGMEVRSVGNSQTLKE
TALIEAFNLKAAIEYTMKNVEAAKEALTDMPPRAEEELDPVTLHNSALINMDSDPTGGFKKLNFLLQSPPFPPETFANLLL
LYCKPSHGFYDLAADVLAENPQYAGKLLSPDLYDYLQAAIGRYKSPEEAFRRFDELATRHVEQLRRLTKQIQDARIARDN
DAIKRAINEYDEALEAYIPGLMAMASIYWDMELYSNVEKIFRQSAEFCSEHEVWKLNVAHTFFMQDNHYKEAIRYYEPV
VKKNADNLLGVTAIVLANLCVSYIMTSQNEEAEELMRKVEKEEERSSMQDPDKPCFHLCIINLVIGTLYCAKGNYEFGVS
RIIKSLEPYDKKLETDTWYYAKRCFLALIENLAKHMIVLKDSSFTEIMAFLNEAEKHGKDIRVVFNEGKHQSRTIASEARML
KKMFLKLRDGAPLGGGSGGSMDKDCEMKRTTLDSPLGKLELSGCEQGLHEIKLLGKGTSAADAVEVPAPAAVLGGPEP
LMQATAWLNAYFHQPEAIEEFPVPALHHPVFQQESFTRQVLWKLLKVVKFGEVISYQQLAALAGNPAATAAVKTALSG
NPVPILIPCHRVVSSSGAVGGYEGGLAVKEWLLAHEGHRLGKPGGDYKDDDDK

3. IFT-A subunits

CHE-11 Flag (NP_506047.5)

MKPFLIEWAPHCGWICVVTQDETTGEANVAFSDHSGSVQEKGPSKPGSVSCVRWHPKKQFVVVGWKDGGVCFIPKG
GNVSHTVVETYPFPNQGVDWSHDGTVLMTLHNPSSVHLYSYMVIGEEISTSNIMQIELNDQITLWCKRLSYDKFKPSKI
SVTDDDSGVDESPFGSKESLAERRDEKSTVPKGTEFLFAGKSGTIYGVDNDRQRTIHKLDSEILFMGYCETISIIIVFTRDCF
IFHLAKGTSEMRCAERVKVKLGGKSEKYSLELDDGILVMCYGEKEIRVWDLIKEENGTIALDVNKGFQPDETINVVTVNG
KRGVITAATSLNNIAEWKRKRTDTNVESAWNLSPSTHVDSQVSLIRWSPILSTAALITEEDLVLIGENSLTVKMRGKMAA
IQTSSNSFTLLHATSGVSQDLKLSIPSAKGICLGEKQLVVWNEDTVVTYDVQTSLATIQCTSFSCNTTSVAIVNQNLYCIEK
DKIFARTLQGTLRQEISLPEIEGDPEILEVNRCWMAVATTNGFIRIYNLSAKDAQQEHNSKYIIENVKNFYKFHTIRINHTG
NKVAVSYLEDVSTVAERLLVYDAELDAVSYFSFDRGMTDTQEYETQAELAHTSSGRPVTAAARKMAREQSRFQMMNH
RPGAFEWDENDARYLVVECIHVEPESTDQRVLTAFVTSEHGIQLQGMQQKNLHCGKLVSVSVPNFYFVRKSGWDEED
NRDERTIGKTLVAKCLREFLGNENCDESTRKAMMDFSFYLTIGSMDAAFKAIQFIKSDSVWDHMASMSIKTRRLDVAM
VCLGHMKNVRGARAVRRSQQNGENDSMKCAALAIELSMLEEALIIYAQNERYDLMNKLYQSQNMWSSAFEIAETKD
RIHLRNTHYNYAKYLEARRDQASIEAAIENYEKAGVHAFEVFRMLKDYPKQIEQYVRRKREESLYSWWGAYLESVGELE
GAISFYSSAKDYYCMVRVKCIQGKTDEAARLAEESKDKAACYLIGRMYENDGDVVKAVKFFTKARALSSAIRLAKEHDM
KDRLANLCLMAGGSELVSAARYYEDLPGYAHKAVMLYHKAGMIGRALDLAFRTEQFSALDLITKDLDAGTDPKILRRAA
EFFENNQNYEKAVNFLCLAKEFSGAVQLCKNRNVRVSDKFAELMTPTKDDMPNVQERKQVLETVAELCLQQGAYSAA
AKKFTQAGDKLSAMRALLKSGDIQKIRFFANTARNKEIYILAANFLQTTDWQDNQQTMKDIETFYTKSQSFEHLGNFYK
SVAIIEAEHLRTLDKSMGALEMAAVCVLEAEQKNMSTTGLDALKEDLKKYVVQLRKLQSVLEVMKNDAADGMRQLTT
LAEESIDDDIVPCTRLFALIIEDHASRKNWKPAYRAITGLQKKVPNVDLETFVETSTLDKVCDEMRMERVTKKKKEEVESD
GEEVDFSHSLRRQNVSGAPDYKDDDDK

CHE-11 SNAP Flag

MKPFLIEWAPHCGWICVVTQDETTGEANVAFSDHSGSVQEKGPSKPGSVSCVRWHPKKQFVVVGWKDGGVCFIPKG
GNVSHTVVETYPFPNQGVDWSHDGTVLMTLHNPSSVHLYSYMVIGEEISTSNIMQIELNDQITLWCKRLSYDKFKPSKI
SVTDDDSGVDESPFGSKESLAERRDEKSTVPKGTEFLFAGKSGTIYGVDNDRQRTIHKLDSEILFMGYCETISIIIVFTRDCF
IFHLAKGTSEMRCAERVKVKLGGKSEKYSLELDDGILVMCYGEKEIRVWDLIKEENGTIALDVNKGFQPDETINVVTVNG
KRGVITAATSLNNIAEWKRKRTDTNVESAWNLSPSTHVDSQVSLIRWSPILSTAALITEEDLVLIGENSLTVKMRGKMAA
IQTSSNSFTLLHATSGVSQDLKLSIPSAKGICLGEKQLVVWNEDTVVTYDVQTSLATIQCTSFSCNTTSVAIVNQNLYCIEK
DKIFARTLQGTLRQEISLPEIEGDPEILEVNRCWMAVATTNGFIRIYNLSAKDAQQEHNSKYIIENVKNFYKFHTIRINHTG
NKVAVSYLEDVSTVAERLLVYDAELDAVSYFSFDRGMTDTQEYETQAELAHTSSGRPVTAAARKMAREQSRFQMMNH
RPGAFEWDENDARYLVVECIHVEPESTDQRVLTAFVTSEHGIQLQGMQQKNLHCGKLVSVSVPNFYFVRKSGWDEED
NRDERTIGKTLVAKCLREFLGNENCDESTRKAMMDFSFYLTIGSMDAAFKAIQFIKSDSVWDHMASMSIKTRRLDVAM
VCLGHMKNVRGARAVRRSQQNGENDSMKCAALAIELSMLEEALIIYAQNERYDLMNKLYQSQNMWSSAFEIAETKD
RIHLRNTHYNYAKYLEARRDQASIEAAIENYEKAGVHAFEVFRMLKDYPKQIEQYVRRKREESLYSWWGAYLESVGELE
GAISFYSSAKDYYCMVRVKCIQGKTDEAARLAEESKDKAACYLIGRMYENDGDVVKAVKFFTKARALSSAIRLAKEHDM
KDRLANLCLMAGGSELVSAARYYEDLPGYAHKAVMLYHKAGMIGRALDLAFRTEQFSALDLITKDLDAGTDPKILRRAA
EFFENNQNYEKAVNFLCLAKEFSGAVQLCKNRNVRVSDKFAELMTPTKDDMPNVQERKQVLETVAELCLQQGAYSAA
AKKFTQAGDKLSAMRALLKSGDIQKIRFFANTARNKEIYILAANFLQTTDWQDNQQTMKDIETFYTKSQSFEHLGNFYK
SVAIIEAEHLRTLDKSMGALEMAAVCVLEAEQKNMSTTGLDALKEDLKKYVVQLRKLQSVLEVMKNDAADGMRQLTT
LAEESIDDDIVPCTRLFALIIEDHASRKNWKPAYRAITGLQKKVPNVDLETFVETSTLDKVCDEMRMERVTKKKKEEVESD
GEEVDFSHSLRRQNVSGAPMDKDCEMKRTTLDSPLGKLELSGCEQGLHEIKLLGKGTSAADAVEVPAPAAVLGGPEPL
MQATAWLNAYFHQPEAIEEFPVPALHHPVFQQESFTRQVLWKLLKVVKFGEVISYQQLAALAGNPAATAAVKTALSG
NPVPILIPCHRVVSSSGAVGGYEGGLAVKEWLLAHEGHRLGKPGLDYKDDDDK

DAF-10 Flag (ABC88647.1)

MRPNLLWVDKILDENNEAGVCIYDLAFKPDGSELLLAADNKVYLFDVNEGGQMQTLKGHKDLVYTVAWSHNGELFAS
GGADKLVILWNEKHEGTLRYSHTDVIQCMMFNPCNQILLTCALNEFGLWSTADKNVIKQRSVVRCCSCAWNTDGTIF
AIGHGDGTITLRKGTNATEEPSIIIQRDNEPIWGIAFSSNRTFASRDSQGNPMGIDEIMAVIDWNKTLSFYSLDGTFIESK
NLEFEPHCISYCLNGEYLLIGGSDKILKIYTRKGVLLGTVAQMDHWIWSVTVRPNSQTVAMGCVDGTIACYNLVFSTVH
CVDHARYANRKSMTDVFVQNLEYRTSSNICCHDLVKKMSLYDTKLAVQLSDKIQIYKQTGGVSKNERRKQLKYTLQDTI
RKDLSFSLMVVTHGHLVVCNDEKLECYDFKGIKKRSWNMKSIVRYLRVLGGPAHRETLVLGTTDGGVYKVFIDNDYPILL
DSRKTAIKCIDINANRTVLASIEDTLVCKWSDIATGETLLQEPGCYSVVFNTVNENLFAFTTNNMLHVRTLAAPGHTTRG
VGYVLGFVKNRTFCLVQYNLIPLEVPYTIHLYQYIERGDFKEALRIACLGVVKNDWKYLANKALDALEFDVARKAYKRVR
DRKMLRMVWELKKMKSNGEPDAILRATILAYTKKFREAAKIFKENGFENRAMELFTDMRMFDDVQEVMTTASGETK
KMLMRKRASWARDANQPKIAAEMLISSGDLDKAALLIIDNDWLELAIEISHKIDRSDLETMKKLSAYFIRKHEFGLASRIF
QSINDMKSIVDMHVNAGHWTDAFAIADRHPKYVEDVYLPYARFLAERDRFEEAQKAFHRAGKEQEAMHVLEQLTSN
SVNENRFADAGFYYWLLSQQYLDRSQTEENLTLLNKAKEAASLADAYYAYYPVFIFCSQPFSFERNENILNMARYLTFTP
YIDNISKVFVYFTIAKIANEMGAYKSARTALDQLTNLRVLPQFELDGQIEVMTLNIRAKPFTDVESMQPMCYRCGLNNPL
LGGMSCIHCETPFIISFVSFDILPLIEFKIENDISFDEAKELIESEPPLSDDDYNPLRGLKKGIKEIILNRESLSKLEQGHVIIQTF
PPPLAPKFLFNVMPSITIAQCKGCNKVFDLDDFEMACLRKGHCPFCRTSYDRNEAFFVDEEEDEDNTNIPSFGQFSRFSG
APDYKDDDDK

DAF-10 Halo Flag

MRPNLLWVDKILDENNEAGVCIYDLAFKPDGSELLLAADNKVYLFDVNEGGQMQTLKGHKDLVYTVAWSHNGELFAS
GGADKLVILWNEKHEGTLRYSHTDVIQCMMFNPCNQILLTCALNEFGLWSTADKNVIKQRSVVRCCSCAWNTDGTIF
AIGHGDGTITLRKGTNATEEPSIIIQRDNEPIWGIAFSSNRTFASRDSQGNPMGIDEIMAVIDWNKTLSFYSLDGTFIESK

NLEFEPHCISYCLNGEYLLIGGSDKILKIYTRKGVLLGTVAQMDHWIWSVTVRPNSQTVAMGCVDGTIACYNLVFSTVH
CVDHARYANRKSMTDVFVQNLEYRTSSNICCHDLVKKMSLYDTKLAVQLSDKIQIYKQTGGVSKNERRKQLKYTLQDTI
RKDLSFSLMVVTHGHLVVCNDEKLECYDFKGIKKRSWNMKSIVRYLRVLGGPAHRETLVLGTTDGGVYKVFIDNDYPILL
DSRKTAIKCIDINANRTVLASIEDTLVCKWSDIATGETLLQEPGCYSVVFNTVNENLFAFTTNNMLHVRTLAAPGHTTRG
VGYVLGFVKNRTFCLVQYNLIPLEVPYTIHLYQYIERGDFKEALRIACLGVVKNDWKYLANKALDALEFDVARKAYKRVR
DRKMLRMVWELKKMKSNGEPDAILRATILAYTKKFREAAKIFKENGFENRAMELFTDMRMFDDVQEVMTTASGETK
KMLMRKRASWARDANQPKIAAEMLISSGDLDKAALLIIDNDWLELAIEISHKIDRSDLETMKKLSAYFIRKHEFGLASRIF
QSINDMKSIVDMHVNAGHWTDAFAIADRHPKYVEDVYLPYARFLAERDRFEEAQKAFHRAGKEQEAMHVLEQLTSN
SVNENRFADAGFYYWLLSQQYLDRSQTEENLTLLNKAKEAASLADAYYAYYPVFIFCSQPFSFERNENILNMARYLTFTP
YIDNISKVFVYFTIAKIANEMGAYKSARTALDQLTNLRVLPQFELDGQIEVMTLNIRAKPFTDVESMQPMCYRCGLNNPL
LGGMSCIHCETPFIISFVSFDILPLIEFKIENDISFDEAKELIESEPPLSDDDYNPLRGLKKGIKEIILNRESLSKLEQGHVIIQTF
PPPLAPKFLFNVMPSITIAQCKGCNKVFDLDDFEMACLRKGHCPFCRTSYDRNEAFFVDEEEDEDNTNIPSFGQFSRFSG
APMEIGTGFPFDPHYVEVLGERMHYVDVGPRDGTPVLFLHGNPTSSYVWRNIIPHVAPTHRCIAPDLIGMGKSDKPDL
GYFFDDHVRFMDAFIEALGLEEVVLVIHDWGSALGFHWAKRNPERVKGIAFMEFIRPIPTWDEWPEFARETFQAFRTT
DVGRKLIIDQNVFIEGTLPMGVVRPLTEVEMDHYREPFLNPVDREPLWRFPNELPIAGEPANIVALVEEYMDWLHQSP
VPKLLFWGTPGVLIPPAEAARLAKSLPNCKAVDIGPGLNLLQEDNPDLIGSEIARWLSTLEISDYKDDDDK

DYF-2 Flag (ABC42046.1)

MSLKVIPCTLTKNQEVFKCVSAQLQYRRGEEEHGSGPIIHRWRPNGHTVAVACANNTVIYYDKKGNVIDALNPTGKLIDI
AWDKEGDVLAIAVANTGTIYLWDVNSRNTDTVESGATSSKELPTCLAWSPSTPTLVIGNNAGNIVVYNHRTSRRIAVM
GKHQRSVTQITVTPEDYVISCSDDNTLSVTTLEGTTVSTTTTNGEPTNMDYGSVNGKGGSGVTMVSVVIGKKILMLAHY
NALDEPVNLQFQEKYGNIHSYRWFNDGYILIGFDRGYIISISAHNNEIGSELVSFLEYRGYLASIAVSTSFNKLLTIGDNMV
KVRDLDELTTVTMLTEIETEKNLSEIEVTEDGQLVAVSSQSGVLSIFVTKMPTLAASYNNSICYLTNLTQVTVVAEVEKKGS
STLELNIEPTVMGLGPLNLAVANNNTVFFYDYHTPAQMQAAQQLQSTQSAAEKPTIVAAEPINRVEYLSTVTNIQLNY
MYAAVNFGSRLRLHRIRNSEDNVSIEFPEANRNATLYSYALTENFLIFTTSNNYIVYFSLSEWAIVSEYRHVVPVRSIFPHP
TNVVCCCFDDRLEAMIYSAVDDEVFRLPSVGSSAHYKGAIWETFTIDKNTFAVFDSQNIYVFLLSKQHIQGESVIYVSATR
LPHAYVPLSLNKGIVTCLMSNGKLSSVLLDSHKTESVISDKSETVIDDILTRSLLMHRWSTAWKICIHSNDGSHWNQFAM
AALLDSDVGMAIKIFREIGDAAMVTALELIETIEEKNLLHAQIYTILSRYDDAEQLYLESSRPMEALNMRRDLLEWPKALV
LAETMNPKEIPYLSKEYAQELELTGDHANSLANYEKGVMENPQNLPELQEHNEICQSGIARMAIKTGDLRRGVQLAKQL
EGRVVKRDCAIILEQMKQYTEAAQLYEVGLFYDRAAAVCLKANAWAKVGELLDHVKSPKIHIQYGKIMEKEKKYKVAVK
CYETGRDYDNQVRLLLDPLNDPDEAVRVVRESRSIEGAKLVAKFFVKLGDYNSAIQFLVMSQCVQEAFELAEKNNAVRE
YAKAIEQHGNISQALELAEYYNRVNDMFMAAKFYTQAGQYNNAINLLFKNGDDENCVALAVDCGIKSKDKTLNNKLVK
FLLGEDGNVKDPAQLFRLYVGLGRTKDAAQTAVVVAQIHQAKGNYRIARDLLFQMHQQLREKMMRIPLDMNKSLMA
IHSYIIVKALINRKETLLAARLLIRTCGEIQRFPTHVVPILTSSVVICTQANLKKSAHKFAAQLMTPEYRPKIHEKYKKKIEDIV
RKGGNQKDLVEENTPCPICDDLMPAYAMSCDNCKSLVPYCILTGRHIVASDFSRCPHCEMPGFYSEFRKLSILNENCYM
CGGDLKGAIPEDAKAYLEKMEQDYKGAPDYKDDDDK

DYF-2 superfolder GFP Flag

MSLKVIPCTLTKNQEVFKCVSAQLQYRRGEEEHGSGPIIHRWRPNGHTVAVACANNTVIYYDKKGNVIDALNPTGKLIDI
AWDKEGDVLAIAVANTGTIYLWDVNSRNTDTVESGATSSKELPTCLAWSPSTPTLVIGNNAGNIVVYNHRTSRRIAVM
GKHQRSVTQITVTPEDYVISCSDDNTLSVTTLEGTTVSTTTTNGEPTNMDYGSVNGKGGSGVTMVSVVIGKKILMLAHY
NALDEPVNLQFQEKYGNIHSYRWFNDGYILIGFDRGYIISISAHNNEIGSELVSFLEYRGYLASIAVSTSFNKLLTIGDNMV
KVRDLDELTTVTMLTEIETEKNLSEIEVTEDGQLVAVSSQSGVLSIFVTKMPTLAASYNNSICYLTNLTQVTVVAEVEKKGS
STLELNIEPTVMGLGPLNLAVANNNTVFFYDYHTPAQMQAAQQLQSTQSAAEKPTIVAAEPINRVEYLSTVTNIQLNY

MYAAVNFGSRLRLHRIRNSEDNVSIEFPEANRNATLYSYALTENFLIFTTSNNYIVYFSLSEWAIVSEYRHVVPVRSIFPHP
TNVVCCCFDDRLEAMIYSAVDDEVFRLPSVGSSAHYKGAIWETFTIDKNTFAVFDSQNIYVFLLSKQHIQGESVIYVSATR
LPHAYVPLSLNKGIVTCLMSNGKLSSVLLDSHKTESVISDKSETVIDDILTRSLLMHRWSTAWKICIHSNDGSHWNQFAM
AALLDSDVGMAIKIFREIGDAAMVTALELIETIEEKNLLHAQIYTILSRYDDAEQLYLESSRPMEALNMRRDLLEWPKALV
LAETMNPKEIPYLSKEYAQELELTGDHANSLANYEKGVMENPQNLPELQEHNEICQSGIARMAIKTGDLRRGVQLAKQL
EGRVVKRDCAIILEQMKQYTEAAQLYEVGLFYDRAAAVCLKANAWAKVGELLDHVKSPKIHIQYGKIMEKEKKYKVAVK
CYETGRDYDNQVRLLLDPLNDPDEAVRVVRESRSIEGAKLVAKFFVKLGDYNSAIQFLVMSQCVQEAFELAEKNNAVRE
YAKAIEQHGNISQALELAEYYNRVNDMFMAAKFYTQAGQYNNAINLLFKNGDDENCVALAVDCGIKSKDKTLNNKLVK
FLLGEDGNVKDPAQLFRLYVGLGRTKDAAQTAVVVAQIHQAKGNYRIARDLLFQMHQQLREKMMRIPLDMNKSLMA
IHSYIIVKALINRKETLLAARLLIRTCGEIQRFPTHVVPILTSSVVICTQANLKKSAHKFAAQLMTPEYRPKIHEKYKKKIEDIV
RKGGNQKDLVEENTPCPICDDLMPAYAMSCDNCKSLVPYCILTGRHIVASDFSRCPHCEMPGFYSEFRKLSILNENCYM
CGGDLKGAIPEDAKAYLEKMEQDYKGAPMSKGEELFTGVVPILVELDGDVNGHKFSVRGEGEGDATNGKLTLKFICTT
GKLPVPWPTLVTTLTYGVQCFARYPDHMKQHDFFKSAMPEGYVQERTISFKDDGTYKTRAEVKFEGDTLVNRIELKGID
FKEDGNILGHKLEYNFNSHNVYITADKQKNGIKANFKIRHNVEDGSVQLADHYQQNTPIGDGPVLLPDNHYLSTQSVLS
KDPNEKRDHMVLLEFVTAAGITHGMDELYKGGDYKDDDDK

IFTA-1 Flag (NP_508940.4)

MPPMLNVMANYNEKTIGKLTMSVFRKFNLGLPEHGQLHFAEWNYNSNYIACGGALGKLKVVKIGTDATDLNKSPNAA
TLVVNQALEGHNATVMNATWNENNQKLTTSDTSGLIIVWGMFNEQWCEEMINNRNKSVVVSICWNLEGTKIAIAYA
DGNVIVGTLEGNRIWNKELEIQLAACEWAPDGDMLIFGTADGKVSVFDDSGSHFLDIPMHCLEAEDLEQALAKKEHQK
EEIVCLKYWSPTLKSKTILDEMERDFERKLEKDREVTGTAIFTNFPTKPPPKELPEHEKNTEPYQPVPPDRPRFVVAYARG
MMQLMRSLNDPEPVVVSIPNFKITGAKWSPNGAFLAVCGNDSDKDEPTFSKIHFLSAYGHIVGYFQTNDSCITGICWES
TGLRMAIAAAGTLLIGQIRPEFKWGSIEETIVYVYQKEELYQYGIMFYDYKTDEKTVKTVTHFENMAFYREHCVLINRQD
DGVIPHYFCQLCNSIGTSLDYNVTTVRPKFACVNGICAVIASEDRYFIWHFVLPKFNSVQAGIHVPGKSGDYVLEEQQRTI
EYGTKRLLGSKDEICALCIGDTFFMMALLSGGIYRVSLNDGVITNSYPVSPSINSIKLNCTFTRLAVIKLVEQVPFQFLLYEF
DGDELKLIYTSDKRDVWDYEWDQNNSNMLALKDKQKILICDGNSILEQSSVNGSILLFQNLVVTAVNIEKILLTPENPTKT
CIVEVMIKAKQDVMNLVNAMKLEEAIDYAERSPHSELWSMIANYAVFKHAFDCAEHAFVKLGDYAGVQLVKKLRNIQS
NDLRNAEIYAYRDTLEEAKTAFLQADRRDLAVEMYKKVGDYASVYDLIRNDDDDEGKCDAFRNMAETHYEMMEWEE
AAKAYSYCGDTANQIDCLIRGNLFGELEVLARTLSDDSEFMEVMGDAFTSRGMCDQAVECYLRRSLPQKALHACKELN
QWQKAQFIADANHMENVEGLLGKFAVEMRGESDEKSLSALALYMRAGRHLDAAKIAFDIAKDRKSKYVPYEELKQCY
VLGAVLVENHRQTIKELRKIDKHNFLEDALDDESGLSAEQSRILENTWRGAEAFHFMIMAQQHFFENRIKDALQTSLILS
DYEEFLDPAEVHSMIALAAANVNQFGICSKAMMRLEAFEEFDDAEKEEMRNLSFRLFSENPPVNPNSAKVACSVCDAK
IDPYDLQCSECQTKFPVCIASGRLILDNIFWLCPRCKHRAHQHEIPKYNCCPLCHDMESFRVPGAPDYKDDDDK

ZK328.7a Flag (NP_001022993.2)

MDSESDDNPNDPEDRKKWGHKDVEHWRAVSNVHYYAREGYFGTAILVCDGRLATIKDPALAILKGVCLTLLGKIPDAIR
HLETFVTDNDVALGALHALKWAHASAFNPDNKSIVEIETEISTRARNEKTPYTSYATASEVLYFAGEYQKSKQMLDIARK
RATEKHAKHYCLLGWIELALGKKQKSTQELFEKAGGQEYPDGNIGRCKILEGHHSAPEMKVAANELAISTIHFLPGHIEK
AKASIMMKDWRGVMDCIMNADQPEGSNPYIEVLRTVHGICYAGEVSMLKRTLQLLLKSLDENEATNHVLYARITKLLV
SISGRDEKILRHARDFLTRALKISRKPDYVALSMRIAFGLGGAKEVSTLSQELVALDCEDSYAVLSSVVSMLMISRVSDARA
QFDILPSAHPKLLESPLYYLIASVLAKQSKDKSFENFRQHIENLVEMLRNQLQSFPFGLDYLSLFSSDLLYSAVEQCFDFYPL
VPIKAPDDCMKLTAKTLQMIYDVAPGLAHCTLQLARNSYLCSNTNAAEKWIEKVLDKDDSLADAHILRAELILDRGGKIT
DADDALVTGLNFNFKLRETSLYHLIKSKTFKKRNENDEAIKTLKMALQIPRKEPSKNLFQPKESADTHKISVQLELIDTLQH
MKRIQEAETTMTDALAEWAGQPEQDQLVIAQAQLYLTKGHVERALGILKKIQPGQSNFHLSRIKMAEIYLEEKKDKRM
FAACYRELLKVEATPGSYSLLGDAFMKVQEPEDAINFYEQALKMQSKDVQLAEKIGEAYVMAHLYSKAVNFYESSMNIY
KDKNMRLKLANLLLKLRNFEKCEKVLRAPFERDPEPVGTETIQTYIQFLLLLAECHEMMDNVPEAMNDFEKAKSLHSRIQ

DKTLTAALKKEGARICNLQAELLYRRREFSQAVDICKQALAYHETDLKANLLLSKIFKEENKWTLVLQPCQTVIQVDPHN
DEANSILADFYYIRSEAAHASTSYTTLLNTNPQHWHALSRVVELFCRNGEQNAAEKHLDRAKEVNPRCVTESGYNVCRG
RFEWYTGDQNEALRYYSRTKDSAAGWREKALYYMIDICLNPDNEIIIDENSVENPETTIVEEASEQQKLAKYYLDLLGKLP
TTDRFLLAQNFIRMHTTDKSAIQAALDEFNRMAFNADRSQVTNVGAVFGVARGHVLLKQVQKAKTVLKMVNGRVW
NFDDSDYLEKCWLMLADIYINQNKNDQAVTFLDLVFKYNCNCLKAFELYGYMREKEQKYVEAYKMYEKAFMATKERN
PGFGYKLAFTYLKAKRLFACIETCQKVLDLNPQYPKIKKEIMDKAKALIRTGAPDYKDDDDK

C25H3.12 Flag (NP_495107.1)
MIILENEANEPGFRIQQRAESETGKKGRFGGILKENPIKGFSSETLTRPLTGLFRKTGKSQRKTDDDDSQETIAAPPTNFP
NMARISATIESVQINDEYAGYRDRNPETGSKLTLNEGAGVFGNAMHPLTRYFKVGDVDVSILGRSFPTEKTVDEEGPWT
AQSLFNSLESRIKKERIDAKDQPSDSRSRNARETLISSKYGAPDYKDDDDK

8.4. Supplementary movies

Prefixes *Ce* and *Mm* is used to denote the respective proteins from *C.elegans* and mouse model organisms.

Movie S1 (Related to Figure 5.2): The *Ce*OSM-6 subunit is adequate and essential for the complete activation of *Ce*OSM-3 motor, along with *Ce*DYF-1 subunit.
(Top left panel) Devoid of any adaptor proteins, *Ce*OSM-3 failed to display any directional movement on surface-attached microtubules due to its inherent autoinhibition. **(Top right panel)** The *Ce*DYF-1/OSM-6 adaptor could allosterically activate the *Ce*OSM-3 motor to maximum velocity while **(bottom left panel)** the *Ce*DYF-1/OSM-5 could only introduce the basal activation. The adaptor proteins, *Ce*DYF-1/OSM-6 and *Ce*DYF-1/OSM-5 are labeled through SNAP tag with Alexa^{647} dye on the *Ce*DYF-1 subunit and GFP tags on the *Ce*OSM-6 and *Ce*OSM-5 subunits. Microtubules are labeled with ATTO^{550}. White arrows illustrate the colocalized movement of the respective adaptors by the unlabeled motor. Delay time between the channels per frame is 50 ms. Videos are sped up by three-fold (scale bar: 5 µm).

Movie S2 (Related to Figure 5.6): Phenylalanines can efficiently substitute for the strictly conserved tyrosine motif in *Ce*DYF-1, for the complete activation for *Ce*OSM-3 but not alanines.
(Left panel) The allosteric activation of *Ce*OSM-3 motor put forward by the wild type *Ce*DYF-1/OSM-6 adaptor is eliminated by introducing alanine mutations in the *Ce*DYF-1^{Ala}/OSM-6 complex. **(Right panel)** However, phenylalanine residues can effectively rescue this loss of full activation by the *Ce*DYF-1^{Phe}/OSM-6 complex, where the wild type tyrosines are substituted with

phenylalanines. The *Ce*OSM-6 adaptor is labeled through the GFP tag and the mutated constructs, *Ce*DYF-1^{Ala} and *Ce*DYF-1^{Phe} adaptors, are labeled by SNAP tag with Alexa^{647} dye. Microtubules are labeled with ATTO^{550}. Delay time between the channels per frame is 50 ms. Videos are sped up by three-fold (scale bar: 5 µm).

Movie S3 (Related to Figure 5.8 B): The *Mm*KIF-17 motor is an autoinhibited motor *in vitro* that can be activated by eliminating its autoinhibitory C-terminal domains.

(Left panel) Wild type *Mm*KIF-17 motors were autoinhibited, and remained static on the surface or exhibited non-directed diffusion on surface-attached microtubules. **(Right panel)** The elimination of the autoinhibitory C-terminus in the truncated *Mm*KIF-17$^{1-747}$ allowed then to exhibit robust processive movement. The motor proteins are labeled via SNAP tag with Alexa^{647} dye, and the microtubules are labeled with ATTO^{550}. Video is sped up by three-fold (scale bar: 5 µm).

Movie S4 (Related to Figure 5.8 A): The nonspecific binding of the autoinhibitory C-terminus to the glass surface in microtubule filament gliding assay, activates the autoinhibited mouse *Mm*KIF-17 motor.

The full-length *Mm*KIF-17 motors are affixed to the glass surface through their C-termini as illustrated in Figure 5.8 A, in microtubule filament gliding assays. The attachment of the C-terminus to the surface freed the catalytic head domains from its autoinhibitory partners and the motors were able to efficiently glide the ATTO^{550} labeled microtubules in velocities that were comparable to the speed of C-terminally truncated *Mm*KIF-17$^{1-747}$ motor (Movie S3, right panel and Figure 5.8 B). Video is sped up by ten-fold (scale bar: 10 µm).

Movie S5 (Related to Figure 5.9 & 5.10): The mouse 'On–switch' adaptors are capable of activating the *C. elegans Ce*OSM-3 motor, but not the mouse *Mm*KIF-17.

(Top panels) The mouse *Mm*IFT-70 **(left)** adaptor was unsuccessful in interacting with the *Mm*KIF-17 and hence failed to activate its motor. The *C.elegans Ce*DYF-1 **(middle)** also could not interact or activate the *Mm*KIF-17 motor. The motors and the corresponding adaptor proteins were detached and largely remained immobile on the surface, although the *Mm*KIF-17 motor also exhibited some intermittent diffusion. **(Right)** However, *Mm*IFT-70 could efficiently bind and

activate the autoinhibited *Ce*OSM-3 motor to robust movement on microtubule filaments, as observed by their colocalized movement. The motor proteins *Mm*KIF-17 and *Ce*OSM-3 are labeled by SNAP tag with Alexa^{647} dye, and the adaptors, *Mm*IFT-70 and *Ce*DYF-1 by SNAP tag with Alexa^{488} dye. **(Bottom panels)** The mouse homologs for *Ce*DYF-1/OSM-6, *Mm*IFT-70/IFT-52 adaptor could completely activate the *Ce*OSM-3 motor similar to the *Ce*DYF-1/OSM-6 adaptor. **(Left)** Here, the mouse adaptor *Mm*IFT-70 has been kept unlabeled while the *Mm*IFT-52 subunit is labeled by a GFP tag. The *Ce*OSM-3 motor is labeled by SNAP tag with Alexa^{647} dye. **(Middle)** Here, the *Mm*IFT-70 adaptor is labeled by SNAP tag with Alexa^{647} dye and *Mm*IFT-52 with GFP tag, while keeping the motor unlabeled. Microtubules are labeled with ATTO^{550}. Videos are sped up by three-fold (Delay time between the channels per frame is 50 ms) (scale bar: 5 µm).

Movie S6 (Related to Figure 5.13): Mouse *Mm*IFT-46/IFT-56 and *C.elegans Ce*DYF-6/DYF-13 adaptors interact with the *Mm*KIF-17 and *Ce*OSM-3 motors, still allowing them to retain their autoinhibited state.

(Top panels) Both, *Mm*KIF-17 **(left)** and *Ce*OSM-3 **(right)** motors showed binding to the mouse *Mm*IFT-46/IFT-56 adaptor, but could not get activated to exhibit any directional movement, and remained mostly immobile or displayed intermittent diffusion as illustrated by white arrows. **(Bottom panels**) Similarly, both *Mm*KIF-17 **(left)** and *Ce*OSM-3 **(right)** motors also showed efficient interaction with the *C.elegans* adaptor *Ce*DYF-6/DYF-13, but failed to orchestrate any directional movement and remained either immobile or displayed intermittent diffusion. The adaptor *Mm*IFT-56, is labeled via Halo tag with Alexa^{488} dye, and *Ce*DYF-13 by SNAP tag with Alexa^{488} dye, while the motor proteins *Mm*KIF-17 and *Ce*OSM-3 are labeled via SNAP tag with Alexa^{647} dye. Microtubules are labeled with ATTO^{550}. Videos are sped up by three-fold (Delay time between the channels per frame is 50 ms) (scale bar: 5 µm).

9. Abbreviations

A.a	Amino acids
ATP	Adenosine triphosphate
bBSA	Biotinylated bovine serum albumin
BSA	Bovine serum albumin
C-terminal	Carboxy terminal
DMSO	Dimethyl sulfoxide
E. coli	*Escherichia coli*
EDTA	Ethylenediaminetetraacetic acid
EGTA	Ethylene-bis(oxyethylenenitrilo)tetraacetic acid
sfGFP	Superfolder Green fluorescent protein
HEPES	4-(2-hydroxyethyl)-1-piperazineethanesulfonic acid
IFT	Intraflagellar transport
LB	Luria broth
N	Number of events
N-terminal	Amino terminal
PBS	Phosphate-Buffered Saline
PIPES	Piperazine-1,4-bis(2-ethanesulfonic acid)
QCC	Quadripartite complex
RL	Run length
Sf9	*Spodoptera frugiperda 9*
S.O.C.	Super optimal catabolite
SD	Standard deviation
TAE	Tris-acetate-EDTA
TBS	Tris-Buffered Saline
TEMED	N,N,N',N'-Tetramethylethylenediamine
TIRF	Total internal reflection fluorescence
v	Velocity

10. References

1. Campbell, I.D., *The Croonian lecture 2006. Structure of the living cell.* Philos Trans R Soc Lond B Biol Sci, 2008. **363**(1502): p. 2379-91.
2. Brady, S.T., *A novel brain ATPase with properties expected for the fast axonal transport motor.* Nature, 1985. **317**(6032): p. 73-5.
3. Vale, R.D., T.S. Reese, and M.P. Sheetz, *Identification of a novel force-generating protein, kinesin, involved in microtubule-based motility.* Cell, 1985. **42**(1): p. 39-50.
4. Schliwa, M. and G. Woehlke, *Molecular motors.* Nature, 2003. **422**(6933): p. 759-65.
5. Mavroidis, C., A. Dubey, and M.L. Yarmush, *Molecular machines.* Annu Rev Biomed Eng, 2004. **6**: p. 363-95.
6. Hirokawa, N., S. Niwa, and Y. Tanaka, *Molecular motors in neurons: transport mechanisms and roles in brain function, development, and disease.* Neuron, 2010. **68**(4): p. 610-38.
7. Vale, R.D., *The molecular motor toolbox for intracellular transport.* Cell, 2003. **112**(4): p. 467-80.
8. Hartman, M.A. and J.A. Spudich, *The myosin superfamily at a glance.* J Cell Sci, 2012. **125**(Pt 7): p. 1627-32.
9. Hirokawa, N. and Y. Noda, *Intracellular transport and kinesin superfamily proteins, KIFs: structure, function, and dynamics.* Physiol Rev, 2008. **88**(3): p. 1089-118.
10. Verhey, K.J., N. Kaul, and V. Soppina, *Kinesin assembly and movement in cells.* Annu Rev Biophys, 2011. **40**: p. 267-88.
11. Hook, P. and R.B. Vallee, *The dynein family at a glance.* J Cell Sci, 2006. **119**(Pt 21): p. 4369-71.
12. Martin, M., et al., *Cytoplasmic dynein, the dynactin complex, and kinesin are interdependent and essential for fast axonal transport.* Mol Biol Cell, 1999. **10**(11): p. 3717-28.
13. Roberts, A.J., et al., *Functions and mechanics of dynein motor proteins.* Nat Rev Mol Cell Biol, 2013. **14**(11): p. 713-26.
14. Cochran, J.C., *Kinesin Motor Enzymology: Chemistry, Structure, and Physics of Nanoscale Molecular Machines.* Biophys Rev, 2015. **7**(3): p. 269-299.
15. Woehlke, G. and M. Schliwa, *Walking on two heads: the many talents of kinesin.* Nat Rev Mol Cell Biol, 2000. **1**(1): p. 50-8.
16. Okten, Z., et al., *Myosin VI walks hand-over-hand along actin.* Nat Struct Mol Biol, 2004. **11**(9): p. 884-7.
17. Yildiz, A., et al., *Kinesin Walks Hand-Over-Hand.* Science, 2004. **303**(5658): p. 676-678.
18. Miki, H., et al., *All kinesin superfamily protein, KIF, genes in mouse and human.* Proc Natl Acad Sci U S A, 2001. **98**(13): p. 7004-11.
19. Hirokawa, N., et al., *Kinesin superfamily motor proteins and intracellular transport.* Nat Rev Mol Cell Biol, 2009. **10**(10): p. 682-96.
20. Endow, S.A., F.J. Kull, and H. Liu, *Kinesins at a glance.* J Cell Sci, 2010. **123**(Pt 20): p. 3420-4.
21. Schnitzer, M.J. and S.M. Block, *Kinesin hydrolyses one ATP per 8-nm step.* Nature, 1997. **388**(6640): p. 386-90.
22. Carter, N.J. and R.A. Cross, *Mechanics of the kinesin step.* Nature, 2005. **435**(7040): p. 308-12.
23. Rice, S., et al., *Thermodynamic properties of the kinesin neck-region docking to the catalytic core.* Biophys J, 2003. **84**(3): p. 1844-54.
24. Yun, M., et al., *A structural pathway for activation of the kinesin motor ATPase.* EMBO J, 2001. **20**(11): p. 2611-8.
25. Hirose, K., et al., *Large conformational changes in a kinesin motor catalyzed by interaction with microtubules.* Mol Cell, 2006. **23**(6): p. 913-23.

26. Block, S.M., *Kinesin motor mechanics: binding, stepping, tracking, gating, and limping.* Biophys J, 2007. **92**(9): p. 2986-95.
27. Hyeon, C. and J.N. Onuchic, *Internal strain regulates the nucleotide binding site of the kinesin leading head.* Proc Natl Acad Sci U S A, 2007. **104**(7): p. 2175-80.
28. Endow, S.A., *Determinants of molecular motor directionality.* Nat Cell Biol, 1999. **1**(6): p. E163-7.
29. Endow, S.A. and H. Higuchi, *A mutant of the motor protein kinesin that moves in both directions on microtubules.* Nature, 2000. **406**(6798): p. 913-6.
30. Mandelkow, E. and A. Hoenger, *Structures of kinesin and kinesin-microtubule interactions.* Curr Opin Cell Biol, 1999. **11**(1): p. 34-44.
31. Sack, S., et al., *X-ray structure of motor and neck domains from rat brain kinesin.* Biochemistry, 1997. **36**(51): p. 16155-65.
32. Sablin, E.P., et al., *Direction determination in the minus-end-directed kinesin motor ncd.* Nature, 1998. **395**(6704): p. 813-6.
33. Hammond, J.W., et al., *Autoinhibition of the kinesin-2 motor KIF17 via dual intramolecular mechanisms.* J Cell Biol, 2010. **189**(6): p. 1013-25.
34. Kaan, H.Y.K., D.D. Hackney, and F. Kozielski, *The Structure of the Kinesin-1 Motor-Tail Complex Reveals the Mechanism of Autoinhibition.* Science, 2011. **333**(6044): p. 883-885.
35. Coy, D.L., et al., *Kinesin's tail domain is an inhibitory regulator of the motor domain.* Nature Cell Biology, 1999. **1**(5): p. 288-292.
36. Hackney, D.D., N. Baek, and A.C. Snyder, *Half-site inhibition of dimeric kinesin head domains by monomeric tail domains.* Biochemistry, 2009. **48**(15): p. 3448-56.
37. Imanishi, M., et al., *Autoinhibition regulates the motility of the C. elegans intraflagellar transport motor OSM-3.* The Journal of cell biology, 2006. **174**(7): p. 931-937.
38. Sonar, P., et al., *Kinesin-2 from C. reinhardtii Is an Atypically Fast and Auto-inhibited Motor that Is Activated by Heterotrimerization for Intraflagellar Transport.* Current Biology, 2020. **30**(6): p. 1160-1166.e5.
39. Ren, J., et al., *Coiled-coil 1-mediated fastening of the neck and motor domains for kinesin-3 autoinhibition.* Proc Natl Acad Sci U S A, 2018. **115**(51): p. E11933-E11942.
40. Akhmanova, A. and J.A. Hammer, 3rd, *Linking molecular motors to membrane cargo.* Curr Opin Cell Biol, 2010. **22**(4): p. 479-87.
41. Macaskill, A.F., et al., *Miro1 is a calcium sensor for glutamate receptor-dependent localization of mitochondria at synapses.* Neuron, 2009. **61**(4): p. 541-55.
42. Morfini, G., et al., *JNK mediates pathogenic effects of polyglutamine-expanded androgen receptor on fast axonal transport.* Nat Neurosci, 2006. **9**(7): p. 907-16.
43. Stagi, M., et al., *Unloading kinesin transported cargoes from the tubulin track via the inflammatory c-Jun N-terminal kinase pathway.* FASEB J, 2006. **20**(14): p. 2573-5.
44. Sato-Yoshitake, R., et al., *The phosphorylation of kinesin regulates its binding to synaptic vesicles.* J Biol Chem, 1992. **267**(33): p. 23930-6.
45. Echard, A., et al., *Interaction of a Golgi-associated kinesin-like protein with Rab6.* Science, 1998. **279**(5350): p. 580-5.
46. Scholey, J.M., *Kinesin-2: a family of heterotrimeric and homodimeric motors with diverse intracellular transport functions.* Annu Rev Cell Dev Biol, 2013. **29**: p. 443-69.
47. Brunnbauer, M., et al., *Regulation of a heterodimeric kinesin-2 through an unprocessive motor domain that is turned processive by its partner.* Proc Natl Acad Sci U S A, 2010. **107**(23): p. 10460-5.
48. Doodhi, H., et al., *KAP, the Accessory Subunit of Kinesin-2, Binds the Predicted Coiled-Coil Stalk of the Motor Subunits.* Biochemistry, 2009. **48**(10): p. 2248-2260.

49. Takeda, S., et al., *Kinesin superfamily protein 3 (KIF3) motor transports fodrin-associating vesicles important for neurite building.* J Cell Biol, 2000. **148**(6): p. 1255-65.
50. Jimbo, T., et al., *Identification of a link between the tumour suppressor APC and the kinesin superfamily.* Nat Cell Biol, 2002. **4**(4): p. 323-7.
51. Huang, C.J., C.C. Huang, and C.C. Chang, *Association of the testis-specific TRIM/RBCC protein RNF33/TRIM60 with the cytoplasmic motor proteins KIF3A and KIF3B.* Mol Cell Biochem, 2012. **360**(1-2): p. 121-31.
52. Mohamed, M.A.A., W.L. Stepp, and Z. Ökten, *Reconstitution reveals motor activation for intraflagellar transport.* Nature, 2018. **557**(7705): p. 387-391.
53. Bhogaraju, S., B.D. Engel, and E. Lorentzen, *Intraflagellar transport complex structure and cargo interactions.* Cilia, 2013. **2**(1): p. 10.
54. Ishikawa, H. and W.F. Marshall, *Intraflagellar Transport and Ciliary Dynamics.* Cold Spring Harb Perspect Biol, 2017. **9**(3).
55. Prevo, B., J.M. Scholey, and E.J.G. Peterman, *Intraflagellar transport: mechanisms of motor action, cooperation, and cargo delivery.* Febs j, 2017. **284**(18): p. 2905-2931.
56. Rosenbaum, J.L. and G.B. Witman, *Intraflagellar transport.* Nature Reviews Molecular Cell Biology, 2002. **3**(11): p. 813-825.
57. Scholey, J.M., *Intraflagellar transport.* Annu Rev Cell Dev Biol, 2003. **19**: p. 423-43.
58. Mirvis, M., T. Stearns, and W. James Nelson, *Cilium structure, assembly, and disassembly regulated by the cytoskeleton.* Biochem J, 2018. **475**(14): p. 2329-2353.
59. Anvarian, Z., et al., *Cellular signalling by primary cilia in development, organ function and disease.* Nat Rev Nephrol, 2019. **15**(4): p. 199-219.
60. Taschner, M. and E. Lorentzen, *The Intraflagellar Transport Machinery.* Cold Spring Harb Perspect Biol, 2016. **8**(10).
61. Jordan, M.A., et al., *The cryo-EM structure of intraflagellar transport trains reveals how dynein is inactivated to ensure unidirectional anterograde movement in cilia.* Nat Cell Biol, 2018. **20**(11): p. 1250-1255.
62. Stepanek, L. and G. Pigino, *Microtubule doublets are double-track railways for intraflagellar transport trains.* Science, 2016. **352**(6286): p. 721-4.
63. Badano, J.L., et al., *The Ciliopathies: An Emerging Class of Human Genetic Disorders.* Annual Review of Genomics and Human Genetics, 2006. **7**(1): p. 125-148.
64. Bisgrove, B.W. and H.J. Yost, *The roles of cilia in developmental disorders and disease.* Development, 2006. **133**(21): p. 4131-43.
65. Chevalier-Larsen, E. and E.L. Holzbaur, *Axonal transport and neurodegenerative disease.* Biochim Biophys Acta, 2006. **1762**(11-12): p. 1094-108.
66. Moyer, J.H., et al., *Candidate gene associated with a mutation causing recessive polycystic kidney disease in mice.* Science, 1994. **264**(5163): p. 1329-33.
67. Pazour, G.J., et al., *The intraflagellar transport protein, IFT88, is essential for vertebrate photoreceptor assembly and maintenance.* J Cell Biol, 2002. **157**(1): p. 103-13.
68. Murcia, N.S., et al., *The Oak Ridge Polycystic Kidney (orpk) disease gene is required for left-right axis determination.* Development, 2000. **127**(11): p. 2347-55.
69. Kozminski, K.G., et al., *A motility in the eukaryotic flagellum unrelated to flagellar beating.* Proceedings of the National Academy of Sciences of the United States of America, 1993. **90**(12): p. 5519-5523.
70. Hao, L., et al., *Analysis of intraflagellar transport in C. elegans sensory cilia.* Methods Cell Biol, 2009. **93**: p. 235-66.
71. Williams, C.L., et al., *Direct evidence for BBSome-associated intraflagellar transport reveals distinct properties of native mammalian cilia.* Nat Commun, 2014. **5**: p. 5813.

72. Ishikawa, H. and W.F. Marshall, *Efficient live fluorescence imaging of intraflagellar transport in mammalian primary cilia.* Methods Cell Biol, 2015. **127**: p. 189-201.
73. Cole, D.G., et al., *Chlamydomonas kinesin-II-dependent intraflagellar transport (IFT): IFT particles contain proteins required for ciliary assembly in Caenorhabditis elegans sensory neurons.* J Cell Biol, 1998. **141**(4): p. 993-1008.
74. Mueller, J., et al., *The FLA3 KAP subunit is required for localization of kinesin-2 to the site of flagellar assembly and processive anterograde intraflagellar transport.* Mol Biol Cell, 2005. **16**(3): p. 1341-54.
75. Kozminski, K.G., P.L. Beech, and J.L. Rosenbaum, *The Chlamydomonas kinesin-like protein FLA10 is involved in motility associated with the flagellar membrane.* J Cell Biol, 1995. **131**(6 Pt 1): p. 1517-27.
76. Liang, Y., et al., *FLA8/KIF3B phosphorylation regulates kinesin-II interaction with IFT-B to control IFT entry and turnaround.* Dev Cell, 2014. **30**(5): p. 585-97.
77. Engel, B.D., et al., *The role of retrograde intraflagellar transport in flagellar assembly, maintenance, and function.* J Cell Biol, 2012. **199**(1): p. 151-67.
78. Chien, A., et al., *Dynamics of the IFT machinery at the ciliary tip.* Elife, 2017. **6**.
79. Wong-Riley, M.T. and J.C. Besharse, *The kinesin superfamily protein KIF17: one protein with many functions.* Biomol Concepts, 2012. **3**(3): p. 267-282.
80. Marande, W. and L. Kohl, *Flagellar kinesins in protists.* Future Microbiol, 2011. **6**(2): p. 231-46.
81. Inglis, P.N., et al., *The sensory cilia of Caenorhabditis elegans.* WormBook, 2007: p. 1-22.
82. Signor, D., et al., *Two heteromeric kinesin complexes in chemosensory neurons and sensory cilia of Caenorhabditis elegans.* Mol Biol Cell, 1999. **10**(2): p. 345-60.
83. Snow, J.J., et al., *Two anterograde intraflagellar transport motors cooperate to build sensory cilia on C. elegans neurons.* Nature Cell Biology, 2004. **6**(11): p. 1109-1113.
84. Ou, G., et al., *Functional coordination of intraflagellar transport motors.* Nature, 2005. **436**(7050): p. 583-587.
85. Prevo, B., et al., *Functional differentiation of cooperating kinesin-2 motors orchestrates cargo import and transport in C. elegans cilia.* Nat Cell Biol, 2015. **17**(12): p. 1536-45.
86. Burghoorn, J., et al., *Mutation of the MAP kinase DYF-5 affects docking and undocking of kinesin-2 motors and reduces their speed in the cilia of Caenorhabditis elegans.* Proc Natl Acad Sci U S A, 2007. **104**(17): p. 7157-62.
87. Evans, J.E., et al., *Functional modulation of IFT kinesins extends the sensory repertoire of ciliated neurons in Caenorhabditis elegans.* J Cell Biol, 2006. **172**(5): p. 663-9.
88. Brunnbauer, M., et al., *Torque generation of kinesin motors is governed by the stability of the neck domain.* Mol Cell, 2012. **46**(2): p. 147-58.
89. Stepp, W.L., et al., *Kinesin-2 motors adapt their stepping behavior for processive transport on axonemes and microtubules.* EMBO Rep, 2017. **18**(11): p. 1947-1956.
90. Vukajlovic, M., et al., *How kinesin-2 forms a stalk.* Molecular biology of the cell, 2011. **22**(22): p. 4279-4287.
91. Vukajlovic, M., *Regulation of the subunit assembly and the catalytic activity in heteromeric kinesin-2 from Caenorhabditis elegans*, in *Faculty of Biology*. 2012, Ludwig-Maximilian Universität: Munich.
92. Yi, P., C. Xie, and G. Ou, *The kinases male germ cell-associated kinase and cell cycle-related kinase regulate kinesin-2 motility in Caenorhabditis elegans neuronal cilia.* Traffic, 2018. **19**(7): p. 522-535.
93. Cavalier-Smith, T., *The phagotrophic origin of eukaryotes and phylogenetic classification of Protozoa.* Int J Syst Evol Microbiol, 2002. **52**(Pt 2): p. 297-354.

94. Engelke, M.F., et al., *Acute Inhibition of Heterotrimeric Kinesin-2 Function Reveals Mechanisms of Intraflagellar Transport in Mammalian Cilia.* Curr Biol, 2019. **29**(7): p. 1137-1148 e4.
95. Funabashi, T., et al., *Ciliary entry of KIF17 is dependent on its binding to the IFT-B complex via IFT46-IFT56 as well as on its nuclear localization signal.* Mol Biol Cell, 2017. **28**(5): p. 624-633.
96. Jiang, L., et al., *Kinesin family 17 (osmotic avoidance abnormal-3) is dispensable for photoreceptor morphology and function.* FASEB J, 2015. **29**(12): p. 4866-80.
97. Lim, Y.S. and B.L. Tang, *A role for Rab23 in the trafficking of Kif17 to the primary cilium.* J Cell Sci, 2015. **128**(16): p. 2996-3008.
98. Jenkins, P.M., et al., *Ciliary targeting of olfactory CNG channels requires the CNGB1b subunit and the kinesin-2 motor protein, KIF17.* Curr Biol, 2006. **16**(12): p. 1211-6.
99. Setou, M., et al., *Kinesin superfamily motor protein KIF17 and mLin-10 in NMDA receptor-containing vesicle transport.* Science, 2000. **288**(5472): p. 1796-802.
100. Nakayama, K. and Y. Katoh, *Ciliary protein trafficking mediated by IFT and BBSome complexes with the aid of kinesin-2 and dynein-2 motors.* J Biochem, 2018. **163**(3): p. 155-164.
101. Taschner, M., et al., *Crystal structures of IFT70/52 and IFT52/46 provide insight into intraflagellar transport B core complex assembly.* The Journal of Cell Biology, 2014. **207**(2): p. 269-282.
102. Taschner, M., et al., *Intraflagellar transport proteins 172, 80, 57, 54, 38, and 20 form a stable tubulin-binding IFT-B2 complex.* Embo j, 2016. **35**(7): p. 773-90.
103. Katoh, Y., et al., *Overall Architecture of the Intraflagellar Transport (IFT)-B Complex Containing Cluap1/IFT38 as an Essential Component of the IFT-B Peripheral Subcomplex.* J Biol Chem, 2016. **291**(21): p. 10962-75.
104. Taschner, M., S. Bhogaraju, and E. Lorentzen, *Architecture and function of IFT complex proteins in ciliogenesis.* Differentiation, 2012. **83**(2): p. S12-22.
105. Mukhopadhyay, S., et al., *TULP3 bridges the IFT-A complex and membrane phosphoinositides to promote trafficking of G protein-coupled receptors into primary cilia.* Genes Dev, 2010. **24**(19): p. 2180-93.
106. Behal, R.H., et al., *Subunit interactions and organization of the Chlamydomonas reinhardtii intraflagellar transport complex A proteins.* J Biol Chem, 2012. **287**(15): p. 11689-703.
107. Bredrup, C., et al., *Ciliopathies with skeletal anomalies and renal insufficiency due to mutations in the IFT-A gene WDR19.* Am J Hum Genet, 2011. **89**(5): p. 634-43.
108. Piperno, G., et al., *Distinct mutants of retrograde intraflagellar transport (IFT) share similar morphological and molecular defects.* The Journal of cell biology, 1998. **143**(6): p. 1591-1601.
109. Iomini, C., et al., *Retrograde intraflagellar transport mutants identify complex A proteins with multiple genetic interactions in Chlamydomonas reinhardtii.* Genetics, 2009. **183**(3): p. 885-96.
110. Efimenko, E., et al., *Caenorhabditis elegans DYF-2, an orthologue of human WDR19, is a component of the intraflagellar transport machinery in sensory cilia.* Mol Biol Cell, 2006. **17**(11): p. 4801-11.
111. Blacque, O.E., et al., *The WD repeat-containing protein IFTA-1 is required for retrograde intraflagellar transport.* Mol Biol Cell, 2006. **17**(12): p. 5053-62.
112. Cortellino, S., et al., *Defective ciliogenesis, embryonic lethality and severe impairment of the Sonic Hedgehog pathway caused by inactivation of the mouse complex A intraflagellar transport gene Ift122/Wdr10, partially overlapping with the DNA repair gene Med1/Mbd4.* Dev Biol, 2009. **325**(1): p. 225-37.
113. Tsao, C.C. and M.A. Gorovsky, *Tetrahymena IFT122A is not essential for cilia assembly but plays a role in returning IFT proteins from the ciliary tip to the cell body.* J Cell Sci, 2008. **121**(Pt 4): p. 428-36.
114. Lee, E., et al., *An IFT-A protein is required to delimit functionally distinct zones in mechanosensory cilia.* Curr Biol, 2008. **18**(24): p. 1899-906.

115. Verhey, K.J. and J.W. Hammond, *Traffic control: regulation of kinesin motors.* Nature Reviews Molecular Cell Biology, 2009. **10**(11): p. 765-777.
116. Fan, Z.C., et al., *Chlamydomonas IFT70/CrDYF-1 is a core component of IFT particle complex B and is required for flagellar assembly.* Mol Biol Cell, 2010. **21**(15): p. 2696-706.
117. Baker, S.A., et al., *IFT20 links kinesin II with a mammalian intraflagellar transport complex that is conserved in motile flagella and sensory cilia.* J Biol Chem, 2003. **278**(36): p. 34211-8.
118. Follit, J.A., et al., *Characterization of mouse IFT complex B.* Cell Motil Cytoskeleton, 2009. **66**(8): p. 457-68.
119. Green, M.R. and J. Sambrook, *Molecular Cloning: A Laboratory Manual*. 2012: Cold Spring Harbor Laboratory Press.
120. Corpet, F., *Multiple sequence alignment with hierarchical clustering.* Nucleic acids research, 1988. **16**(22): p. 10881-10890.
121. Carbonell, L.F., M.J. Klowden, and L.K. Miller, *Baculovirus-mediated expression of bacterial genes in dipteran and mammalian cells.* J Virol, 1985. **56**(1): p. 153-60.
122. Miller, L.K., *Baculoviruses as gene expression vectors.* Annu Rev Microbiol, 1988. **42**: p. 177-99.
123. Luckow, V.A., et al., *Efficient generation of infectious recombinant baculoviruses by site-specific transposon-mediated insertion of foreign genes into a baculovirus genome propagated in Escherichia coli.* J Virol, 1993. **67**(8): p. 4566-79.
124. Laemmli, U.K., *Cleavage of structural proteins during the assembly of the head of bacteriophage T4.* Nature, 1970. **227**(5259): p. 680-5.
125. Fygenson, D.K., E. Braun, and A. Libchaber, *Phase diagram of microtubules.* Phys Rev E Stat Phys Plasmas Fluids Relat Interdiscip Topics, 1994. **50**(2): p. 1579-1588.
126. Bradford, M.M., *A rapid and sensitive method for the quantitation of microgram quantities of protein utilizing the principle of protein-dye binding.* Anal Biochem, 1976. **72**: p. 248-54.
127. Green, N.M., *Avidin.* Adv Protein Chem, 1975. **29**: p. 85-133.
128. Fish, K.N., *Total internal reflection fluorescence (TIRF) microscopy.* Curr Protoc Cytom, 2009. **Chapter 12**: p. Unit12 18.
129. Howard, J., A.J. Hudspeth, and R.D. Vale, *Movement of microtubules by single kinesin molecules.* Nature, 1989. **342**(6246): p. 154-8.
130. Vale, R.D., et al., *Direct observation of single kinesin molecules moving along microtubules.* Nature, 1996. **380**(6573): p. 451-3.
131. Cleetus, A., G. Merck, and Z. Ökten, *Retracing the evolution of kinesin-2 deployment from mouse to worm.* bioRxiv, 2020: p. 2020.08.17.254268.
132. Scheidel, N. and O.E. Blacque, *Intraflagellar Transport Complex A Genes Differentially Regulate Cilium Formation and Transition Zone Gating.* Curr Biol, 2018. **28**(20): p. 3279-3287 e2.
133. Wong, R.W., et al., *Overexpression of motor protein KIF17 enhances spatial and working memory in transgenic mice.* Proc Natl Acad Sci U S A, 2002. **99**(22): p. 14500-5.
134. Guillaud, L., M. Setou, and N. Hirokawa, *KIF17 dynamics and regulation of NR2B trafficking in hippocampal neurons.* J Neurosci, 2003. **23**(1): p. 131-40.
135. Stepp, W.L. and Z. Okten, *Resolving kinesin stepping: one head at a time.* Life Sci Alliance, 2019. **2**(5).
136. Hoeprich, G.J., et al., *Kinesin's neck-linker determines its ability to navigate obstacles on the microtubule surface.* Biophys J, 2014. **106**(8): p. 1691-700.
137. Shastry, S. and W.O. Hancock, *Neck linker length determines the degree of processivity in kinesin-1 and kinesin-2 motors.* Curr Biol, 2010. **20**(10): p. 939-43.
138. Jensen, L.J., et al., *STRING 8--a global view on proteins and their functional interactions in 630 organisms.* Nucleic Acids Res, 2009. **37**(Database issue): p. D412-6.

139. Pan, X., et al., *Mechanism of transport of IFT particles in C. elegans cilia by the concerted action of kinesin-II and OSM-3 motors.* The Journal of cell biology, 2006. **174**(7): p. 1035-1045.

Acknowledgement

It was a great pleasure to work on this thesis under the guidance of Dr. Zeynep Ökten. I offer my heartfelt gratitude to my supervisor for her kind invitation to work on this project. Thank you, Zeynep, for encouraging and guiding me throughout the years with your supervision, patience, and valuable insights.

I feel highly indebted to Georg Merck, my colleague and partner in this project, for his support has always being available whenever required. I knew whom to ask when I needed purified microtubules. Thank you, Georg.

I would like to extend my sincere thanks to Punam for supporting me with viruses and protocols for numerous experiments and also for being a good friend. I will miss the wonderful chai talks.

I want to thank Hieu for your wholehearted support and management of the lab. It was always a difficult time when you were not present in the lab.

I also take this opportunity to express my thanks and regards to my lab mates, Mohammed, for his kind support and discussions throughout the time; Willi for helping me in data analysis with MATLAB; Angela and Peter for allowing me to contribute in the Myosin project; Suelo for teaching me all the new assays when I joined the lab and all the other E22/E27 members for attending my status reports and subsequent discussions during the thesis. They all had a very significant role in the successful completion of this project.

I couldn't have gone through this project without the never ending love & support of my family, especially my dear wife Swathi and my parents. I thank my family for their assistance and care.